MICRO SHEET INCREMENTAL HYDROFORMING PROCESS UTILIZING ULTRA HIGH PRESSURE

HIDEKI SATO

Supervised by

Professor Ken-ichi Manabe

March 2016

Department of Mechanical Engineering,
Graduate School of Science and Engineering,
TOKYO METROPOLITAN UNIVERSITY
1-1 Minamiosawa Hachioji 192-0397
Tokyo, JAPAN

A DISSERTATION SUBMITTED IN PARTIAL FULFILLMENT OF THE REQUIREMENTS FOR DEGREE OF PHILOSOPHY IN DEPARTMENT OF MECHANICL ENGINEERING, TOKYO METROPOLITAN UNIVERSITY

Acknowledgments

Firstly, I appreciate my supervisor Prof. Ken-ichi Manabe for his continuous support and patience. He taught me what a fundamental principle is, and how I should think and act to achieve a breakthrough innovation. This study could not be possible without his earnest guidance.

I am grateful and thankful to Prof Zhengyi Jiang to support my study abroad and research in University of Wollongong, Australia. I experienced the study in the different the environment and countries, which was good opportunity to expand my research field.

I would also like to acknowledge the other two members of my thesis committee: Prof. Ming Yang and Prof. Satoru Takahashi for their time, logical and practical comments.

This research was supported by Research Fellowships of the Japan Society for the Promotion of Science (JSPS) for Young Scientists. I would like to appreciate JSPS for their financial support of this study.

The design of MHDD and MUDD tool sets and development of MUDD system was supported by Mr. Kuniyoshi Ito and staff members at Micro Fabrication Laboratory. Without their supports, the complex, miniature and high precision MUDD apparatus cannot be developed and the MUDD process cannot be experimentally realized. I appreciate their professional and attentive assistances.

I would also like to acknowledge Dr. Dongbin Wei of University of Technology, Sydney for his suggestions of a basic idea about micro sheet hydroforming. Furthermore, I am thankful to Prof, Sergei Alexandrov for his guidance of theoretical model and his helpful from theoretical aspect.

The advice about the tribology in micro forming and the attitude for the fundamental and innovative researches from Dr. Tetsuhide Shimizu is indispensable for the clarification of size effect in MHDD and my research life. To design the hydraulic system for MHDD and MUDD, I got many useful advices based on the micro fluid mechanics from Prof. Satoshi Ogata and Dr. Ken Yamamoto. Dr. Marko Vilotic supported my life of research internship in National Chung Cheng University in Taiwan, and helped the correction of my Ph. D. thesis. Mr. Luo Liang at University of Wollongong also help me to solve the problems about the micro fluid behavior in MHDD and my study life in University of Wollongong. I am very grateful for their big support and advices for my research.

I am particularly thankful to the members of “Professional seminar” in TMU for their strict and incisive comments and warm and gracious attitudes for training my scientific and engineering insights.

The members of the Engineering Plasticity Laboratory warmly and constantly supported my personal and research life in the lab. Dr. Tsuyoshi Furushima has showed me what a mature researcher should think, act and achieve from his attitude. He has also kindly supported my personal research life in the lab. Mr. Kazuo Tada has supported the technical problems in development of the machines and experimental work. The members of micro ultra deep drawing team, Mr. Daiki Kondo

and Mr. Takayuki Mano, contributed to the development of MUDD system, the analytical research using FE simulation, and the experimental work. This challenging research could not be realized without their novel ideas and efforts. Dr. Zicheng Zhang taught me FE simulation and showed me the strict attitude for the research. My colleges, Shusaku Furusawa, Hitomi Tsunezaki, Yuki Kinoshita and Kei Tsushima encouraged and worked hard together. The graduated seniors I respect, Dr. Supriadi Sugeng, Mr. Yuta Noda, Mr. Masahiro Ogawa, Mr. Takuma Ikeda, Mr. Satoshi Miyajima, Mr. Tetsuro Masuda, Mr. Shuhei Iwaoka, Mr. Toshiji Morishima, Mr. Mitsuhiro Shimada and Mr. Yuta Suzuki, warmly guided and taught me what the laboratory life is and how we should face the research. The graduated lovely juniors, Ikuko Akutsu, Yusuke Imagawa, Xu Chen, Masato Yagi, Dai Kobayashi, Kenta Takahashi and Tomoko Nakayama, shared the hard but satisfying research life. In addition, the present lab members, Kohei Aoto, Yutaro Hirose, Kazuki Matsuhita, Tomomasa Nakamori, Naoki Mashiwa, Kenta Itai, Kanta Sasaki, Keita Shukuno and Mari Hioki supported my Ph. D. life. I am grateful and thankful to all of the members in Engineering Plasticity Laboratory.

Finally, I would like to thank my family for being so patient with me and giving me their best supports throughout the course of my study. And above all, I appreciate Nan who mentally supported and persistently encouraged me during my Ph. D. student life.

Hideki Sato
March 2016

Micro Sheet Incremental Hydroforming Process Utilizing Ultra High Pressure

Chapter 2 Design of MHDD Based on Scale Dependence

Chapter 3 Development of MHDD System and Its Basic Drawing Characteristics

Chapter 4 Process Design of MUDD Using High Pressure and Incremental Control

Chapter 5 Development of MUDD System and Its Experimental Verification

Chapter 6 Conclusions

List of symbols

Symbol	Explanation
a	Constant for plane strain yield criterion
c	Clearance between blank and punch
c_1	Clearance between die and 1st punch in MUDD
c_2	Clearance between die and 2nd punch in MUDD
d	Grain size
h	Constant gap between die and blank holder
n	Work hardening exponent
p	Fluid pressure
p_c, p_r	Counter and radial pressures
p_{cr}	Critical blank holding pressure
p_{dry}	Normal pressure at RCA under dry friction
p_{fmin}	Minimum required fluid pressure for friction holding effect
p_h	Required fluid pressure for hydrodynamic lubrication
p_{total}	Normal pressure acting on the total surface under lubrication condition
p_{CL}	Hydrostatic pressure reduced by the enclosed lubricant in the CLPs
q	Blank holder pressure in flange area
q_d	Contact pressure at die shoulder
r_0	Current rim radius
r_1, r_2, r_3, r_4	Radii at points A, B, C and D in Fig. 2.1
r_{d1}	1st die shoulder radius in MUDD
r_{d2}	2nd die shoulder radius in MUDD
r_p, r_d	Punch and die shoulder radii
r_{p1}	1st punch shoulder radius in MUDD
r_{p2}	2nd punch shoulder radius in MUDD
r_{pi1}	1st punch inner shoulder radius in MUDD
S	Punch stroke
t	Blank thickness
x	Distance from cup center
w	Width of OPLs
w_{ave}	Average width of OPLs
y	Height from cup bottom
A, B, C	Parameters to determine contact angle at die shoulder Φ

A_f	Contact area in flange area
A_c, A_o	Area of CLPs and OLPs
A_{o-dry}	Dry friction area in OLPs
$A_{o-fluid}$	Lubricated area by fluid pressure in OLPs
D	Cup diameter
D_0	Blank diameter $(= 2R_0)$
D_d	Die diameter $(= 2R_d)$
D_p	Punch diameter $(= 2R_p)$
D_{p1}	1st punch diameter in MUDD
D_{p2}	2nd punch diameter in MUDD
E	Young's modulus
E_o	Reduced modulus of buckling of sheet metal
F_o	Tangent modulus of buckling of sheet metal
H	Cup height
I	Geometrical moment of inertia per unit width
K	Strength coefficient
L	Length of side wall
L_c	Contact length between the blank and punch side wall
M	Bending moment per unit width in die shoulder
M_B	Relative moment per unit width for bending resistance of blank
M_p	Relative bending moment per unit width caused by counter pressure applied to side wall
N	Ratio of thickness to grain size $(= t/d)$
P	Punch force
P_{al}	Allowance punch force at punch side wall
$P_{max(p_r=0)}$	Maximum punch force without radial pressure
$P_{max(p_r>0)}$	Maximum punch force with radial pressure
P_E	Effective punch force
P_M	Measured punch force
P_p	Force acting on the punch oppositely by counter pressure
P_S, P_F, P_B, P_{UB}	Pure drawing, friction, bending and unbending forces
$\bar{P}_E$	Normalized effective punch force
$\bar{P}_{Emax}$	Normalized maximum effective punch force
$\bar{P}_F$	Normalized friction force
$\bar{P}_M$	Normalized measured punch force
Q	Blank holder force per unit width

V_1, V_2, V_3, V_4	Volumes at die shoulder, side wall, punch shoulder and punch bottom areas
$\alpha_o, \alpha_c, \alpha_{RC}$	Fractions of OLPs, CLPs and RCA
$\bar{\alpha}_c, \bar{\alpha}_o$	Fractions of nominal CLPs and OLPs
α_B	Functions of γ_0 and γ_1 $(= (\gamma_0 - \gamma_1)/\gamma_0\gamma_1)$
α_H	Functions of γ_0 and γ_1 $(= \gamma_0 + \gamma_1)$
α_D	Functions of γ_0 and γ_1 $(= (\gamma_0 + \gamma_1)^2/(\gamma_0 - \gamma_1)^3)$
β_0	Relative current blank radius $(= r_0/R_0)$
β_1	Relative radius at entrance of die shoulder $(= r_0/R_1)$
β_2	Relative radius at exit of die shoulder $(= r_0/R_2)$
β^*	Function of β_0, β_1 and β_2
γ_0	Current drawing ratio $(= r_0/R_p)$
γ_1	Drawing ratio at entrance of die shoulder $(= r_1/R_p)$
δ	Elongation
δ_d	Relative punch diameter to thickness $(= D_p/t)$
ε_0	Material constant
ε_{eq}	Equivalent strain
ε_n	Nominal strain
ε_t	Thickness strain
ε_u	Strain at tensile strength
$\varepsilon_\varphi, \varepsilon_\theta$	Meridional and circumferential strains
$\bar{\varepsilon}_{eq}$	Average equivalent strain
λ	Scale factor $(= R_0/w)$
μ	Average friction coefficient
μ_c	Friction coefficient in CPLs
μ_d	Friction coefficient for dry friction in OLPs
μ_{fluid}	Friction coefficient in lubricated OLPs by fluid pressure
μ_h	Friction coefficient in hydraulic lubrication
μ_k	Kinetic friction coefficient used in FEM
μ_s	Static friction coefficient used in FEM
ξ	Taper angle of die and 1st punch in MUDD
σ_b, σ_{ub}	Bending and unbending stresses
σ_d, σ_f	Pure drawing and friction stresses
σ_{eq}	Equivalent stress
σ_n	Nominal stress
σ_r	Compression stress at flange area by radial pressure
σ_y	Yield stress

σ_B	Tensile strength
$\sigma_\varphi, \sigma_\theta$	Meridional and circumferential stresses
$\bar{\sigma}_{eq}$	Average equivalent stress
Φ	Contact angle at die shoulder
Φ_c	Bending angle to make contact between the blank and punch side wall
Φ_e	Angle of no contact area in entrance of die shoulder
ω_{cr}	Allowable specific wrinkle height
Δf	Flatness at bottom of cup
Δs	1st punch displacement in MUDD process
Δt	Flange pressing amount in MUDD process
ΔP_{Emax}	Reduction of maximum effective punch force by radial pressure
$\Delta \bar{P}_{Emax}$	Normalized reduction of maximum effective punch force by radial pressure
$\Delta \sigma_\varphi$	Reduction of meridional stress at side wall by applying radial pressure
DR	Drawing ratio $(= R_0/R_p)$
DR_1	Drawing ratio at 1st drawing in MUDD
DR_2	Drawing ratio at 2nd drawing in MUDD
LDR	Limiting drawing ratio

Chapter 1

Introduction

1.1. Background

The demand for micro components with an ultra fine, complicated shape, and high shape accuracy has been increasing in order to improve the performance of medical devices, precision equipment, communication devices, and micro-electromechanical systems (MEMS), as well as to achieve multifunctional, compact, and highly integrated devices. According to Yole Development market analysis of May 2015 [1-1], especially micro sensors market is expected of the raped growth and the whole MEMS industry is preparing to exceed 20 billion US$ by 2020 as shown in **Fig. 1.1**.

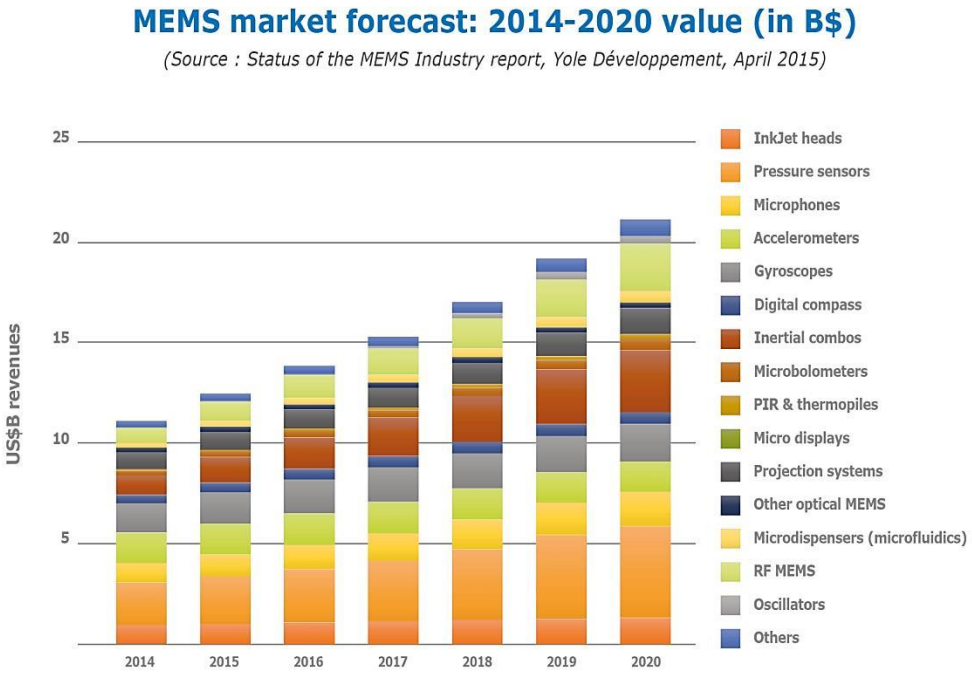

Fig. 1.1 2014-2020 MEMS market forecast by Yole Development [1-1].

01 Introduction

To reduce the product size by half or more and also reduce costs, the MEMS market is calling for new technologies to meet their challenges. As a production method for micro components, the conventional metal forming was scaled down to micro scale due to its process simplicity, high production capability, minimized or zero material waste, and near-net-shape production. Scaled down technologies, such as micro blanking, micro extrusion, micro bending, micro forging, and micro deep drawing (MDD), have been developed since more than 10 years ago [1-2]. These forming technologies are adopted to produce the lead frame, micro pin, micro gears, micro screw, micro spring, bipolar place, and many others. These micro components fabricated by micro forming are summarized in **Table 1.1**.

The three dimensional micro components are known as a complex shape and are hard to fabricate. Previously, a hybrid forming method of micro bending and laser welding was adopted for fabricating the three dimensional micro components with complex shape as shown in **Fig. 1.2** [1-14]. This technique can apply various shapes by changing the blank material; however, it cannot say that the produce quality is high enough due to the welding line. To fabricate the seamless three dimensional micro components, micro deep drawing (MDD) process was scaled down. The components fabricated by MDD have been adapted to the various applications, especially in medical, electrics and telecommunication devices. Yang developed a micro pump valve which is used at medical solution injection equipment as shown in **Fig. 1.3** [1-15]. The micro deeper cup shape components was used in probe pin used for electric characteristics measuring [1-16] and advanced medical equipment [1-17]. Thus, various shapes and sizes, such as shallow or deep containers, irregular shape, were demanded in MDD. However, these conventional technologies need many steps to achieve the long and tiny shape. It takes a long forming cycle and costs a lot because many tools and machines are required to conduct several steps. Additionally, it is difficult to apply further complication and miniaturization of components. As mentioned above, further simple and flexible micro forming technology is a technique emergency to supply the demand in MEMS markets.

Table 1.1 Adoption examples of micro forming in micro parts and its applications.

Applications	Micro parts	Forming process	Reference
Image sensor 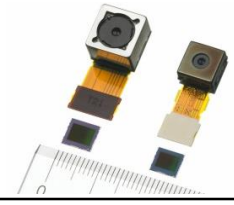	Lead frame 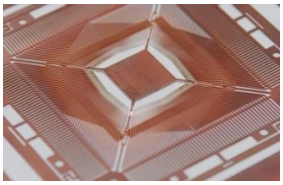	Micro blanking	[1-3, 1-4]
Micro HDD 	Magnetic disk head 	Micro blanking, Micro bending	[1-5, 1-6]
Fuel injector 	Orifice plate 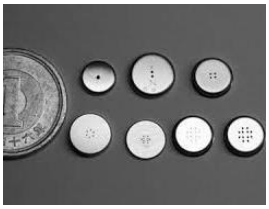	Micro deep drawing Micro piercing	[1-7, 1-8]
USB adapter 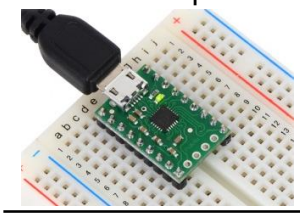	Micro pin 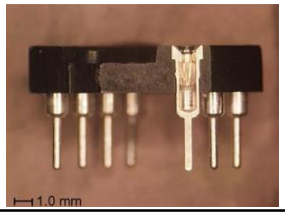	Micro extrusion	[1-9, 1-1]
Micro fuel cell 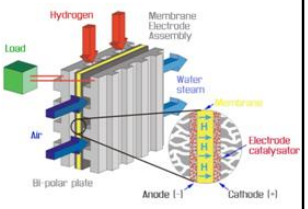	Bipolar plate 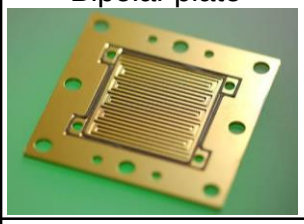	Micro embossing, Micro bulging	[1-10, 1-11]
Coronary artery stent 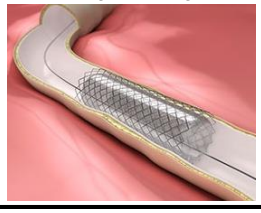	Stent 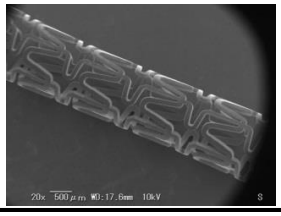	Micro laser cutting	[1-12, 1-13]

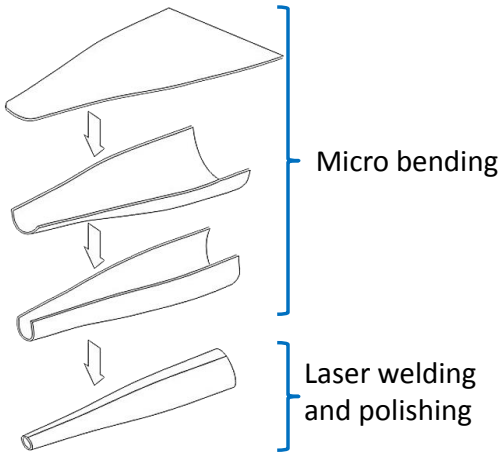

Fig. 1.2 Hybrid forming method of micro bending and laser welding for complex shape [1-14].

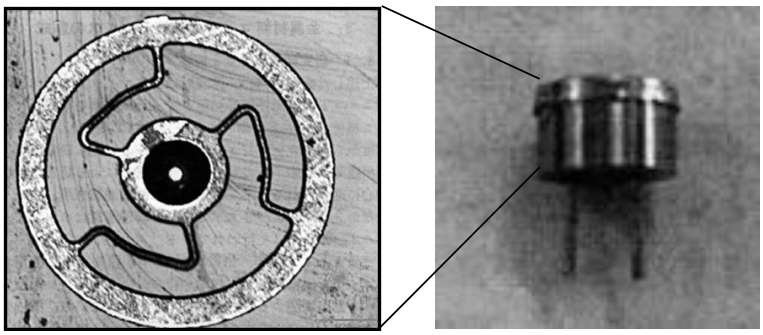

(a) Micro valve pump

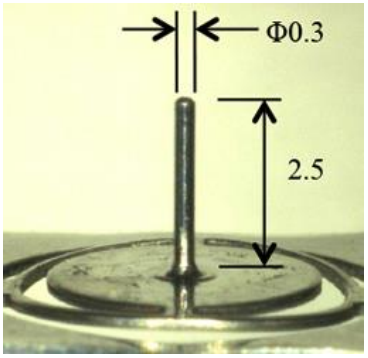

(b) Micro deeper cup for probe pin

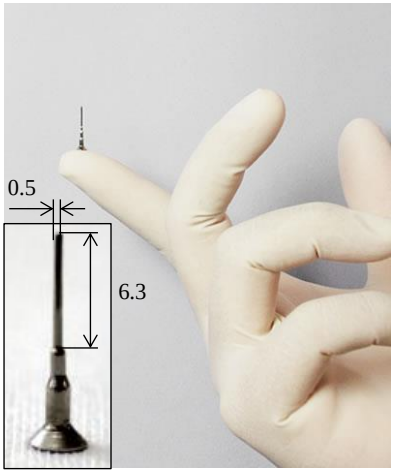

(c) Micro deeper cup for advanced medical equipment

Fig. 1.3 Examples of formed products and applications in micro deep drawing [1-15]-[1-17].

1.2. Macro Sheet Forming for High Aspect Ratio Products

In macro metal forming, several techniques for high aspect ratio products, such as pressure, heating, vibration, and process control, were developed. These techniques have the potentials to realize the high flexibility, decrease of number of process, high shape accuracy, good surface property and high forming limit. Therefore, it is believed that these techniques can solve the problems in micro scale. In this section, the techniques for high aspect ratio products developed in macro scale are reviewed and the effectiveness of these techniques and the feasibility of their advantages in micro scale are discussed.

1.2.1. Pressure aided forming

The pressure in deep drawing is useful to fabricate the complex shape components due to its flexibility. The pressure is generally generated by the fluid medium, air, rubber and other materials. There are several methods of the deep drawing using the pressure and it can be classified as follows,

(a) Hydromechanical deep drawing
(b) Radial pressure assisted hydromechanical deep drawing
(c) Rubber pat forming
(d) Deep drawing with high pressured water jet

Kasuga et al., developed the hydromechanical deep drawing –pressure lubricated method– as shown in **Fig. 1.4(a)** [1-18]. In this method, the hydrostatic pressure is applied from the die cavity during deep drawing process. The application of fluid pressure can induce fracture prevention effects, such as friction holding effect, hydrodynamic lubrication effect, pre-bulging effect, and compression effect of blank edge by radial pressure [1-19]. Based on this hydromechanical deep drawing, Nakamura et al., developed the radial pressure assisted hydromechanical deep drawing in which the radial pressure is applied to blank edge to enhance the material flow and improve the tribological behavior as shown in **Fig. 1.5 (a)** [1-20]. To improve the work environment, the hydroforming method was developed in which the rubber sheet is used to prevent the leakage of fluid medium as shown in **Fig. 1.6** [1-21]. Moreover, the fluid pressure is easily controlled in this method due to no leakage. The mechanisms for each effect in these forming methods are shown in **Fig. 1.7** and expressed as follows;

(a) Friction holding effect

When the blank contacts with the punch at side wall, the friction between the blank and punch side wall occurs and it reduces the meridional stress applied to the blank at punch shoulder. This

effect is called as the friction holding effect and it can prevent the fracture at punch shoulder by the reduction of applied force to the blank.

(b) Pre-bulging effect

When the counter pressure is applied before the deep drawing process starts, the blank deformed to the punch side. This pre-bulging deformation is helpful to induce the friction holding at early stage by the contact between the blank and punch. Furthermore, by compressing the bulged blank, the blank near the punch shoulder becomes thick and the allowance applied force can be improved. To obtain this thickening behavior, the lubricant and material flow at flange are at pre-bulging stage is important to prevent the thinning.

(c) Hydrodynamic lubrication effect

When the fluid medium leeks between the blank and die, the hydrodynamic lubrication occurs. It can reduce the friction coefficient between the blank and die significantly and improve the tribological behavior.

(d) Variable die radius effect

To decrease the maximum applied force to the blank, the die radius is set up the large until the maximum applied force, and then set up the designed value by controlling the fluid pressure during the process.

(e) Compression effect of blank edge by radial pressure

By applying the radial pressure at blank edge, the compression stress can be applied at flange area. It can reduce the meridional stress at flange area and enhances the material flow.

(f) Both sides hydrodynamic lubrication effect

By applying the radial pressure at blank edge, the hydrodynamic lubrication occurs not only between the blank and die, but also between the blank and blank holder. The further improvement of tribological behavior can be obtained by this both sides hydrodynamic lubrication effect.

Due to these effects in hydromechanical deep drawing, the drawing ratio of 2.92 and aspect ratio of 1.84 can be achieved in the hydromechanical deep drawing as shown in **Fig. 1.4(b)**, and the drawing ratio of 3.31 and aspect ratio of 2.4 can be obtained in radial pressure assisted hydromechanical deep drawing **Fig. 1.5(b)**. This forming method also can reduce the springback and improve the shape accuracy [1-22].

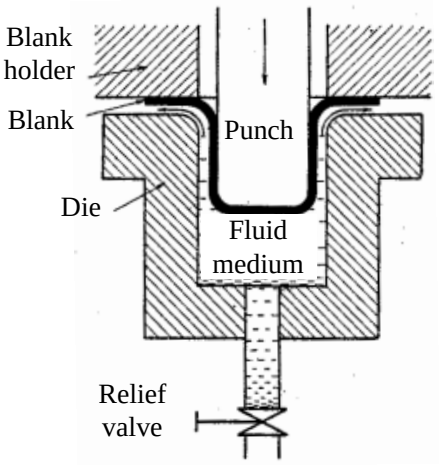

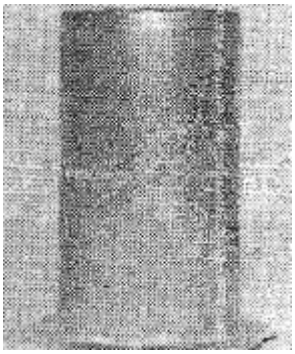

DR=2.92
H=91.7mm
D=49.98mm
H/D=1.84
t=0.6mm

(a) Schematic of forming principle (b) Example of drawn cup

Fig. 1.4 Hydromechanical deep drawing (pressure lubricated method) [1-18, 19].

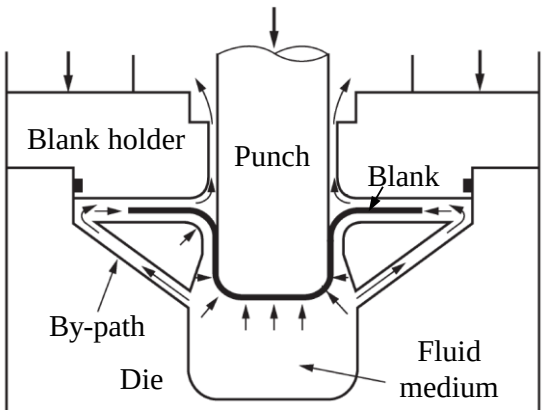

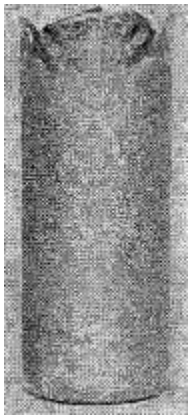

DR=3.31
H=72mm
D=29.9mm
H/D=2.4
t=0.8mm

(a) Schematic of forming principle (b) Example of drawn cup

Fig. 1.5 Radial pressure assisted hydromechanical deep drawing [1-20].

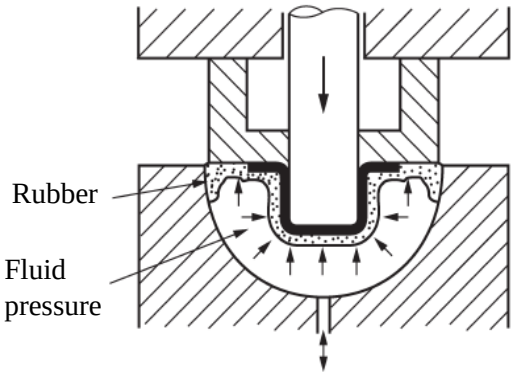

DR=2.4
H=100mm
D=125mm
H/D=0.8
t=1.0mm

(a) Schematic of forming principle (b) Example of drawn cup

Fig. 1.6 Hydromechanical deep drawing (hydroform method) [1-21].

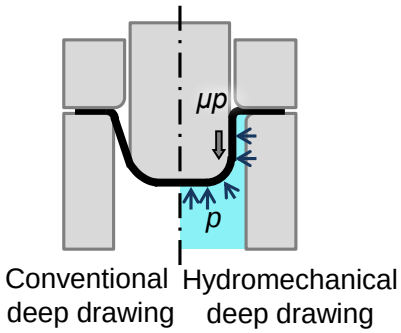

(a) Friction holding effect

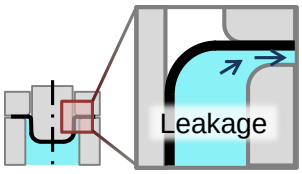

(b) Hydrodynamic lubrication effect

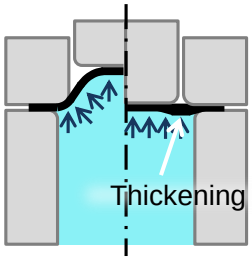

(c) Pre-bulging effect

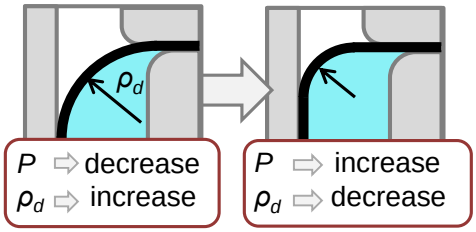

(d) Variable die radius effect

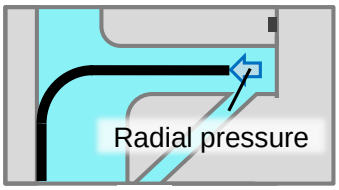

(e) Compression effect of blank edge by radial pressure

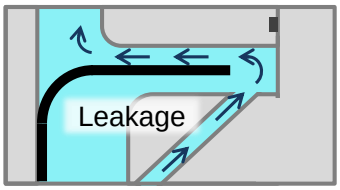

(f) Both side hydrodynamic lubrication effect

Fig. 1.7 Principle of fracture restriction effects in hydromechanical deep drawing.

In the hydromechanical deep drawing, the cycle time is low because the fluid medium should be filled in the die cavity after the process. In addition, when the lubricant is used, the degreasing and clearing processes are required. To solve this problem and improve the productivity, Yamazaki et al., developed a deep drawing using high pressure jet water to improve the tribological behavior without the lubricant [1-23]. The high pressure jet water is applied from punch shoulder to reduce the contact between the blank and die as shown in **Fig. 1.8(a)** [1-24]. Thus, the tribological property can be improved with the high productivity and without lubricant. Using this method, the drawn cup with high surface quality and the drawing ratio of 1.8 can be fabricated as shown in **Fig. 1.8(b)**.

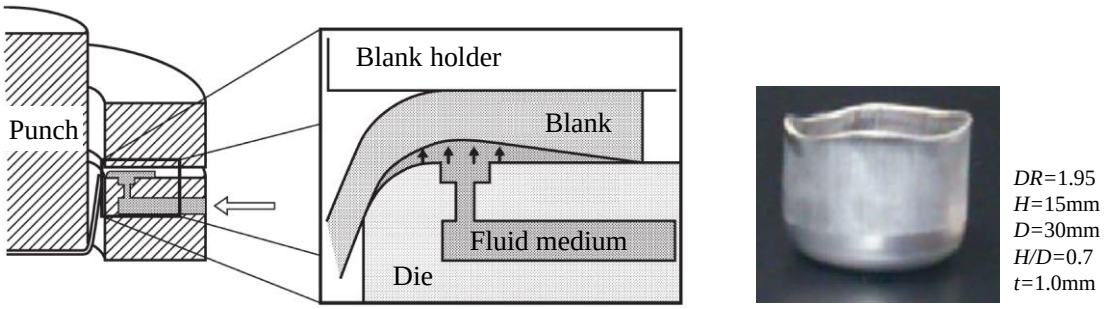

(a) Schematic of forming principle (b) Example of drawn cup

Fig. 1.8 Deep drawing using high pressure jet water [1-24].

Instead of the fluid pressure, the rubber pat is used in rubber pat forming as shown in **Fig. 1.9**. The guerin process shown in **Fig. 1.9(a)** is generally used for the bending, bulging, embossing, shallow recessing and shearing. The marform process shown in **Fig. 1.9(b)** is generally used for deep drawing [1-25]. This marform process also can be obtained the friction holding effect to improve the drawability and is suitable to fabricate the complex shape components. As compared with the hydromechanical deep drawing, the forming process is much simple due to no control of the fluid pressure during the process, although the failure of forming machine occurs due to the fracture of rubber pat. This rubber part forming of marform process can fabricate the drawn cup with the drawing ratio of 2.6 and aspect ratio of 1.4 in one step as shown in **Fig. 1.9(c)**. Though the redrawing process, the drawing ratio of 5.38 and aspect ratio of 4.3 can be achieved.

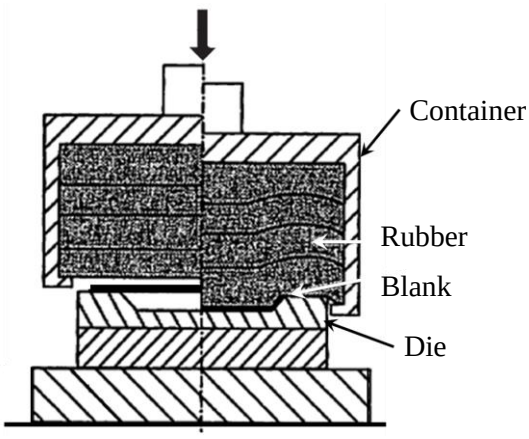

(a) Schematic of guerin process

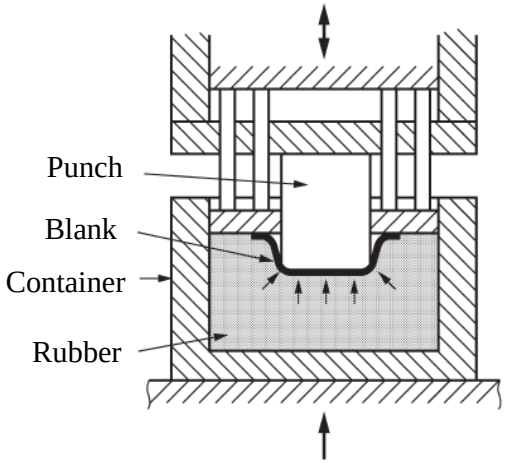

(b) Schematic of marform process

DR=2.6
H=36.1mm
D=25.4mm
H/D=1.4
t=0.8mm
N=1

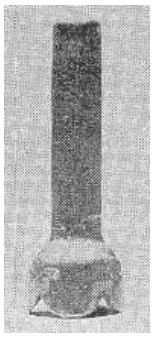

DR=5.38
H=86mm
D=20mm
H/D=4.3
t=0.8mm
N=2

(c) Examples of drawn cups by marform process

Fig. 1.9 Rubber pat forming [1-25].

1.2.2. Heat aided forming

The heating is widely used to enhance the ductility of material and decrease the drawing resistance in deep drawing. It is also useful to change the material properties during the process. The deep drawing using heating can be classified as follows;

(a) Deep drawing using strain induced transformation

(b) Deep drawing by local heating and cooling

Kawai et al., developed the deep drawing using strain induced transformation in which the strain induced transformation is used to obtain the quite large ductility and strength and improve the drawability [1-26]. In this process, the heating medium is applied to the blank near the punch shoulder from the nozzle as shown in **Fig. 1.10**. By controlling the temperature of the blank appropriately, the strain induced transformation can be obtained and the drawability can be improved.

The local heating and cooling technique is also used in deep drawing process [1-27]. In this deep drawing using the heating and cooling, the blank at flange area is heated to reduce the drawing resistance and the blank at punch shoulder and side wall is cooled to enhance the allowable force applied to the blank as shown in **Fig. 1.11**(a). The drawn cup with drawing ratio of 5.0 and aspect ratio of 3.l3 can be obtained [1-28].

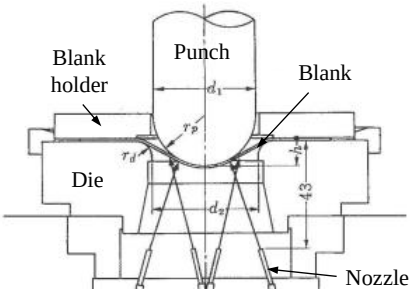

Fig. 1.10 Schematic of deep drawing using strain induced transformation [1-26].

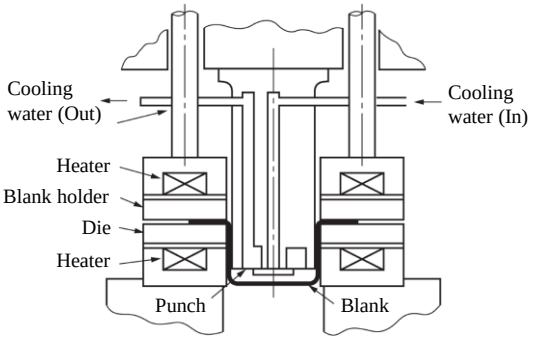

(a) Schematic of forming principle

DR=5.0
H=109mm
D=33mm
H/D=3.3
t=0.5mm
N=1

(b) Example of drawn cup

Fig. 1.11 Deep drawing by heating and cooling [1-27, 28].

1.2.3. Vibration aided forming

The vibration is useful in deep drawing to enhance the material flow and improve the tribological behavior. This method can be classified as follows;

(a) Deep drawing using ultra sonic vibration

(b) Deep drawing with hydraulic pressure and tool vibration

Jimma et al., developed the deep drawing using ultra sonic vibration as shown in **Fig. 1.12** [1-29, 30]. The ultra sonic vibration can restrict the wrinkling because the blank holder pressure in thickness direction becomes large. It also can improve the material flow because the blank at flange area is subjected to the large compression and flows in the meridional direction. In addition, the delayed fracture can be prevented due to the decrease of residual stress.

Kataoka et al., developed the deep drawing with hydraulic pressure and tool vibration as shown in **Fig. 1.13** [1-31]. The limiting drawing ratio (LDR) of 2.1 can be achieved using all of the hydraulic pressure, ultrasonic vibration of die and mechanical vibration of punch, although the LDR is less than 1.8 when only the hydraulic pressure is used as shown in **Fig. 1.14**. It is because the vibrations of punch and die under hydraulic pressure can make a gap between the blank and tools and apply the lubricant. Therefore, the tribological behavior can be improved.

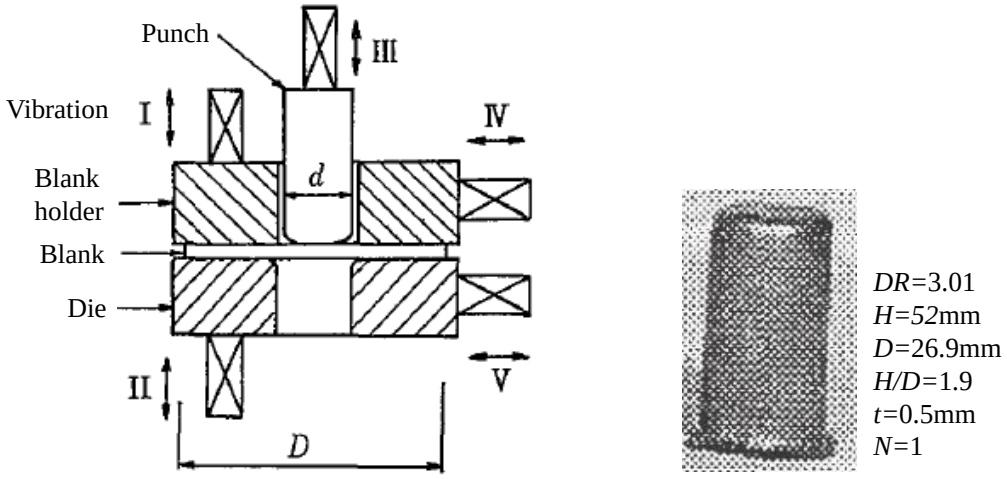

(a) Schematic of forming principle (b) Example of drawn cup

Fig. 1.12 Deep drawing using ultra sonic vibration [1-29].

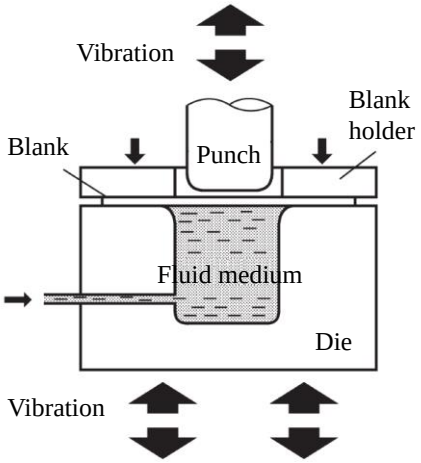

Fig. 1.13 Schematic of deep drawing with hydraulic pressure and tool vibration [1-31].

Additional conditions	Marks							
	A	B	C	D	E	F	G	H
Hydraulic counter pressure (H)					○	○	○	○
Ultrasonic vibration of die (U)		○		○		○		○
Mechanical vibration of punch (M)			○	○			○	○

(a) Drawing condition

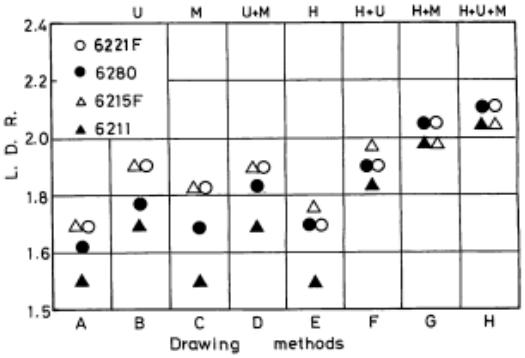

(b) Result

Fig. 1.14 Effects of hydraulic pressure, ultrasonic vibration of die and mechanical vibration of punch on limit drawing ratio [1-31].

1.2.4. Material flow control techniques

In the deep drawing using material flow control, the blank is not deformed by traction of punch, but by the material flow at flange area. This method can significantly improve the drawability. This method can be classified as follows;

(a) Friction aided deep drawing using rubber

(b) Friction aided deep drawing using tapered blank holder divided into several segments

(c) Deep drawing using flange pressing

The friction aided deep drawing using rubber shown in **Fig. 1.15(a)** was developed to realize the punchless deep drawing [1-32, 33]. This forming method does not use the punch to deform the blank, but uses the rubber ring to enhance the material flow. By continuing the cycle several times, the cup with drawing ratio of 3.42 and aspect ratio of 2.4 can be obtained as shown in **Fig. 1.15(b)** [1-34]. The quite long cup with the drawing ratio of 12 and aspect ratio of 14 also can be fabricated by continuing the cycle more than 150 times.

Hassan et al., uses a tapered blank holder divided into four segments in friction aided deep drawing as shown in **Fig. 1.16(a)** [1-35]. It consists of the stationary base and four movable segments that have similar planes of slightly taper angle of 5°, the movable segments can slide radially under a constant speed over the tapered surfaces of the stationary base. By moving the drawing segments repeatedly, the friction force in the meridional direction occurs between the blank and tools and it enhances the material flow into the die cavity. Thus, the blank is deformed by the movable segments and the cup with the drawing ratio of 3.67 and aspect ratio of 2.1 can be obtained as shown in **Fig. 1.16(b)**.

Iizuka uses the flange pressing by the solid punch to improve the durability of rubber method and nonuniform material flow in movable segments method [1-36]. In this method, the blank is pressed by the solid punch and the ironing and drawing are induced by stretch and shrink flange deformation as shown in **Fig. 1.17(a)**. Thus, the long drawn cup with the aspect ratio of 18 (**Fig. 1.17(b)**) and uniform thickness distribution can be fabricated.

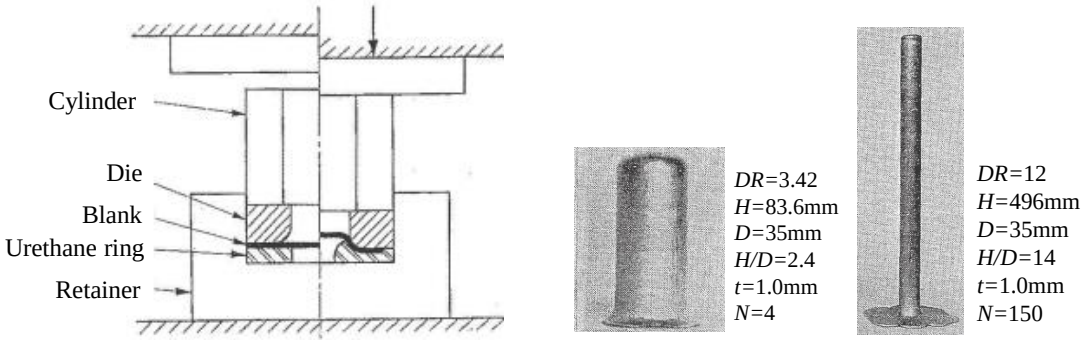

(a) Schematic of forming principle (b) Examples of drawn cups

Fig. 1.15 Friction aided deep drawing using rubber [1-34].

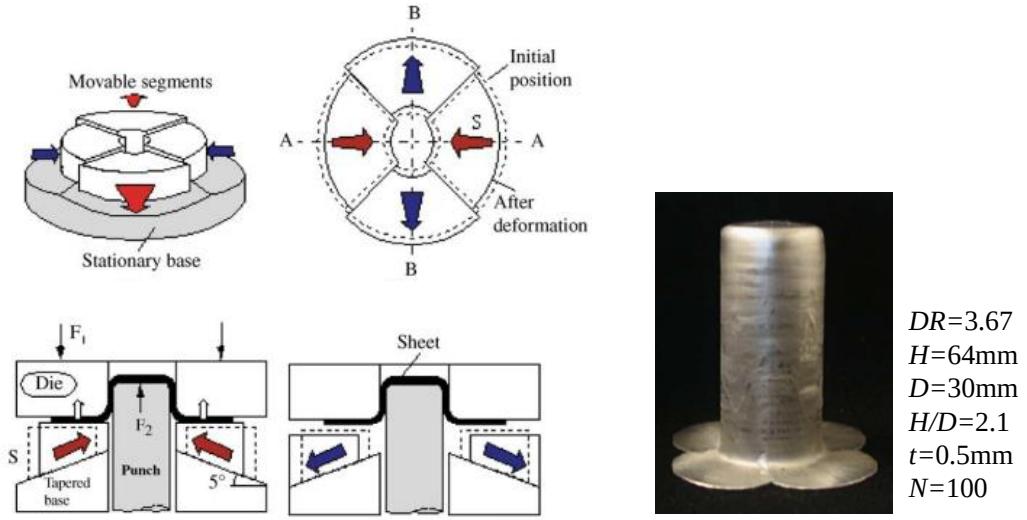

(a) Schematic of forming principle (b) Example of drawn cup

Fig. 1.16 Friction aided deep drawing using divided tapered blank holder [1-35].

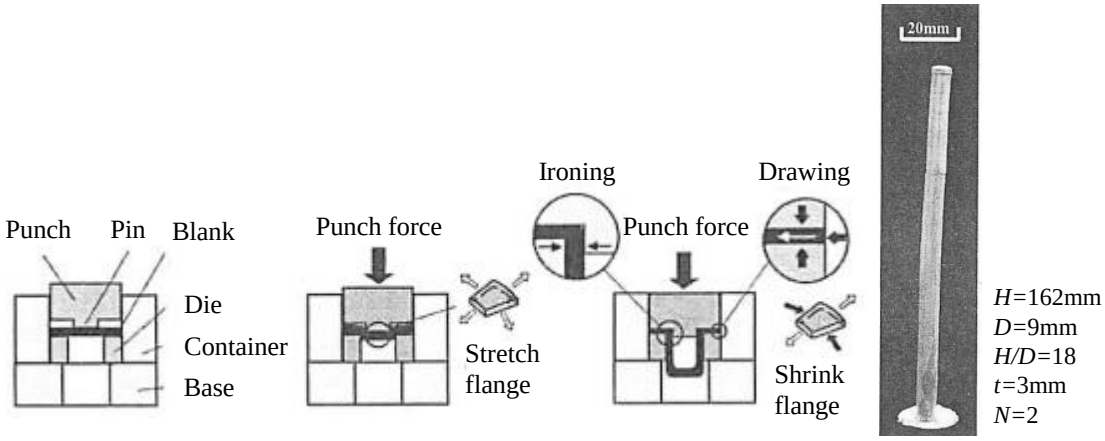

(a) Schematic of forming principle (b) Example of drawn cup

Fig. 1.17 Deep drawing using flange pressing [1-36].

1.2.5. Process control techniques

Manabe et al., developed the variable control methods for blank holder force and punch speed in deep drawing [1-37, 38]. In this method, the blank holder force is changed and controlled during deep drawing process to avoid the fracture and wrinkle limit as shown in **Fig. 1.18** [1-39]. This method can improve the LDR by optimizing the process control path as shown in **Fig. 1.19**. Furthermore, the uniform thickness distribution can be obtained. In addition, the variable blank holder force control using segment blank holder was developed by Yagami et al., [1-40]. The blank holder is divided into several segments and the blank holder force of each segments are optimized during the process as shown in **Fig. 1.20**. This technique is useful for the deep drawing of non-asymmetric components and realizes the appropriate material flow.

On the other hand, in the punch speed control, the punch speed is controlled and changed during the process to reduce the forming time and enhance the forming limit for the strain rate sensitive material as shown in **Fig. 1.21** [1-38]. This technique also can achieve the improvement of forming limit as shown in **Fig. 1.22**.

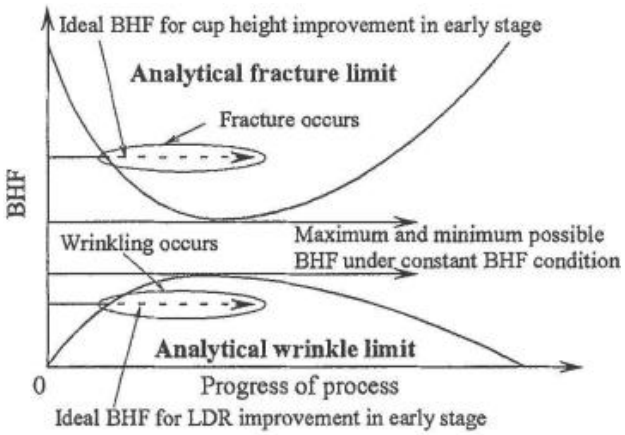

Fig. 1.18 Concept of variable blank holding force in deep drawing [1-39].

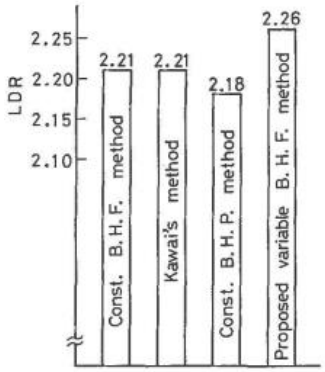

Fig. 1.19 Comparison of LDRs for various blank holding methods [1-37].

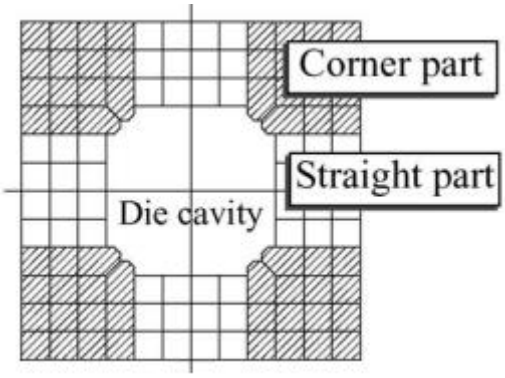

Fig. 1.20 Schematic of segmented blank holder [1-40].

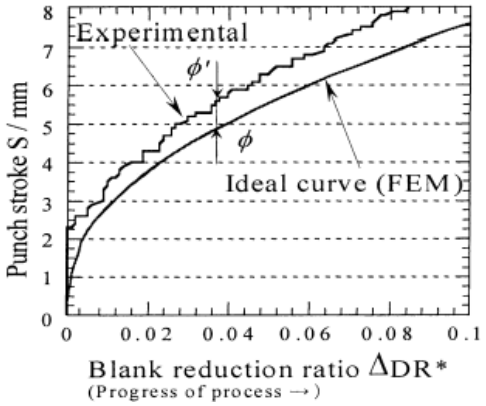

Fig. 1.21 Image of punch speed control in deep drawing process [1-38].

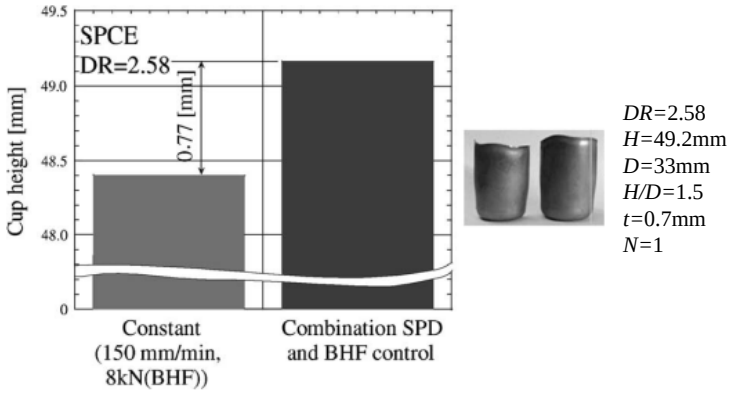

Fig. 1.22 Comparison of cup heights for different control methods [1-38].

1.2.6. Utilization of unique tooling

The tapered blank holder in deep drawing [1-41] is used to enhance the material flow as shown in **Fig. 1.23**. The large taper angle of blank holder can improve the LDR as shown in **Fig. 1.24**. It is effectively improved even only by the small taper angel. It is because the tapered blank holder can restrict the wrinkling in quite small blank holder force. Thus, the tapered blank holder can easily improve the forming limit without additional expensive equipment.

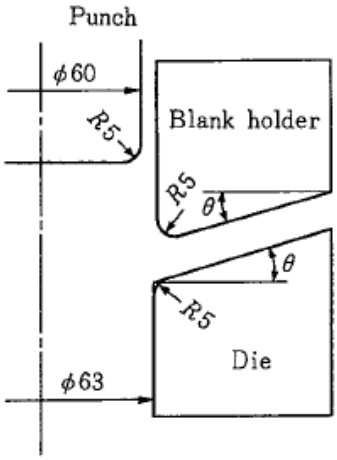

Fig. 1.23 Schematic of deep drawing with tapered blank holder [1-41].

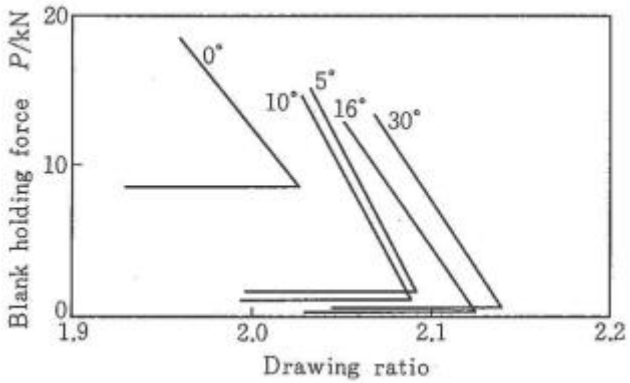

Fig. 1.24 Effect of inclination of blank holder surface on fracture or wrinkle limit in deep drawing (SPCC, t=1.0mm) [1-41].

1.2.7. Incremental forming

The incremental forming [1-42, 43] is generally known as the forming method using the single point tool as shown in **Fig. 1.25**. This method can be classified as follows;

(a) Single point incremental forming

(b) Incremental forming using single point rotated tool

(c) Revers bulging method

In this forming method, the single point tool is in the continuous contact with the sheet metal and is moved under the computer numerical control (CNC) in three dimensional space. From the appropriate control of forming tool, the flexible shape can be fabricated without the die as shown in **Fig. 1.26**. Although its productivity is not high enough, it can save the cost of die and can apply any complex shape components. Furthermore, by the strain allocation as shown in **Fig. 1.27**, the high deformability, high forming limit and uniform thickness distribution can be obtained. This principle is called the strain allocation [1-44]. As mentioned above, the incremental forming is a high-mix and low volume forming technique.

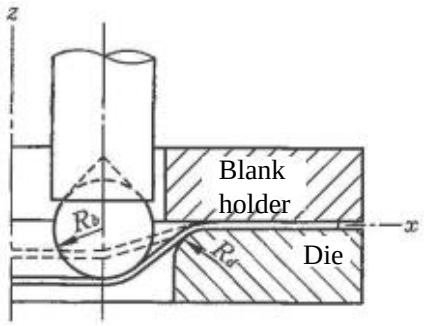

(a) Single point incremental forming

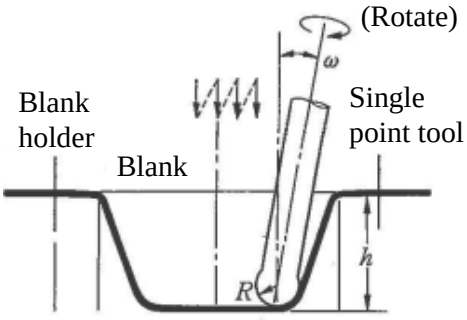

(b) Single point rotate tool

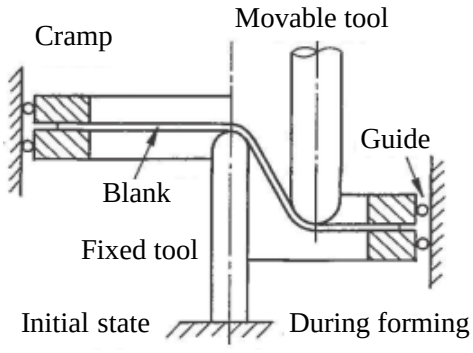

(c) Revers bulging method

Fig. 1.25 Schematic of several type of incremental forming [1-42].

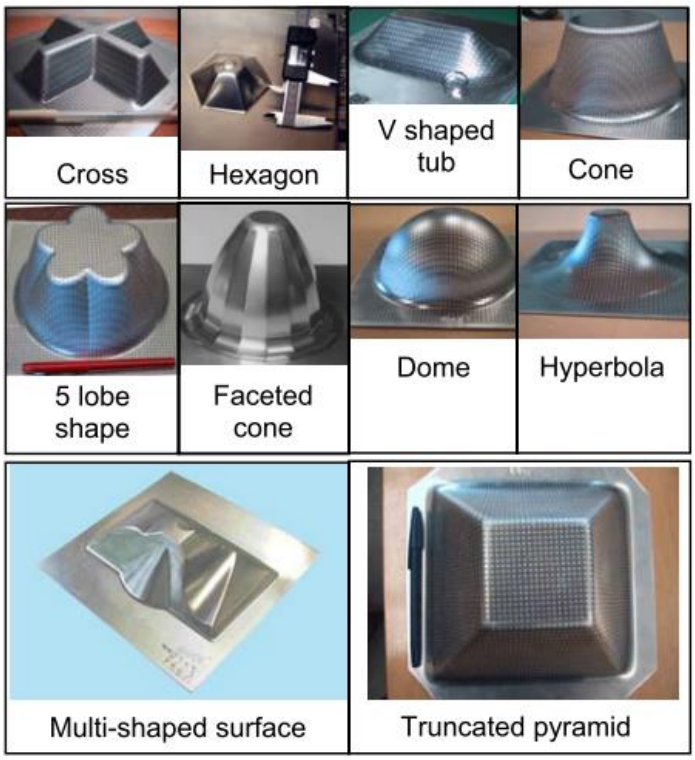

Fig. 1.26 Several shape applications in incremental forming [1-43].

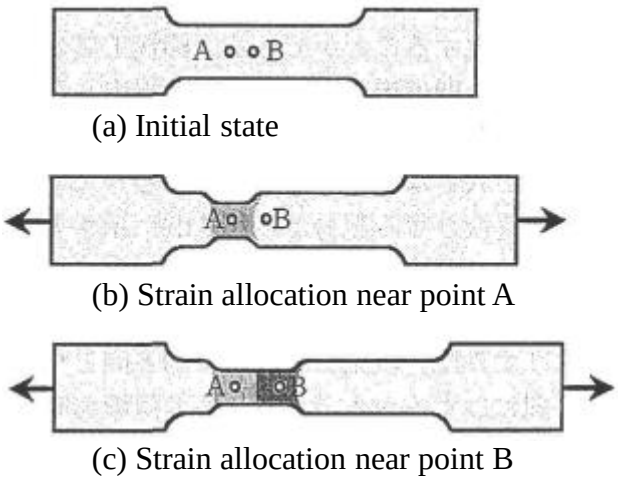

Fig. 1.27 Mechanism of improving ductility by strain allocation [1-44].

1.2.8. Characterization of each macro sheet forming

The characterization and advantages for each forming technique can be summarized in **Table 1.2**. The sheet hydroforming has a high superiority for improving the forming limit, shape accuracy, and applying the dieless and complex shape. Additionally, the friction aided and incremental forming also have these advantages. The forming limit, complex shape, shape accuracy and dieless or punch less are important factor for miniaturization due to the low formability and accuracy, difficulty of handling and limitation of tooling miniaturization in micro forming as explained in Section 2. It seems that these forming techniques have a high feasibility to solve the problems in micro scale.

On the other hand, the productivity is also important factor and should be considered to respond the high volume production. **Fig. 1.28** shows the effectiveness of each forming technique for improving forming limit and decreasing the number of processes. The friction aided deep drawing can fabricate the quite long product; however, it needs a number of processes and its productivity is low. On the other hand, heat aided deep drawing, rubber forming and sheet hydroforming have a good productivity, although its feasible aspect ratio is lower than the friction aided deep drawing.

From the above discussion, the sheet hydroforming technique is expected to be suitable for micro sheet forming.

Forming principle		Important factor for miniaturization					
		Forming limit			Complex shape	Dimensional accuracy	Diless/ punchless
		High allowable applied force	Decrease of applied force	Decrease of friction force			
Heating	Strain induced transformation		○			○	
	Local heating/ cooling	◎	○			○	
Pressure	Hydraulic pressure		○	◎	○	○	○
	Flexible tool		○	○	○	○	○
Vibration	Ultrasonic			○		○	
	Vibraction under fluid pressure			◎		○	○
Material flow control	Friction aided		◎				○
	Divided tapered blank holder		○			○	
	Flange pressing		◎				◎
Process control	Blank holder force control	○	○	○		○	
	Punch speed control		○			○	
Inrcemental	Incremental forming		◎		◎		◎
Unique tooling	Tapered blank holder		○			○	

Table 1.2 Characterization and advantages for each forming technique

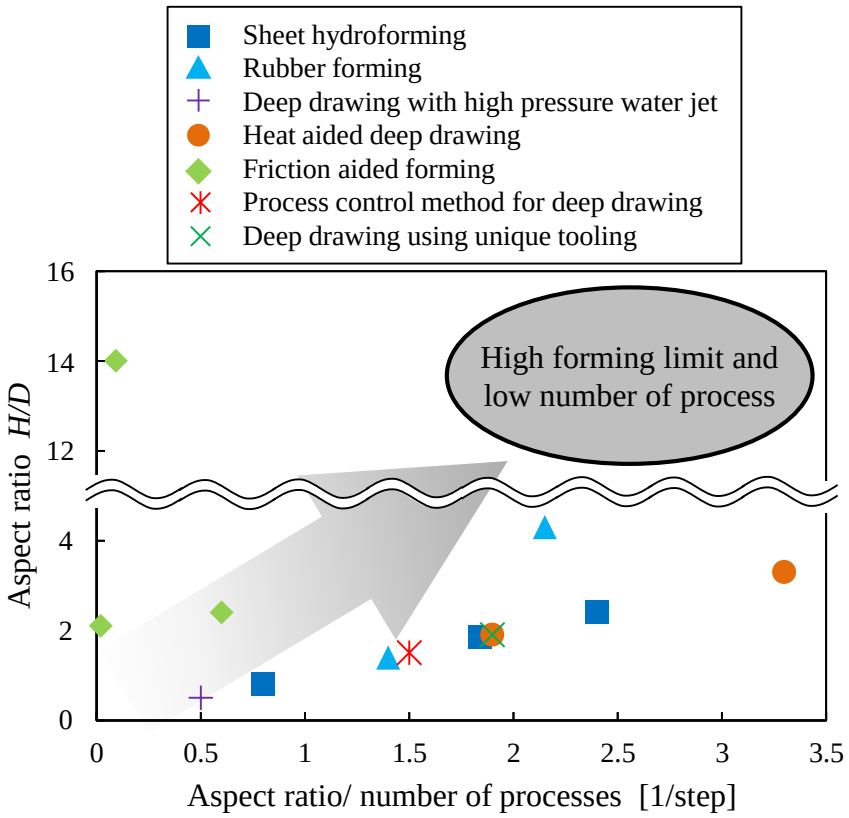

Fig. 1.28 Effectiveness of each forming technique for improving forming limit and decreasing the number of processes.

1.3. Problems and Size Effects in Micro Forming

With scaling down to micro scale, some unexpected behaviors are resulted in the processing parameters, the processing or testing results. These problems cause that the conventional macro forming cannot be simply scaled down to micro scale. Size effects are known as unique characteristics with miniaturization. It can be categorized by density, shape and microstructure as shown in **Fig. 1.29** [1-45].

The density of defects decreases with decreasing the target size. The point defects (e. g. small pores), line defects (e. g. dislocation lines) and interface areas (e. g. grain boundaries) normally exist in the material; however, these defects disappear when the material size is scaled down to certain size. It causes the scale dependence of the scatter of results and material strength.

The relative dimensions among line, area, and volume are changed with scaling down. With decreasing the target size, the ratios of the surface area and volume to the sample size decrease because the surface area of a part is proportional to the third power of its size r^3 and the surface goes with the second power r^2. When the sample size becomes 1/10, the surface area and volume becomes 1/100 and 1/1000, respectively. Therefore, the surface effects (e. g. surface tension) are stronger than the volume effects (e. g. inertia) in micro scale.

The microstructure does not change when the target size decreases. For example, the surface roughness and grain size depends on the material properties itself and does not change when the sample size decreases. The ratio of this microstructure to sample size relatively increases. It causes the change of material properties and tribological behavior in micro scale.

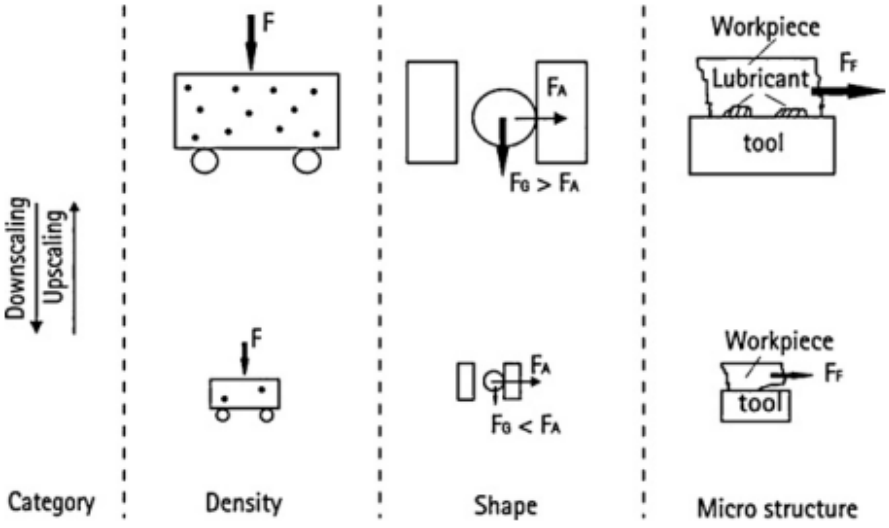

Fig. 1.29 Categories for size effects. [1-45]

1.3.1. Size effects on material properties

The material properties have scale dependences because the microstructure in the material, such as grain size and surface roughness, does not change although its specimen size decreases. It significantly influences the formability and quality in micro forming. In this section, the size effects of grain size and surface roughness on material properties are introduced and the material properties in micro scale are described.

(1) Grain size

The ratio of thickness to grain size is an important parameter to describe the material flow in micro scale. This ratio decreases with scaling down because the grain size does not change with decreasing the thickness. Previous research focused on this ratio to investigate the grain size effect on material properties. Lai et al., conducted the tensile test using CuNi18Zn20 with grain size of 40μm and thicknesses of 0.1, 0.5 and 1.0mm [1-46]. They revealed that the flow stress decreases with the decrease of the specimen size as shown in **Fig. 1.30**. The similar behavior was reported by Fu et al., as shown in **Fig. 1.31** [1-47]. They conducted the tensile test using pure copper with different grain sizes and thicknesses and clarified that the flow stress and ductility decreases with deceasing the ratio of specimen size to grain size. This behavior is explained by so called surface layer model as shown in **Fig 1.32** [1-48]. The moving dislocations pile up at grain boundary, but cannot pile up in the surface grains during the deformation. Therefore, the grain size located on the surface shows the less hardening and causes the low flow stress in metal foil.

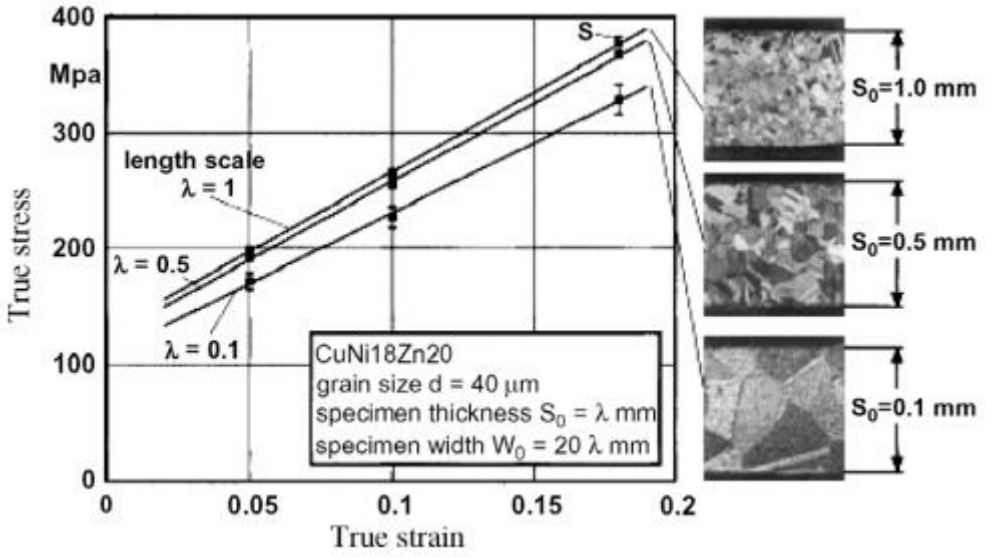

Fig. 1.30 Flow stress curves of CuNi18Zn20 for different values of the length scale [1-46].

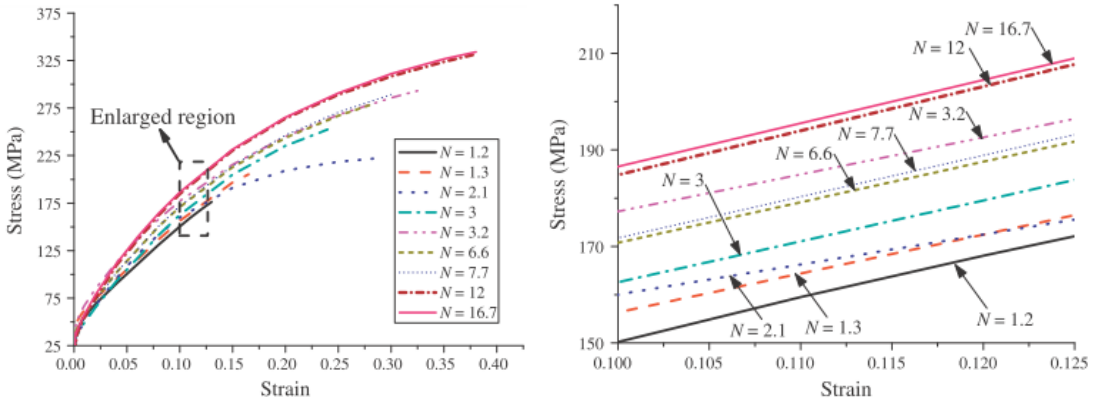

(a) Overall view (b) Enlarged view

Fig. 1.31 Experimental results of tensile tests for different ratios of thickness to grain size ($N = t/d$) [1-47].

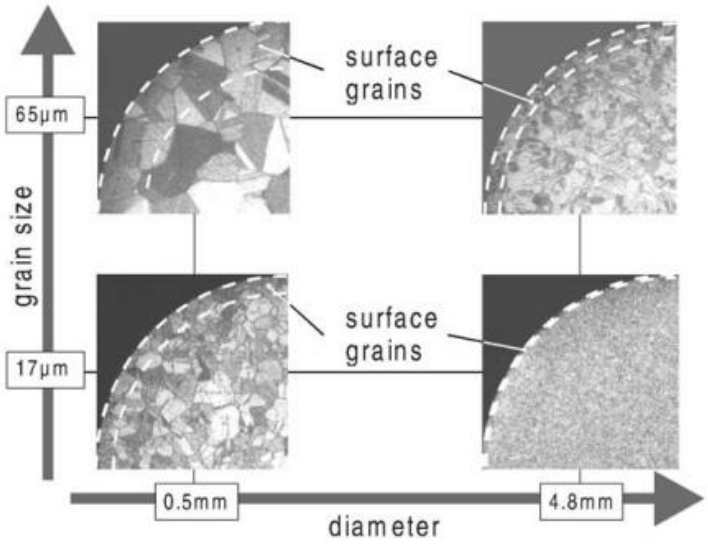

Fig. 1.32 Share of surface grains [1-48].

(2) Surface roughness

Oh the other hand, Furushima et al., reported that the free surface roughening behavior also influences the ductile fracture of metal foil [1-49]. They conducted the tensile test using pure copper foil with thicknesses of 0.05, 0.1, 0.3 and 0.5mm. It was clarified that the fracture strain does not only depend on the thickness itself as shown in **Fig. 1.33(a)**, but also depends on the ratio of increase in surface roughness as shown in **Fig. 1.33(b)**. They implied that the local deformation is caused by free surface roughening and it leads the fracture in micro scale with the large ratio of surface roughness to thickness.

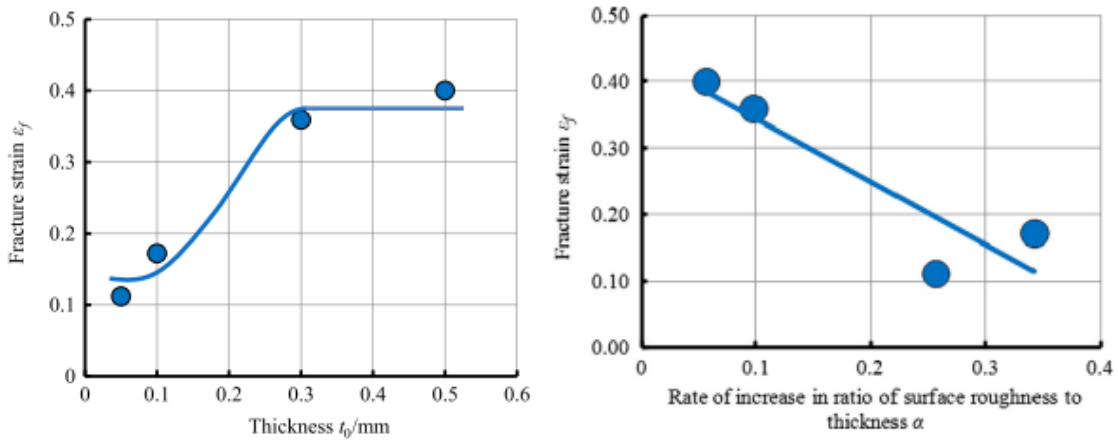

(a) Effect of thickness

(b) Effect of rate of increase in ratio of surface roughness to thickness

Fig. 1.33 Effect of thickness and rate of increase in ratio of surface roughness to thickness on fracture strain [1-49].

1.3.2. Size effect on variation and scatter

The miniaturization of target size also influences the geometrical accuracy and scatter of formed parts. The bending test for different grain sizes and thicknesses shows that the maximum bending force decreases as the thickness decreases in the case of fine grain, but it increases in the case of coarse grain as shown in **Fig. 1.34** [1-50]. When only single grain exists along the thickness, the yield strength increases although it increases when the ratio of thickness to grain size is over 1. It means that the characteristic for each grain dominants the material behavior. Therefore, the strain distribution for coarse grained material becomes inhomogeneous as shown in **Fig. 1.35**. Thus, the scatter of bending force increases with decreasing the ratio of thickness to grain size as shown in **Fig. 1.34**.

The springback angle, which is an important parameter for the accuracy of formed parts, is also affected by this ratio. The springback angle increases as the ratio of thickness to grain size decreases as shown in **Fig. 1.36** [1-51]. Particularly, it exceeds 20 degree at the thickness of 0.1mm although it is under 5 degree in thickness of 0.6mm. It can be said that the springback is one of significant problems for the product accuracy in micro forming.

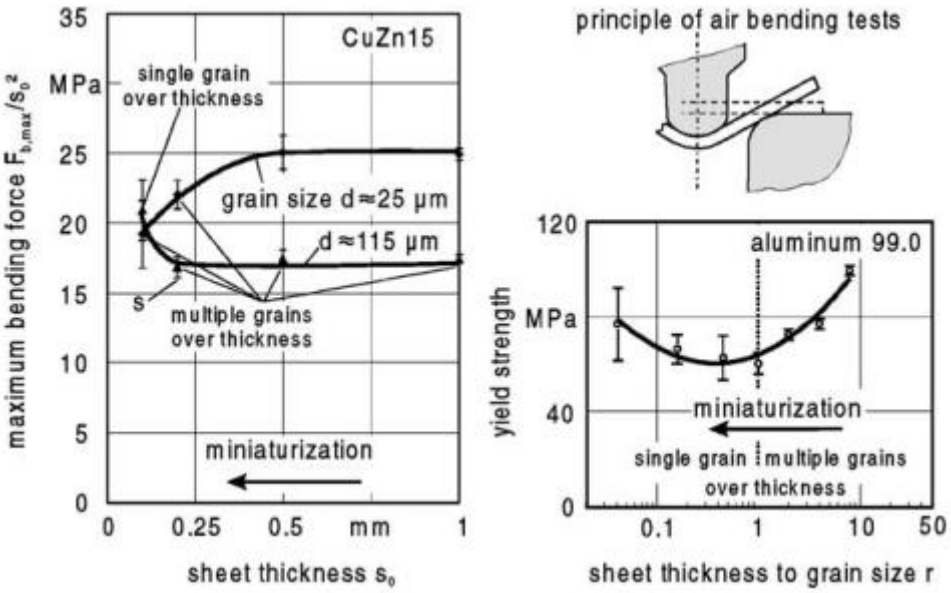

(a) On bending forces (b) On yield strength

Fig. 1.34 Effect of thickness and grain size miniaturization in bending test [1-50].

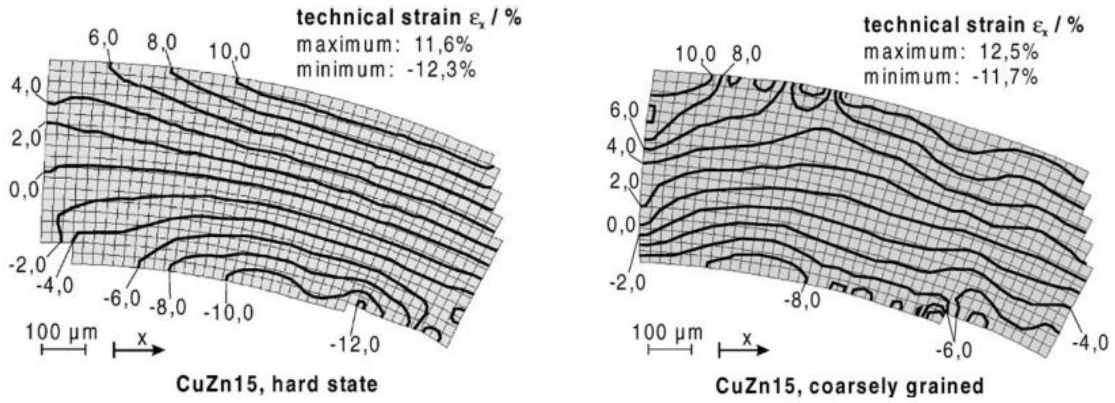

(a) Fine grained material (b) Coarse grained material

Fig. 1.35 Strain distributions of fine and coarse grained materials [1-50].

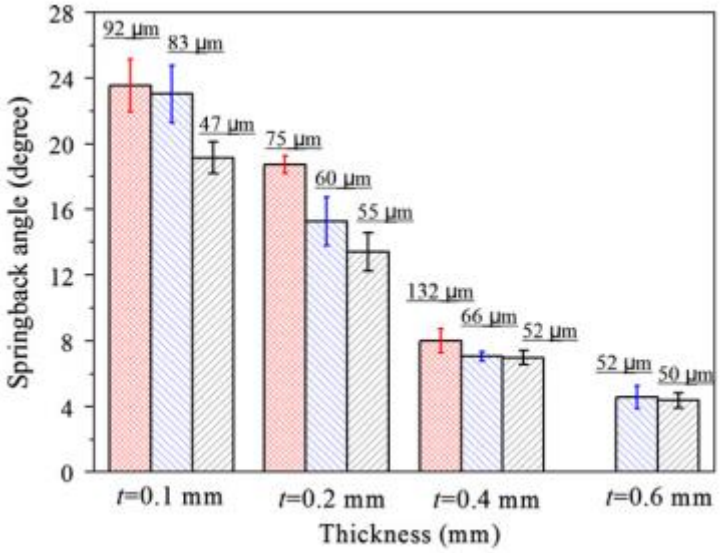

Fig. 1.36 Effects of thickness and grain size on springback angle [1-51].

1.3.3. Size effect on friction

The tribological behavior depends on the several parameters, such as the, the contact state between the material and tools, the contact pressure, the lubricant condition and the surface topography. Particularly, the surface topography plays an important role for the friction and its microstructure does not change as the sample size decreases. Accordingly, the size effect on friction occurs and many researchers investigated it in micro forming. In this subsection, the previous studies about size effect on friction and its friction model and lubricant pockets model, are introduced.

(1) Scale dependence in lubricated friction

The size effect in friction is generally explained that the friction increases with miniaturization. One of representative reports of size effect on friction in micro bulk forming is the double-cup-extrusion test [1-52]. The upper punch moves down and causes the material to form two cups with the lower and upper cup heights. In the theoretical case of no friction, both of cups have the same height, whereas the higher friction prevents the deformation of the lower cup as shown in **Fig. 1.37**. Therefore, the ratio of upper cup height to lower cup height can evaluate the friction. The experiment and FE results of the double-cup-extrusion show that the cup height ratio increases with miniaturization as shown in **Fig. 1.38**. It means that the friction increases distinctly with decreasing the specimen size.

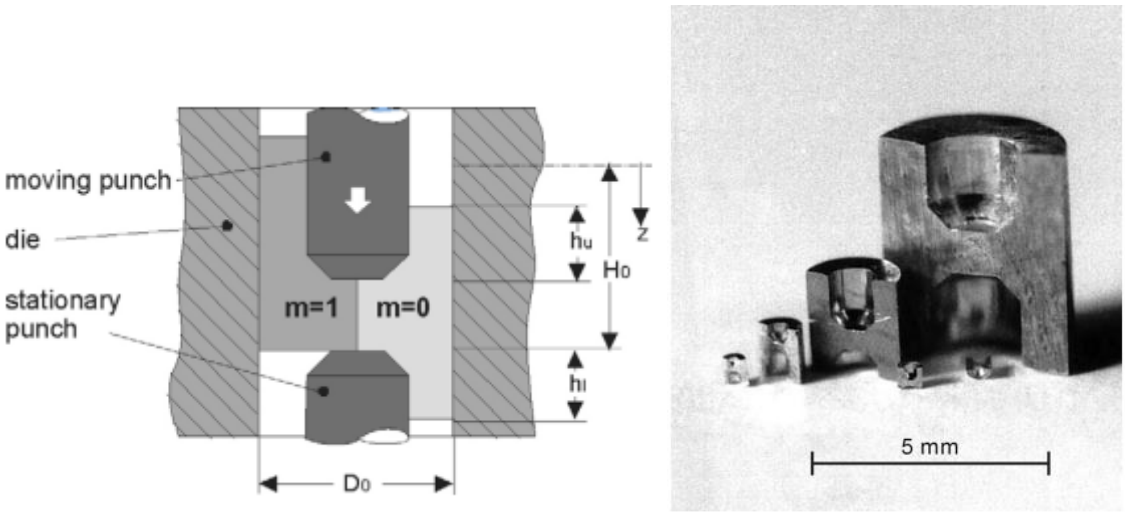

(a)Schematic of friction dependent material flow (b) Specimens with different diameters

Fig. 1.37 Set up of double-cup-extrusion test and its specimens [1-52].

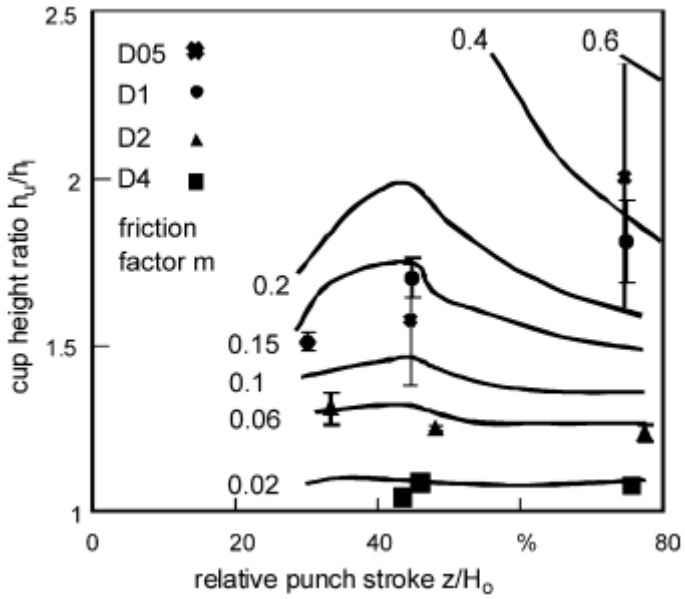

Fig. 1.38 Effect of cup height ratio on friction factor in FEA and experiment [1-52]

The same behavior was reported in micro sheet forming by Vollertsen et al., [1-53]. Under the blank holder force, the strip is drawn by a punch into the die, whereby the punch force is measured as shown in **Fig. 1.39**. The punch force consists of bending force at the die shoulder and friction force at flange area. Because the bending force for certain work piece and certain die shoulder radius can be theoretically calculated, the share of the friction force can be determined. The experimental result shows that the friction coefficient decreases as the specimen dimensions decrease as shown in **Fig. 1.40**, and its dependence on contact pressure is also changed with decreasing the size.

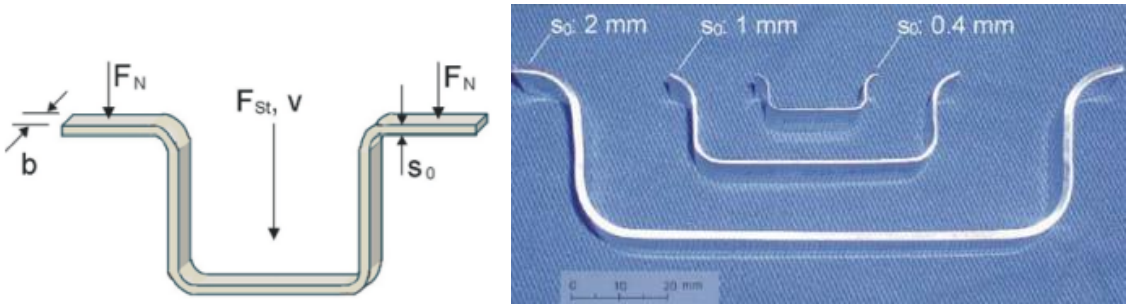

(a) Principle of strip drawing test (b)Specimens with different specimen sizes

Fig. 1.39 Set up of strip drawing test and its specimen [1-53]

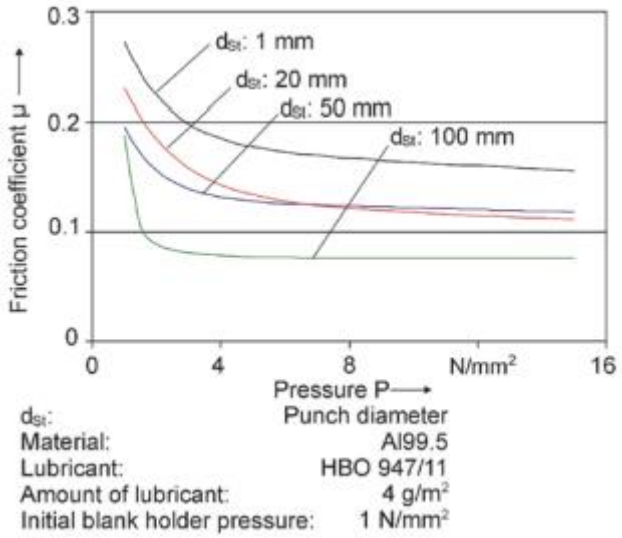

Fig. 1.40 Friction functions of different process dimensions [1-53].

(2) Lubricant pocket model

The size effect on friction can be explained by open lubricant pockets (OLPs). In this area, the roughness valleys connect with the edge of surface and cannot keep the lubricant as shown in **Fig. 1.41**. When the specimen size decreases, the contact area is reduced significantly while the size of single topography feature remains approximately constant. Therefore, the fraction of OLPs increases drastically in micro scale as shown in **Fig. 1.42**. It leads the increase of contact between the material and tool and the increase of friction.

To model this behavior, Engel developed the mechanical-rheological model distinguishing between open and closed lubricant pockets (CLPs), both being influenced by scaling [1-52]. In this model, considered the fractions of OLPs, CLPs and real contact area (RCA), the normal pressure acting on the total surface under lubrication condition p_{total} is led. It can be expressed by;

$$p_{total} = p_{dry} + \left(1 - \frac{1 - \alpha_{RC}}{\lambda}\right) p_{CL} \qquad (1.1)$$

where p_{dry} is the normal pressure at RCA under dry friction, p_{CL} is the hydrostatic pressure reduced by the enclosed lubricant in the CLPs, α_{RC} is the fraction of RCA, and λ is the scale factor. With some assumptions for the relative parameters, this mechanical-rheological model can distinguish the size effect on friction under the lubricant as shown in **Fig. 1.43**.

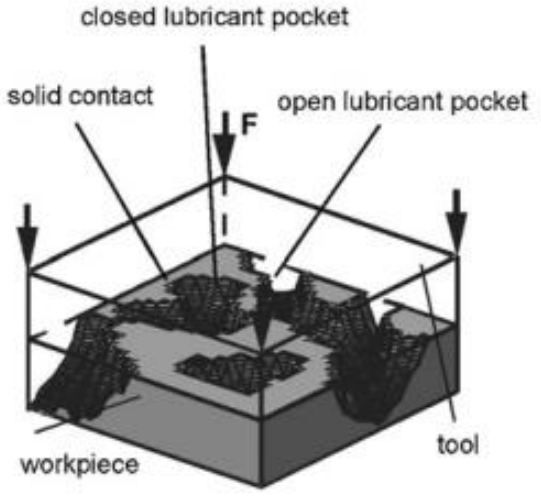

Fig. 1.41 Schematic of open and closed lubricant pockets [1-54].

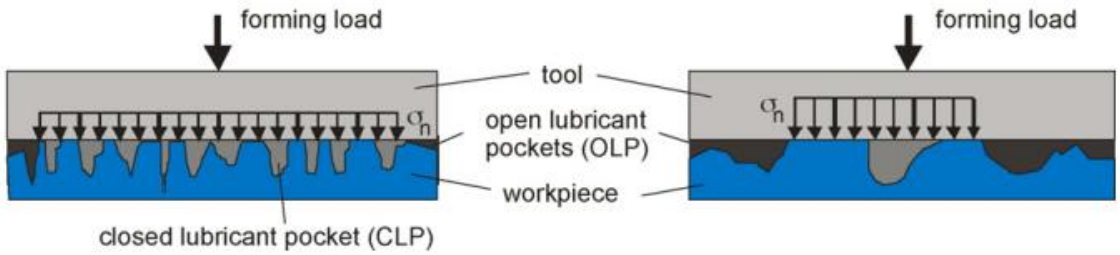

(a) At conventional length scale (b) At micro scale

Fig. 1.42 Contact state in different length scales [1-54].

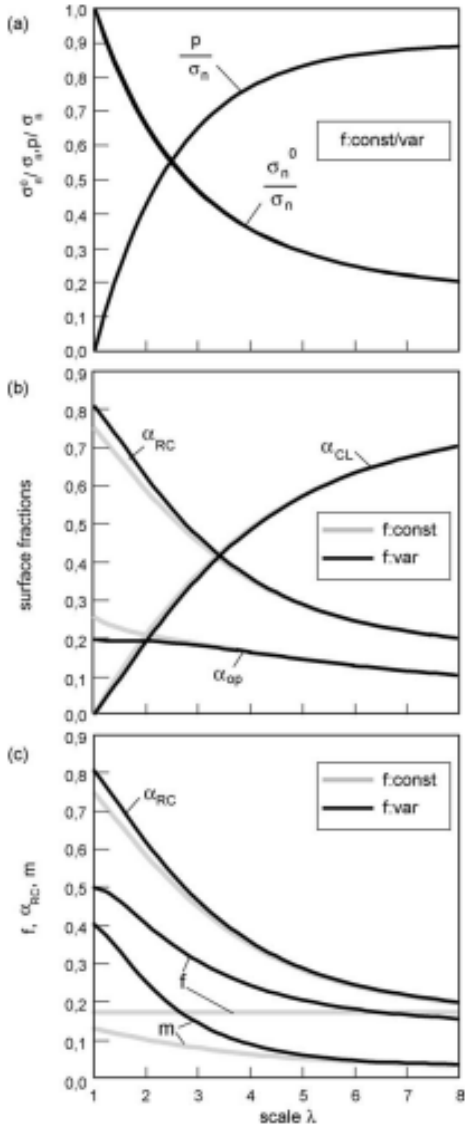

Fig. 1.43 Effect of scaling factor λ on p and σ_n^0 normalized to σ_n (a), on α_r, α_c and α_o (b), and on m, f and α_r (c) [1-52].

Peng et al., proposed the friction model based on the OLPs and CLPs considering a function of RAC and normal press p_{total}/σ_y by introducing size/scale factor λ [1-55]. They considered the flattening behavior under dry friction and lubricant to describe the tribological behavior in OLPs and CLPs as shown in **Fig. 1.44**. Based on this model, the hydrostatic pressure reduced by enclosed lubricant in CLPs can be calculated. They also applied this model to the ring compression test in FEM and observed that the influence of friction size effects to the ring compression process as shown in **Fig. 1.45**.

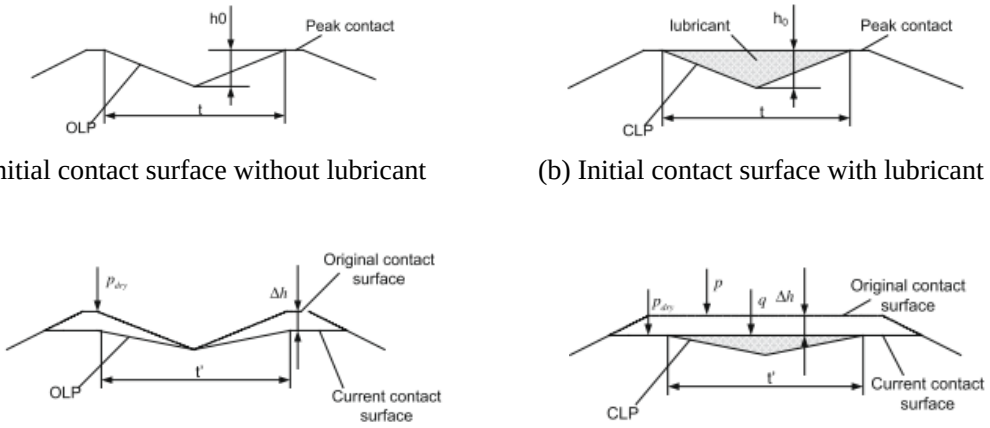

(a) Initial contact surface without lubricant (b) Initial contact surface with lubricant

(c) Current contact surface without lubricant (d) Current contact surface with lubricant

Fig. 1.44 Deformation of material in microscopic view [1-55].

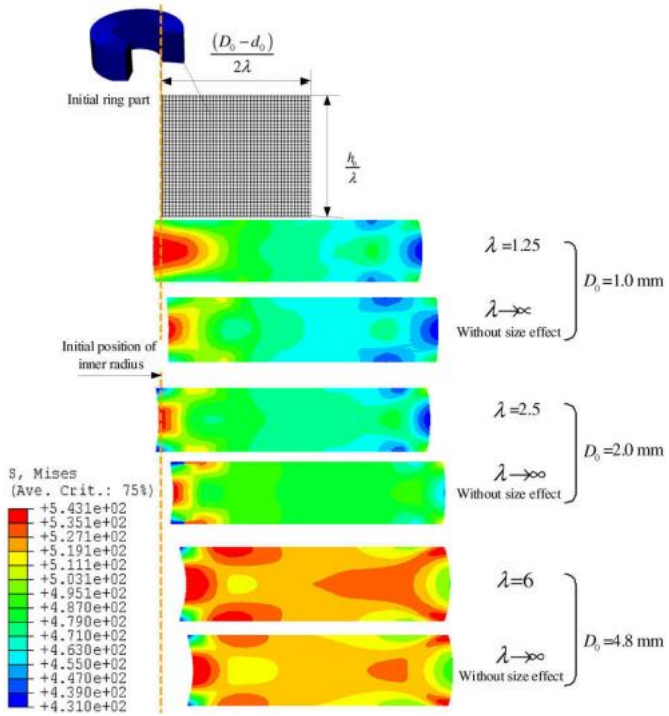

Fig. 1.45 Ring parts after compression and radial displacements in various scales [1-55].

1.3.4. Effect of features size

As mentioned in Section 2.1, the ratio of specimen size to gain size decreases as the specimen size decreases and significantly influences the material properties. This effect on material behavior can be divided by two different types of size effects. One is grain size effects in which the grain size increases while the feature/specimen size is kept constant as shown in **Fig. 1.46(a)** [1-56]. The other is feature/specimen size effects in which the feature/specimen size decreases while the grain size is kept constant as shown in **Fig. 1.46(b)**. Thus, the feature size effect occurs and affects the material behavior when the feature or specimen size itself decreases. Most of literatures about grain size effects explained in Section 2.1 are not purely mentioned about the grain size effect, but are including this feature size effects [1-56, 57].

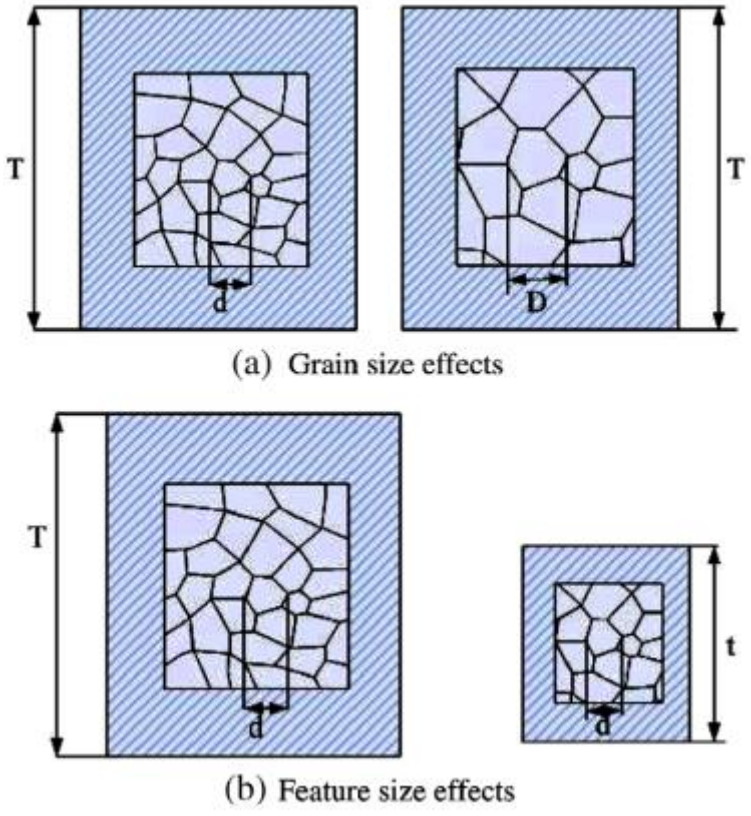

Fig. 1.46 Grain size effects and feature size effects with the decreasing of the scale. [1-56]

This feature size effect is not only affected by the specimen size itself, but also affected by the ratio of tooling dimension to specimen size. Mahabunphachai et al., investigated the feature size effect on flow stress under micro hydraulic bulge testing (**Fig. 1.47**) using the stainless steel foil [1-57]. The different grain sizes of 9.3, 10.6 and 17μm and different bulge diameters of 2.5, 5.0, 10, 20 and 100mm were used under the constant thickness of 51μm to change the grain size and feature size parameters. For the grain size effect, the flow stress continuously decreases with decreasing the grain size at the high strain level as shown in **Fig. 1.48(a)**. On the other hand, the feature size effect on flow stress is shown to have a critical point in which the material behavior is changed as shown in **Fig. 1.48(b)**.

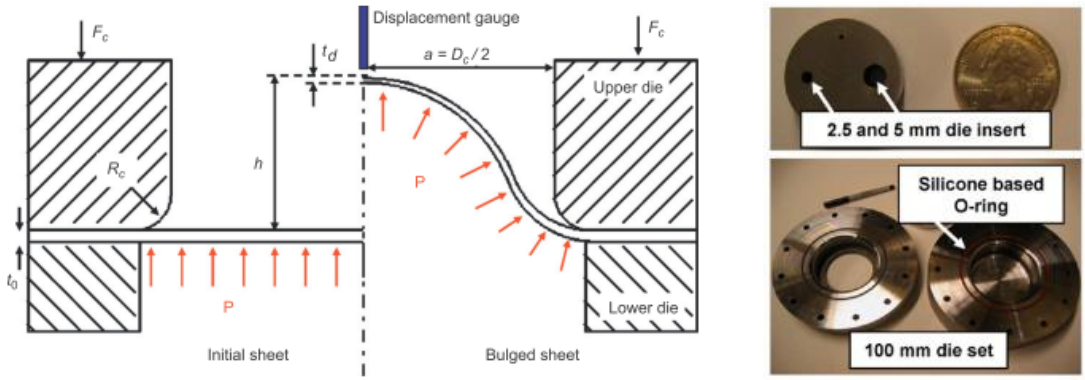

(a) Schematic of hydraulic bulge test (b) Die sets with different bulge diameters

Fig. 1.47 Micro hydraulic bulge test [1-57].

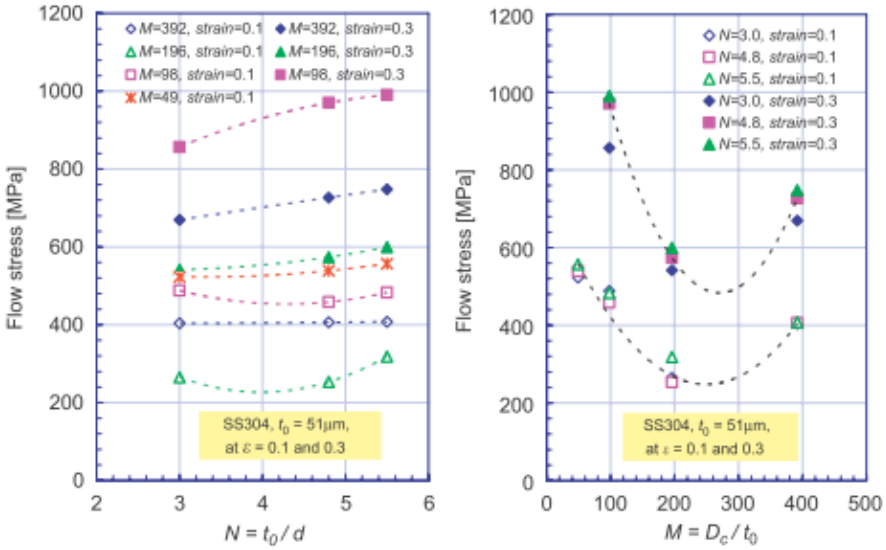

(a) Grain size effect (b) Feature size effect

Fig. 1.48 Grain size effect and feature size effect on flow stress at two strain levels in micro hydrostatic bulge test [1-57].

The feature size effect was investigated not only in material testing, but also in the micro forming process. Gao et al., conducted the roll-to-plate micro/meso-imprinting as shown in **Fig. 1.49** [1-58]. The feature height decreases and the rolling force increases with decreasing the groove width as shown in **Fig. 1.50**. It means that the material flow deteriorates and flow stress increases as the feature size decreases.

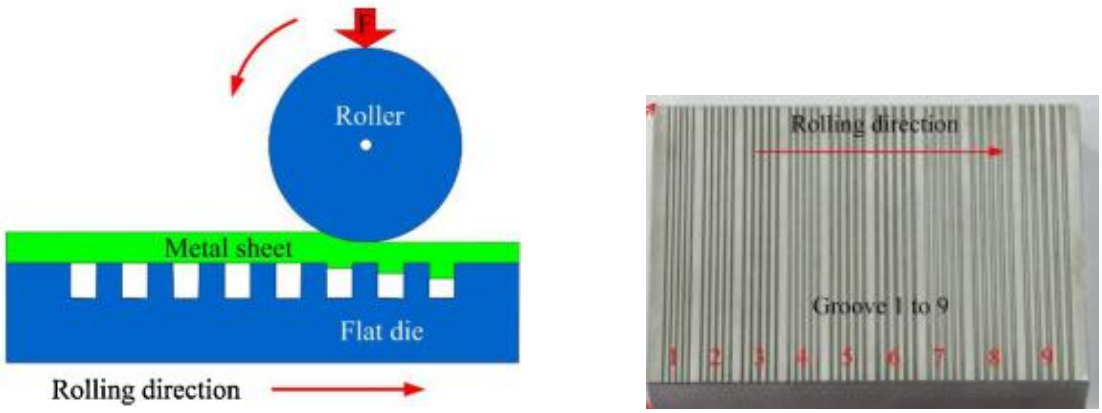

(a) Schematic of micro/meso-imprinting process (b) Die set with different groove width

Fig. 1.49 Micro/meso-imprinting process [1-58].

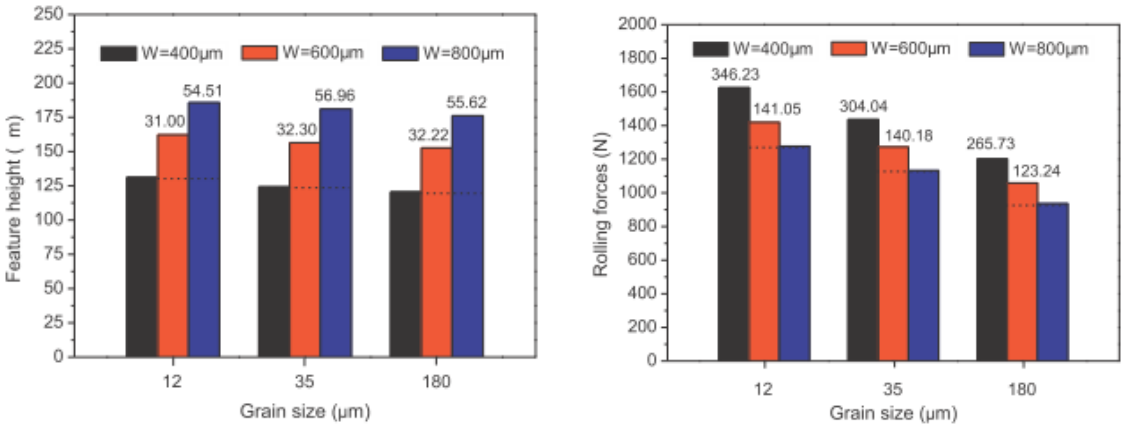

(a) Feature height (b) Rolling force

Fig. 1.50 Effect of groove width and grain size on feature height and rolling force in micro/meso-imprinting process [1-58].

The hydraulic and dynamic pressure forming for micro channel shown in **Fig. 1.51** were conducted [1-59, 60]. The normalized forming depth decreases as the feature size decreases and has a certain point to change its behavior as shown in **Fig. 1.52**. In addition, the surface roughness for all grain sized specimens has a tendency to increase with the feature size of micro channel and the tendency becomes more apparent for the coarse grained specimen. At large groove width, the surface roughness for coarse grain is higher than that for fined grain; however, it becomes opposite in the case of small groove width. This may be attributed to the combined effect of plastic strain and strain incompatibility when the feature size and grain size changes.

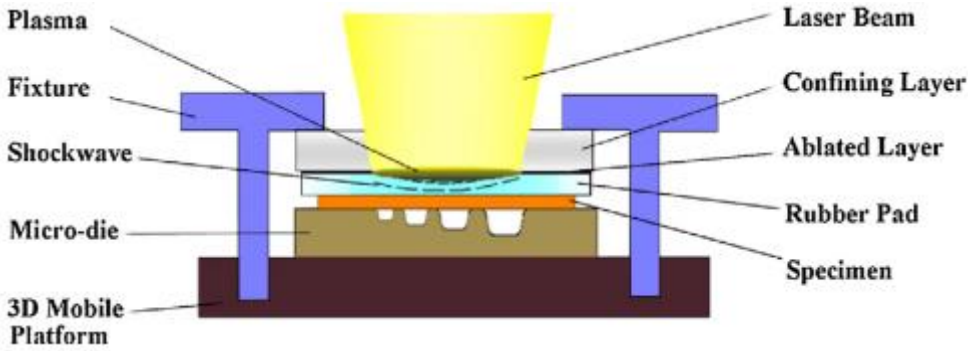

Fig. 1.51 Schematic of microscale laser dynamic forming for different channel sizes [1-59].

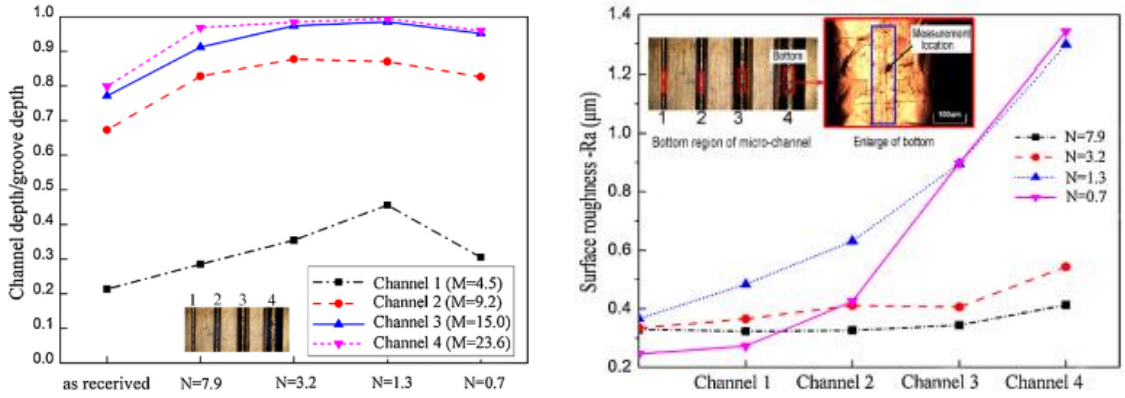

(a) On normalized channel depth (b) On surface roughness

Fig. 1.52 Experimental results of grain size and feature size effects in microscale dynamic forming [1-60].

The micro deep drawing (MDD) for various feature size shown in **Fig. 1.53** was also conducted and its feature size effect was clarified [1-61, 62]. Saotome et al., revealed that the calculation results has a good agreement with experimental results in large tooling feature size, but have a big difference in small tooling feature size as shown in **Fig. 1.54**. The calculation results do not consider the bending effect. Therefore, this difference between the calculation and experimental results shows that the bending deformation is significant and dominant in MDD.

Thus, the material flow and flow stress not only depends on the grain size, but also the tooling feature size. The ratio of tooling feature size to the specimen size and grain size is also the important parameter to describe the material behavior in micro forming.

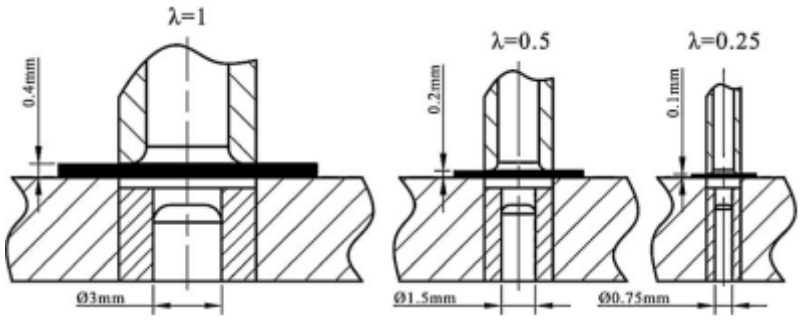

Fig. 1.53 Schematic of MDD for different size scaled tooling sets [1-61].

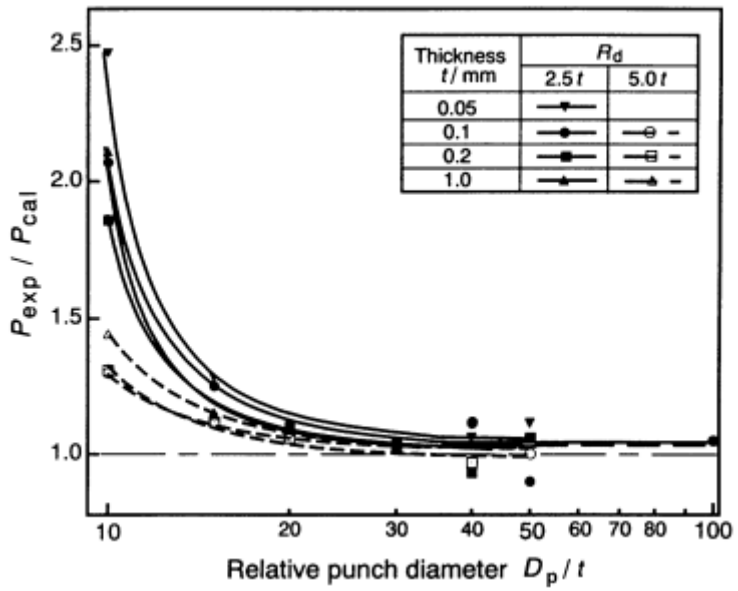

Fig. 1.54 Difference between the experimental and calculation results for punch force for various tooling conditions in MDD [1-62].

1.3.5. Effect of range of the process window

As mentioned above, the several size effects occur in micro scale and they deteriorate the material properties, material flow, tribological behavior and forming accuracy. These problems cause the decrease of forming limit in micro forming.

Saotome et al., conducted the MDD using SPCE with thickness of 0.05, 0.1, 0.2, 1.0mm, and various tooling condition [1-62]. The limit drawing ratio (LDR) increases as the punch diameter decreases as shown in **Fig. 1.55**. It means that the drawability increases with scaling down to micro scale with the relative punch diameter to thickness D_p/t. The effect of blank holder pressure was clearly recognized above D_p/t of 40 and as D_p/t increases. The effect of die shoulder radius on drawability is seen clearly below D_p/t of 15. Thus, LDR also can be improved by the blank holder pressure and die shoulder radius.

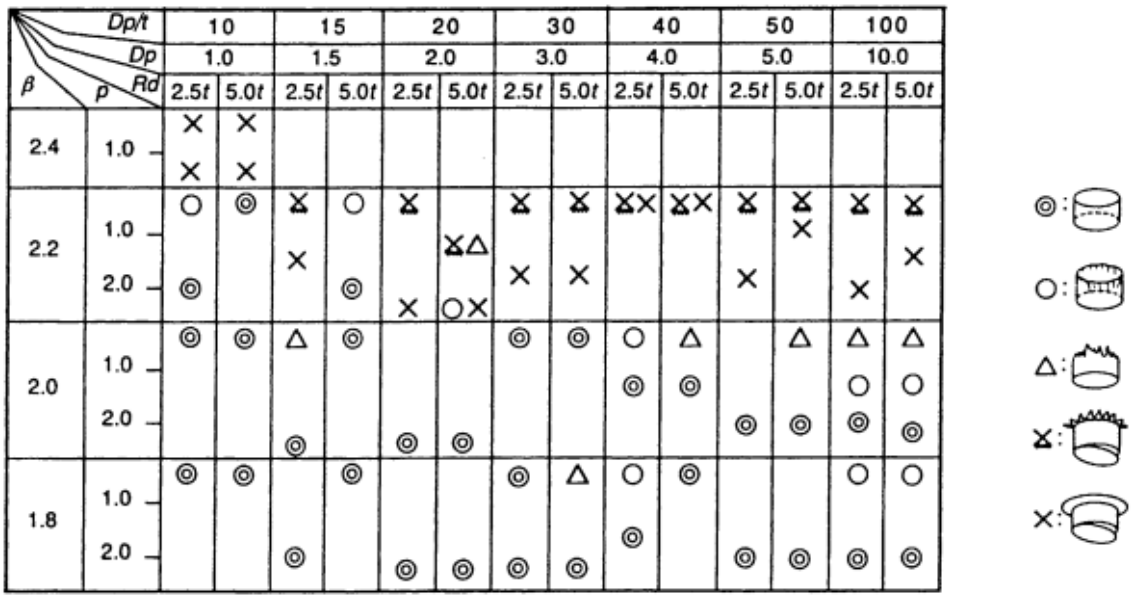

Fig. 1.55 Micro deep drawing results for various tooling condition (SPCE, t =0.1mm) [1-62].

Vollertsen et al., investigated the effect of size scale, blank holder force, and punch force speed on LDR in MDD using Al99.5 pure aluminum with 0.02mm to 1.0mm thickness [1-63, 64]. The LDR in MDD is significantly smaller than that in milli scale deep drawing as shown in **Fig. 1.56**. It is because the fracture limit is shifted downward with scaling down. The increase of punch speed can improve the fracture limit and the process window in MDD as shown in **Fig. 1.57**. It is because the increase of punch speed can decrease the friction coefficient by hydrodynamic lubrication. However, the LDR cannot increase by increasing the punch speed. The LDR is not dependent on the punch speed and friction coefficient.

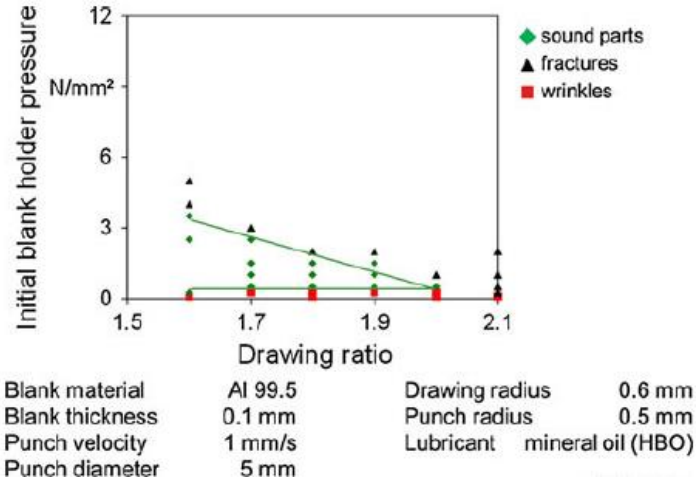

(a) Milli scale (t =0.1mm, D_p =5mm)

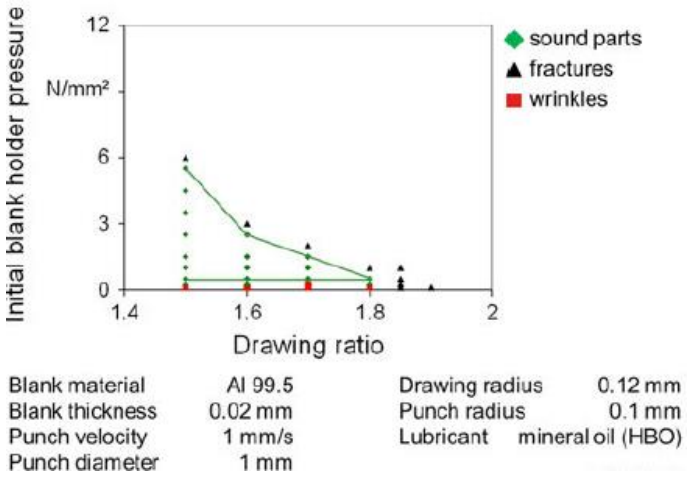

(b) Micro scale (t =0.02mm, D_p =1mm)

Fig. 1.56 Process windows of deep drawing at different scales [1-63].

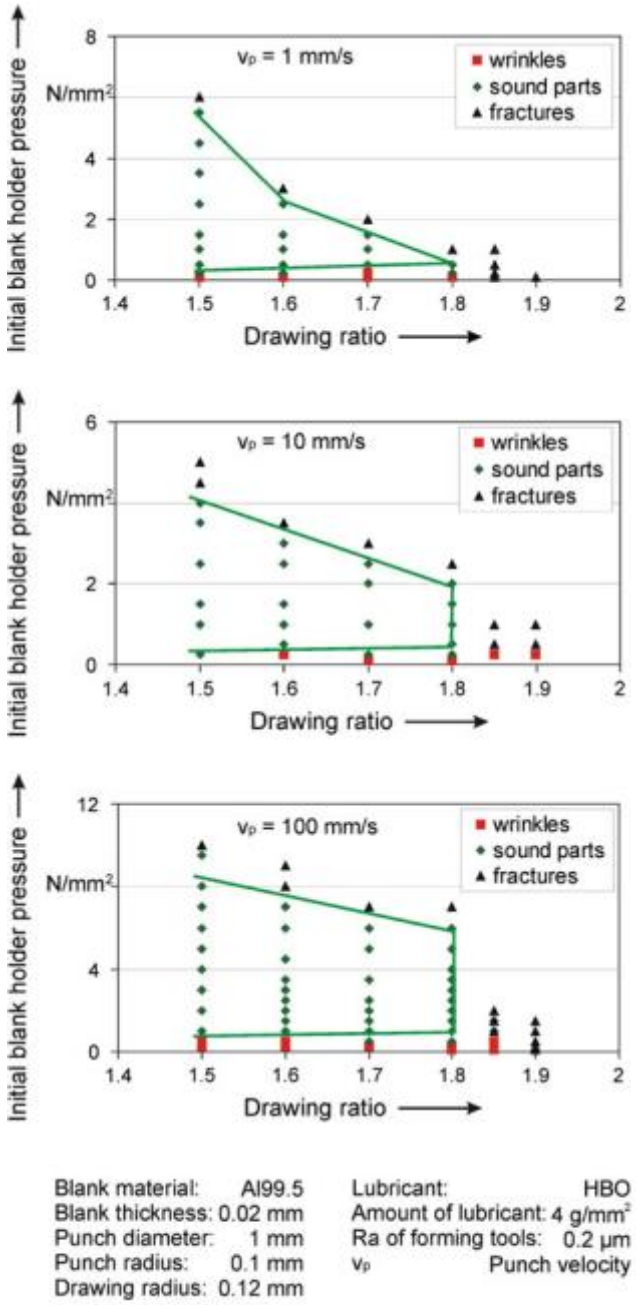

Fig. 1.57 Process windows of micro deep drawing with different punch speeds [1-64]

Chen et al., investigated the grain size effect on LDR in MDD using annealed stainless steel with 0.02mm and 0.05mm thickness [1-65]. The LDR increases with the decreases of the ratio of thickness to grain size except 0.02mm thickness as shown in **Fig. 1.58**. The thicker foils have higher LDR among the foils with the same the ratio of thickness to grain size. The similar tendency for the effect of grain size on LDR was also observed in MDD using ultra fined grained copper made by the equal channel angular pressing (ECAP) as shown in **Fig. 1.59** [1-66].

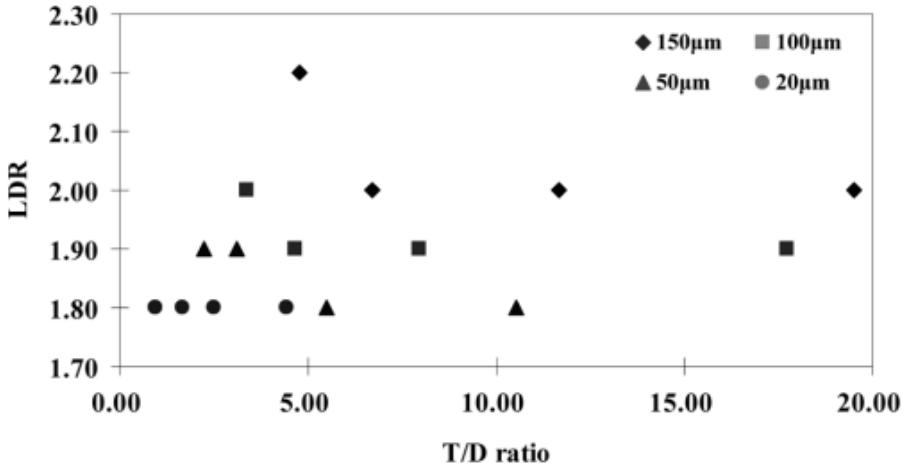

Fig. 1.58 Limit drawing ratio for various ratios of thickness to grain size using annealed stainless steel foils [1-65].

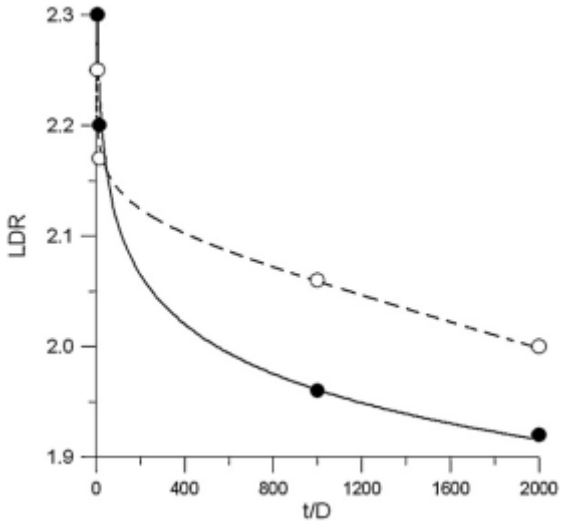

Fig. 1.59 Limit drawing ratio for various ratios of thickness to grains using ultra fine grained copper made by ECAP (closed symbols: experimental results, open symbols: FEM results) [1-66].

1.3.6. Problems in tools and machines

In order to design a press macro forming tools and machines, the number of processes required to form components is determined and the processes are designed. Then, the tools, press machines, and transfer device required to perform the processes are prepared. However, there are design issues unique to micro forming that must be overcome before the processes can be designed. In general, compared with the conventional macro forming, much higher accuracy is required for transfer, positioning, force and stroke position controls. If a machine satisfying these advanced control requirements is designed using the conventional design concept of macro forming, the apparatus becomes large and costly, hindering the achievement of the saving of energy, space, and resources, which should be realized with micro factories. Therefore, these difficulties in micro scale should be considered to design the micro forming tools and machines. They can be classified and characterized as follows;

＜Tool accuracy＞

As the target size becomes 1/1000, the required precision for the micro forming apparatus also becomes 1/1000. It means that the high precision is required for tool. Particularly, it is difficult to make the shoulder area or inside of die. To fabricate the micro components, these difficulties about tool accuracy should be considered.

＜Limitation of tooling size miniaturization＞

There is a limit for the minimum size of tools due to the difficulties to manufacture the tools. In addition, the strength of tools decreases with scaling down to micro scale and the tiny tools are easily broken. The minimum size based on not only manufacturability but also durability of tools should be considered to fabricate the tools.

＜Handling＞

The high accuracy is also required for the transfer, force, and position controls. To achieve the required accuracy using the conventional equipment, the large and expensive equipment is required. The miniaturization of apparatus size and a new handling concept to solve the above difficulties are required.

1.4. Micro Sheet Forming for High Aspect Ratio Products

As mentioned in Section 2, the techniques for high aspect ratio products, such as pressure, heat and incremental control methods, can effectively improve the forming limit and quality of components. It is expected that these techniques can achieve the high aspect ratio. However, when the targets size is scale down to micro scale, the problems in process, tools and machines occur as mentioned in Section 3. These difficulties in micro forming should be overcome to develop the micro sheet forming for high aspect ratio. In this section, the previous micro/milli sheet forming using these techniques is reviewed to highlight the problem of conventional forming method. Thereafter, the approach to achieve the further improvement of forming limit, quality and miniaturization is proposed.

1.4.1. Conventional micro deep drawing for high aspect ratio cups

Previously, the pressure, heating, multi stage and coating techniques were applied into the micro deep drawing (MDD). Manabe et al., conducted a micro redrawing process using stainless steel with 0.023mm thickness [1-67]. They can successfully fabricate the micro cup with diameter of 0.45 and aspect ratio of 1.1.

Vollertsen et al., developed the laser micro deep drawing in which the laser induces the shock waves and it uses to deform the blank [1-68]. Using the aluminum foil with 0.05mm thickness, the micro cup with the diameter of 4.0mm and aspect ratio of aspect ratio of 0.39 was fabricated. Irthiea et al., [1-69] developed the micro deep drawing using flexible tools in which the rubber material is put in die cavity to generate the pressure and induce the several effects as mentioned in Section 3.1. The micro cup with the diameter of 4.0mm and aspect ratio of 1.25 can be successfully drawn.

Yang et al., developed the heat assisted micro deep drawing using electrical heating [1-70]. They successfully fabricated the micro cup with the diameter of 1mm and aspect ratio of 0.57.

Furthermore, some coating techniques were applied in micro sheet forming to improve the tribological behavior in micro scale. Hu et al., applied the diamond like carbon (DLC) films on the die to improve the tribological behavior in MDD under dry friction [1-71]. It was found that the DLC film can reduce the friction force even in micro scale, and the micro cup with the diameter of 1mm, aspect ratio of 0.5. Shimizu et al., applied the high power impulse magnetron sputtering (HIPIMS) to deposit the TiAlN films on the die for MDD, which can make the coating file with fine smooth surface and high hardness properties [1-72]. In addition, they also applied the micro texturing of DLC film coating in MDD to improve the tribological characteristics under dry sliding friction [1-73].

These micro sheet forming for techniques for high aspect ratio products and drawn micro cups

are summarized in **Fig. 1.60**.

Principle of forming method	Schematic of micro deep drawing	Appearance of drawn micro cup	References
Multi steps		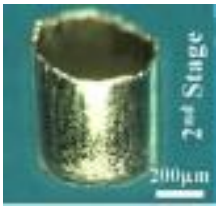 *H/D*=0.57 *D*=0.45mm	[1-67]
Pressure (Laser shock)	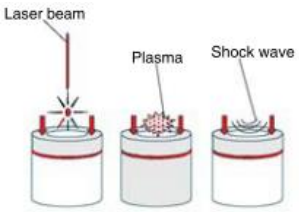	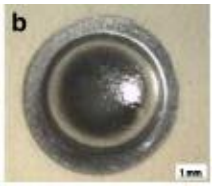 *D/H*=0.39 *D*=4mm	[1-68]
Pressure (Flexible tools)	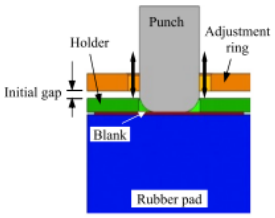	 *H/D*=1.25 *D*=4mm	[1-69]
Heating (Electrical heating)	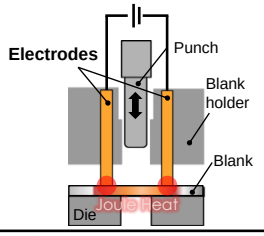	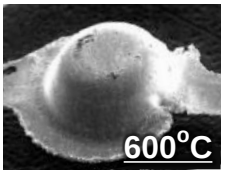 *H/D*=0.57 *D*=1mm	[1-70]
Coating (DLC film)	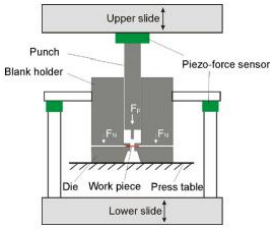	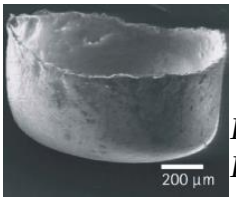 *H/D*=0.54 *D*=1mm	[1-71]

Fig. 1.60 Micro sheet forming for high aspect ratio products and appearance of drawn micro cups.

1.4.2. Micro incremental forming

The incremental forming is scaled down to micro scale by Saotome et al. [1-74]. They developed single point micro incremental hammering and fabricate the tiny car body with the length of 0.6mm, wide of 0.4mm and height of 0.1nn as shown in **Fig. 1.61**. Obikawa et al. developed a micro incremental forming by single point tool and successfully fabricate deeper tiny car body [1-75]. Kuboki et al. developed a micro incremental in-plan bending and conducted the in-plan bending for metal foil with thickness of 0.1mm [1-76]. Thus, the micro incremental forming was developed and applied to the complex shape components; however, it cannot apply the deep micro component due to the low ductility of metal foil. Furthermore, the shape accuracy and productivity is quite low with this forming method.

Principle of forming method	Schematic of micro incremental forming	Appearance of application	References
Single point incremental hammering	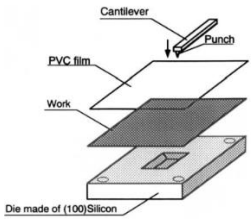	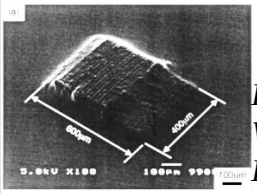 *L*=0.6mm *W*=0.4mm *H*=0.1mm	[1-74]
Incremental forming by single point tool	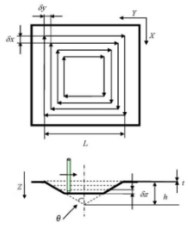	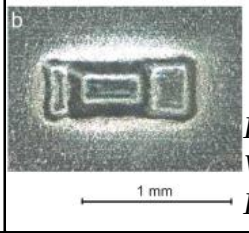 *L*=1.0mm *W*=0.4mm *H*=0.23mm	[1-75]
Incremental in-plane bending	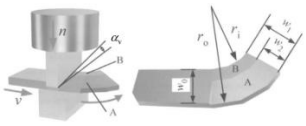	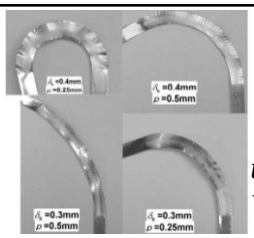 *t*=0.1mm *W*=0.5mm	[1-76]

Fig. 1.61 Micro incremental forming and its applications.

1.4.3. Difficulties and possibility of micro sheet forming for high aspect ratio products

Fig. 1.62 shows the comparison of aspect ratios between macro and micro sheet forming. When the target size decreases, the aspect ratio of most of sheet forming, such as heat aided deep drawing, multi steps deep drawing and pressure aided deep drawing, decreases. It is because the size effect causes the decrease of forming limit as mentioned in Section 3.5. It seems that the single technique alone cannot achieve the high aspect ratio in micro scale. On the other hand, the fiction aided deep drawing which is one of incremental forming technique can achieve the quite high aspect ratio in macro scale. It is expected that this technique can achieve the quite high forming limit and fabricate the micro cup with the high aspect ratio because the material is not deformed by the traction of punch, but deformed by the material flow without the applied force to the material. However, this forming method cannot be simply applied to micro scale. The complex tooling structure used in punchless forming cannot be scaled down to micro scale due to the limitation of space in tool sets and the difficulty to fabricate the complex tools. Moreover, the large contact pressure and friction between the material and tools easily results the seizure and adhesion especially in micro scale in which the lubricant cannot be kept.

The miniaturization, complex shape and high shape accuracy are also important factor for micro forming. The dieless forming, such as incremental forming using the single point tool, sheet hydroforming, does not use the tiny and complex shape die, which is difficult to manufacture, to fabricate the workpiece. Therefore, these techniques are useful to achieve the miniaturization and fabricate the complex shape components. Furthermore, the sheet hydroforming technique can achieve the high shape accuracy by the fluid pressure. As mentioned above, the sheet hydroforming technique is effective to solve the problem in tools and achieve the miniaturization, complex shape and high shape accuracy. However, this technique alone cannot achieve the high aspect ratio as shown in **Fig. 1.62**.

Thus, due to some difficulties in micro forming, the potential of each technique cannot be brought out. In addition, due to the deterioration of material properties and tribological characteristics in micro scale, it seems that the utilization of single technique alone cannot solve the problems in micro scale. A new concept for micro sheet forming is required to achieve the further improvement of forming limit, the further miniaturization of target size, and fabricate the complex shape components with high accuracy.

From these discussions, the micro sheet hydroforming and micro incremental forming are focused in this study. The micro sheet hydroforming has some advantages of high shape accuracy, shape complication and friction reduction. These can effectively solve the problem in tools and tribology in micro incremental forming, such as friction aided deep drawing. On the other hand, the

micro incremental forming can significantly improve the forming limit due to the material flow and local deformation. It is possible to achieve the high aspect ratio in micro scale. Thus, the combination of micro sheet hydroforming and micro incremental forming effectively solves the problems in micro scale and achieve the high aspect ratio. So, a novel forming technique, micro incremental sheet hydroforming, is proposed. The concept of MUDD can be summarized in **Fig. 1.63**.

In this study, particularly, the deep drawing process is focused and a micro ultra deep drawing (MUDD) process using the ultra high pressure and incremental controls of tools and pressure is developed. This process is developed on the basis of micro hydromechanical deep drawing (MHDD) which is a scaled down technique of macro hydromechanical deep drawing. Based on MHDD, the incremental control techniques, such as the press motion control, pressure control and local deformation, are combined. Thus, the micro ultra deep drawing for the high aspect ratio and high shape accuracy is developed.

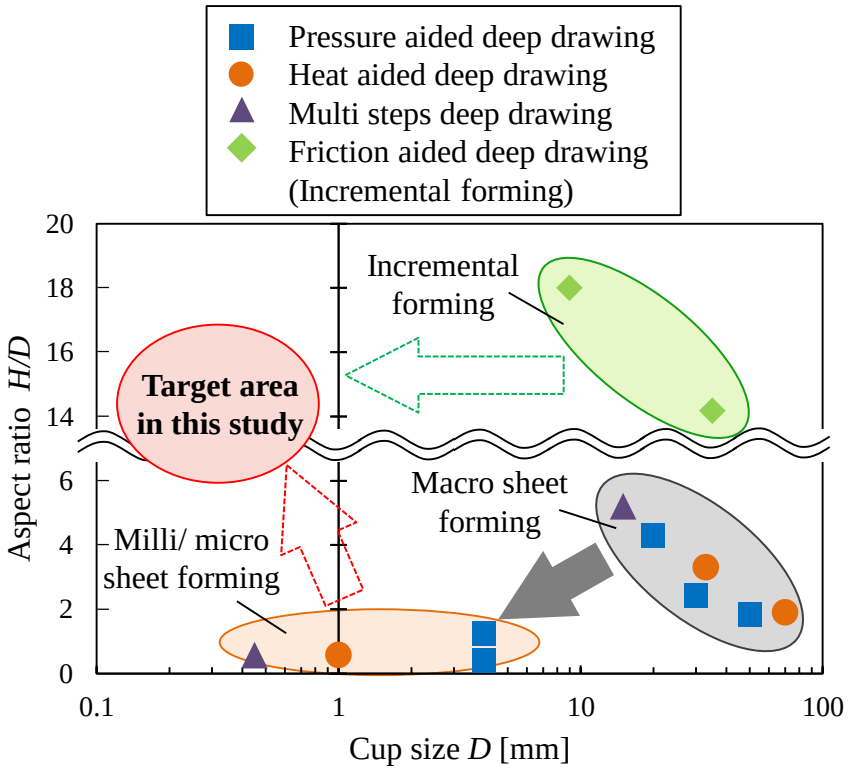

Fig. 1.62 Comparison of aspect ratios between macro and micro sheet forming.

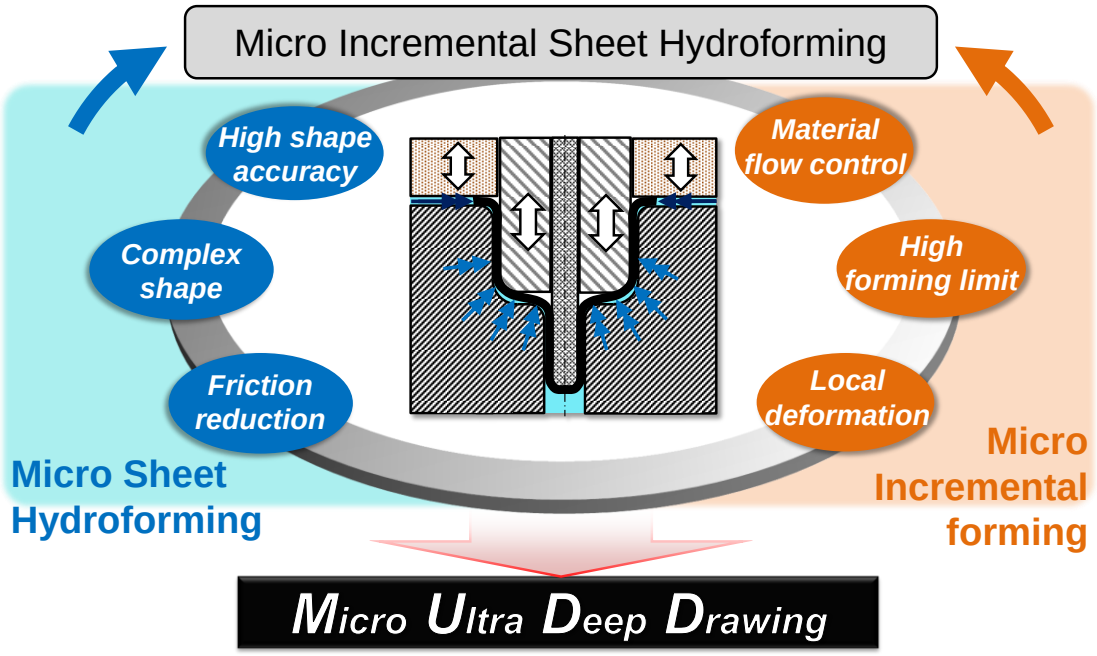

Fig. 1.63 Concept of micro incremental sheet hydroforming.

1.5. Motivation and Objectives

The forming limit, shape complication, high precision, and miniaturization for micro components are important factors to realize the multifunctional, compact, and highly integrated devices. The scaled down technologies of conventional metal forming is applied to achieve these due to its process simplicity, high production capability and low cost. However, due to several problems in micro scale, such as size effects, process and machine difficulties, the conventional metal forming cannot be simply scaled down to micro scale. In micro scale, it is difficult to fabricate the tiny and complex shape tools and the required accuracy significantly increases; hence, the miniaturization of target size with high accuracy is difficult to achieve. Moreover, with scaling down, the delamination of ductility, strength and material and the increase of friction are resulted in due to the grain, tribological, and feature size effects. Therefore, the forming limit significantly decreases and the miniaturization and fabrication of complex shape component cannot be achieved.

Several techniques are developed to improve the forming limit, flexibility and quality in macro sheet forming, such as pressure, heating, vibration, material flow control, process control, and incremental formings. These forming methods can realize the decrease of applied force to material, the increase of allowance applied force, the improvement of tribological behavior, and the high flexibility for three dimensional complex components. Particularly, the sheet hydroforming has several functions to improve the tribological behavior and forming limit, and fabricate the complex components with high accuracy. In addition, the incremental forming, such as the friction aided deep drawing, can achieve the quite high aspect ratio by the material flow control and local deformation. If these forming techniques are applied to the micro scale, it is expected that the high aspect ratio, shape accuracy, and shape complication can be achieved. However, the micro sheet hydroforming cannot achieve the high aspect ratio because the size effect causes the decrease of forming limit. Furthermore, one of incremental forming technique, friction aided deep drawing, cannot be simply scaled down due to the limitation of tools and tribological problem. Therefore, it is difficult to achieve the high aspect ratio, high shape accuracy and shape complication using conventional micro sheet forming.

From this background, a novel forming method, micro incremental sheet hydroforming is proposed in this study. In this method, the micro sheet hydroforming and micro incremental forming are combined to solve the problems in each technique and enhance each advantage. In this study, the deep drawing process in micro incremental sheet hydroforming is focused and a micro ultra deep drawing is newly developed by combing the incremental forming technique based on the micro hydromechanical deep drawing (MHDD). However, MHDD process has not been studied previously. Furthermore, its basic drawing characteristics may be different from the conventional macro hydromechanical deep drawing due to the size effects. Particularly, the tribological behavior and the

basic drawing characteristic under the fluid pressure in MHDD may be different from conventional macro hydromechanical deep drawing due to several size effects.

According to the strategy shown in **Fig. 1.64**, the main research tasks are shown below;

1. *Design of micro hydromechanical deep drawing based on scale dependence*
2. *Development of micro hydromechanical deep drawing system and its basic drawing characteristics*
3. *Process design of micro ultra deep drawing using ultra high pressure and incremental control*
4. *Development of micro ultra deep drawing system and its experimental verification*

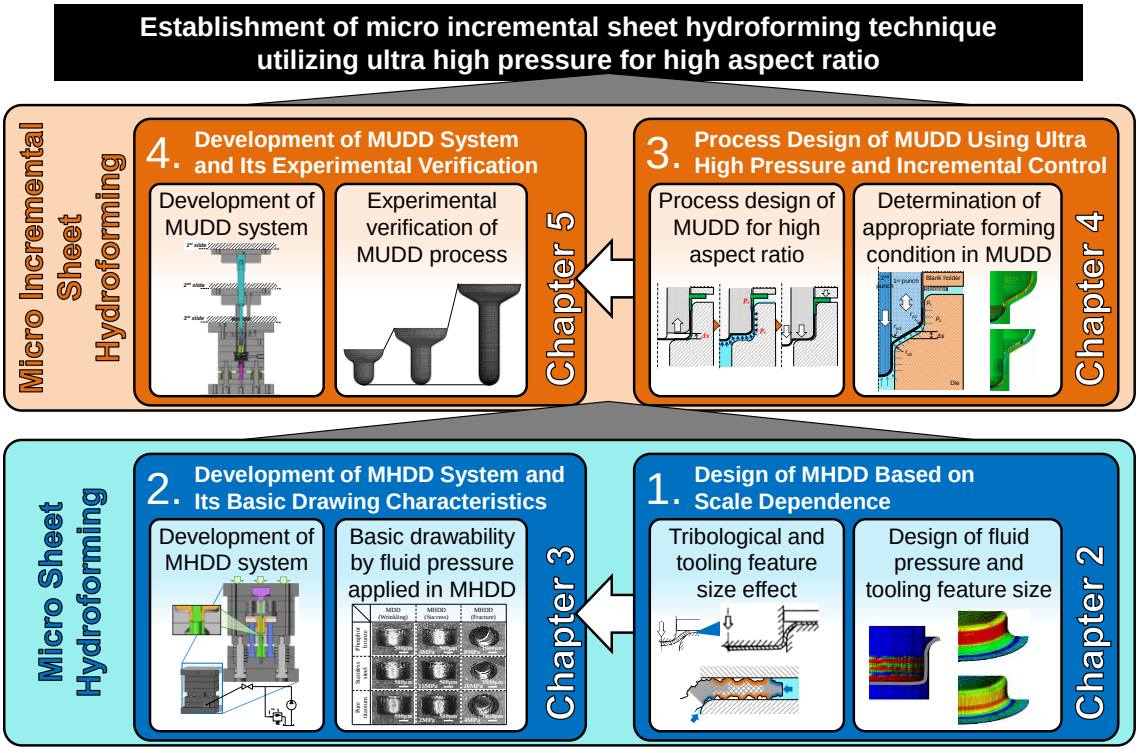

Fig. 1.64 Strategy and organization of this study.

1.6. Outline of Thesis

This thesis consists of six chapters. The contraction of this thesis is shown in **Fig. 1.63**. Brief explanations for each chapter are drawn as follows.

Chapter 1 introduces the background of micro sheet forming, its difficulties and size effect. Several techniques in macro sheet forming are also reviewed to analyze the effective forming technique or combination for micro sheet forming. Consequently, the challenge and approach in this study is stated.

Chapter 2 designs the MHDD process based on the scale dependence, such as tribological size effect and tooling feature size. The theoretical model for punch force, friction holding effect, hydrodynamic lubrication effect and compression effect of blank edge by radial pressure, and a new friction model for MHDD are developed with considering the fluid pressure and OLPs. The effect of relative tooling feature size on deformation behavior in MHDD is investigated not only using the theoretical model but also using finite element method (FEM) simulation which can consider the blank deformation. The relative punch diameter to thickness D_p/t represents the relative tooling feature size and set up at D_p/t=20, 38 and 100. The results show the application of counter pressure can improve the shape accuracy and drawability due to the decrease of maximum meridional stress by friction holding effect. However, the required fluid pressure for friction holding and hydrodynamic lubrication effects p_f and p_h increases as D_p/t and r_p/t decreases, respectively. It was clarified that the application of ultra high pressure $p \geq$100MPa, the small punch shoulder radius, and the large die shoulder radius are required to obtain these effects to improve the drawability and shape accuracy in MHDD. On the other hand, the lubrication in OLPs under fluid pressure is also investigated in MHDD. It is experimentally clarified that the fluid medium can be maintained in OLPs. Based on this behavior, it is theoretically revealed that the application of radial pressure can effectively reduce the friction force in micro scale. It is concluded that the ultra high pressure and radial pressure can improve the tribological behavior by inducing the hydrodynamic lubrication and the lubricated OLPs.

Chapter 3 presents the development of micro hydromechanical deep drawing (MHDD) system based on the design guideline proposed in Chapter 2. Design concepts for new MHDD are proposed to realize the simple apparatus with high accuracy. In addition, the basic effect of fluid pressure on deformation behavior in MHDD is investigated using the stainless steel, phosphor bronze, and pure titanium foils with 20 and 50μm thicknesses. As results, the shape accuracy, the wrinkling and fracture limit can be improved by applying the appropriate counter pressure in MHDD. However, the hydrodynamic lubrication cannot be induced in MHDD due to the high sealablity at die shoulder under high relative tooling feature size. It causes the increase of friction force with increasing the fluid pressure and the fracture at punch shoulder at high fluid pressure. Therefore, it was clarified

that the fluid pressure is effective to improve the winkling limit and shape accuracy in MHDD; however, the advantages of ultra high fluid pressure cannot be obtained and the quite high aspect ratio cannot be achieved by the simple application of fluid pressure in MHDD.

Chapter 4 presents the design of new forming process, micro ultra deep drawing (MUDD), using FEM simulation to obtain the advantage of ultra high pressure without the fracture and achieve the quite high aspect ratio. A new MUDD process has a 2nd punch in inside of 1st punch to perform the all of processes at the same axis. MUDD process consists of repeating three stages: (1) making the space between the 1st drawing punch and blank by lifting up the 1st punch, (2) applying the ultra high pressure stage toward this space so as to be disappeared, and (3) lifting down the 1st and 2nd punches and controlling the thickness at flange area by the compression of blank by the 1st punch and die. The FEM results show that the micro cup with total drawing ratio of 3.8 can be fabricated in MUDD, but cannot be fabricated in conventional micro deep drawing (MDD) and MHDD. It is because the application of ultra high pressure toward the space between the 1st punch and blank can control the material flow. The contact between the blank and 2nd punch also induces the friction holding effect, and it can prevent the thickness reduction at 2nd punch shoulder. The forming conditions to control the material flow and deformation area properly are designed. It was found that the thickness reduction at 2nd punch shoulder can be avoided by the high friction coefficient, the use of stopper, the small 1st punch inner shoulder radius, the proper counter pressure, and the low punch displacement. Using the appropriate forming conditions, the long micro cup with drawing ratio of 7.0 and aspect ratio of 4.6 can be fabricated by FEM.

Chapter 5 develops a new MUDD system with triple action servo press machine and ultra high hydraulic system to realize the proposed MUDD process experimentally. The triple action servo press machine can control the blank holder, 1st and 2nd punches independently and incrementally. In addition, the ultra high hydraulic system with designed maximum applicable pressure of 400MPa is developed. In the performance test, it was clarified that the ultra high pressure of 200MPa can be successfully generated and maintained. Moreover, the movement of blank holder, 1st and 2nd punches can be controlled independently and incrementally with minimum control amount of 1μm. Using the developed the MUDD system, the micro cup with diameter of 0.5mm, aspect ratio of 0.9 and drawing ratio of 3.8 can be fabricated. The designed MUDD process by FEM simulation can be realized in experiment using the developed MUDD system with triple action press machine and ultra high hydraulic system.

Chapter 6 concludes the contribution and innovation of this study and suggests the remaining problems and future works.

Reference

[1-1] Yole Development: Status of the MEMS Industry 2015, Industry and Market Report, May 2015.

[1-2] M. Geiger, M. Kleiner, R. Eckstein, N. Tiesler, U. Engel, Microforming, CIRP Annals-Manufacturing Technology, 50, (2001), 445-462.

[1-3] http://www.sony.co.jp/SonyInfo/News/Press/201010/10-137/

[1-4] http://leadframe.sdi.com.tw/_english/01_semi_lead_frame/00_overview.php

[1-5] http://www.slashgear.com/watch-made-from-micro-hdd-is-a-geeks-dream-08358675/

[1-6] http://datacent.com/datarecovery/hdd/samsung

[1-7] http://denso-europe.com/denso-celebrates-40th-anniversary-of-gasoline-injection-business/

[1-8] T. Shiratori, Application example of orifice plate, Press Working (in Japanese), 51-6, (2013)62-63.

[1-9] https://www.pololu.com/product/1308

[1-10] http://enefield.eu/category/field-trials/technology/

[1-11] http://www.dnp.co.jp/news/1189383_2482.html

[1-12] http://www.kokocas.com/pci.html

[1-13] http://www.tosei.co.jp/technology/laser_case_0602.html

[1-14] R. Nagai, N. Naoto, Realization of manifest need ~Foundation of creating innovation~, Japan Marketing Journal (in Japanese), 32-128, (2013), 107-121.

[1-15] M. Yang, Fabrication of micro pump and valve with metallic material, Journal of the Japan Society for Technology of Plasticity (in Japanese), 49-570, (2008), 654-658.

[1-16] http://www.suzukinet.co.jp/lab/technology/deep-drawn/post.php

[1-17] http://www.noguchi-ss.co.jp/advantage/

[1-18] K. Nakamura, T. Nakagawa, Fracture mechanism and fracture control in deep drawing with hydraulic counter pressure ‐studies on hydraulic counter pressure forming Ⅰ‐, Journal of the Japan Society for Technology of Plasticity (in Japanese), 25-284, (1984), 831-838.

[1-19] K. Nakamura, T. Nakagawa, Radial pressure assisted hydraulic counter pressure deep drawing ‐studies on hydraulic counter pressure forming Ⅱ‐, Journal of the Japan Society for Technology of Plasticity (in Japanese), 26-288, (1985), 73-80.

[1-20] S. Fukui, K. Yoshida, K. Abe, Deep drawing for thin sheet using hydroform method, Journal of the Japan Society for Technology of Plasticity (in Japanese), 2-10, (1961), 715-726.

[1-21] K. Nakamura, B. Guo, Effect of fluid pressure on shape accuracy of cylindrical drawn shells, Journal of the Japan Society for Technology of Plasticity (in Japanese), 32-367, (1991), 1029-1034.

[1-22] Y. Yamazaki, M. Yoshida, Effect of pressurized liquid method in cylindrical deep-drawing, The Proceedings of 48th Japanese Joint Conference for the Technology of Plasticity (in Japanese),

(1997), 341-344.
[1-23] Y. Horikoshi, T. Kuboki, M. Murata, K. Matsui, M. Tsubokura, Die design for deep drawing with high-pressured water jet utilizing computer fluid dynamics based on Reynolds' equation, Journal of Materials Processing Technology, 218, (2015), 99-106.
[1-24] M. Fukuda, K. Yamaguchi, Press forming using rubber – cylindrical and square cup deep drawing –, Journal of the Japan Society for Technology of Plasticity (in Japanese), 20-222, (1979), 566-573.
[1-25] N. Kawai, M. Gotoh, T. Matsuda, Profitable employments of strain-induced transformation in press forming, Journal of the Japan Society for Technology of Plasticity (in Japanese), 15-156, (1974), 11-18.
[1-26] Y. Watanabe, Warm Forming of Stainless Steel, Journal of the Japan Society for Technology of Plasticity (in Japanese), 23-375, (1992), 396-403.
[1-27] S. Yoshihara, H. Yamamoto, K. Manabe, H. Nishimura, Formability enhancement in magnesium alloy deep drawing by local heating and cooling technique, Journal of Materials Processing Technology, 143-144, (2003), 612-615.
[1-28] T. Jimma, Y. Kasuga, N. Iwaki, O. Miyazawa, E. Mori, K. Ito, H. Hatano, An application of ultra sonic vibration to the deep drawing process, Journal of the Japan Society for Technology of Plasticity (in Japanese), 23-256, (1982), 458-464.
[1-29] T. Jimma, Y. Kasuga, N. Iwaki, O. Miyazawa, E. Mori, K. Ito, H. Hatano, An application of ultra sonic vibration to the deep drawing process, Journal of Materials Processing Technology, 80-81, (1998), 406-412.
[1-30] S. Kataoka, Deep drawing process of aluminum alloy sheet with hydraulic counter pressure and vibration to tool system with use of volatile lubricants, Journal of Japan Institute of Light Metals (in Japanese), 48-2, (1998), 78-82.
[1-31] N.A. Maslennikov, Russians develop 'punchless' drawing, Metalworking Production, 16, (1957), 1417-1420.
[1-32] M.A. Hassan, N. Takakura, K. Yamaguchi, Friction aided deep drawing of sheet metals using polyurethane ring and auxiliary metal punch. part 1: experimental observations on the deep drawing of aluminium thin sheets and foils, International Journal of Machine Tools & Manufacture, 42, (202), 625-631.
[1-33] M. Fukuda, K. Yamaguchi, Press forming using rubber – punchless drawing –, Journal of the Japan Society for Technology of Plasticity (in Japanese), 20-224, (1979), 781-788.
[1-34] M.A. Hassan, R. Suenaga, N. Takakura, K. Yamaguchi, A novel process on friction aided deep drawing using tapered blank holder divided into four segments, Journal of Materials Processing Technolgy, 159, (2005), 418-425.
[1-35] T. Iizuka, Fabrication of ultra long cup by the deep drawing of thin sheet using press

compression, The Proceedings of the 3rd Integrated Advanced Conference in the Light Metal Educational Foundation, (2013), 47-53.

[1-36] K. Manabe, H. Hamano, H. Nishimura, A new variable blank holding force method in deep drawing of sheet materials, Journal of the Japan Society for Technology of Plasticity (in Japanese), 29-330, (1988), 740-747.

[1-37] K. Manabe, H Koyama, S. Yoshihara, T. Yagami, Development of a combination punch speed and blank-holder fuzzy control system for the deep-drawing process, Journal of Materials Processing Technology, 125-126, (2002), 440-445.

[1-38] H. Koyama, K. Manabe, S. Yoshihara, Development of database and FEM assisted intelligent control press forming system, Journal of the Japan Society for Technology of Plasticity (in Japanese), 43-503, (2002), 1162-1167.

[1-39] T. Yagami, K. Manabe, M. Yang, H. Koyama, Intelligent sheet stamping process using segment blankholder modules, Journal of Materials Processing Technology, 155-156, (2004), 2099-2105.

[1-40] T. Tatenami, Y. Nakamura, T. Ohata, Effect of inclination of blank holder surface in cylindrical deep drawing process, Journal of the Japan Society for Technology of Plasticity (in Japanese), 30-340, (1989), 696-702.

[1-41] S. Matsubara, CNC Incremental forming, Journal of the Japan Society for Technology of Plasticity (in Japanese), 35-406, (1994), 1258-1263.

[1-42] J. Jeswiet, F. Micari, G. Hirt, A. Bramley, J. Duflou, J. Allwood, Asymmetric single point incremental forming of sheet metal, CIRP Annals – Manufacturing Technology, 54, (2005), 88-114.

[1-43] K. Kitazawa, Incremental forming for new reuse technology, Journal of the Japan Society for Technology of Plasticity (in Japanese), 42-4889, (2001), 1001-1007.

[1-44] F. Vollertsen, Categories of size effects, Production Engineering Research and Development, 2, (2008), 377-383.

[1-45] T.A. Kals, R. Eckstein, Miniaturization in sheet metal working, Journal of Materials Processing Technology, 103, (2000), 95-101.

[1-46] M. W. Fu, W. L. Chan, Geometry and grain size effects on the fracture behavior of sheet metal in micro-scale plastic deformation, Materials and Design, 32, (2011), 4738-4746.

[1-47]U. Engel, R. Eckstein, Microforming –form basic research to its realization, Journal of Materials Processing Technology, 125-126, (2002), 35-44.

[1-48] T. Furushima, H. Tsunezaki, K. Manabe, S. Alexandrov, Ductile fracture and fee surface roughening behaviors of pure copper foils for micro/meso-scale forming, International Journal of Machine Tools & Manufacture, 76, (2014), 34-48.

[1-49] U. Engel, R. Eckstein, Microforming – form basic research to its realization, Journal of Materials Processing Technology, 125-126, (2002), 35-44.

[1-50] J.G. Lie, M.W. Fu, J.Lu, W.L. Chan, Influence of size effect on the springback of sheet metal foils in micro-bending, Computational Materials Science, 50, (2011), 2604-2614.

[1-51] U. Engel, Tribology in microforming, Wear, 260, (2006), 265-273.

[1-52] F. Vollertsen, Z. Hu, Tribological size effects in sheet metal forming measured by a strip drawing test, Annals of the CIRP, 55-1, (2006), 291-294.

[1-53] S. Weidel, U. Engel, Characterisation of the flattening behavior of modeled asperities, Wear, 266, (2009), 596-599.

[1-54] L. Peng, X. Lai, H.J. Lee, J.H. Song, J. Ni, Friction behavior modeling and analysis in micro/meso scale metal forming process, Materials and Design, 31, (2010), 1953-1961.

[1-55] X. Lai, L. Peng, P. Hu, S. Lan, J. Ni, Material behavior modelling in micro/meso-scale forming process with considering size/scale effects, Computational Materials Science, 43, (2008), 1003-1009.

[1-56] S. Mahabunphachai, M. Koc, Investigation of size effects on material behavior of thin sheet metals using hydraulic bulge testing at micro/meso-scales, International Journal of Machine Tools & Manufacture, 48, (2008), 1014-1029.

[1-57] Z. Gao, L. Peng. P. Yi, X. Lai, Grain and geometry size effects on plastic deformation in rool-to-plate micro/meso-imprinting process, Journal of Materials Processing Technology, 219, (2015), 28-41.

[1-58] X. Wang, Y. Ma, Z. Shen, Y. Gu, D. Zhang, T. Qiu, H. Lie, Size effects on formability in microscale laser dynamic forming of copper foil, Journal of Materials Processing Technology, 220, (2015), 173-183.

[1-59] S. Mahabunphachai, M. Koc, Fabrication of micro-channel arrays on thin metallic sheet using internal fluid pressure: Investigations on size effects and development of design guidelines, Journal of Power Sources, 175, (2008), 363-371.

[1-60] M.W. Fu, B. Yang, W.L. Chan, Experimental and simulation studies of micro blanking and deep drawing compound process using copper sheet, Journal of Materials Processing Technology, 213, (2013), 101-110.

[1-61] Y. Saotome, K. Yasuda, H. Kaga, Microdeep drawability of very thin sheet steels, Journal of Materials Processing Technology, 113, (2001), 641-647.

[1-62] F. Vollertsen, Effects on the deep drawing diagram in micro forming, Production Engineering Research and Development, 6, (2012), 11-18.

[1-63] F. Vollertsen, Z. Hu, Analysis of punch velocity dependent process window in micro deep drawing, Production Engineering Research and Development, 4, (2010), 553-559.

[1-64] C.H. Chen, J.T. Gau, R.S. Lee, An experimental and analytical study on the limit drawing ratio of stainless steel 304 foils for microsheet forming, Materials and Manufacturing Processes, 24 (2009), 1256-1265.

[1-65] A. Molotnikov, R. Lapovok, C.F. Gu, C.H.J. Davies, Y. Estrin, Size effects in micro cup drawing, Materials Science and Engineering A, 550, (2012), 312-319.

[1-66] Y. Kasuga, N. Nozaki, Pressu lubricated deep drawing (1st report, conception of the mechanism, characteristics and possibilities), Transactions of the Japan Society of Mechanical Engineers (in Japanese), 24-146, (1958), 720-727.

[1-67] K. Manabe, T. Shimizu, H. Koyama, M. Yang, K. Ito, Validation of FE simulation based on surface roughness model in micro-deep drawing, Journal of Materials Processing Technology, 204, (2008), 89-93.

[1-68] F. Vollertsen, H.S. Niehoff, H. Wielage, On the acting pressure in laser deep drawing, Production Engineering Research and Development, 3, (2009), 1-8.

[1-69] I. Irthiea, G. Green, S. Hashim, A. Kriama, Experimental and numerical investigation on micro deep drawing process of stainless steel 304 foil using flexible tools, International Journal of Machine Tools & Manufacture, 76, (2014), 21-33.

[1-70] H. Tanabe, M. Yang, Design and evaluation of heat assisted microforming system, Steel Research International, Special features, (2011), 1020-1024.

[1-71] Z. Hu, Z. Schubnov, F. Vollertsen, Tribological behavior of DLC-films and their application in micro deep drawing, Journal of Materials Processing Technology, 212, (2012), 647-652.

[1-72] T. Shimizu, H. Komiya, T. Watanabe, Y. Teranishi, H. Nagasaka, K. Morikawa, M. Yang, HIPIMS deposition of TiAlN films on inner wall of micro dies and its applicability in micro-sheet metal forming, Surface & Coating Technology, 250, (2014), 44-51.

[1-73] T. Shimizu, T. Kakegawa, M. Yang, Micro-texturing of DLC thin film coatings and its tribological performance under dry sliding friction for microforming operation, Procedia Engineering, 81, (2014), 1884-1889.

[1-74] Y. Saotome, T. Okamoto, An in-situ incremental Microforming system for three-dimensional shell structures of foil materials, Journal of Materials Processing Technology, 113, (2001), 636-640.

[1-75] T. Obikawa, S. Satou, T. Hakutani, Dieless incremental micro-forming of miniature shell objects of aluminum foils, International Journal of Machine Tools & Manufacture, 49, (2009), 906-915.

[1-76] T. Kuboki, A. Azire, Y. Jin, A new incremental in-plane bending of thin sheet metals for micro machine components by using a tillable punch, CIRP Annals – Manufacturing Technology, 63, (2014), 249-252.

[1-77] M. Koc, S. Mahabunphachai, Feasibility investigations on a novel micro-manufacturing process for fuel cell bipolar plates: Internal pressure-assisted embossing of micro channels with in-die mechanical bonding, Journal of Power Sources, 172, (2007), 725-733.

Chapter 2
Design of MHDD Based on Scale Dependence

2.1. Introduction

In conventional macro hydromechanical deep drawing (HDD), there are the fracture prevention effects to improve the forming limit, such as the friction holding effect, the hydrodynamic lubrication effect and compression effect of blank edge by radial pressure [2-1]. Furthermore, the fluid pressure can improve the shape accuracy. Therefore, to design the process, fluid pressure and tooling conditions in macro HDD, these effects and characteristics are considered. However, the design guideline of conventional macro HDD cannot be simply applied to micro hydromechanical deep drawing (MHDD) because the deformation behavior and the required fluid pressure may change due to the size effects. Therefore, the design guideline for MHDD should be established on the basis of the scale dependence.

One of important phenomena in MHDD is the fluid behavior. It can induce hydrodynamic lubrication and reduce the friction force significantly [2-2]. The characteristics of fluid behavior in the micro scale however, are still not clear. Not only hydrodynamic lubrication but also the boundary and mixed lubrications exist during the MHDD process. To analyze these lubrication conditions in micro forming, the surface topography, especially the open lubricant pockets (OPLs) and closed lubricant pockets (CLPs), must be considered [2-3, 4].

In addition, the tooling feature size also significantly influences the material and deformation behavior in micro forming as mention in Chapter 1. The ratio of tooling feature size to minimum manufacturable thickness becomes small in micro scale because the thinning of manufacturable foil thickness is limited with scaling down the target size and shape. It was reported that this relative tooling feature size affects the drawability in micro deep drawing and its drawing characteristics are close to the deep drawing for thick sheet [2-5, 6]. Thus, the relative tooling feature size may also affect the deformation behavior of blank and cause the scale dependences of effects of fluid pressure on shape accuracy and forming limit in MHDD.

As mentioned above, the effects of fluid behavior, the ratio of the punch diameter to the minimum thickness, OPLs and CPLs on tribological behavior and drawing characteristics need to be examined in order to establish the design guideline of MHDD. This is the main objective of this section.

From the above, the basic drawing characteristics and tribological behavior in MHDD are investigated based on the relative tooling feature size and tribological size effect and the proper fluid pressure, tooling conditions for MHDD process are designed using theory and finite element method (FEM). The theoretical model in MHDD and a new friction model for MHDD considering the OLPs and CLPs are developed. The finite element method (FEM) is also conducted to evaluate the drawing characteristics more accurate by considering the blank deformation.

2.2. Theory of MHDD

The theoretical model for MHDD was made under the following assumptions:

(1) The thickness of the blank is constant, and then the normal strain in thickness direction is zero as shown in **Fig. 2.1**.
(2) The distribution of equivalent stress in the flange and die shoulder areas is replaced with uniform distribution.
(3) The blank material is assumed to present the isotropic rigid plasticity.

2.2.1. Geometrical description

From the geometrical relationship based on the above assumptions, the current rim radius r_0 can be presented by

$$r_0 = \sqrt{{R_0}^2 + {r_1}^2 - \frac{V_1 + V_2 + V_3 + V_4}{\pi t}} \tag{2.1}$$

where V_1, V_2, V_3 and V_4 are the volumes in die shoulder, side wall, punch shoulder and punch bottom areas, respectively. These can be expressed as follows:

$$V_1 = 2\pi t\Phi\left(r_d + \frac{t}{2}\right)\left(r_1 - \left(r_d + \frac{t}{2}\right)\sin\frac{\Phi}{2}\right) \tag{2.2}$$

$$V_2 = \pi t(r_2 + r_3) \times \sqrt{(r_2 - r_3)^2 + \{S - (r_d + r_p + t)(1 - \cos\Phi)\}^2} \tag{2.3}$$

$$V_3 = 2\pi t\Phi\left(r_p + \frac{t}{2}\right)\left(r_4 + \left(r_p + \frac{t}{2}\right)\sin\frac{\Phi}{2}\right) \tag{2.4}$$

$$V_4 = \pi t{r_4}^2 \tag{2.5}$$

The contact angle Φ changes as the punch travels and it is geometrically determined. Manabe et al. [2-7] derived the contact angle using the punch stroke S by assuming the blank shape as the straight at clearance between die and punch. It is given by:

$$\Phi = \cos^{-1}\frac{-B + \sqrt{B^2 - 4A \cdot C}}{2A} \tag{2.6}$$

where the parameters A, B and C can be obtained, respectively, as:

$$A = \frac{(S - r_p - r_d)^2}{(c + r_p + r_d)^2} + 1 \tag{2.7}$$

$$B = \frac{2(r_p + r_d)(S - r_p - r_d)}{(c + r_p + r_d)^2} \tag{2.8}$$

$$C = \frac{(r_p + r_d)^2}{(c + r_p + r_d)^2} - 1 \tag{2.9}$$

where S is the punch stroke and c is the clearance between the die and punch as shown in **Fig. 2.1**.

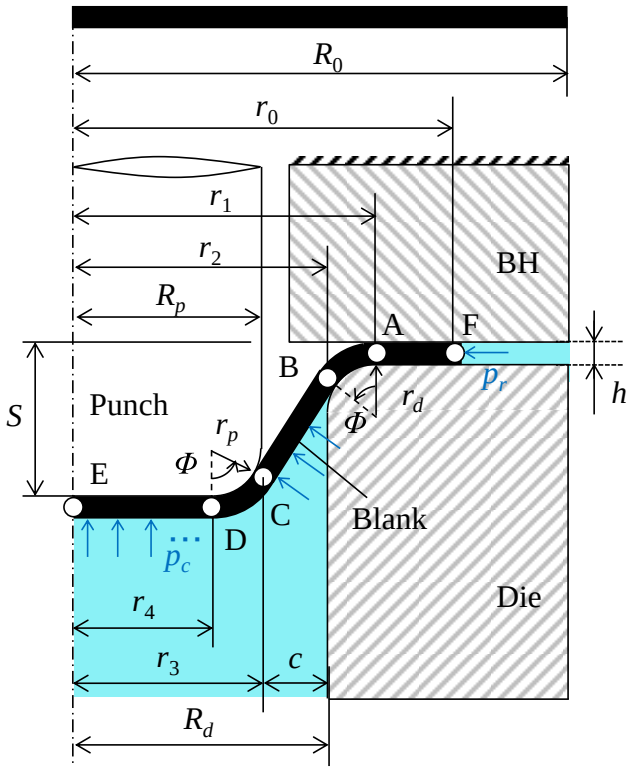

Fig. 2.1 Geometrical parameters in MHDD process.

2.2.2. Constitutive equations

In the case under consideration, Mises's equivalent strain is expressed by:

$$\varepsilon_{eq} = \sqrt{\frac{2}{3}\left({\varepsilon_{\varphi}}^2 + {\varepsilon_{\theta}}^2\right)} \tag{2.10}$$

Because of the volume constant ($\varepsilon_{\varphi} + \varepsilon_{\theta} = 0$), Eq. (2.10) can be rewritten as

$$\varepsilon_{eq} = \frac{2}{\sqrt{3}}\varepsilon_{\varphi} \tag{2.11}$$

Swift's law is used for the constitutive equation of the blank material and it is expressed by:

$$\sigma_{eq} = K\left(\varepsilon_{eq} + \varepsilon_0\right)^n \tag{2.12}$$

where σ_{eq} is the equivalent stress, K is the strength coefficient, n is the work hardening exponent, ε_0 is the material constant and ε_{eq} is the equivalent strain. Kawai [2-8] defined the average circumferential stress $\bar{\varepsilon}_{\theta}$ in the flange and die shoulder areas using an average radius in flange area $\bar{r}(=(r_0 + r_2)/2)$ as follows:

$$|\bar{\varepsilon}_{\theta}| = \frac{1}{2}\ln\frac{{R_0}^2 - {r_0}^2 + \bar{r}^2}{\bar{r}^2} \tag{2.13}$$

The equation for equivalent strain in this theory is integrated to Mises yield criterion, in which Mises and Tresca yield criterions are combined in Kawai's equations. From Eqs. (2.11) and (2.13), the equivalent strain can be expressed as

$$\varepsilon_{eq} = \bar{\varepsilon}_{eq} = \frac{2}{\sqrt{3}}\bar{\varepsilon}_{\varphi} = \frac{2}{\sqrt{3}}|\bar{\varepsilon}_{\theta}| = \frac{1}{\sqrt{3}}\ln\frac{{R_0}^2 - {r_0}^2 + \{(r_0 + r_2)/2\}^2}{\{(r_0 + r_2)/2\}^2} \tag{2.14}$$

2.2.3. Equilibrium equations

Fig. 2.2 shows the stress state in flange and die shoulder areas. The theory for the deep drawing of a circular cup can be derived as an axisymmetric model. By assuming the membrane stress state, the force equilibrium relation in meridional direction in flange area can be expressed as

$$\frac{d\sigma_\varphi}{dr}+\frac{\mu(q+p_C)}{t}+\frac{\sigma_\varphi-\sigma_\theta}{r}=0 \tag{2.15}$$

where μ is the friction coefficient, q is the blank holder pressure caused by constant gap in MDD ($p_c=0$MPa), p_c is the counter pressure and σ_φ and σ_θ are the meridional and circumferential stresses, respectively. Any plane strain yield criterion for isotropic incompressible material can be written as $\sigma_\varphi-\sigma_\theta=a\sigma_{eq}$. In particular, $a=1$ for Tresca yield criterion and $a=2/\sqrt{3}$ for Mises yield criterion. In what follows, it is assumed that $a=1.1$ in this study using Mises yield criterion. Therefore

$$\sigma_\varphi-\sigma_\theta=1.1\sigma_{eq} \tag{2.16}$$

In the flange area, the boundary conditions are as $r=r_0,\ \sigma_\varphi=-p_r$. From Eqs. (15) and (16), the meridional stress at the entrance of die shoulder ($r=r_1$) in **Fig. 2.1** is given by

$$\sigma_{\varphi 1}=1.1\sigma_{eq}\ln\frac{r_0}{r_1}+\frac{\mu(q+p_c)(r_0-r_1)}{t}-p_r \tag{2.17}$$

For the die shoulder area, the force equilibrium relations in meridional and thickness direction can be expressed as

$$\frac{d(rt\sigma_\varphi)}{d\varphi}+(r_d+t/2)t\sigma_\theta\cos\Phi-(r_d+t/2)r\mu(q_d-p_c)=0 \tag{2.18}$$

$$\frac{\sigma_\varphi}{r_d+t/2}-\frac{\sigma_\theta}{r}\sin\Phi-\frac{q_d-p_c}{t}=0 \tag{2.19}$$

where q_d is the contact pressure at die shoulder area in MDD (p_c =0MPa). From Eqs. (2.18) and (2.19), the relationship between σ_φ and σ_θ is expressed as

$$\frac{d(rt\sigma_\varphi)}{d\varphi}-\mu rt\sigma_\varphi+(\cos\Phi+\mu\sin\Phi)(r_d+t/2)t\sigma_\theta=0 \tag{2.20}$$

Since the thickness is assumed to be constant and $(r_d+t/2)\ll r_1$, considered the friction around the die shoulder, the meridional stress at the exit of die shoulder ($r=r_2$) in Fig. **2.1** $\sigma_{\varphi 2}$ is given by

$$\sigma_{\varphi 2}=e^{\mu\Phi}\left\{1.1\sigma_{eq}\ln\frac{r_1}{r_2}+\sigma_{\varphi 1}\right\} \tag{2.21}$$

From Eqs. (2.17) and (2.21), the meridional stress at the exit of die shoulder is obtained by

$$\sigma_{\varphi 2} = e^{\mu\Phi}\left\{1.1\sigma_{eq}\ln\frac{r_0}{r_2} + \frac{\mu(q+p_c)(r_0-r_1)}{t} - p_r\right\} \tag{2.22}$$

Here, Eq. (2.22) considers the pure drawing stress $\sigma_d = 1.1\sigma_{eq}\ln r_0/r_2$ and the friction stress in flange area $\sigma_f = \mu(q+p_c)(r_0-r_1)/t$. The influence of friction around die shoulder is considered by using the coefficient $e^{\mu\Phi}$.

The bending stress σ_b is caused at the entrance of die shoulders at point A in **Fig. 2.1** and the unbending stress σ_{ub} is caused at the exit of die shoulder at point B in **Fig. 2.1**. Masuda et al. derived σ_b and σ_{ub} using a bending moment per unit width M at the entrance of die shoulder (at point A in **Fig. 2.1**) [2-9]. By assuming that the blank at the entrance of die shoulder is subjected to the plastic bending deformation, the bending moment per unit width M can be expressed as

$$M = \frac{1.1\sigma_{eq}t^2}{4} \tag{2.23}$$

and the bending stress σ_b can be obtained by

$$\sigma_b = \sigma_{ub} = \frac{1.1\sigma_{eq}t}{4(r_d + t/2)} \tag{2.24}$$

Considered the bending and unbending stresses σ_b, σ_{ub}, the meridional stress at the exit of die shoulder in Eq. (2.22) can be rewritten as

$$\sigma_{\varphi 2} = e^{\mu\Phi}(\sigma_d + \sigma_f + \sigma_b - \sigma_r) + \sigma_{ub} \tag{2.25}$$

Finally, from Eqs. (2.22)-(2.25), the meridional stress at the exit of die shoulder $\sigma_{\varphi 2}$ can be determined as

$$\sigma_{\varphi 2} = e^{\mu\Phi}\left(1.1\sigma_{eq}\ln\frac{r_0}{r_2} + \frac{\mu(q+p_c)(r_0-r_1)}{t} - p_r\right) + (1+e^{\mu\Phi})\frac{1.1\sigma_{eq}t}{4(r_d+t/2)} \tag{2.26}$$

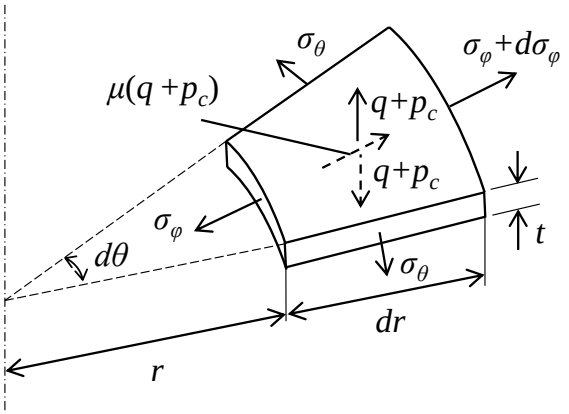

(a) At Flange area

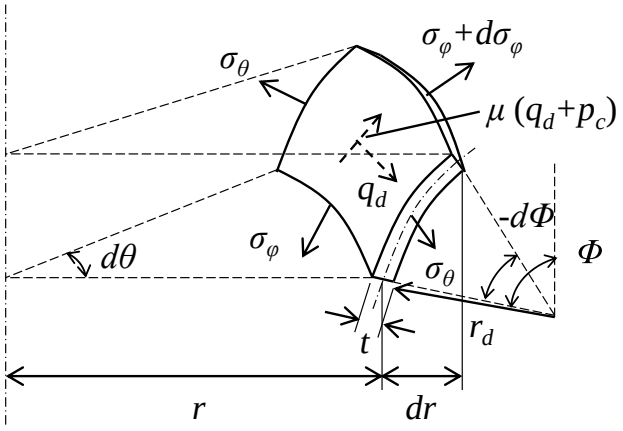

(b) At die shoulder area

Fig. 2.2 Stress state at flange and die shoulder area.

2.2.4. Blank holder pressure in constant gap method

A constant gap method shown in **Fig. 2.3** is adopted in which the gap between blank and blank holder is fixed. In this method, the edge of blank contacts with the blank holder and the blank holder force Q is generated. Due to the gap between the blank and die in the flange area, the blank does not have contact with the inner radius part of the flange area. It has an angle of non-contact area at the entrance of the die shoulder Φ_e. Based on the equilibrium of moment, the blank holder force per unit width for constant gap method can be obtained by

$$Q = \frac{M}{r_0 - r_1 + (r_d + t/2)\sin\Phi_e} \tag{2.27}$$

From Eqs. (2.24) and (2.27), the blank holder pressure q caused by constant gap in MDD (p_c =0MPa) can be obtained by

$$q = \frac{1.1\sigma_{eq}t^3}{4\{r_0 - r_1 + (r_d + t/2)\sin\Phi_e\}^2} \tag{2.28}$$

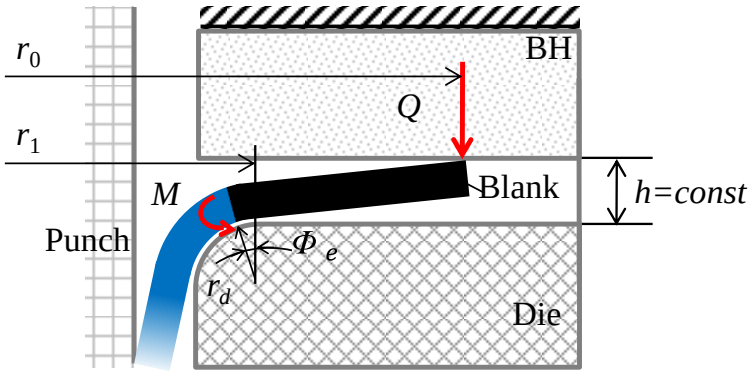

Fig. 2.3 Equilibrium of moment in flange area.

2.2.5. Scale dependent friction model in MHDD

In micro forming, the material surface cannot be considered as smooth but instead, contains many peaks and valleys called 'roughness' [2-3]. The roughness and the extent of the valleys become relatively large as compared to the size of the workpiece with scaling down. The valleys which connect to the edge of the blank cannot retain the lubricant. This area is called OLPs, as shown in **Fig. 2.4**. With the decrease in specimen size, the fraction of OLPs increases. Thus, the lubricant cannot be kept during conventional micro forming and it results in an increase in the friction force. This means that the OLPs must be considered when the tribological behavior of micro forming is studied.

The relationship among OLPs, CLPs and real contact area (RCA) [2-10] can be expressed as

$$\alpha_o + \alpha_c + \alpha_{RC} = 1 \tag{2.29}$$

where α_o, α_c and α_{RC} are the fractions of OLPs, CLPs and RCA, respectively. In the real contact state, RCA exists in both OLPs and CLPs areas; hence, the nominal OLPs include OLPs itself and RCA in OLPs area. In the same manner the nominal CLPs does CLPs itself and RCA. Using the nominal OLPs and CLPs, the relationship among OLPs, CLPs and RCA in Eq. (2.29) can be simplified and rewritten by

$$\bar{\alpha}_o + \bar{\alpha}_c = 1 \tag{2.30}$$

where, $\bar{\alpha}_o$ and $\bar{\alpha}_c$ are the fraction of nominal OLPs and CLPs, respectively.

The scale factor λ can be expressed by the ratio of width of OLPs w to blank radius R_0 as follows,

$$\lambda = R_0/w \tag{2.31}$$

The width of OLPs w does not change when the scale becomes small. In the macro case, the scale factor λ is usually larger than 10, and in the micro case, λ is close to 0.

For MHDD, the double side friction acts because the contact state in flange area should be modelled as shown in **Fig. 2.4**. Furthermore, the nominal contact area at die side and blank holder side are different. Here, the total nominal contact area on both die and blank holder sides in flange part A_t, the nominal OLPs and CLPs on both die and blank holder sides A_c and A_o can be expressed by

$$A_t = \pi\{2{r_0}^2 - {r_1}^2 - {r_2}^2\} \tag{2.32}$$

$$A_o = 2\pi w\{2r_0 + r_1 + r_2\} \tag{2.33}$$

$$A_c = A_t - A_o \tag{2.34}$$

The fraction of nominal OLPs $\bar{\alpha}_o$ can be obtained by

$$\bar{\alpha}_o = \frac{A_o}{A_t} = \frac{2w(2r_0 + r_1 + r_2)}{2{r_0}^2 - {r_1}^2 - {r_2}^2} = \frac{2(2\beta_0 + \beta_1 + \beta_2)}{\lambda\left(2{\beta_0}^2 - {\beta_1}^2 - {\beta_2}^2\right)} = \frac{1}{\lambda\beta^*} \tag{2.35}$$

where the relative current blank radius $\beta_0 = r_0/R_0$, the relative radius at the entrance of die shoulder radius $\beta_1 = r_1/R_0$, the relative radius at the exit of die shoulder $\beta_2 = r_2/R_0$ and $\beta^* = \left(2{\beta_0}^2 - {\beta_1}^2 - {\beta_2}^2\right)/\{2(2\beta_0 + \beta_1 + \beta_2)\}$. When $\lambda \leq 1/\beta^*$, only OLPs exists in the flange area and $\bar{\alpha}_o = 1$.

Considered the scale factor λ, the average friction coefficient in flange area μ can be calculated as follows,

$$\mu = \frac{A_o\mu_{dry} + (A_t - A_o)\mu_c}{A_t} = \frac{\mu_{dry} + (\lambda\beta^* - 1)\mu_c}{\lambda\beta^*} \tag{2.36}$$

where μ_c is the friction coefficients in CLPs and μ_{dry} is the friction coefficient for dry friction in OLPs.

For MHDD, the fluid medium may insert into the OLPs by applying the fluid pressure as shown in **Fig. 2.5**. In this area, the friction behavior is different from the dry friction. As the fluid pressure increases, the friction coefficient in lubricated OLPs by fluid pressure shown in **Fig. 2.5** decreases, and the hydrodynamic lubrication can be obtained when the fluid pressure exceeds the certain value. Thus, in MHDD, the lubricated OLPs by fluid pressure exist in addition to CLPs and OLPs with dry friction. To model this friction model, Eq. (2.36) is rewritten as,

$$\mu = \frac{A_{o-dry}\mu_{dry} + A_{o-fluid}\mu_{fluid} + (A_t - A_o)\mu_c}{A_t}$$

$$= \frac{\left(1 - \bar{\alpha}_f\right)\mu_{dry} + \bar{\alpha}_f\mu_{fluid} + (\lambda\beta^* - 1)\mu_c}{\lambda\beta^*} \tag{2.37}$$

where the dry friction area in nominal OLPs $A_{o-dry} = \left(1 - \bar{\alpha}_f\right)A_o$, the lubricated area by fluid pressure in nominal OLPs $A_{o-fluid} = \bar{\alpha}_f A_o$, μ_{fluid} is the friction coefficient in lubricated OLPs by fluid pressure, and $\bar{\alpha}_f$ is the ratio of the lubricated nominal OLPs by fluid pressure to whole nominal OLPs. $\bar{\alpha}_f$ is changed by pressurization methods as shown in **Fig. 2.5**. $\bar{\alpha}_f = 0$ for no fluid pressure, $\bar{\alpha}_f = 1/4$ for counter pressure, $\bar{\alpha}_f = 1/2$ for radial pressure, $\bar{\alpha}_f = 3/4$ for counter and radial pressures. Moreover, $\bar{\alpha}_f = 1$ when $\bar{\alpha}_o = 1$ at any pressurization methods. When the hydrodynamic lubrication occurs, $\mu = \mu_h$ which is the friction coefficient in hydraulic lubrication.

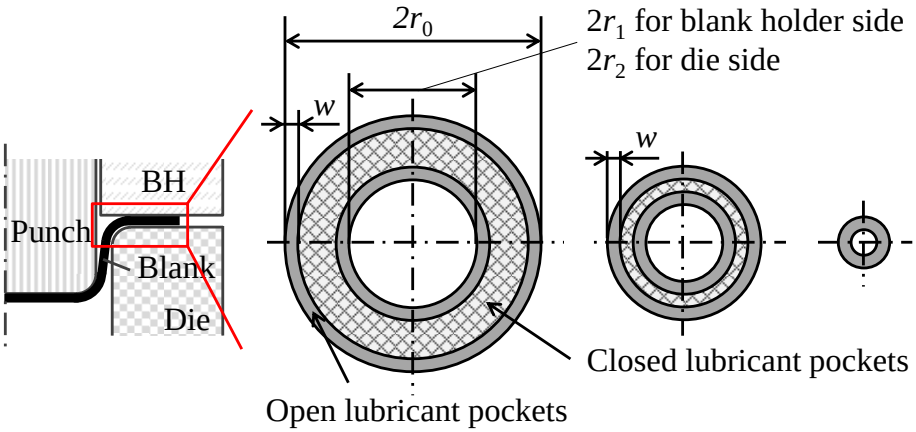

Fig. 2.4 The change of fraction of OLPs in flange area with the decrease of blank size.

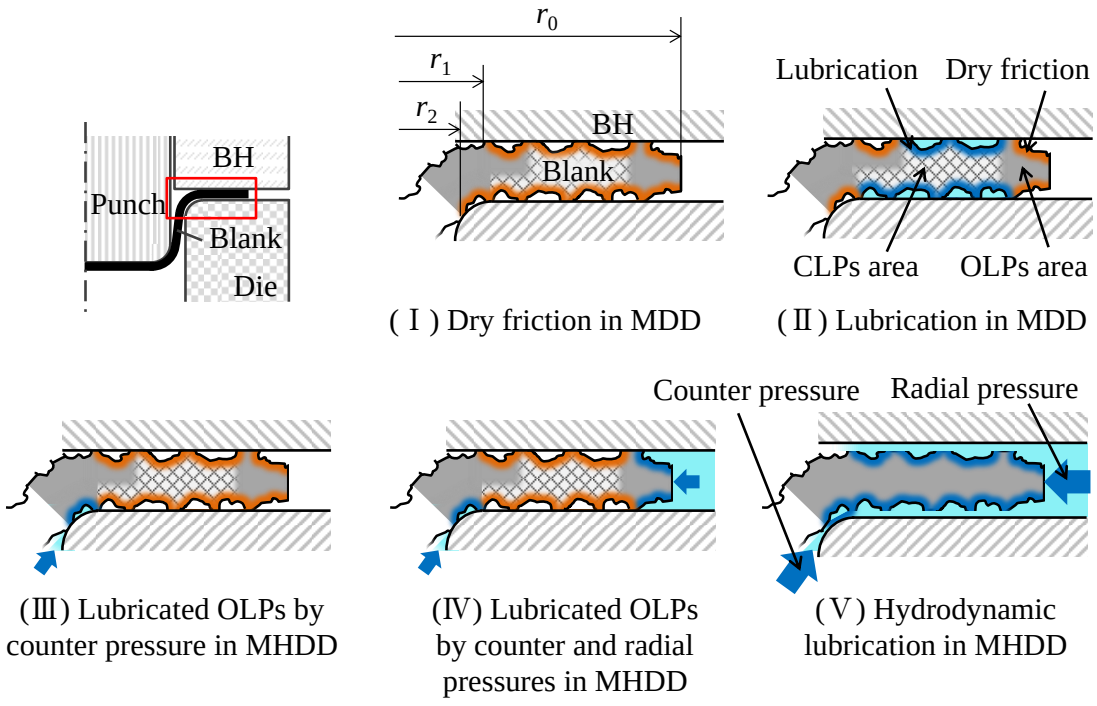

Fig. 2.5 Examples of lubrication conditions considering OLPs and CLPs in MDD and MHDD.

2.2.6. Effective punch and friction forces in MHDD

The punch force P was used to evaluate the change of friction force by applying the counter pressure in experiment and theory. From the meridional stress at the exit of die shoulder as shown in Eq. (2.26), P can be presented as

$$P = 2\pi r_2 t \sin\Phi \left[e^{\mu\Phi} \left\{ 1.1\sigma_{eq} \ln\frac{r_0}{r_2} + \frac{\mu(q+p_c)(r_0-r_1)}{t} - p_r \right\} + 1.1\sigma_{eq}\frac{t}{4(r_d+t/2)}\left(1+e^{\mu\Phi}\right) \right] \quad (2.38)$$

This punch force consists of the drawing, friction, bending and unbending forces P_S, P_F, P_B and P_{UB}. In the same tooling dimension, P_S, P_B and P_{UB} are approximately constant even if the counter pressure is changed. The change of counter pressure only influences the friction force as shown in Eq. (2.38). Therefore, the different punch forces for each counter pressure shows the change of friction force. In the experiment, the force acting on the punch oppositely by counter pressure P_p is included in the measured punch force P_M. For this reason, the effective punch force P_E in which P_M is subtracted from P_p is used to evaluate the change of friction force by applying counter pressure. It can be expressed as

$$P_E = P_M - P_p = P_S + P_F + P_B + P_{UB} \quad (2.39)$$

This P_E similarly consists of P_S, P_F, P_B and P_{UB}. Therefore, the difference of P_E at each counter pressure can evaluate the change of friction force. The friction force P_F is also calculated theoretically. From Eq. (2.38), the friction force can be obtained by

$$P_F = 2\pi r_2 t \sin\Phi \left(1-e^{\mu\Phi}\right)\left\{ 1.1\sigma_{eq}\ln\frac{r_0}{r_2} + \frac{\mu(q+p_c)(r_0-r_1)}{t} - p_r + \frac{1.1\sigma_{eq}t}{4(r_d+t/2)} \right\} \quad (2.40)$$

On the other hand, the application of radial pressure can apply the compression stress to the blank edge and the punch force can be reduced. This reduction of punch force by radial pressure ΔP_{Emax} can be expressed by

$$\Delta P_{Emax} = P_{max(p_r=0)} - P_{max(p_r>0)} = 2\pi r_2 t \sin\Phi\, p_r \quad (2.41)$$

where $P_{max(p_r=0)}$ and $P_{max(p_r>0)}$ are the maximum punch forces without and with radial pressure, respectively.

The normalized values are used when P_E, P_F and ΔP_{Emax} are calculated. Using the tensile strength, the allowance punch force at punch side wall can be obtained by

$$P_{al} = 2.2\pi r_2 t \sin\Phi\, \sigma_B(1+\varepsilon_u) \quad (2.42)$$

where ε_u is the strain at tensile strength.

The normalized effective punch force normalized $\bar{P}_E$, the normalized friction force $\bar{P}_F$ and the normalized reduction of punch force by radial pressure $\Delta\bar{P}_{Emax}$ can be expressed by

$$\bar{P}_E = \frac{P_E}{P_{al}} = \frac{P}{P_{al}} = \frac{P}{1.1\sigma_B(1+\varepsilon_u)} \tag{2.43}$$

$$\bar{P}_F = \frac{P_F}{P_{al}} = \frac{P_F}{1.1\sigma_B(1+\varepsilon_u)} \tag{2.44}$$

$$\Delta\bar{P}_{Emax} = \frac{\Delta P_{Emax}}{P_{al}} = \frac{p_r}{1.1\sigma_B(1+\varepsilon_u)} \tag{2.45}$$

2.2.7. Scale dependence of required fluid pressure in MHDD

(1) Friction holding effect

To make the contact between the blank and punch at side wall, the blank should be bent the bending angle Φ_c by the relative bending moment per unit width caused by counter pressure applied to side wall M_p as shown in **Fig. 2.6**. Based on the equilibrium of moments, the relative moment per unit width for bending resistance of blank M_B and M_p can be expressed as follows,

$$M_B = \frac{EI}{r_p} = \frac{Et^3}{12r_p} \tag{2.46}$$

$$M_p = \frac{L^2}{2\cos^2\Phi_c} p_c \tag{2.47}$$

where I is the geometrical moment of inertia per width and L is the length of side wall. When the blank is bent to make the contact between the blank and punch side wall, M_p should be higher than that M_B. Therefore, from Eqs. (2.46) and (2.47), the minimum required fluid pressure for friction holding effect p_{fmin} can be obtained by

$$p_{fmin} \geq \frac{Et^3\cos^2\Phi_c}{6r_pL^2} = \frac{E\cos^2\Phi_c}{6(r_p/t)\cdot(L/D_p)^2(D_p/t)^2} \tag{2.48}$$

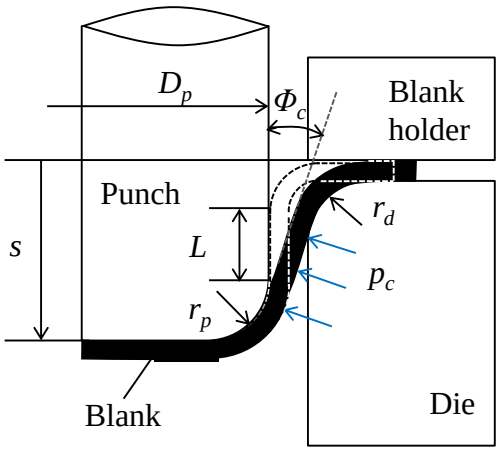

Fig. 2.6 Geometrical parameters in fitting process in MHDD.

(2) Hydrodynamic lubrication effect

The hydrodynamic lubrication occurs when the fluid medium leaks between the blank and tools and the blank does not contact with the tools. Therefore, when the fluid pressure exceeds the contact pressure at die shoulder, the fluid pressure leaks between the blank and tools and the hydrodynamic lubrication can be obtained [2-11]. The required fluid pressure for hydrodynamic lubrication p_h is given by the contact pressure at die shoulder q_d. From Eq. (2.19), it is presented by

$$p_h = q_d = \frac{t\sigma_\varphi}{r_d + t/2} - \frac{t\sigma_\theta}{r}\sin\Phi \tag{2.49}$$

On the basis of Eqs. (2.16) and (2.22), assuming that the friction resistance under the hydrodynamic lubrication is quite small and can be ignored, Eq. (2.49) can be rewritten as

$$p_h = 1.1\sigma_{eq}\left\{\frac{t}{r_d + t/2}\ln\frac{r_0}{r_2} + \frac{t}{r_2}\left(1 - \ln\frac{r_o}{r_2}\right)\sin\Phi\right\}$$

$$= 1.1\sigma_{eq}\left\{\frac{1}{(r_d/t) + 1/2}\ln\frac{r_0}{r_2} + \frac{1}{\left(D_p/t\right)/2 + c/t + (1 - \sin\Phi)(r_d/t)}\left(1 - \ln\frac{r_o}{r_2}\right)\sin\Phi\right\} \tag{2.50}$$

2.2.8. Material and dimensions used in calculation

Stainless steel foil (SUS304-H) with a thickness of 50μm was used. The mechanical properties are listed in **Table 2.1**. The stress-strain curves obtained by a tensile test and calculated by the Swift equation are shown in **Fig. 2.7**. The stress-strain curve was also calculated using power law as a comparison. The tool dimensions are presented in **Fig. 2.8**. The angle of the no contact area at the entrance of the die shoulder in Fig. 2.3 was experimentally measured and was set to $\Phi_e = 12°$. Two types of lubrication conditions were used in the calculation as shown in **Fig. 2.5**. Dry friction conditions were adopted in MDD and lubricated OLPs by counter pressure was assumed in MHDD. The friction coefficients for different lubrications used in calculation are listed in **Table 2.2**. The friction coefficients for each lubrication case were assumed with reference to the friction coefficients shown in the several papers related with tribology [2-4, 12, 13]. Based on the experimental results as mentioned below, the width of OLPs w used in calculation was set up at 175μm.

Table 2.1 Mechanical properties of material used.

Young's modulus E (GPa)	Yield stress σ_y (MPa)	Tensile strength σ_B (MPa)	Material constant ε_0	Work hardening exponent n	Material strength coefficient K (MPa)
193	1217	1331	0.007	0.017	1470

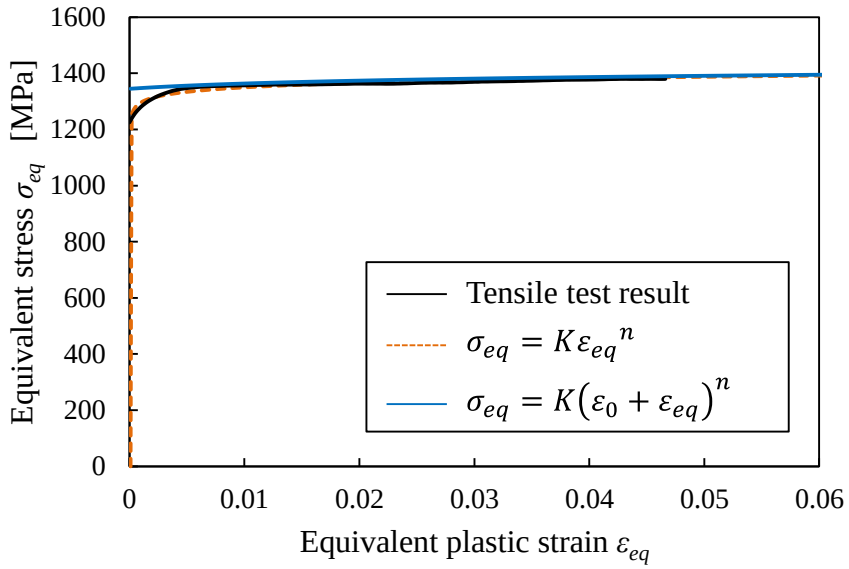

(a) Overall view

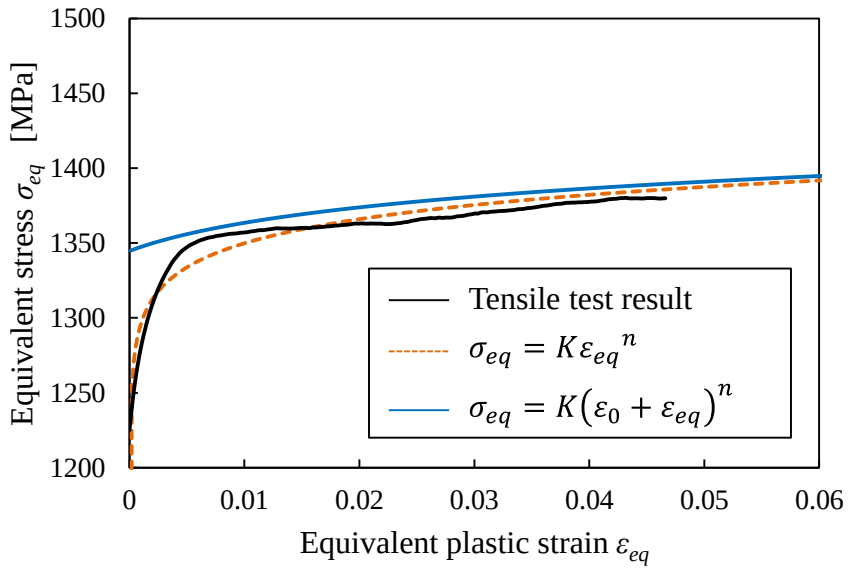

(b) Enlarged view

Fig. 2.7 Stress-strain curves obtained by tensile test and used for calculation.

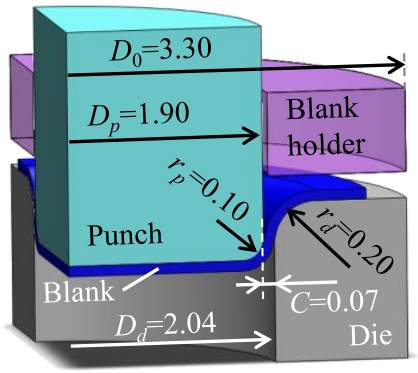

Fig. 2.8 Tooling dimensions of micro hydromechanical deep drawing

Table 2.2 Friction coefficients for each lubrication and area.

Dry friction in OLPs μ_{dry}	Friction coefficient in OLPs μ_c	Lubricate OLPs by fluid pressure μ_h	Friction coefficient in lubricated OLPs by fluid pressure μ_{fluid}	Hydrodynamic lubrication μ_h
0.30	0.30, 0.03	0.03, 0.25	0.03, 0.25	0.005

2.3. FE Model of MHDD

The FEM simulation was carried out with an explicit dynamic finite element code, LS-DYNA ver.971. The stainless steel foil (SUS304-H) of 50μm thickness was employed. For mechanical properties, Young's modulus $E = 193$GPa, yield stress $\sigma_y = 1217$MPa and tensile strength σ_B =1331MPa was used. A real stress-strain curve obtained by tensile test shown in **Fig. 2.7** was input into FEM directly as the plastic stress-strain curve. The 8-node solid element with isotropic elastic-plastic body model was used for the blank, and the tools were treated as rigid bodies as shown in **Fig. 2.9**. The blank has 5 elements in thickness direction, 100 elements in radial direction, and has the 10 integration points in thickness direction. The full model was simulated.

The ratio of punch diameter to thickness D_p/t which represents the target size, the ratio of punch and die shoulder radii to thickness r_p/t, r_d/t are important parameters in relative tooling feature size. D_p/t represents the relative tooling feature size and set up at D_p/t=20, 38, 100. In this FEM, the punch diameter, punch and die radii were changed under the constant minimum thickness t =50μm to evaluate the effect of relative tooling feature size on deformation behavior as shown in **Fig. 2.10**. The tool dimensions used in MHDD are listed in **Table 2.3**. The constant gap method was adopted, in which the gap between the blank holder and die h is fixed. The counter pressure p_c was applied to whole surface of blank and the radial pressure p_r was applied to blank edge. These fluid pressures were assumed as constant during the MHDD process. The static and kinetic friction coefficients between the punch and blank were assumed as μ_s =0.35, μ_k =0.30 in dry friction under all conditions, respectively. The friction coefficients between the die, blank holder and blank are listed in **Table 2.4**.

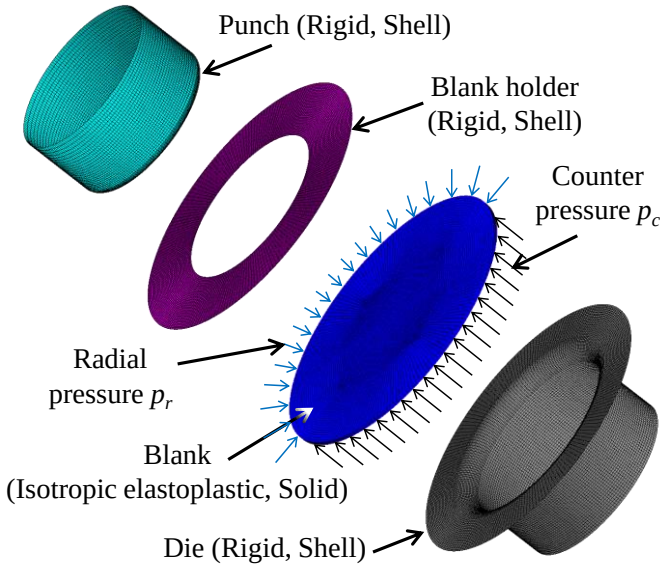

Fig. 2.9 FEM model of MHDD.

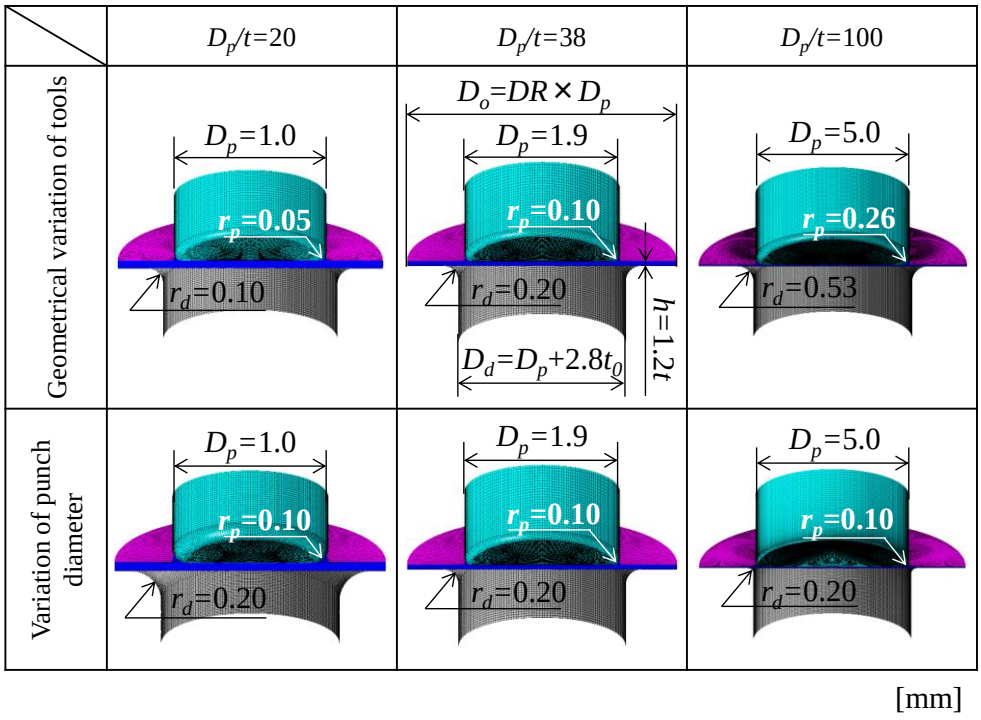

Fig. 2.10 Change of tooling dimension in geometrical variation of tools and variation of punch diameter.

Table 2.3 Tooling dimensions for various D_p/t values.

D_p/t	20	38	100
Blanking punch diameter, D_0 [mm]	1.726	3.300	8.684
Drawing punch diameter, D_p [mm]	1	1.9	5
Drawing punch shoulder radius, r_p [mm]	0.05,	0.10	0.26,
	0.10	0.10	0.10
Drawing die diameter, D_d [mm]	1.142	2.04	5.14
Drawing die shoulder radius, r_d [mm]	0.10	0.20	0.53
	0.20	0.20	0.20
Blank holder constant gap, h [mm]	0.06	0.06	0.06

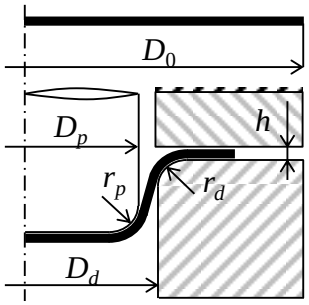

Table 2.4 Friction coefficients between die, blank holder and blank.

Lubrication conditions	Friction coefficients
Dry friction (No lubrication)	μ_s =0.35, μ_k =0.30
Lubrication	μ_s =0.05, μ_k =0.03

2.4. Results and Discussion

2.4.1. Verifications of FEM model and theory of MHDD

Fig. 2.11 shows the ratio of kinetic energy to total energy in FEM model for MHDD. The energy ratio was less than 0.05 during whole drawing process and it was less than 0.01 except of the early stage. The stress wave also cannot be observed during the drawing process. It can be said that the energy ratio is small enough to eliminate the dynamic influence.

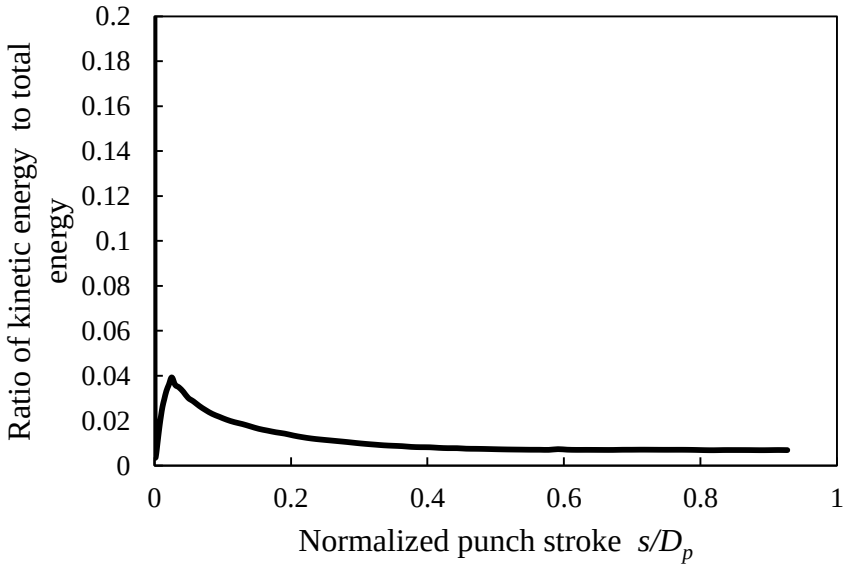

Fig. 2.11 Energy ratio in FEM model for MHDD (D_p/t =38, p_c =30MPa).

Fig. 2.12 shows the deformation processes of blank during MHDD in FEM and experiment. The flange area flows into the die cavity as the punch travels. The blank shape and material flow at flange area in FEM are in good agreement with experimental results, except for the wrinkling at cup edge. It can be found that the FEM model can simulate the deformation behavior in MHDD.

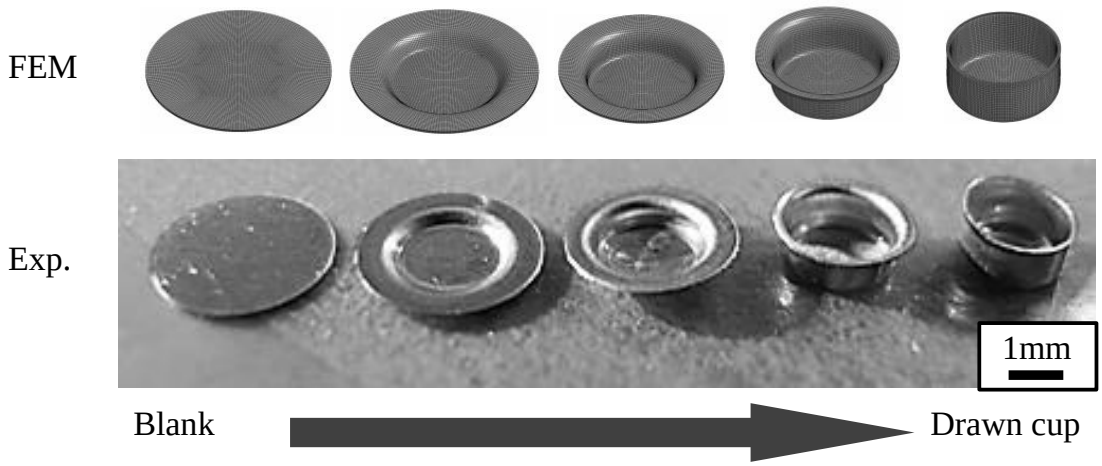

Fig. 2.12 Comparison of deformation processes of blank during MHDD between experiment and FEM (D_p/t =38, p_c =10MPa).

Fig. 2.13 shows the effect of counter pressure on deformation profiles of blank at side wall in experiment and FEM. The fitness in punch side wall can be improved by applying p_c =20MPa in experiment, although it is low at p_c =0MPa. The FEM results also shows that the larger counter pressure, the higher fitness for punch side wall. The contact length between blank and punch side wall L_c has a good agreement between experiment and FEM at p_c =20MPa. The FEM model can qualitatively and quantitatively simulate the deformation behavior of blank by counter pressure.

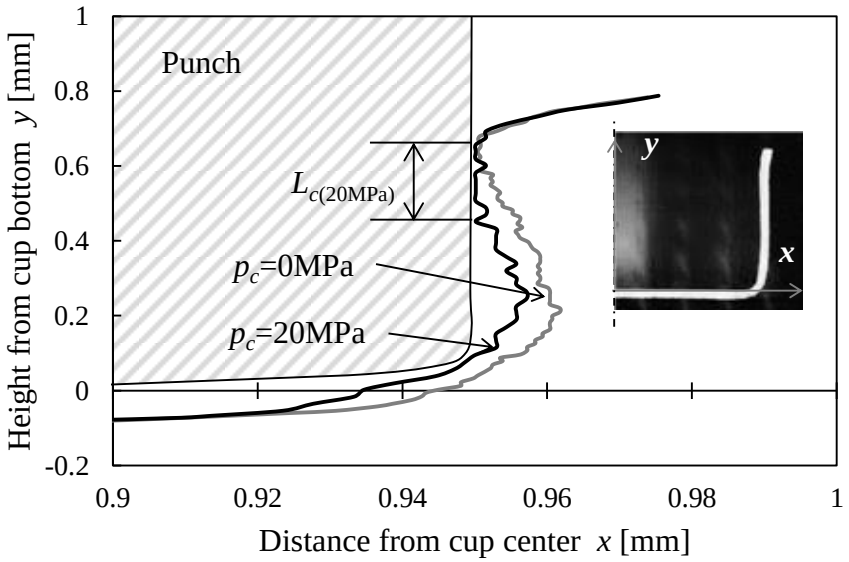

(a) Experiment

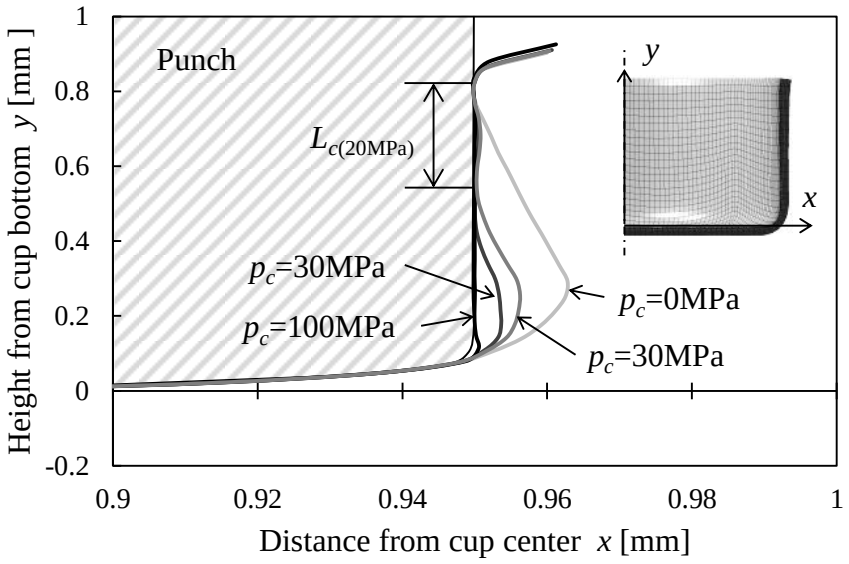

(b) FEM

Fig. 2.13 Deformation profiles of blank at side wall for different counter pressures in experiment and FEM (D_p/t =38).

Fig. 2.14 shows the comparison of experimental and theoretical results of normalized effective punch force-stroke curves. In the experimental results of MDD and MHDD, the punch force-stroke curves increase at the early stage (S/D_p <0.2) and reach the maximum at S/D_p = 0.2. At the middle stage (0.2< S/D_p <0.6), the punch force and the sliding force occurs during passing thought the straight die part in **Fig. 2.8** at the late stage (S/D_p >0.6). The theoretical results can represent the increase and decrease of punch force although it cannot represent the sliding force. The maximum punch forces of the theoretical results are almost as large as the experimental results in MDD and MHDD of μ_{fluid} =0.25. This means that the theoretical results agree with the experimental results. For MHDD of μ_{fluid} =0.03, the effective punch force is much smaller than that in experimental result and theoretical result of μ_{fluid} =0.25. It means that the friction coefficient in OLPs cannot be sufficiently reduced by applying counter pressure of 10MPa. Moreover, it shows that the friction coefficient in OLPs significantly influences the effective punch force in MHDD. The punch force-stroke curves calculated by Swift equation are completely the same as the power law. This is because the stress-strain curves are almost the same for material with a low work hardening exponent. The punch force-stroke is not significantly changed by the approximation of stress-strain curve.

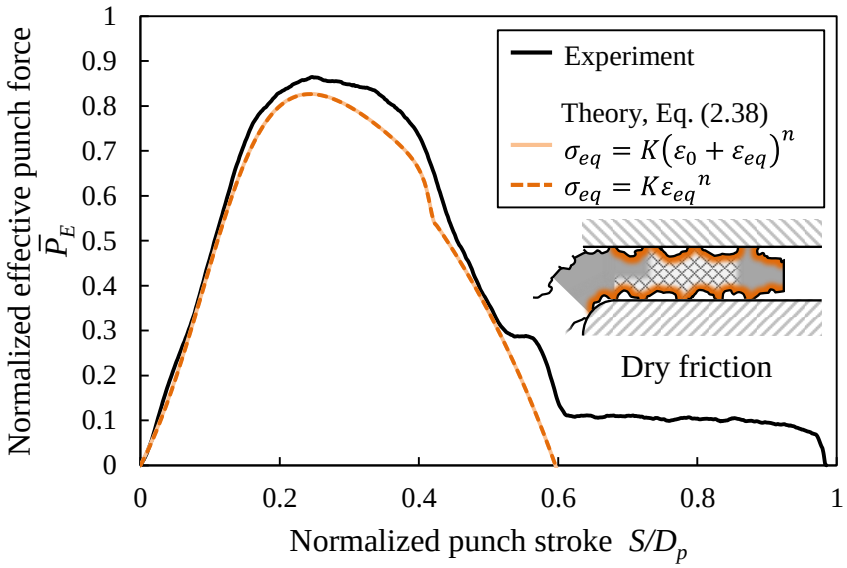

(a) In MDD ($\mu_c = \mu_{dry} = 0.3,\ \bar{\alpha}_f = 0$)

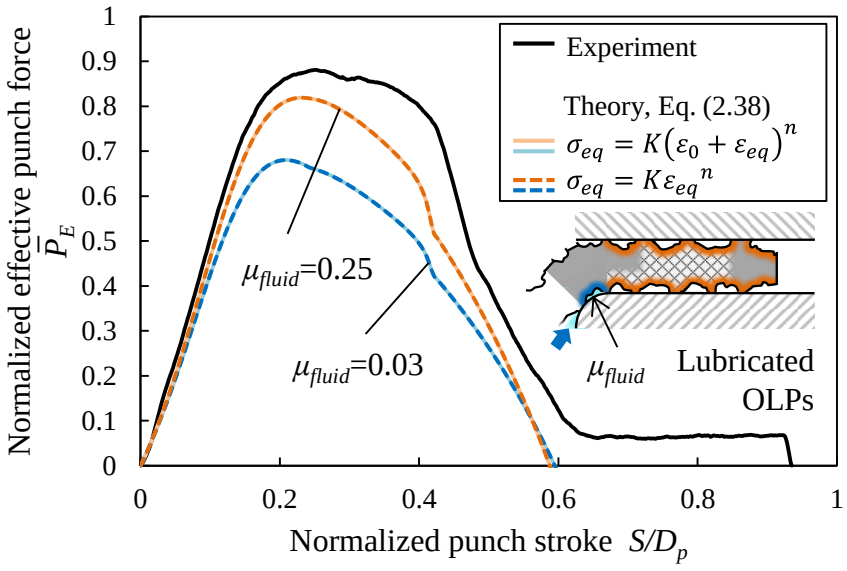

(b) In MHDD (p_c=10MPa, $\mu_c = \mu_{dry} = 0.3,\ \bar{\alpha}_f = 1/4$)

Fig. 2.14 Comparison of experimental and theoretical results of normalized punch force-stroke curves.

2.4.2. Basic deformation characteristics and drawability in MHDD

Fig. 2.15 shows the deformation processes in cross section of blank during MHDD. It can be seen that the blank at flange area flows into the die cavity as with **Fig. 2.12**. It seems that the contact length between the blank and punch at side wall increases as the punch travels. This contact behavior between the blank and punch at side wall is different at different counter pressures as shown in **Fig. 2.16**. For p_c =0MPa, the blank does not contact with the punch at side wall during the drawing process. After the blank was drawn at S/D_p =0.6, the blank near the edge contacts with punch at side wall. By applying p_c =30MPa, the contact timing between the blank and punch at side wall is made quick and the contact length L_c increases. However, the blank still does not contact before S/D_p =0.4 due to the no contact between the blank and punch side wall near the punch shoulder. The blank is difficult to be fitted to the punch side due to the large bending stiffness at punch shoulder. Therefore, the contact between the blank and punch side wall cannot be obtained at low counter pressure. Meanwhile, the adequate contact state can be obtained by applying p_c =100MPa. At p_c =100MPa, the blank contacts with the punch by degrees as the punch travels. The ultra high pressure which is larger than p_c =100MPa, is required to obtain the adequate fitness for punch.

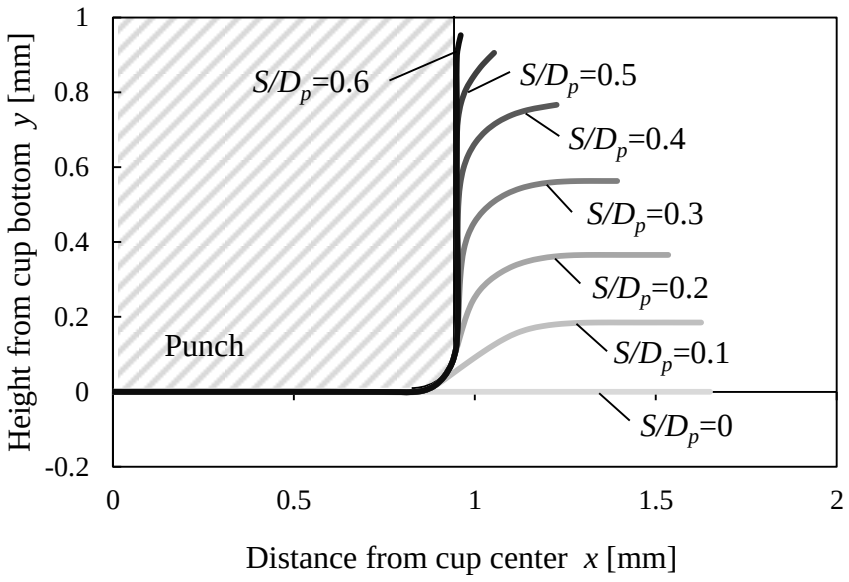

Fig. 2.15 Overall view of deformation processes in cross section of blank during MHDD (D_p/t =38, p_c =30MPa, S: punch stroke).

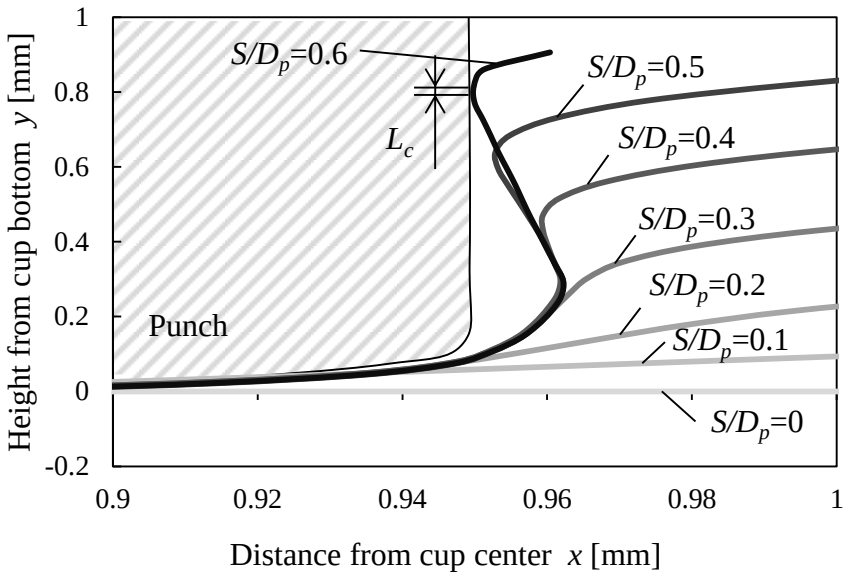

(a) p_c =0MPa

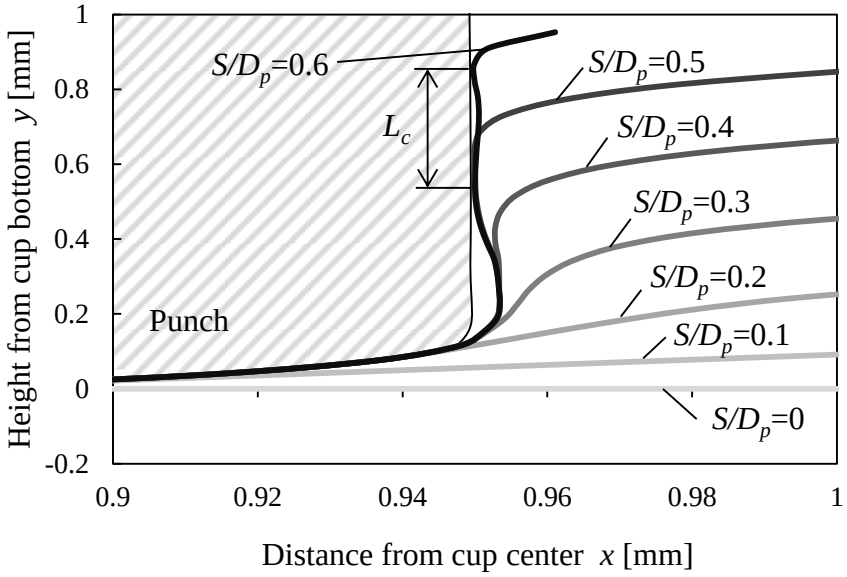

(b) p_c =30MPa

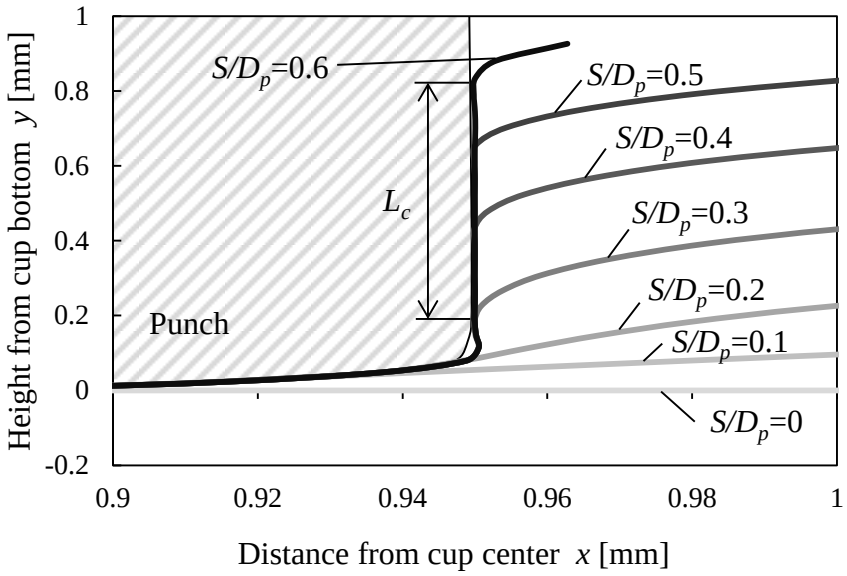

(c) p_c =100MPa

Fig. 2.16 Enlarged view of deformation processes in cross section of blank at punch shoulder during MHDD (D_p/t =38).

Fig. 2.17 shows the effect of counter pressure on thickness strain distribution in FEM. The maximum thickness reduction appears at punch shoulder due to the bending and bulge deformation. The thickness is also reduced at side wall due to the bending and unbending deformations at die shoulder. The same behavior has been observed at conventional macro HDD [2-14]. In addition, the thickness reduction increases at punch shoulder with increasing the counter pressure. The blank holder plays a role of blank holder pressure in MHDD with constant gap. So, the increase of counter pressure causes the increase of blank holder pressure and friction force between blank and blank holder. Therefore, the thickness reduction occurs when the drawing resistance in flange area increases by increasing the friction force at high counter pressure.

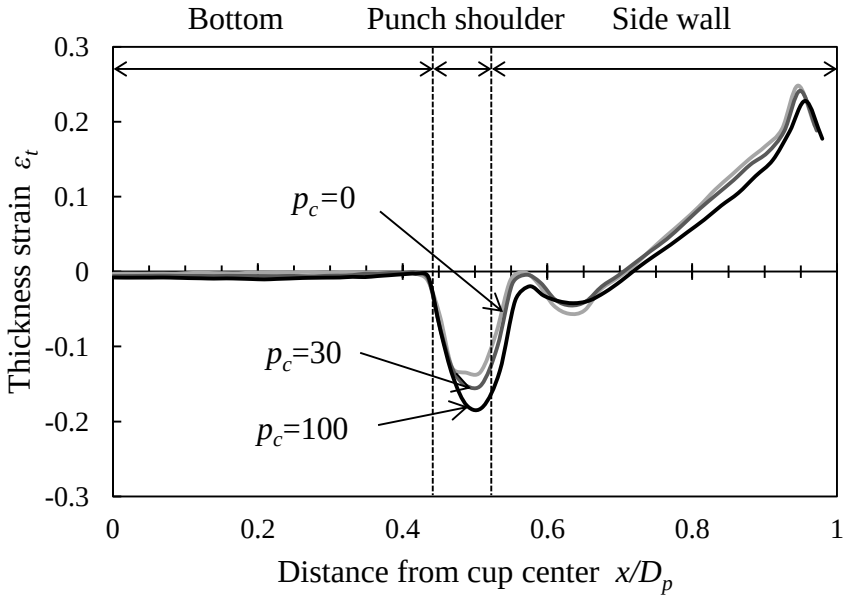

Fig. 2.17 Effect of counter pressure on thickness strain distribution in FEM (D_p/t =38).

Fig. 2.18 shows the shift of locations of maximum meridional stress and fracture by counter pressure applied in MHDD. At low counter pressure p_c =30MPa, the meridional stress become high at punch shoulder at any D_p/t. It is because the friction holding effect is not enough due to the less fitness between the blank and punch side wall as shown **Fig. 2.16**. It induces the fracture at punch shoulder [2-14]. On the other hand, the meridional stress concentration area is shifted to the die shoulder area by applying p_c =180MPa at D_p/t =38 and p_c =80MPa at D_p/t =100 due to the friction holding effect. The required fluid pressure to reduce the meridional stress concentration at

punch shoulder increases as D_p/t decreases. Moreover, the meridional stress at punch shoulder cannot be reduced at D_p/t =20 because the excessive thickness reduction occurs before the friction holding effect is obtained. In conventional macro HDD, it was reported that the fracture normally occurs at die shoulder under the high counter pressure. It is because the reverse bulging deformation occurs at the die shoulder, or the blank side wall is subjected to the high drawing resistance due to the less friction holding effect. The limiting drawing ratio (LDR) can be obtained when this fracture at die shoulder cannot be avoided. It means the forming limit can be improved by avoiding the fracture at punch shoulder by applying counter pressure. From the above results, it was clarified that the ultra high fluid pressure p ≥100MPa is required to improve the drawability in MHDD and it also increases as the size is scaled down to micro scale with decreasing the relative tooling feature size D_p/t.

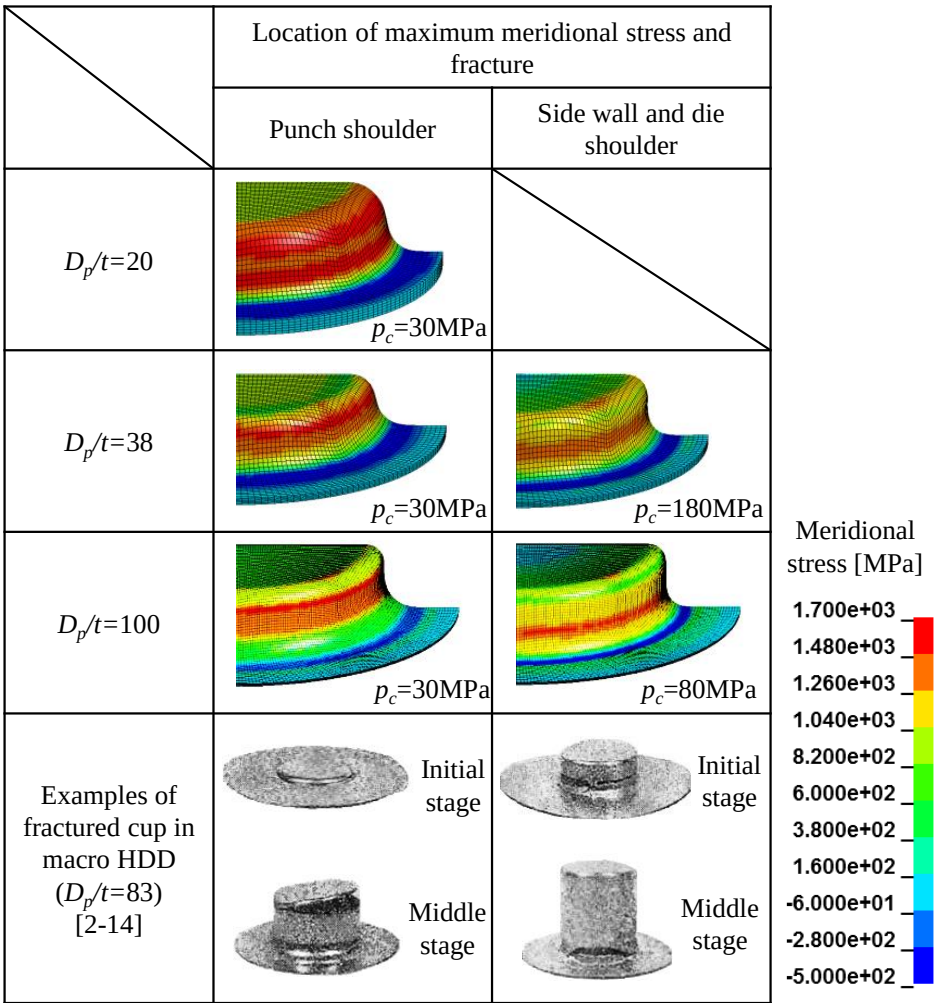

Fig. 2.18 Shift of locations of maximum meridional stress and fracture by counter pressure applied in MHDD (S/D_p =0.25).

2.4.3. Scale dependent strategy for tooling and process variable design in MHDD

(1) Friction holding effect

The friction holding effect can be obtained when the blank contact with the punch side wall and the friction between them reduces the applied load to the blank at punch shoulder. The friction holding effect was evaluated by the contact position from the punch shoulder. **Fig. 2.19** shows the variation of contact region between the blank and punch during MHDD process for different D_p/t values. As shown in the contact pressure distribution in the inserted figure in **Fig. 2.19**, the contact region includes the contact pressure distribution and its area increases as the punch travels. The contact region is zero at the early stage which is the contact stage between blank and punch shoulder at any conditions. From the certain punch stroke, the blank starts to contact with the punch side wall and the contact region increases as the punch travels.

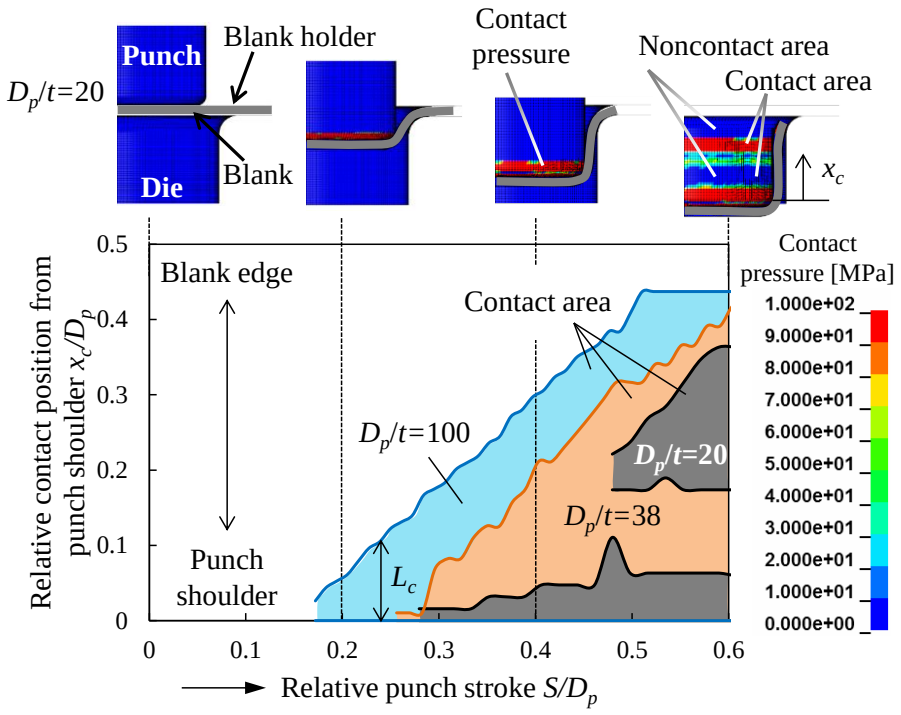

Fig. 2.19 Variation of contact region between blank and punch during MHDD process for different D_p/t values (Geometrical variation of tool, p_c =100MPa).

Fig. 2.20 can be obtained by adding the effect of counter pressure in **Fig. 2.19**. In the case of geometrical variation of tools as shown in **Fig. 2.20(a)**, the contact region between blank and punch exists only at the cup edge at p_c =0MPa. By increasing the counter pressure, the contact region increases and the contact timing becomes earlier. However, as D_p/t decreases, the blank hardly fits with the punch side and the high counter pressure is required to obtain the early contact at the early stage. For the variation of punch diameter as shown in **Fig. 2.20(b)**, the contact region increases at D_p/t =100 and it decreases at D_p/t =20 as compared with the geometrical variation of tools as shown in **Fig. 2.20(a)**.

Fig. 2.21 shows the effect counter pressure on contact length in different D_p/t values, which was calculated from the relationship between the counter pressure and contact region at the certain punch stroke in **Fig. 2.20**. It can be seen that the contact length increases with the increase of the counter pressure. The minimum counter pressure in which the blank contacts to the punch side and the friction holding effect can be obtained differs from D_p/t. In addition, by comparing between the geometrical variation of tools and the variation of punch diameter, it can be seen that the contact length also increases as r_p/t decreases. In the case of D_p/t =20, the excessive thickness reduction at the punch shoulder occurs before the contact region appears at the relative punch stroke S/D_p =0.25.

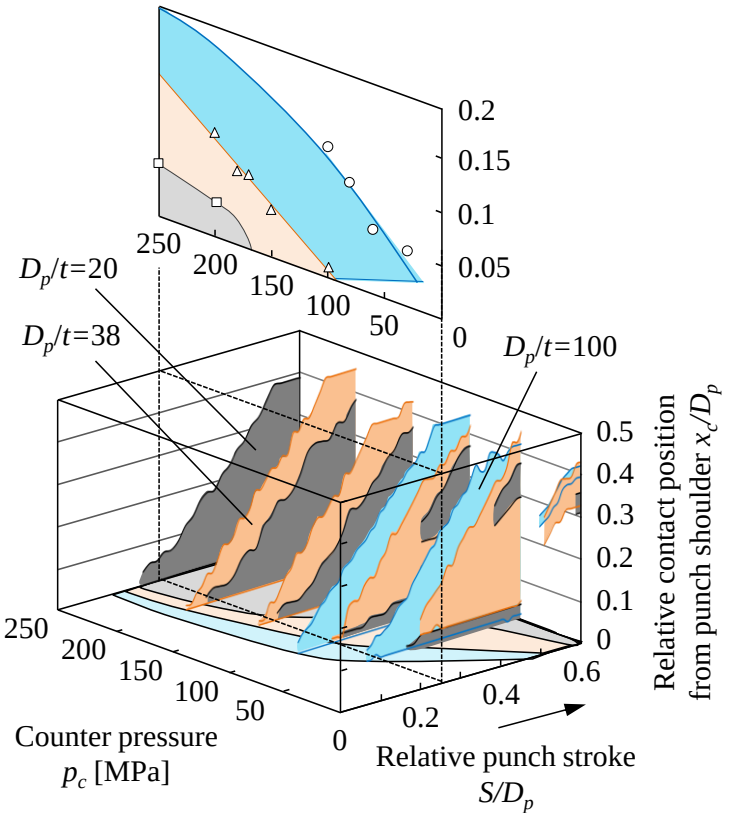

(a) Geometrical variation of tools

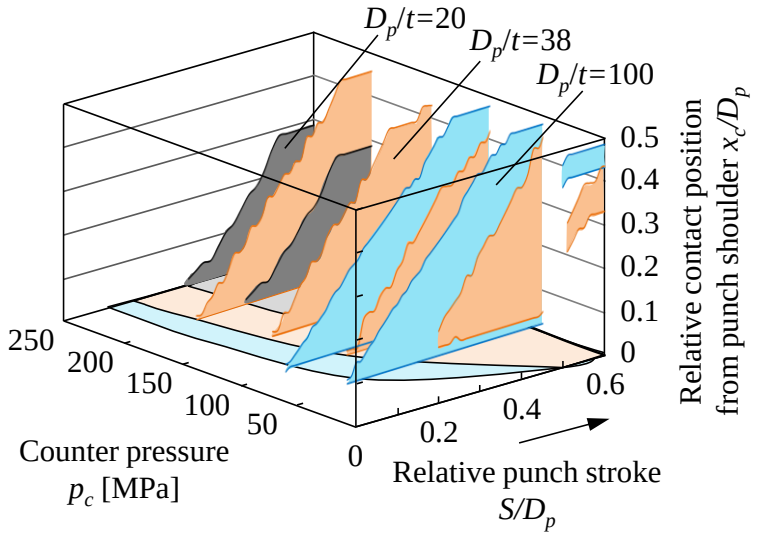

(b)Variation of punch diameter

Fig. 2.20 3-D representation of variation in relative contact region between blank and punch during the process for different counter pressures and D_p/t values.

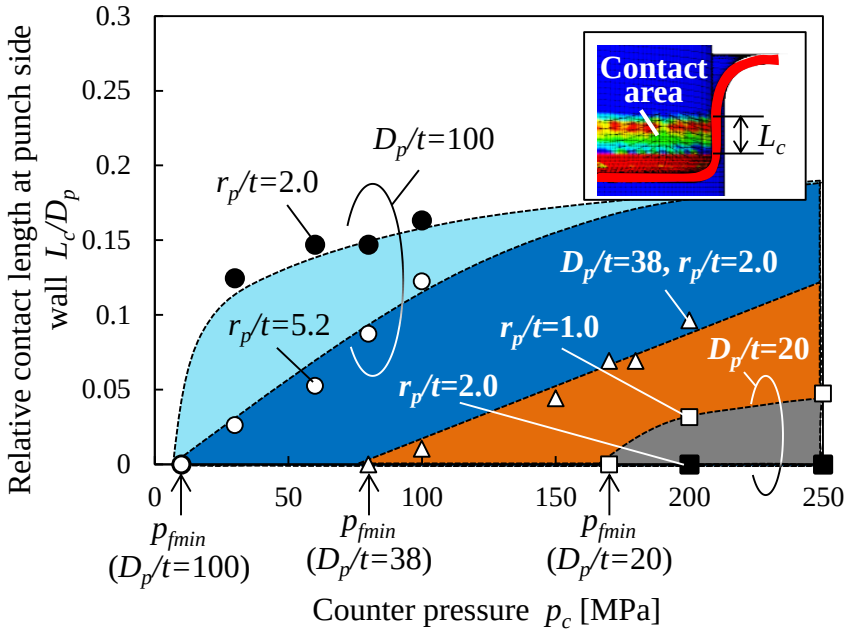

Fig. 2.21 Effect of counter pressure on relative contact length in different D_p/t values (S/D_p =0.25).

Fig. 2.22 shows the effect of D_p/t on minimum required fluid pressure for friction holding effect p_{fmin}. p_{fmin} is defined as the counter pressure when the blank starts to contact with the punch side wall and the friction holding effect is obtained. p_{fmin} increases with decreasing D_p/t at any tooling conditions. For D_p/t =20 in the variation of punch diameter, the friction holding effect cannot be obtained because the thickness reduction increases becomes significant as the counter pressure increases before the friction holding effect occurs. From these results, it was revealed that the minimum required fluid pressure for friction holding effect does not strongly depends on the relative punch shoulder radius to thickness r_p/t, but depends on the relative punch diameter to thickness D_p/t.

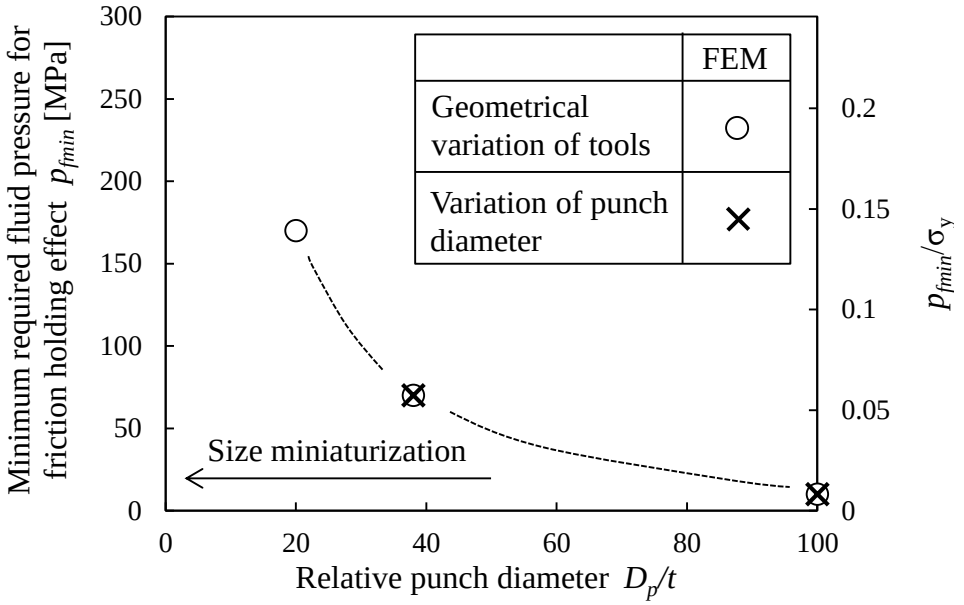

Fig. 2.22 Minimum required fluid pressures for friction holding effect for various D_p/t values (S/D_p =0.25).

(2) Hydrodynamic lubrication effect

The hydrodynamic lubrication is known as the effect to reduce the friction force between the die, blank holder and blank. This effect is important to improve the forming limit in MHDD. When the hydrodynamic lubrication is induced, the force pushing the blank from the contact start point at die shoulder to blank edge occurs by the counter pressure as shown in **Fig. 2.23**. To induce the hydrodynamic lubrication, this force pushing the blank should be larger than the contact reactive force between the blank and die [2-11]. For this reason, the required fluid pressure for hydrodynamic lubrication p_h is calculated from the contact pressure between the blank and die.

Fig. 2.24 shows the effect of D_p/t on required fluid pressure for hydrodynamic lubrication p_h. As the comparison, the theoretical results calculated by Eq. (2.50) are also shown in **Fig. 2.24**. In geometrical variation of tools, p_h increases as D_p/t decreases in both of FEM and theory. On the other hand, p_h is almost constant in variation of punch diameter. It means that p_h does not depend on the relative punch diameter to thickness D_p/t, but mainly depends on the relative die shoulder radius to thickness r_d/t. Similar behavior is experimentally observed in conventional HDD as shown in **Fig. 2.25** [2-15]. The FEM results are qualitatively in a good agreement with theoretical results although the FEM result is lower than that in theoretical results. This difference may be caused by the assumption of uniform thickness and no consideration of blank deformation by fluid pressure in theoretical model. **Fig. 2.26** shows the effects of D_p/t and r_d/t on required fluid pressure for hydrodynamic lubrication p_h. In the same r_d/t, p_h is almost the constant over $D_p/t = 50$; however, it drastically increases under $D_p/t = 50$. Furthermore, the level of p_h uniformly decreases in any D_p/t values. The die shoulder radius should be large to induce the hydrodynamic lubrication in MHDD and the punch diameter also affects it under $D_p/t = 50$.

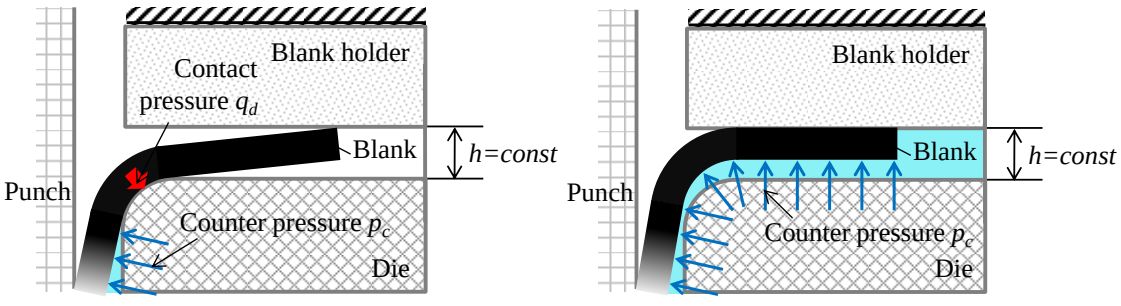

(a) At solid contact between blank and die (b) At hydrodynamic lubrication

Fig. 2.23 Schematics of blank state and forces to induce hydrodynamic lubrication.

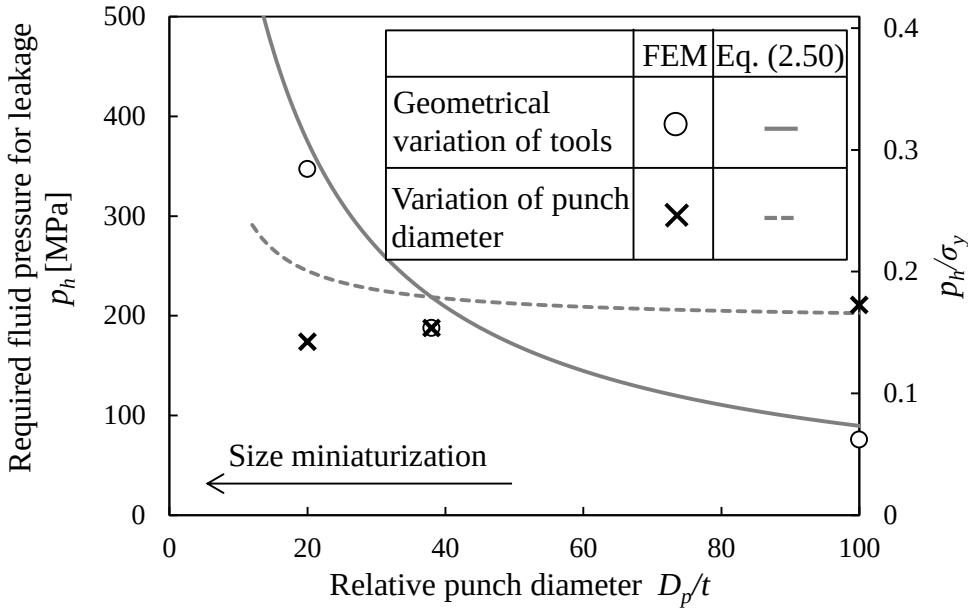

Fig. 2.24 Required fluid pressures for hydrodynamic lubrication in various D_p/t values.

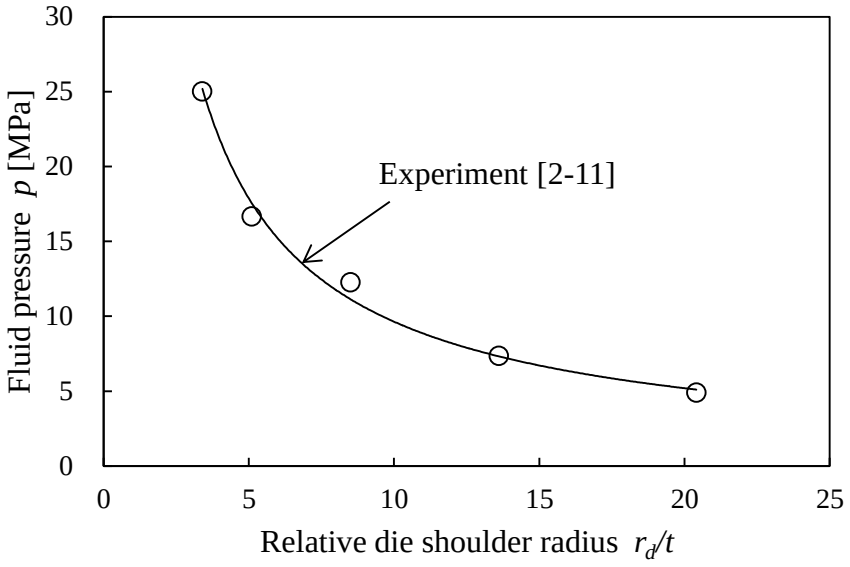

Fig. 2.25 Effect of r_d/t on generated fluid pressure to leak the fluid medium in experiment.

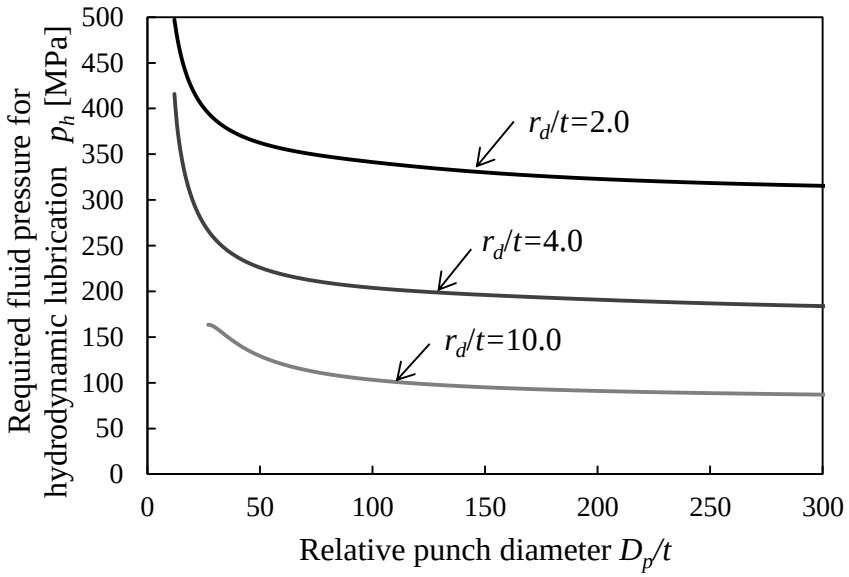

Fig. 2.26 Required fluid pressure for hydrodynamic lubrication in various D_p/t and r_d/t values.

(3) Compression effect of blank edge by radial pressure

The compression effect of blank edge by radial pressure applied to blank edge can reduce the meridional stress by applying the compression stress at flange area to improve the forming limit. To investigate the effect of D_p/t on compression effect, the normalized reduction of maximum effective punch force by applying radial pressure $\Delta\bar{P}_{Emax}$ is evaluated as shown in **Fig. 2.27**. $\Delta\bar{P}_{Emax}$ is almost constant at any D_p/t in both conditions of geometrical variation of tools and variation of punch diameter. It means that $\Delta\bar{P}_{Emax}$ is not depended on any relative tooling feature sizes D_p/t, r_p/t and r_d/t. The FEM results is larger than that in theoretical results. The thickening behavior at flange area is not considered in theoretical model. The area of blank edge and the compression force by radial pressure in theory is smaller than that in FEM. It is the reason why $\Delta\bar{P}_{Emax}$ becomes small in theory.

As mentioned above, the required fluid pressure for the friction holding and hydrodynamic lubrication effects depend on the relative punch diameter and die shoulder radius to thickness D_p/t, r_d/t, respectively, although the compression effect does not depend on any relative tooling feature sizes. Moreover, it was clarified that the ultra high pressure p_c >100MPa is required to improve the forming limit by obtaining the friction holding and hydrodynamic lubrication effects. In conventional macro HDD, the applied fluid pressure is normally less than p_c =30MPa for pure aluminum and p_c =50MPa for mild steel [2-16]. The scaling down of target size in MHDD causes the increase of required fluid pressure.

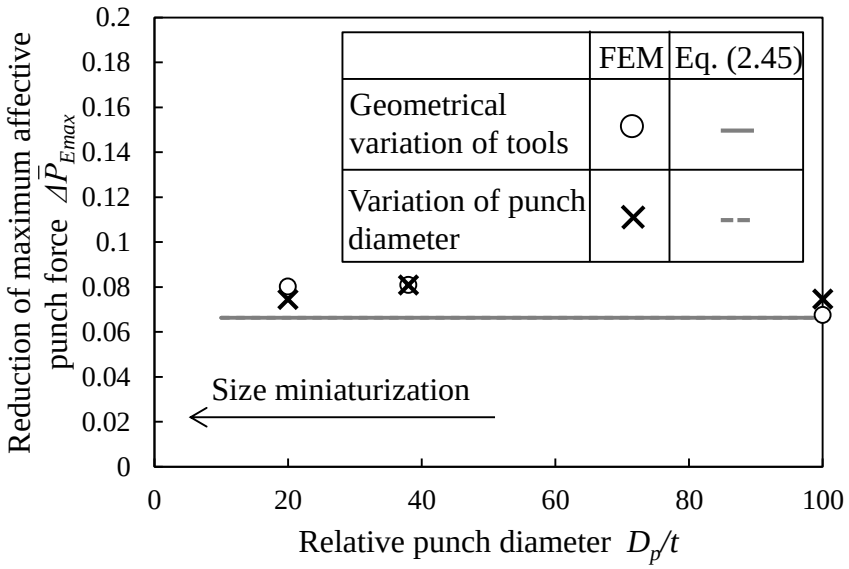

Fig. 2.27 Reductions of maximum effective punch forces by radial pressure applied to blank edge ($p_c = p_r$ =100MPa).

2.4.4. Scale dependence of fracture prevention mechanism in MHDD

(1) Friction holding effect

Fig. 2.28 shows the effects of counter pressure, D_p/t and r_p/t on meridional stress distribution. In geometrical variation of tools, the high applied force at punch shoulder can be reduced by applying p_c =100MPa at D_p/t =100 because the friction holding effect occurs at punch side wall. At D_p/t =20 and 38, the meridional stress at punch shoulder cannot be reduced significantly. It is because the contact region decreases and the contact timing becomes late when the foil thickness become relatively thick to the tool dimension at small D_p/t as shown in **Figs. 2.19** and **20**. Therefore, the friction holding effect cannot be obtained in the case of D_p/t =20 and 38.

On the other hand, in variation of punch diameter, the friction holding effect cannot be obtained at D_p/t =20 and 38, but can be obtained at D_p/t =100 as with geometrical variation of tools. At D_p/t =100, the friction holding effect occurs at p_c =60MPa in variation of punch diameter and it is lower than that in geometrical variation of tools, even though the punch shoulder radius in variation of punch diameter is smaller. It is because the small r_p/t causes the early contact between the blank and punch at the side wall and the increase of contact region as shown in **Fig. 2.21**.

Generally, when the tooling dimensions and material sizes is scaled down in geometrical similarity, p_{fmin} does not change. However, becomes relatively larger than the minimum manufacturable thickness in micro scale, the relative punch diameter D_p/t because the tooling dimensions, although the relative length of side wall L/D_p is almost constant. Therefore, Therefore, the minimum required fluid pressure for friction holding effect p_{fmin} increases as D_p/t decreases as shown in Eq. (2.48). It is because the relative stiffness of blank increases with decreasing D_p/t.

On the other hand, as r_p/t decreasing, L/D_p also decreases at the same time. The effect of L/D_p on p_{fmin} is more significant than the effect of r_p/t because L/D_p is the square parameter as shown in Eq. (2.48). It means that the resultant force by the counter pressure acting on the side wall is larger than the relative bending stiffness with the decrease of r_p/t. Therefore, with decreasing r_p/t, the blank easily contact with the punch side wall and the friction holding effect can be easily obtained as shown in **Figs. 2.21** and **28**.

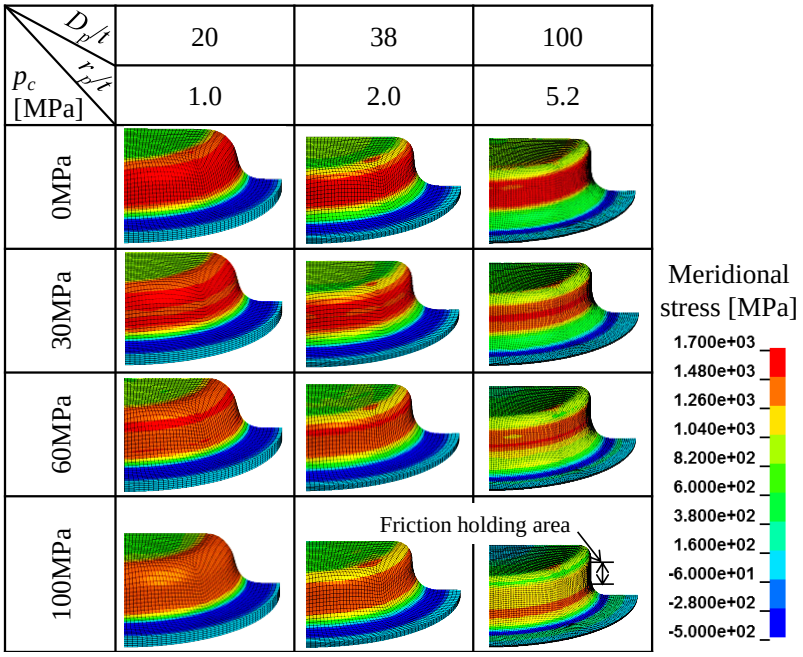

(a) Geometrical variation of tools

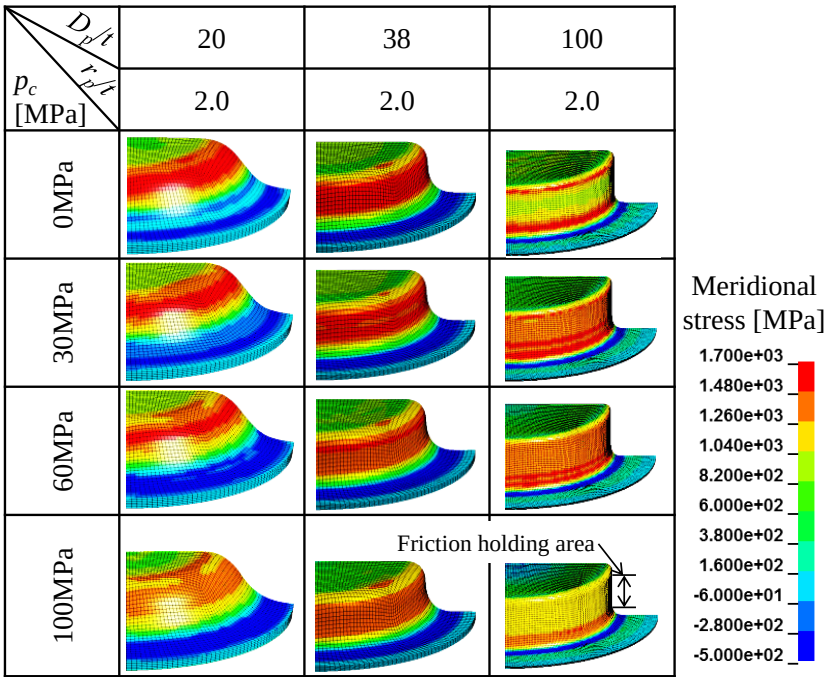

(b) Variation of punch diameter

Fig. 2.28 Effect of counter pressure, D_p/t and r_p/t on meridional stress distribution (s/D_p =0.25).

(2) Hydrodynamic lubrication effect

In conventional macro HDD with constant blank holder force, it was reported that the contact pressure not only at the die shoulder but also at flange area influences the required fluid pressure for hydrodynamic lubrication p_h [2-11]. However, in MHDD with constant gap method, the contact pressure is concentrated at the die shoulder as shown in **Fig. 2.29**. This contact pressure at die shoulder and its area increase as r_d/t decreases in geometrical variation of tools. In addition, the blank and the die does not contact uniformly but contacts at boundary between the flange, side wall and die shoulder. On the other hand, the contact state in variation of punch diameter is almost the same at any r_p/t values. It means that p_h does not depend on D_p/t, but depends on r_d/t as with **Fig. 2.24**. It was clarified that the same tendency, which the required fluid pressure for hydrodynamic lubrication p_h increases with decreasing r_d/t, appears not only in conventional macro HDD but also in MHDD with scaling down of target size.

D_p/t	20	38	100
r_d/t	2.0	4.0	10.6
Contact pressure	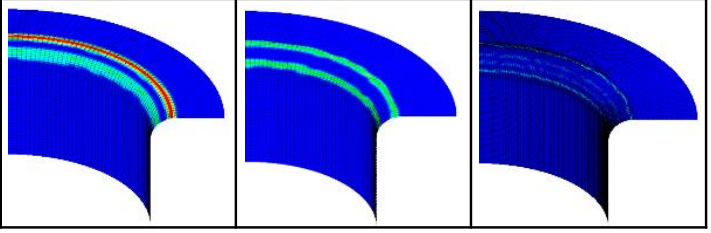		

(a) Geometrical variation of tools

D_p/t	20	38	100
r_d/t	4.0	4.0	4.0
Contact pressure	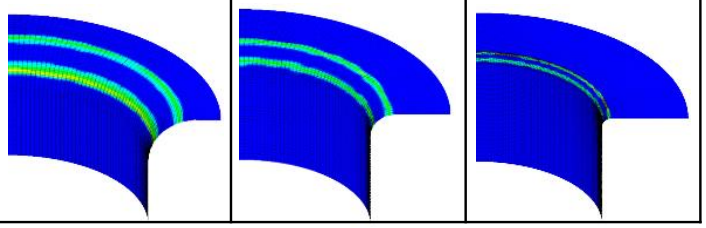		

(b) Variation of punch diameter

Fig. 2.29 Contact pressure distribution at die shoulder for various D_p/t and r_d/t values (p_c =0MPa).

(3) Compression effect of blank edge by radial pressure

Generally, the radial pressure can apply the compression force at blank edge and can improve the forming limit by reducing the meridional tensile stress at side wall [2-15] as shown in **Fig. 2.30**. This reduction of meridional stress at side wall $\Delta\sigma_\varphi$ is almost the same and its reduction amount is also the same with radial pressure p_r at any D_p/t values as shown in **Fig. 2.31**. It means that the meridional stress at side wall is reduced as large as the radial pressure. Moreover, the compression effect of blank edge by radial pressure does not depend on the relative tooling feature size to thickness, but it depends on the flow stress of blank and the radial pressure itself. That is why the compression effect of blank edge by radial pressure is not influenced by D_p/t and r_d/t as shown in **Fig. 2.27**.

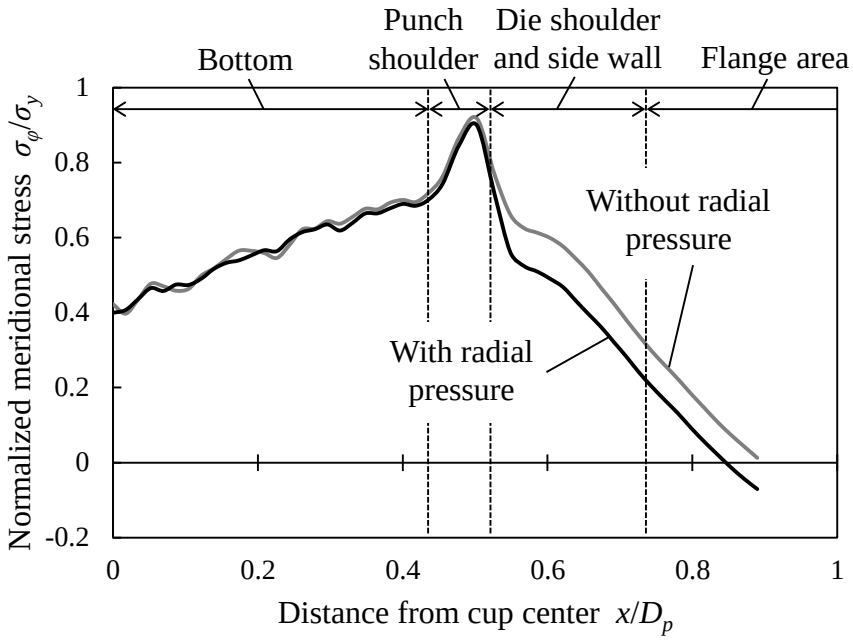

Fig. 2.30 Reduction in meridional stress from flange area to side wall by radial pressure (D_p/t =38).

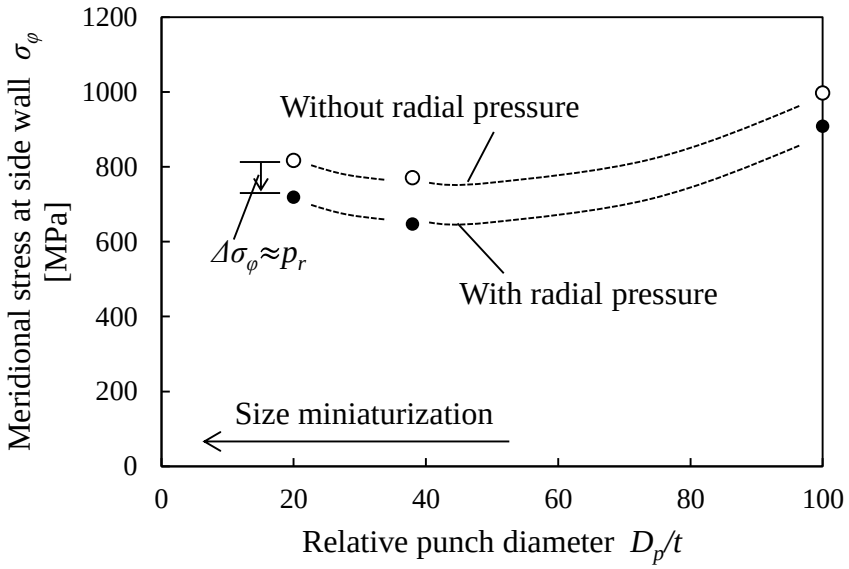

Fig. 2.31 Reductions in meridional stresses at side wall by radial pressure for various D_p/t values in geometrical variation of tools ($\Delta\sigma_\varphi$: Reduction in meridional stress).

2.4.5. Verification and size effect prediction on lubricated OLPs by fluid pressure in MHDD

In MHDD, not only the hydrodynamic lubrication, but also boundary and mixed lubrications exist during the MHDD process. In general, the lubricant cannot be kept in OLPs which connect to the edge of the blank in boundary and mixed lubrications in conventional micro forming [2-3]. On the other hand, if the fluid medium can be filled in the OLPs in MHDD as shown in **Fig. 2.5**, the lubricant can be kept in the OLPs and the friction coefficient can be reduced in micro scale. To confirm this phenomenon, an evaluation test for OLPs utilizing liquid was carried out and the size effect of lubricated OLPs by fluid pressure is theoretically investigated.

(1) Evaluation test for OLPs utilizing liquid

The same material used in the MHDD experiment was used. The blank diameters are D_0 =1.7 and 15mm. The blank is compressed by the tools under the contact pressure of approximately 20MPa and the liquid is filled in the tool as shown in **Fig. 2.31**. The area into which the colored liquid intruded is colored. After the colored liquid is dried, the blank is taken out. Thus, the area into which the liquid intruded can be visualized. The appearance of the blank was observed using a digital microscope and the pictures were digitized.

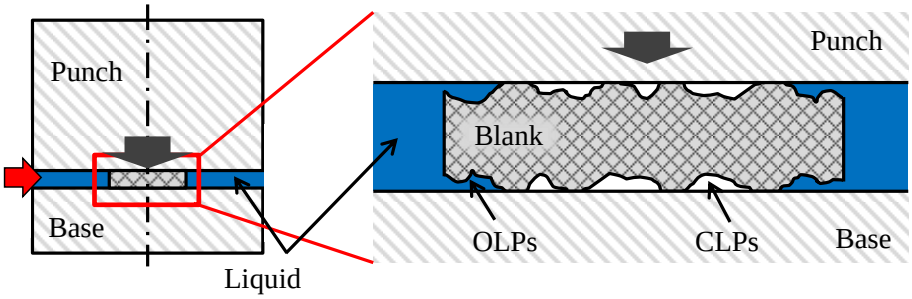

Fig. 2.31 Schematic of evaluation test for OLPs utilizing liquid.

(2) Lubrication model by fluid pressure in MHDD

The friction force and friction coefficient in several lubrication conditions in MDD and MHDD shown in **Fig. 2.5** were calculated. To confirm the tribological size effect in MHDD, the lubricated OLPs by counter and radial pressure was adopted. As a comparison, dry friction and lubrication in MDD, and hydrodynamic lubrication in MHDD were compared. For MHDD with lubricated OLPs by counter and radial pressures, the counter and radial pressures $p_c = p_r$ =100MPa and the friction coefficient in lubricated OLPs by fluid pressure μ_{fluid} =0.03. For hydrodynamic lubrication, they are set up at 180MPa based on Eq. (2.50). The friction coefficients for each condition are listed in **Table 2.2**.

(3) Discussion on lubricated OLPs by fluid pressure in MHDD

Fig. 2.32 shows the appearance of OLPs with the intruded liquid for different blank diameters. For both blank diameters, the outer edge of the blank was colored. This colored area contacts with the blank edge and does not appear in the inner area of the blank as shown in **Fig. 2.33**. This means that the fluid medium was poured into the OLPs. The average widths of the OLPs for D_0 =1.7 and 15mm are approximately w_{ave} =215 and 135μm, respectively. The scale factors for both blank diameters are approximately $\lambda =$ 4.0 and 55.6. Thus, the fraction of OLPs increases as the blank diameter decreases. Similar results were reported in a conventional compression test for a small specimen [2-17]. For a blank diameter of 1.7mm, the width of the OLPs is not uniform. This is because the tool surface is not exactly parallel to the blank surface. This means that the contact area between the blank and the tool is displaced from the center position and alters the shape of the circle. At the blank edge, the shear drop exists because the blank is fabricated by the blanking. In the area of the shear drop, the blank does not have contact with the tool and this area is included in the OLPs. From these results, it could be seen that the fluid medium can be kept at the OLPs by applying the fluid pressure and it induces lubrication in OLPs.

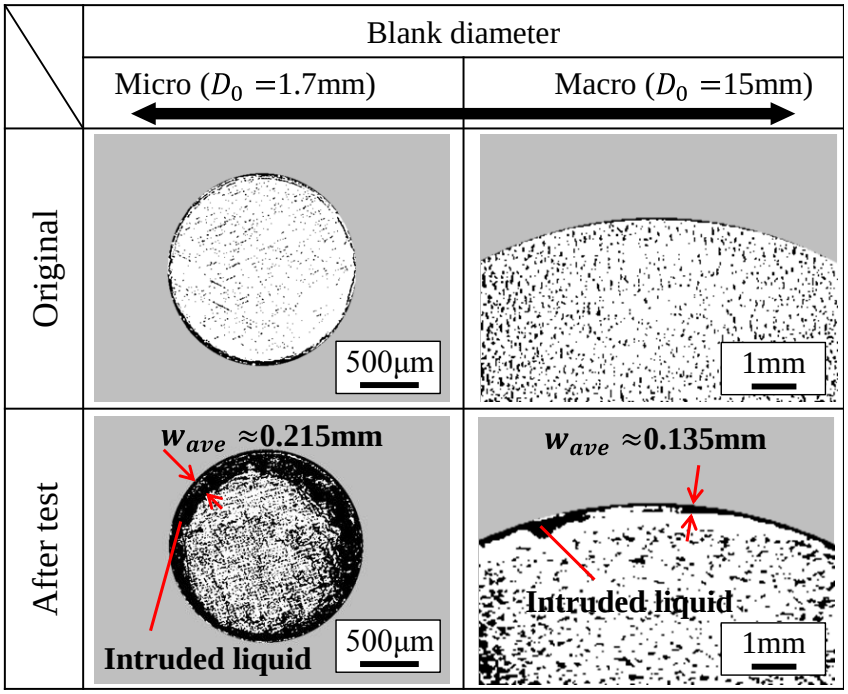

Fig. 2.32 Appearance of OLPs with intruded liquid for different blank diameters.

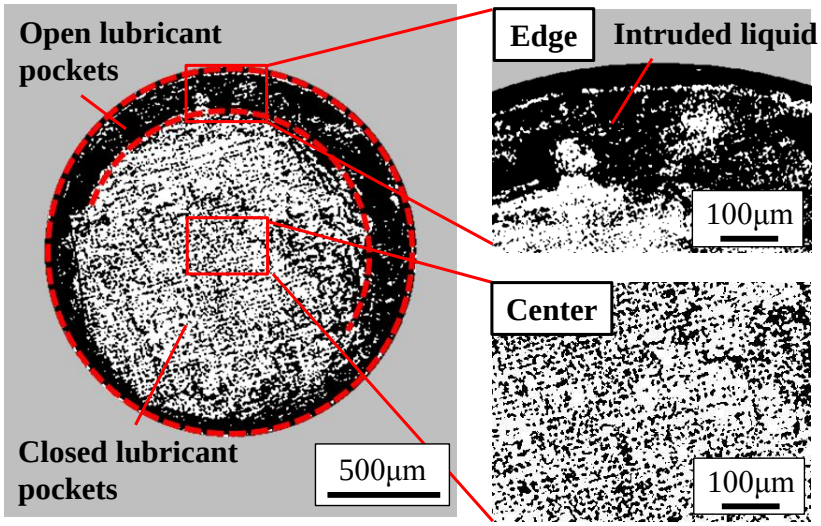

Fig. 2.33 Appearance of OLPs and CLPs on blank (D_0 =1.7mm).

As mentioned above, the OLPs can be filled with the fluid medium by applying fluid pressure. This means that the lubricant can be kept and the friction coefficient can be reduced on OLPs in MHDD. Based on this result, the scale dependences of maximum friction force for different lubrication conditions in MDD and MHDD were calculated as shown in **Fig. 2.34(a)**. In MDD with dry friction, the friction force is constant because the friction coefficients in the OLPs and CLPs are the same. The friction coefficient does not change in macro and micro scales. For MDD with lubrication, the friction force increases with scaling down to micro scale because the fraction of OLPs increases because it cannot keep the lubricant. This causes the increase of the friction coefficient and the friction force in MDD. The same behavior has been reported in previous research into conventional micro forming [2-4]. On the other hand, in MHDD with lubricated OLPs by counter and radial pressures, the friction force decreases with scaling down. This behavior is the opposite of the tribological size effect in conventional micro forming. The OLPs can be filled with the fluid medium by applying fluid pressure. In addition, the fraction of OLPs increases with scaling down, and the friction coefficient can be reduced. Therefore, the average friction coefficient in the flange area decreases with the decrease of specimen size in MHDD with lubricated OLPs by counter and radial pressures as shown in **Fig. 2.34(b)**. In comparison with hydrodynamic lubrication conditions, the friction force in MHDD with lubricated OLPs by counter and radial pressures is large in the macro scale, but is not very different in the micro scale in which λ is under 5. It was found that the friction force can be reduced in the micro scale without hydraulic lubrication by applying fluid pressure to the OLPs.

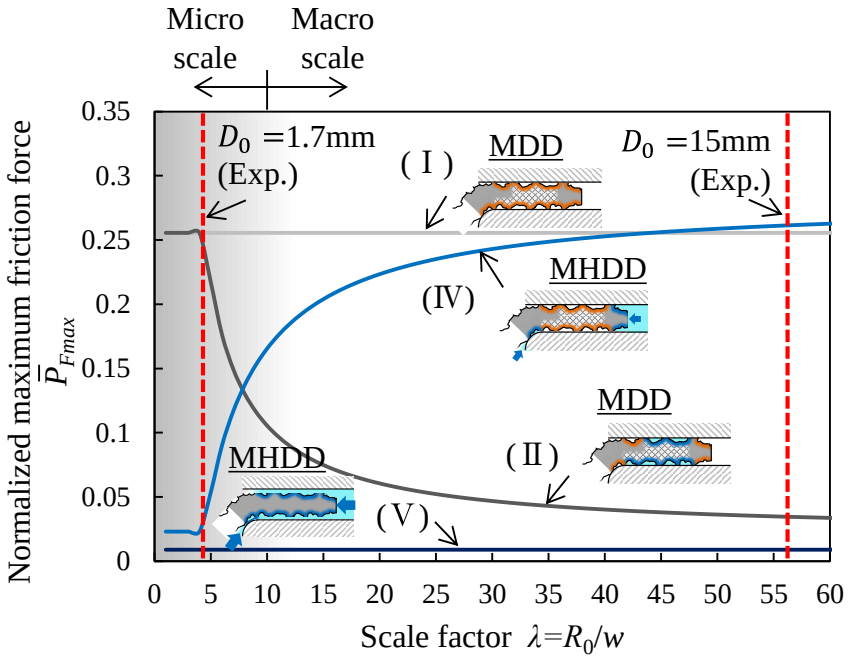

(a) Normalized maximum friction forces

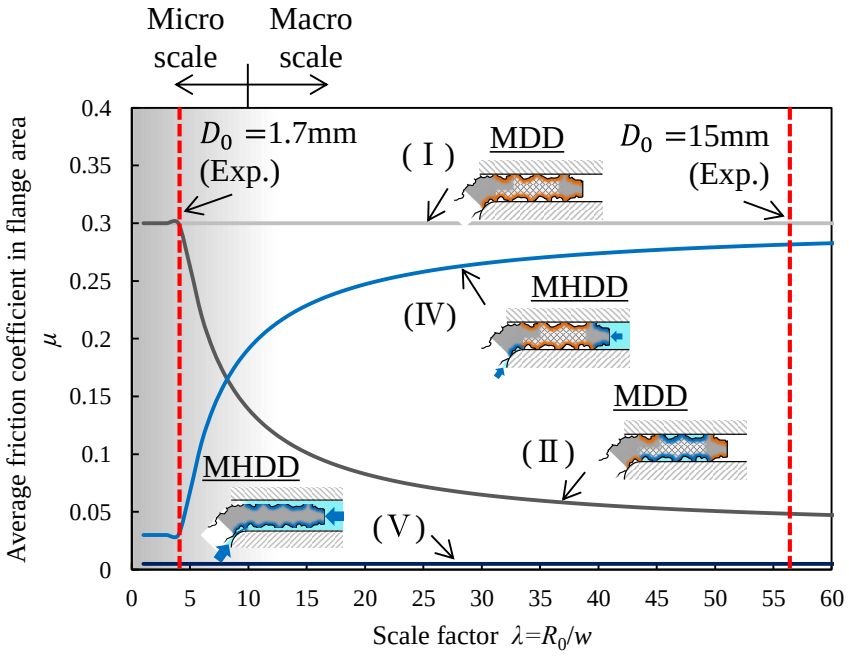

(b) Average friction coefficients

Fig. 2.34 Scale dependences of normalized friction forces and average friction coefficients in flange area at maximum punch force for different lubrication conditions in MDD and MHDD introduced in Eqs. (2.37) and (2.44) ((I) Dry friction, (II) Lubrication, (IV) Lubricated OLPs by counter and radial pressures, and (V) Hydrodynamic lubrication).

2.5. Concluding Remarks

In this chapter, the fluid pressure, tooling conditions to obtain the fracture prevention effects and improve the shape accuracy in MHDD process were designed based on tribological size effect and relative tooling feature size using theory and FEM. The following conclusion may be drawn.

1) The tribological behavior in MHDD is characterized by the high sealablity to induce hydrodynamic lubrication and the lubricated OLPs by fluid pressure, which are caused by the relative tooling feature size and surface topography, respectively. The ultra high pressure p ≥100MPa for stainless steel (p/σ_y ≥0.16) is required to induce the hydrodynamic lubrication in MHDD. The application of radial pressures is also effective to reduce the friction without the hydrodynamic lubrication due to the lubricated OLPs in MHDD.

2) The application of counter pressure can improve the drawability because the location of maximum meridional stress at punch shoulder area is shifted to die shoulder area when the blank contacts with the punch side wall and the friction holding effect is obtained. It was theoretically revealed that r_p/t, L/D_p and D_p/t influences the shape accuracy at side wall and friction holding effect. The required fluid pressure for friction holding effect also becomes more than p_c =100MPa in MHDD with small relative tooling feature size.

3) The parameter about target size D_p/t has a dominant influence on the shape accuracy. The decease of D_p/t results the decrease of the shape accuracy and the friction holding effect due to the increase of relative bending stiffness. The improvement of shape accuracy cannot be expected when D_p/t is too small.

4) When the parameter about the target shape r_p/t and r_d/t decreases, the resultant force by the counter pressure acting on the side wall decrease due to the decrease of relative length of side wall L/D_p decreases. It results the decrease of the shape accuracy and friction holding effect.

As mentioned above, the tribological behavior in MHDD can be improved by applying the ultra high pressure and using lubricated OLPs, although the conventional micro sheet forming has the low lubrication effect and easily causes the adhesion and seizure. Furthermore, the application of ultra high pressure (p_c ≥100MPa) can possibly induce the fracture prevention effects and improve the shape accuracy in MHDD. From the above, the advantages of ultra high fluid pressure in micro sheet hydroforming was clarified. In addition, not only the required fluid pressure, but also the proper

tooling conditions, such as the parameter about the target size D_p/t, the parameters about the target shape r_p/t and r_d/t, in MHDD were revealed. Thus, the MHDD process has the scale dependence and should be considered the above characteristics when its process is designed.

References

[2-1] S.H. Zhang, J. Danckert, Development of hydro-mechanical deep drawing, Journal of Materials Processing Technology, 83, (1998), 14-25.

[2-2] Y. Kasuga, N. Nozaki, Pressure lubricated deep drawing (1st report, conception of the mechanism, characteristic and possibilities), Transactions of the Japan Society of Mechanical Engineers (in Japanese), 24-146, (1958), 720-727.

[2-3] U. Engel, Tribology in microforming, Wear, 260, (2006), 265-273.

[2-4] F. Vollertsen, Z. Hu, Tribological size effects in sheet metal forming measured by a strip drawing test, Annals of the CIRP, 55-1, (2006), 291-294.

[2-5] M.W. Fu, B. Yang, W.L. Chan, Experimental and simulation studies of micro blanking and deep drawing compound process using copper sheet, Journal of Materials Processing Technology, 213, (2013), 101-110.

[2-6] Y. Saotome, K. Yasuda, H. Kaga, Microdeep drawability of very thin sheet steels, Journal of Materials Processing Technology, 113, (2001), 641-647.

[2-7] K. Manabe, K. Soeda, T. Nagashima, H. Nishimura, Adaptive control of deep drawing using the variable blank holding force technique, Journal of the Japan Society for Technology of Plasticity (in Japanese), 33-375, (1992), 423-428.

[2-8] N. Kawai, Critical conditions of wrinkling in deep drawing of sheet metals (1st report, foundations of analyses and results for conditions of no blank-holding), Transactions of the Japan Society of Mechanical Engineers (in Japanese), 26-166, (1960), 850-873.

[2-9] M. Masuda, T. Murota, Revision of engineering plasticity, Yokendo, (in Japanese), (1980), 153-169.

[2-10] L. Peng, X. Lai, H.J. Lee, J.H. Song, J. Ni, Friction behavior modeling and analysis in micro/meso scale metal forming process, Materials and Design, 31, (2010), 1953-1961.

[2-11] Y. Kasuga, K. Kondo, Pressure lubricated deep drawing (3rd report, the pressure generated), Transactions of the Japan Society of Mechanical Engineers (in Japanese), 26-169, (1960), 290-1297.

[2-12] T. Shimizu, M. Yang, K. Manabe, Classification of mesoscopic tribological properties under dry sliding friction for micro forming operation, Wear, 330-331, (2015), 49-58.

[2-13] K. Manabe, T. Shimizu, H. Koyama, M. Yang, K. Ito, Validation of FE simulation based on surface roughness model in micro-deep drawing, Journal of Material Processing Technology, 204, (2008), 89-93.

[2-14] K. Nakamura, T. Nakagawa. Fracture mechanism and fracture control in deep drawing with hydraulic counter pressure – studies on hydraulic counter pressure forming I–, Journal of the Japan Society for Technology of Plasticity (in Japanese), 25-284, (1984), 831-838.

[2-15] K. Nakamura, T. Nakagawa, Radial pressure assisted hydraulic counter pressure deep drawing

– studies on hydraulic counter pressure forming Ⅱ-, Journal of the Japan Society for Technology of Plasticity (in Japanese), 26-288, (1985), 73-80.

[2-17] T. Nakagawa, K. Nakamura, H. Amino, Various applications of hydraulic counter-pressure deep drawing, Journal of Materials Processing Technology, 71, (1997), 160-167.

[2-16] J.H. Deng, M.W. Fu, W.L. Chan, Size effect on material surface deformation behavior in micro-forming process, Materials Science and Engineering A, 528, (2011), 4799-4806.

Chapter 3

Development of MHDD System and Its Basic Drawing Characteristics

3.1. Introduction

In Chapter 2, the micro hydromechanical deep drawing (MHDD) process was analytically designed based on the scaled dependence of tribological behavior and tooling feature size. It was clarified that the ultra high pressure has a possibility to improve the drawability and shape accuracy in micro sheet hydroforming. Furthermore, based on the relative tooling feature size, the appropriate tooling conditions were revealed to improve the shape accuracy and induce the fracture prevention effects, such as the friction holding effect, the hydrodynamic lubrication effect, and the compression effect of blank edge by radial pressure.

To realize the MHDD process, the press machines, tool sets, and hydraulic systems for high fluid pressure are required. Previously, only a few researches previously applied this hydroforming technique in micro sheet forming, such as the embossing using fluid pressure [3-1]. Not only the ultra high pressure, but also the normal level fluid pressure (p <100MPa) has not been applied in the micro deep drawing (MDD). Therefore, the design of guideline of forming system for the micro sheet hydroforming has not been sufficiently established. Additionally, because there is normally a leakage during the hydromechanical deep drawing [3-2], its hydraulic system and sealing method in MHDD are not simple as with the micro embossing [3-3], and micro bulging [3-4] using fluid pressure. Thus, a new concept for MHDD system is required.

In this section, MHDD system with simple structure, compact, and high forming accuracy is developed and its performance tests are carried out. Additionally, the effect of fluid pressure on basic drawing characteristics in MHDD is experimentally investigated.

3.2. Development of MHDD Apparatus

As mention in Chapter 1.3, there are some difficulties in tools and machines with scaling down. In micro scale, the required accuracies for tool, transfer, position and force controls are very high. Furthermore, there is a limitation of tooling size miniaturization due to the difficulty of manufacture of tiny and complex shape and the low stiffness of tiny and long tools.

Based on the difficulties and characteristics in micro scale, the design concept of the new MHDD apparatus is proposed as shown in **Fig. 3.1**. It includes simplification of the forming processes and apparatus structure and can be summarized as follows;

1) Adoption of one-stroke forming to avoid the need for material transfer and positioning control (coaxial multiple processes)
2) Adoption of a constant gap method to avoid the need for highly accurate force control for preventing wrinkling
3) Sealing and generation of stable fluid pressure by decreasing the clearance between tools to avoid the need for ultrafine flow-rate control
4) Adoption of a multi-axis system inside the die to avoid the need for a double-action mechanical press and to simplify the apparatus structure

Through these measures, a simple apparatus is realized, which enables the fabrication of components with a high accuracy by decreasing the number of control targets.

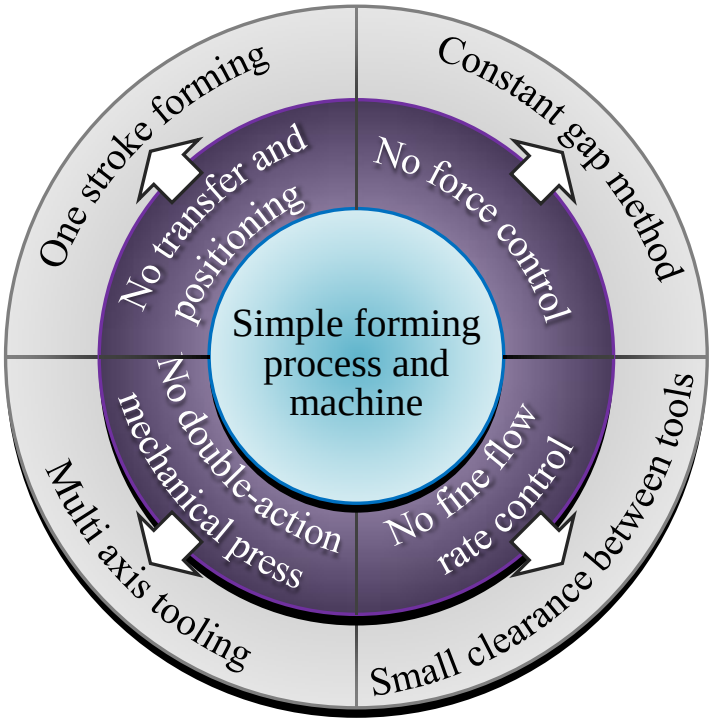

Fig. 3.1 Design concept of new MHDD apparatus.

3.2.1. One-stroke forming

One-stroke forming [3-5] is a forming method in which all the forming processes are carried out coaxially. It was developed to achieve the improvement of shape accuracy, miniaturization of machine, saving of energy and high efficiency.

Generally, the forming process is not finished in one step, but need to divide several steps. It is normally conducted by the transfer press machine which needs many tools and feeding devices. To save a number of tools and machines, space, and improve the shape accuracy, the one-stroke forming is getting a lot of attention, in which the material transfer is unnecessary. Hoden Seimitsu Kako Kenkyusho Co. Ltd. has developed one shot forming using the multi action press in macro scale as shown in **Fig. 3.2** [3-6]. It can conduct the several steps while the punch travels once in axial direction by controlling the movement of inner and outer slides separately. Aisin AW Co., Ltd. and Mori Iron Works Co., Ltd. have developed one-stroke press with multi action press to realize the inline production as shown in **Fig. 3.3** [3-7]. It can fabricate the products in one step, which is previously fabricated in 6~13 steps using the large transfer press. This one-stroke forming can not only miniaturize the machine, but also improve the positioning, avoid the eccentric load, and reduce the load capacity of press machine.

This method also has some advantages in micro scale. The feeding and positioning devices with high accuracy and expensive machine can be unnecessary. For this reason, the MHDD process adopts the one-stroke forming process, in which all the forming processes are carried out coaxially, material transfer becomes unnecessary and high shape accuracy is realized.

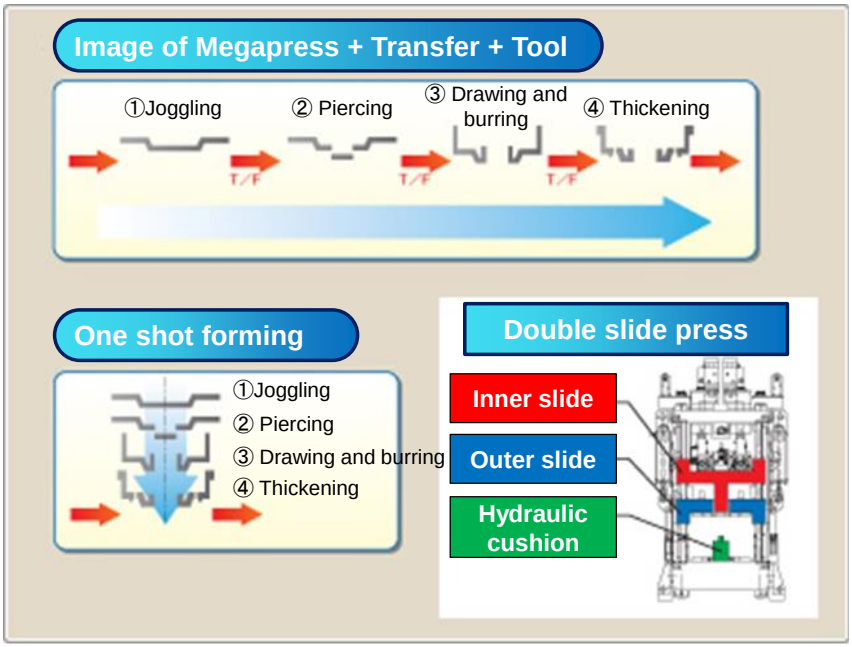

Fig. 3.2 Schematic illustration of 1 stroke forming by double slide servo press [3-6].

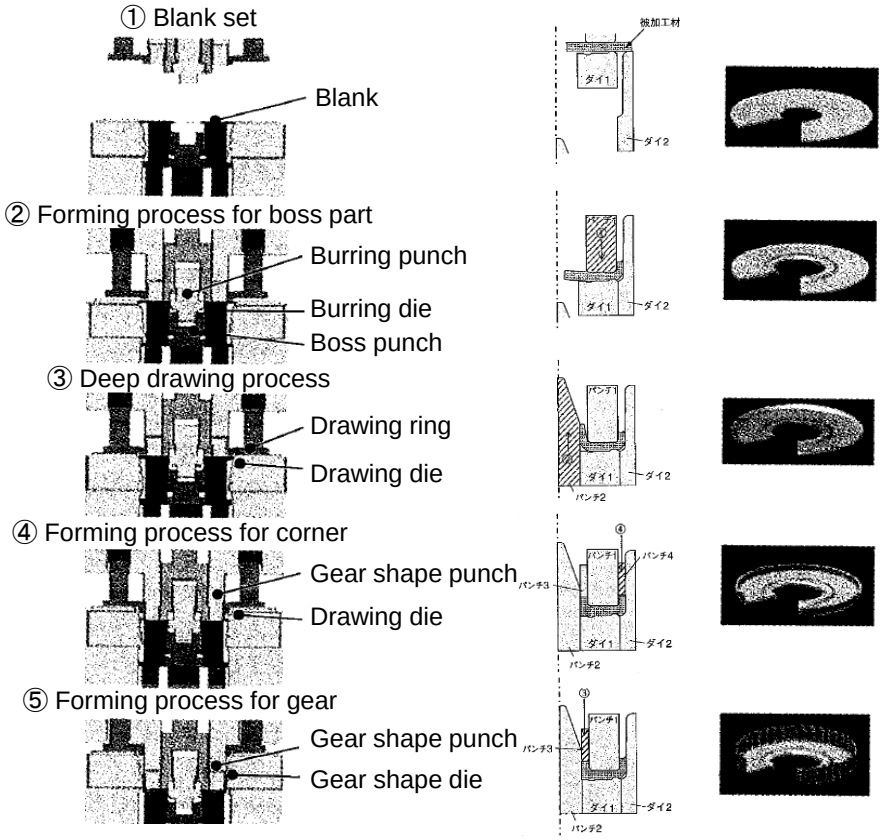

Fig. 3.3 Schematic illustration of one-stroke forming by multi-axis double-acting servo press [3-7].

3.2.2. Blank holder method

The blank holder method is important to eliminate the wrinkling and also affects the generation of fluid pressure in HDD. Therefore, it significantly affects the wrinkling and fracture limits. Manabe et al., classified and characterized the blank holder methods as listed in **Table 3.1** [3-8]. The constant blank holder force method is most popular in macro scale because most of press machine adopts the die cushion. On the other hand, it is difficult to control the blank holder force with high accuracy especially in micro scale. For this reason, the constant gap method, in which the gap between the die and blank holder is fixed during the forming process, was adopted in MHDD. It can stabilize the forming process and improve the productivity because highly accurate force or position controls are unnecessary. As mentioned above, the contact gap method is effective in MHDD.

Table 3.1 Blank holder method in cylindrical deep drawing [3-8].

Blank holder method	Blank holder force H	Blank holder pressure p	Schematic of each blank holder method and blank holder force curves
Constant blank holder force method	Constant	Various	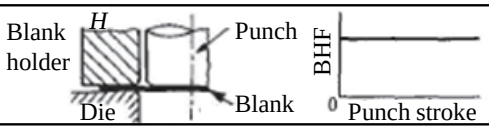
Constant gap method (Flat)	Various	Various	
Constant gap method (Taper)	Various	Various	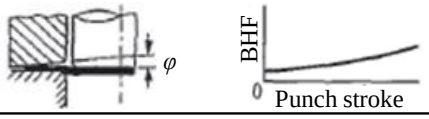
Various blank holder force method	Various	Various	—
Constant blank holder pressure method	Various	Constant	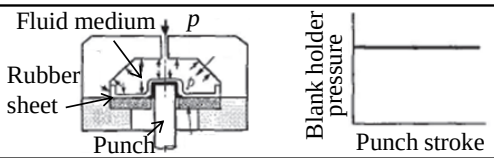
Taper blank holder method	Applicable for any methods	Applicable for any methods	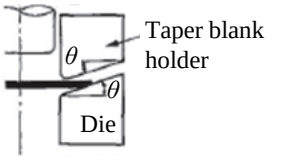

3.2.3. Sealing method

The sealing is important to generate the fluid pressure in HDD. The sealing location can be classified as follows;

1) Sealing between blank and die
2) Sealing at the edge of blank

The sealing between blank and die is required to generate the counter pressure in die cavity, and the sealing at the edge of blank is required to generate the radial pressure at blank edge after the fluid medium leaks between the blank and die as shown in **Fig. 3.4**. On the other hand, the sealing method normally can be classified as follows;

1) By contact pressure between blank and die caused
2) By sealing material

The contact pressure between the blank and die can be controlled by the blank holder force, die shoulder radius, and constant gap [3-9]. This is used to generate the counter pressure in die cavity. O-ring or and other materials are used as the sealing material to generate the radial pressure at blank edge.

However, the edge of blank cannot be sealed in MHDD by the sealing material because there is not space at the edge of blank at the blanking and drawing processes. Therefore, the clearance between the die and the bush was made small, as shown in **Fig. 3.4**, to seal at the edge of blank and generate the radial pressure at the blank edge. Considering the feasible shape accuracy, we adopted a clearance of 1 μm for the MHDD die used in this study.

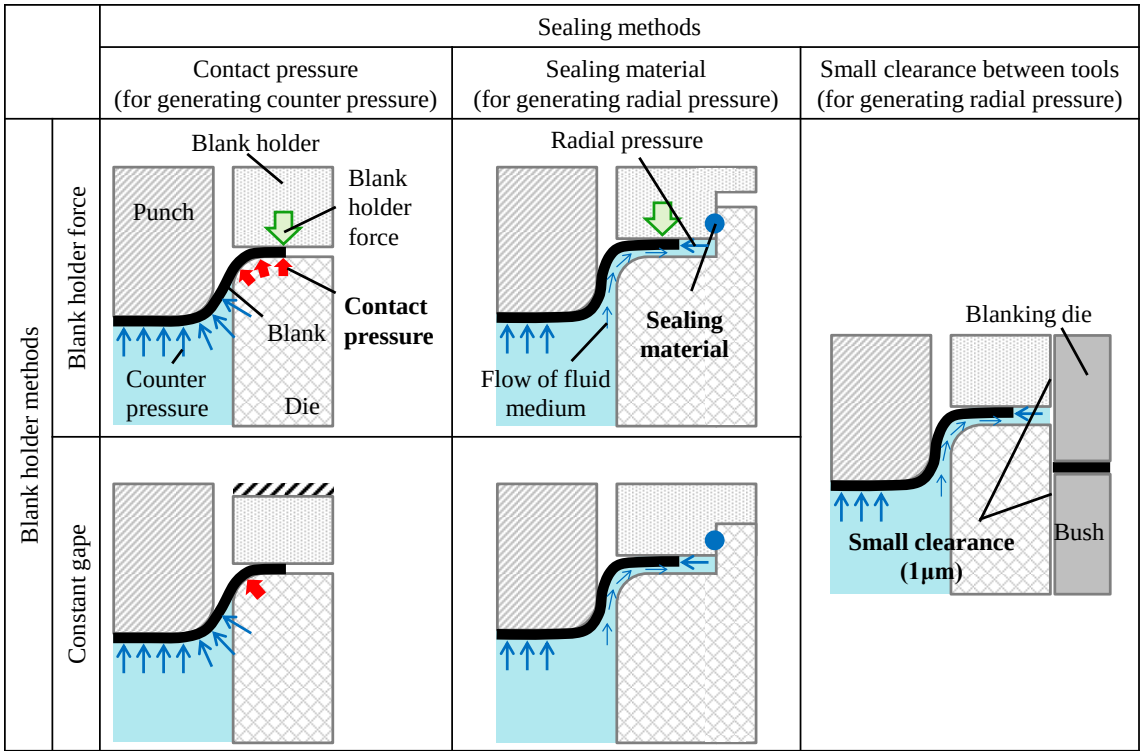

Fig. 3.4 Schematic illustration of pressure generation methods.

3.2.4. Forming processes

Fig. 3.5 shows the forming processes of the developed MHDD apparatus. It is divided 4 stages as follows;

1) The drawing die (blanking punch) is fixed, whereas the upper die including the drawing punch, the blank holder, the blanking die, and the bush moves downward. In this stage, the clearance between the drawing die and the bush becomes small, as a result, the die cavity is sealed and a counter pressure is generated.
2) When the upper die moves further downward, the killer sheet integrated with the blank holder is fixed because of the killer pins, causing the blank holder to be simultaneously fixed. Thus, only the drawing punch, blanking die, and bush move downward during the blanking process.
3) During drawing, the drawing punch moves downward while maintaining a constant gap between the drawing die and the blank holder. By controlling the length of the killer pins, an arbitrary constant gap is maintained.
4) When the stroke reaches the bottom dead point, the upper die starts to move upward and the drawn cup is taken out the knockout process.

As explained above, the four processes, i.e., pressure generation, blanking, drawing, and knockout, are performed coaxially.

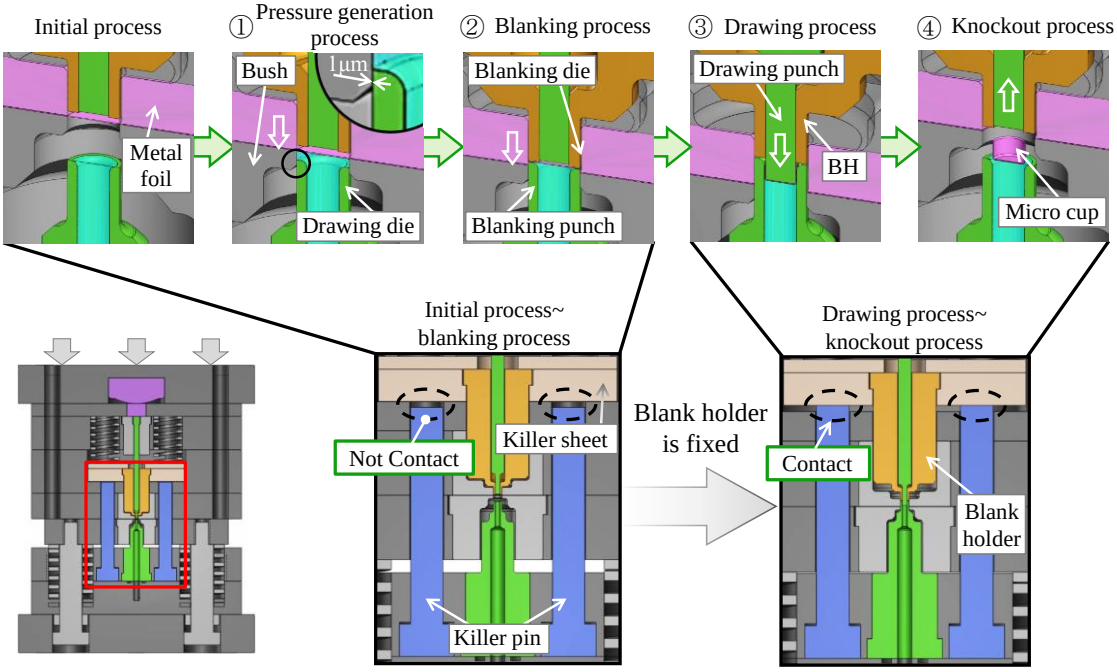

Fig. 3.5 Schematic illustration of MHDD processes and movement of tool.

3.2.5. Outline of MHDD Apparatus

(1) Tooling structure

Fig. 3.6 shows the schematic of the MHDD die and hydraulic system. In general, a multiaxial servo press is used for one-stroke forming, whereas the developed MHDD apparatus adopts a uniaxial servo press to perform one-stroke forming. Therefore, we design a die structure that can reproduce the behavior of a multiaxial servo press inside the die and simplify the structure of the entire MHDD apparatus. Each side of the MHDD die developed is as small as ~100 mm. The drawing die (blanking punch), blanking die, drawing punch, or bush is independently replaceable, accommodating various dimensions of components simply by changing individual parts. In addition, tools with a high shape accuracy were used; the tolerance of the blanking and drawing tools are ±0.001 and ±0.010 mm at the flat and curved parts, respectively. To measure the punch force, an ultra small compression-type load cell with a rating capacity of 20kN (KYOWA : LMR-S-20KN) was incorporated in the die so that the force directly applied to the drawing punch is transferred to the load cell.

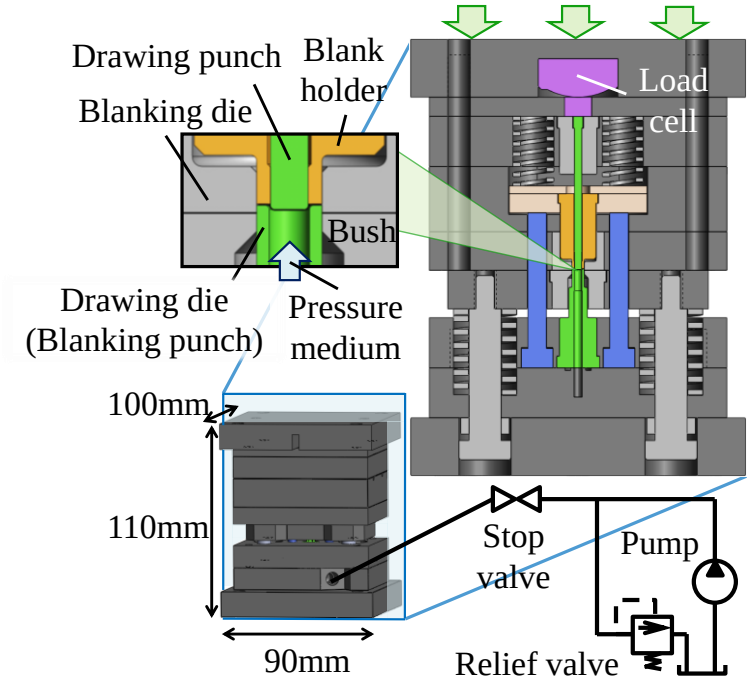

Fig. 3.6 Developed micro hydromechanical deep drawing tool set and hydraulic system.

(2) MHDD system

The desk top servo screw press machine (SEKI CORPORATION: MS50M) shown in **Fig. 3.7** was used with the MHDD apparatus. The specifications of the servo screw press machine were as follows: load capacity, 50 kN; die height, 130 mm; maximum stroke, 37 mm; positioning accuracy, 0.4 μm. Table 1 summarizes the specifications of the MHDD apparatus. In the hydraulic system, a relief valve to control the maximum counter pressure (RIKENKIKI: RV-13), a stop valve to suppress the rate of the flow into the die (RIKENKIKI: V-13C), and a hydraulic pump with a maximum counter pressure of 20 MPa were used. The specification of developed MHDD apparatus is listed in **Table 3.2**.

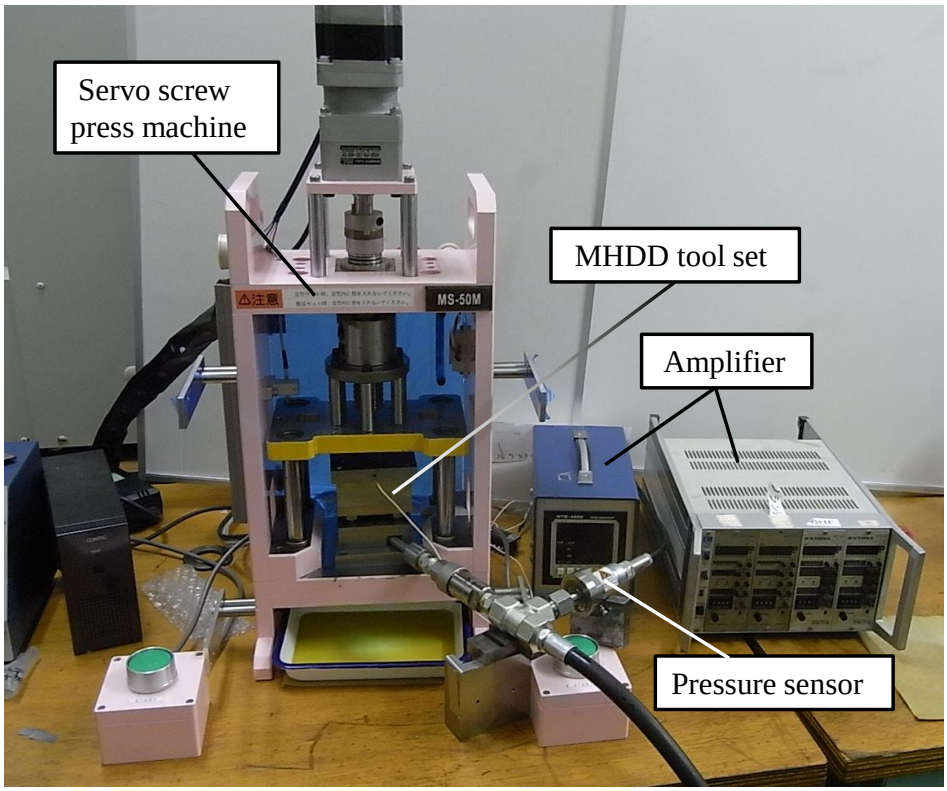

Fig. 3.7 Newly developed MHDD system with servo screw press apparatus.

Table 3.2 Specifications of developed MHDD apparatus.

Apparatus for MHDD system	Load cell	Rating capacity [kN[	20
	Servo screw press machine	Load capacity [kN]	50
		Motion resolution [nm]	400
		Die height [mm]	130
		Maximum stroke [mm]	37
		Maximum instantaneous velocity [mm/s]	28
	Hydraulic system	Pump pressure [MPa]	20
		Relief valve [MPa]	70
		Stop valve	
Tool set	Forming process	One-stroke forming	
	Pressure generation method	1μm clearance between tools	
	Blank holder method	Constant gap method	
	Tolerance	Flat part [mm]	±0.001
		Radius part [mm]	±0.01

3.3. Experiment of MHDD

3.3.1. Materials used

Phosphor bronze foils (C5191-H), stainless steel (SUS304-H), and pure titanium (TR270C-H) with thickness t of 20 and 50μm were used in the experiment. The tensile test was conducted to obtain the mechanical properties of materials used. The dimension of tensile test specimen was determined based on DIN EN 50125-H6x30 standard for the thickness range from 10 to 500μm as shown in **Fig. 3.8**. The video type noncontanct ductilometer (SHIMAZU: DVE-201) was adopted to eliminate the influence to the mechanical properties by contact of strain gauge. **Fig 3.9** shows the used tensile test machine (SHIMAZU AG-50kN IS). The tensile test was conducted with the strain rate 4×10^{-4}/s at the room temperature. The nominal stress-strain curves for each thickness and material are shown in **Figs. 3.19 and 3.11**. The obtained material properties for each thickness and material are listed in **Table 3.3**.

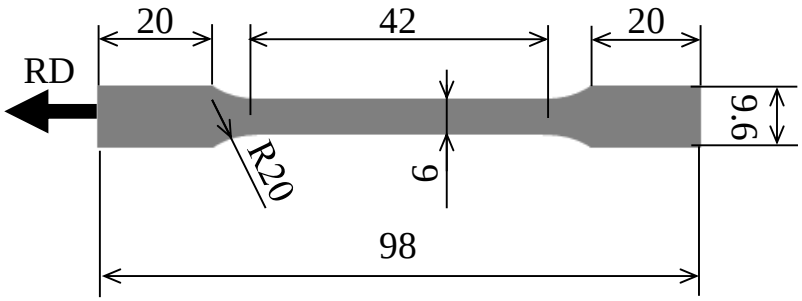

Fig. 3.8 Dimension of tensile test specimen for metal foil.

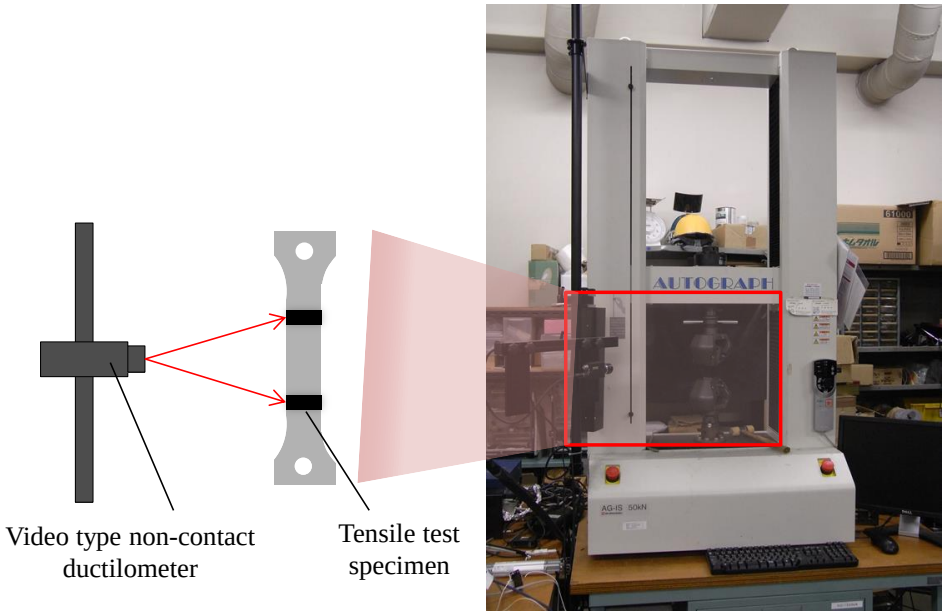

Fig. 3.9 Appearance of tensile test machine and non-contact ductilometer.

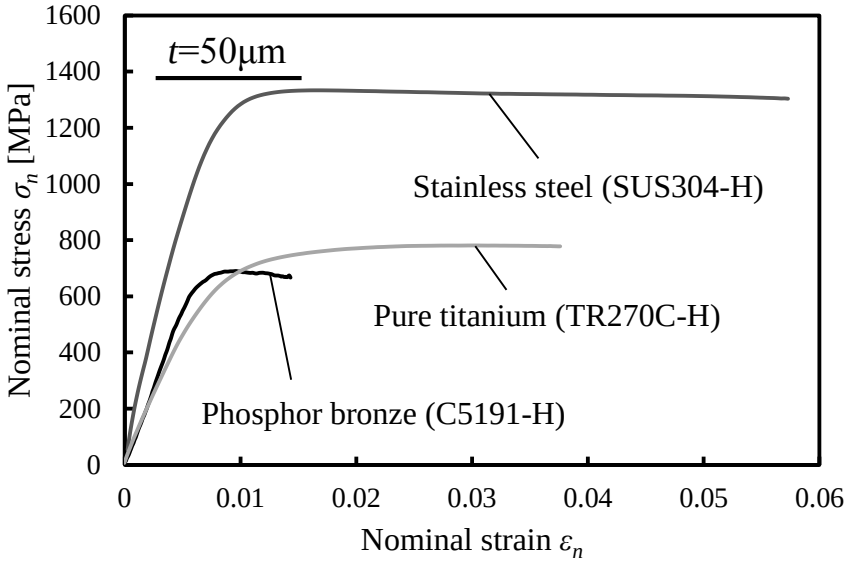

Fig. 3.10 Nominal stress-strain curves for each material with thickness of 50μm.

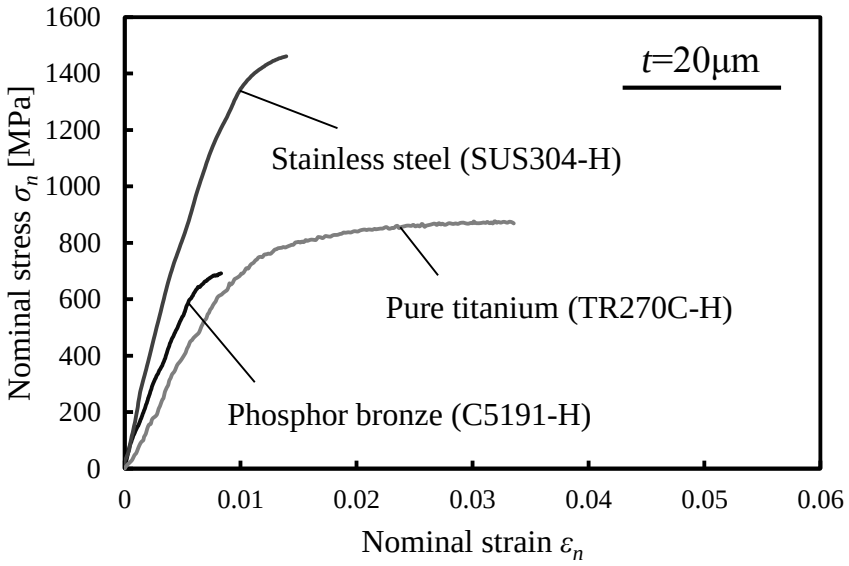

Fig. 3.11 Nominal stress-strain curves for each material with thickness of 20μm.

Table 3.3 Mechanical properties of materials used.

Thickness t [μm]	Material	Young's modulus E [GPa]	Yield stress σ_y [MPa]	Tensile strength σ_B [MPa]	Elongation δ [%]
50	Phosphor bronze (C5191-H)	110	610	687	0.6
	Stainless steel (SUS304-H)	193	1217	1334	2.4
	Pure titanium (TR270C-H)	81	613	782	1.6
20	Phosphor bronze (C5191-H)	104	625	692	0.4
	Stainless steel (SUS304-H)	184	1238	1461	0.6
	Pure titanium (TR270C-H)	75	715	875	1.4

3.3.2. Experimental procedure

Fig. 3.12 shows the appearance of tooling dimension with the drawing ratio D_o/D_p =1.74. Two punch diameters D_p =0.76, 1.90mm were used and the tooling dimensions were changed in geometrical similarity. For D_p =0.76mm, large punch shoulder radius r_p =0.25mm was also used. The tooling dimensions used in experiment is listed in **Table 3.4**. The appearance of drawing die and drawing punch is shown in **Fig. 3.13**. It can be seen that they are almost the same size with mechanical pencil lead as shown in **Fig. 3.13**. To examine the effect of the constant gap on the wrinkling, the experiments were carried out under five conditions, constant gap $h =$ 1.10t, 1.20 t, 1.30 t, 1.40 t, and 2.40 t by the conventional MDD in the dry friction. For MHDD, a forced pressurization was adopted using hydraulic oil (40 ^{o}C, 44 mm^2/s) as a pressure medium. The temperature was controlled by cooling the hydraulic oil with water. The drawing rate was 0.4 mm/s. To observe the drawn micro cups, the microscope (KEYENCE: VHX-900) shown in **Fig. 3.14** was used.

As mentioned in Chapter 2.2, the change of friction force in MHDD was evaluated by the effective punch force P_E. It can be expressed as

$$P_E = P_M - P_p = P_S + P_F + P_B + P_{UB} \tag{3.1}$$

where, P_S is the pure drawing force at the flange, P_F is the friction force between the blank and tools and P_B and P_{UB} is the bending and unbending forces at the die shoulder. In the same tooling conditions, P_S and P_B can be considered to be almost equal even if the fluid pressure increases. Therefore, the change of effective punch force shows the change of friction force.

Table 3.4 List of tooling dimensions used in experiments for each foil thickness.

Foil thickness t [mm]	0.020	0.050
Blank diameter D_0 [mm]	1.320	3.300
Drawing punch diameter D_p [mm]	0.760	1.900
Die diameter D_d [mm]	0.816	2.040
Drawing punch shoulder radius r_p [mm]	0.040	0.100
Drawing die shoulder radius r_d [mm]	0.080, 0.250	0.200
Clearance between punch and die c [mm]	0.028	0.070
Blank holder constant gap h [mm]	0.025	0.055, 0.060, 0.065, 0.070, 0.120

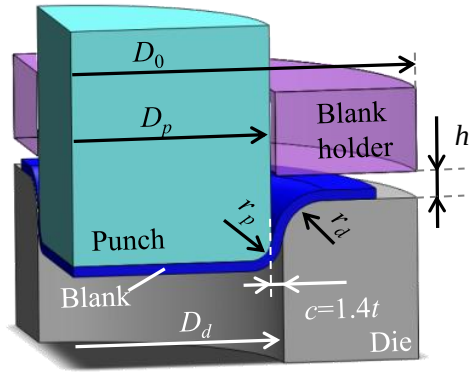

Fig. 3.12 Tool dimensions for MDD and MHDD.

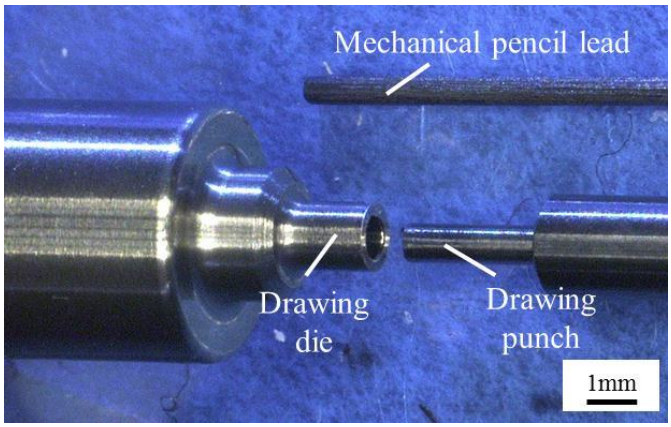

Fig. 3.13 Appearance of micro punch and die for MHDD apparatus.

Fig. 3.14 Appearance of digital microscope.

3.4. Experimental Results

3.4.1. Determination of appropriate constant gap

Fig. 3.15 shows the effect of the constant gap between the blank holder and the drawing die on the punch force-stroke curves in MDD using phosphor bronze with $D_p = 1.9\mathrm{mm}$. As the punch travels, the punch force increases and reaches the maximum punch force. After that, the punch force decreases and the ironing force occurs when the wrinkling flows into the die cavity and is compressed between the punch and die side wall. In the latter half of the forming process, the constant punch force observed is the sliding force generated as a result of the sliding of the cup edge against the die side wall.

At $h = 1.10t$ a normal punch force-stroke curve is obtained. However, for $h > 1.10\,t$, ironing force of wrinkles is observed after the force reaches the maximum; the ironing and the sliding forces increase with increasing constant gap. When the cups formed at $h = 1.10\,t$ and $2.40\,t$ are compared, flange wrinkles are observed in the cups formed at $h = 2.40\,t$, whereas wrinkles are generated only at the cup edge at $h = 1.10\,t$, with reduced the wrinkles height. This result indicates that for large gaps, the blank holder does not function properly, leading to the generation of flange wrinkles. When the flange wrinkles are crushed, the ironing force is generated and the sliding force increases. For small gaps, in contrast, the blank holder functions properly, which reduces the wrinkles height, leading to the suppression of the ironing force and reduction in the sliding force as shown in **Fig. 3.16**. Under the forming conditions adopted in this study, the appropriate constant gap was determined to suppress the wrinkling, although it was impossible to completely prevent wrinkling by controlling the constant gap. For the developed MHDD apparatus, $h = 1.10\,t$ was adopted.

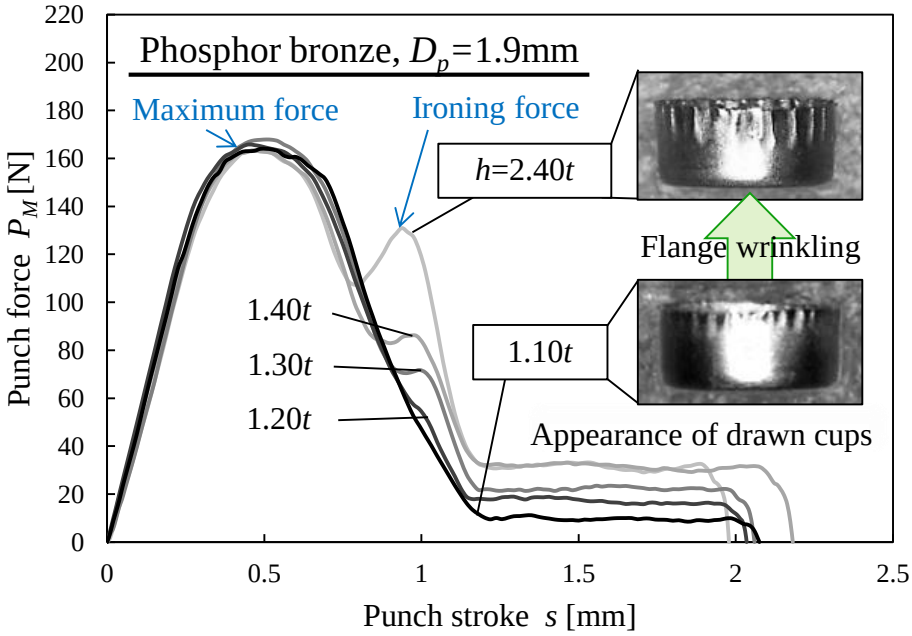

Fig. 3.15 Effect of gap between blank holder and drawing die on punch force-stroke curve (Phosphor bronze, D_p =1, MDD).

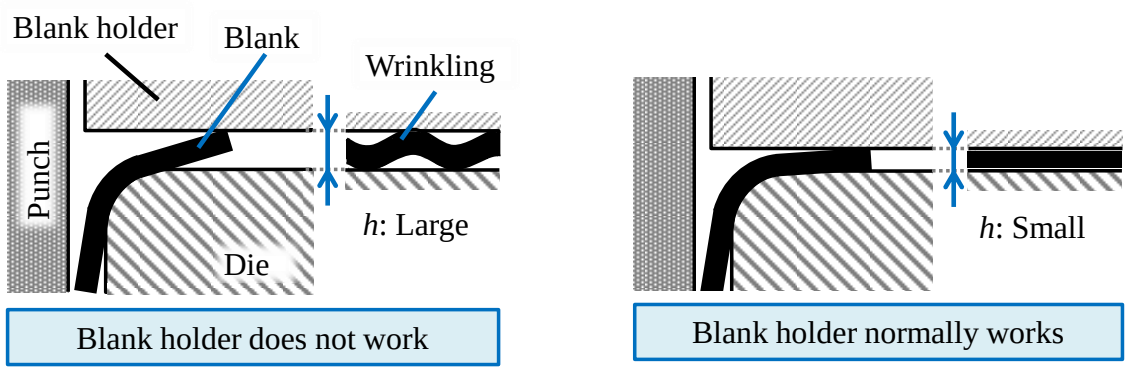

(a) At large constant gap (b) At small constant gap

Fig. 3.16 Schematic of blank state in different constant gaps.

Fig. 3.17 shows the normalize punch force-stroke curves in MDD with D_p =1.9mm, and h =1.10t. The difference of normalized punch force shows the difference of n value and friction force because the punch force is normalized by yield stress. The ironing force appears in stainless steel, although it does not appear in phosphor bronze and pure titanium. It is known that the allowable blank holder pressure to avoid the wrinkling is dependent on Young's modules [3-10]. Young's modules in stainless steel is higher than that of the phosphor bronze and pure titanium, although, it is almost the same between the phosphor bronze and pure titanium. It means that the high blank holder pressure is required in stainless steel. Therefore, the constant gap for stainless steel should be smaller than the appropriate constant gap for the other materials.

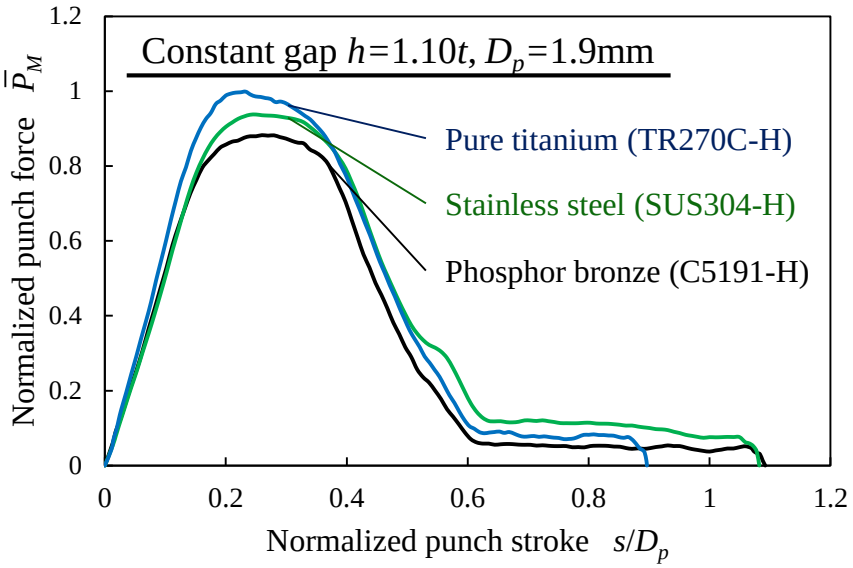

Fig. 3.17 Normalized punch force-stroke curves for each material (Constant gap h =1.10t, D_p =1.9mm, MDD).

3.4.2. Determination of appropriate clearance for generating counter pressure

Fig. 3.18 shows the counter pressure-stroke curve and the punch force-stroke curve during the MHDD process. As shown in **Fig. 3.5**, the forming processes consist of (1) counter pressure generation, (2) blanking, (3) drawing, and (4) pressure release and knockout. Stable counter pressure was found to be generated during drawing when the clearance between the drawing die and the bush was set to 1 μm. The counter pressure did not decrease during the drawing process, which proves that the pressure medium did not leak from the blank edge. Namely, the process is a radial pressure-aided deep drawing by an indirect method in which a compressive force is applied from the blank edge radially inward [3-11]. By this method, the friction force is reduced by the leakage of pressure medium between the blank and blank holder and the meridional stress is also reduced.

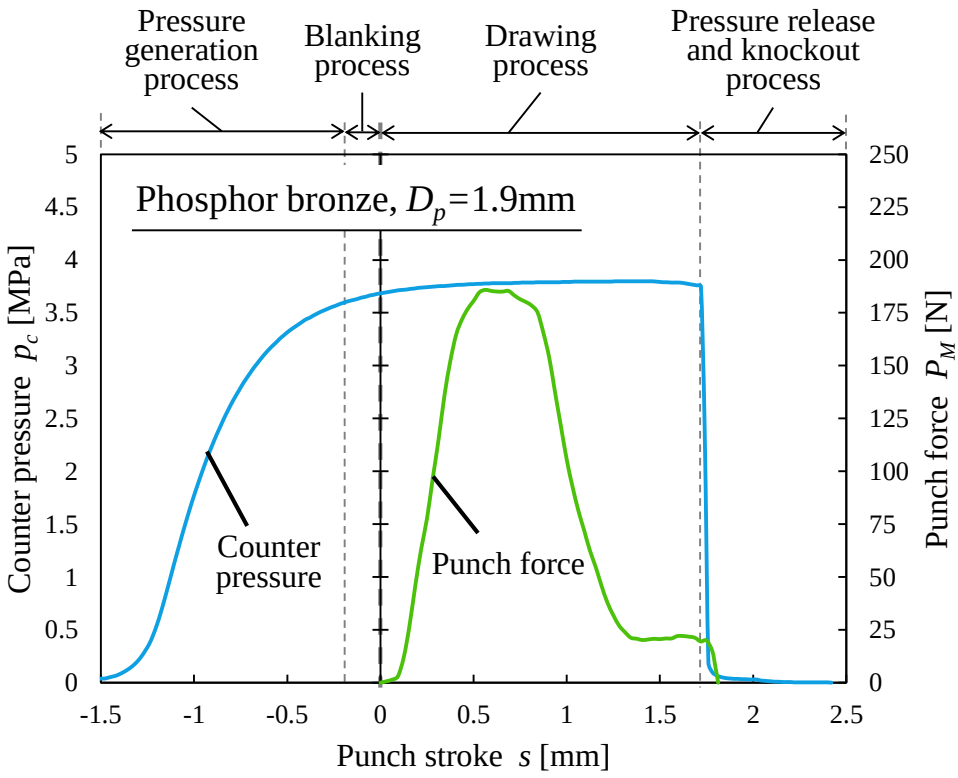

Fig. 3.18 Counter pressure- and punch force-stroke curves during MHDD process (Phosphor bronze, D_p =1.9mm).

3.4.3. Appearance of drawn micro cups

Fig. 3.19 shows the deformation processes of blank during MHDD. It can be seen that the blanking and drawing processes were conducted coaxially when the punch travels once. **Fig. 3.20** shows drawn micro cups obtained under the different punch diameters and punch shoulder radii for MDD and MHDD. At D_p =0.76mm and r_p =0.04 mm, the cups were unsuccessfully drawn. At D_p =1.9mm and r_p =0.10 mm or D_p =0.8mm and r_p =0.25 mm, the cups were successfully drawn for both MDD and MHDD. The MHDD apparatus can be used to form micro cups with diameters ≤ 1 mm. The above results confirmed that the MHDD apparatus with a simple tooling structure and forming processes realized the required performance without the need for large and expensive equipment.

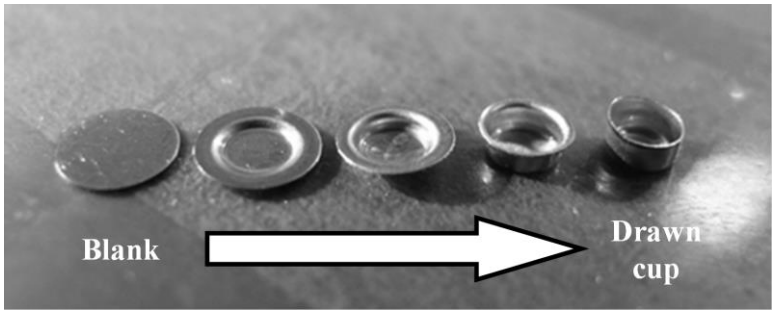

Fig. 3.19 Deformation processes of blank during MHDD (Stainless steel, D_p =1.9mm).

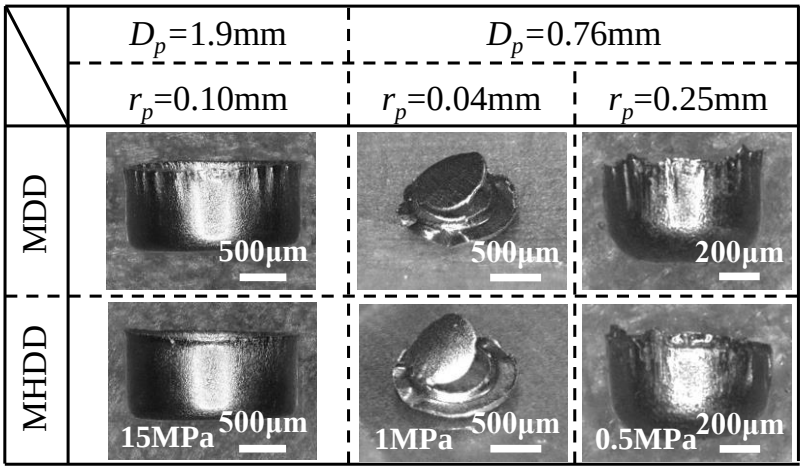

Fig. 3.20 Drawn cups under different scale factors and punch shoulder radii in MDD and MHDD (Stainless steel).

Fig. 3.21 shows the appearance of micro cups obtained by MDD and MHDD. The drawn micro cups with D_p =0.8 and 2 mm are smaller than a rice grain. **Fig. 3.22** shows a cross section of a drawn cup. The micro cup was successfully drawn at D_p =1.9mm and a sharp punch shoulder of r_p =0.10 mm.

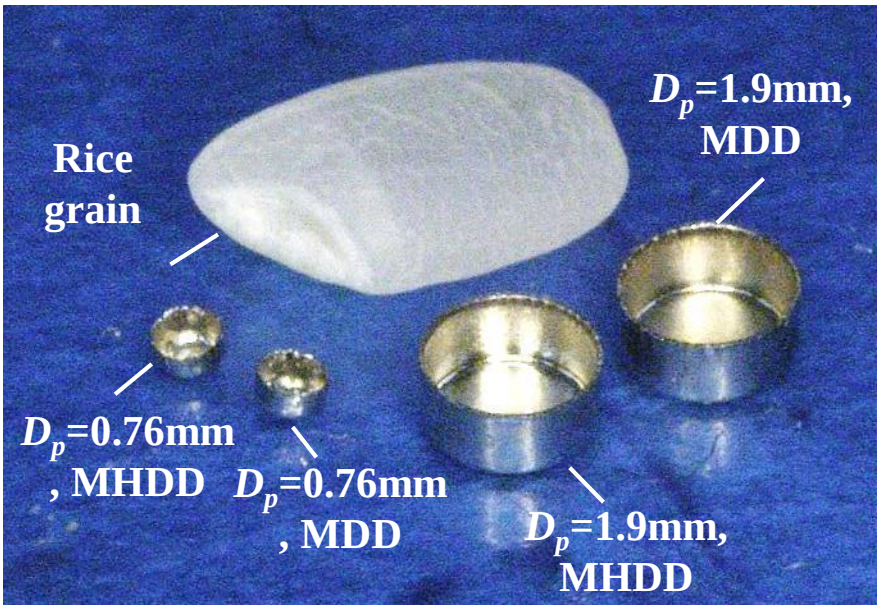

Fig. 3.21 Appearance of different scale cups around a rice grain in MDD and MHDD.

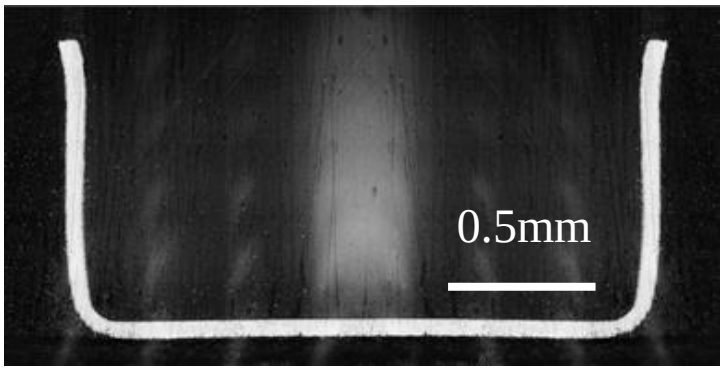

Fig. 3.22 Axial cross section of drawn cup (D_p =1.9mm).

3.4.4. Effect of fluid pressure on drawability

(1) Effect of fluid pressure on wrinkling and fracture in MHDD

Fig. 3.23 shows the appearance of cups of the three materials, fabricated by MDD and MHDD. For stainless steel, wrinkling occurred at the cup edge even for appropriate constant gaps in MDD. In contrast, wrinkling was suppressed at the cup edge obtained by MHDD with applying counter pressure of 15 MPa. The applying counter pressure causes the blank to be pushed against the blank holder. This compressive force acts as the suppressive force of wrinkling. However, when the counter pressure was increased to 20 MPa in MHDD, the cup was fractured at the punch shoulder. The wrinkling prevention effect by the applying counter pressure during MHDD can be observed for all of the three materials and at D_p =0.76mm (**Fig. 3.20**).

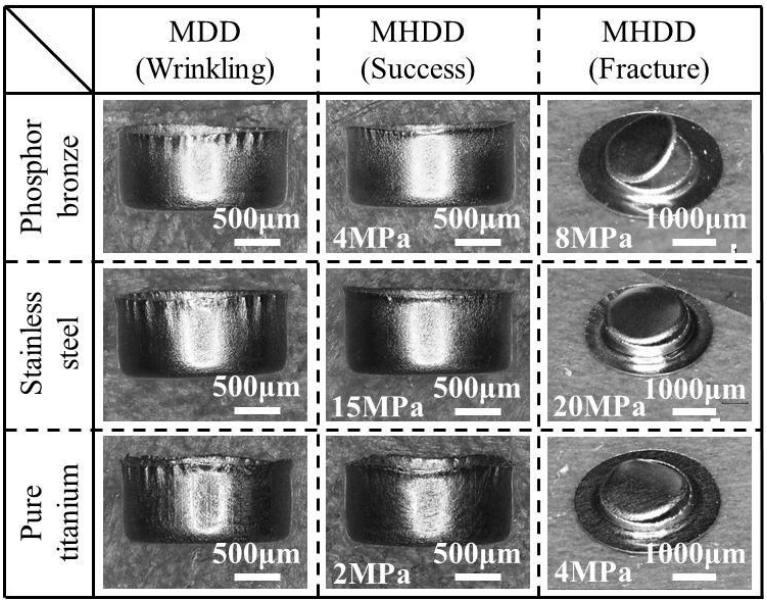

Fig. 3.23 Appearance of wrinkling, success and fracture cups in MDD and MHDD at each material.

Fig. 3.24 shows the effect of counter pressure on the occurrence of wrinkling and fractures during MHDD. When the counter pressure normalized by Young's modulus (p/E) is smaller than a certain value, wrinkling occurs (wrinkling zone), whereas the cups fracture when p/E is larger than a certain value (fracture zone). When p/E falls between these two values, cups without the wrinkles and fractures are obtained (success zone). For the pure-titanium foil, the size of wrinkles decreases with applying the counter pressure (**Fig. 3.23**); however, the cups fracture before wrinkles are completely removed, not showing the successful zone. This is because the friction force for the pure titanium foil becomes too large and the fracture zone shifts to the low-pressure side, leading to the fracture zone merging with the wrinkling zone and the disappearance of the success zone. The successful zone for pure-titanium foils may be obtained by improving the lubrication to decrease the friction force and shift the fracture zone to the high pressure side.

The critical blank holding pressure in cylindrical deep drawing p_{cr} normalized by Young's modulus is predominantly determined by the tool dimensions alone [3-10]. It can be expressed as

$$\frac{p_{cr}}{E_0} = \frac{\omega_{cr}\dfrac{3.82{\gamma_i}^2\delta_d\cdot(DR)}{\{(DR)^2-{\gamma_i}^2\}\alpha_B\alpha_H}\left\{\left(\dfrac{\sigma_D}{E_0}\right)^2-\dfrac{4.77\alpha_B\alpha_D}{{\gamma_i}^2{\delta_d}^4}\right\}}{1+\omega_{cr}\mu\left(3.82{\gamma_i}^2{\delta_d}^2\cdot(DR)\right)\cdot\dfrac{1}{\alpha_H}\left(\dfrac{\sigma_i}{E_0}\right)} \tag{3.2}$$

where

$$E_0=\frac{4EF_0}{\left(\sqrt{E}+\sqrt{F_0}\right)^2},\qquad F_0=\frac{\partial\sigma}{\partial\varepsilon}=Kn\left(\bar{\varepsilon}_{eq}+\varepsilon_0\right)^{n-1},\qquad \sigma_D=1.1\bar{\sigma}_{eq}\ln\frac{r_0}{r_1},\qquad DR=\frac{R_0}{R_p},$$

$$\gamma_0=\frac{r_0}{R_p},\qquad \gamma_1=\frac{r_1}{R_p},\qquad \delta_d=\frac{D_p}{t},\qquad \alpha_B=\frac{\gamma_0-\gamma_1}{\gamma_0\gamma_1},\qquad \alpha_H=\gamma_0+\gamma_1,\qquad \alpha_D=\frac{(\gamma_0+\gamma_1)^2}{(\gamma_0-\gamma_1)^3}$$

and ω_{cr} is the specific wrinkle height. Eq. (3.2) means that the wrinkling zone exists at a certain p/E or less under the same tool conditions and the counter pressure in MHDD functions equivalently to the blank holder.

From the above, the applying appropriate counter pressure in MHDD is considered to prevent the wrinkling and reduce the friction force, leading to the improvement of the forming limit in the MHDD. However, the fracture occurs at punch shoulder before applied fluid pressure reaches the ultra high pressure. It shows that the advantages of ultra high pressure as mentioned in Chapter 2 cannot be obtained in MHDD.

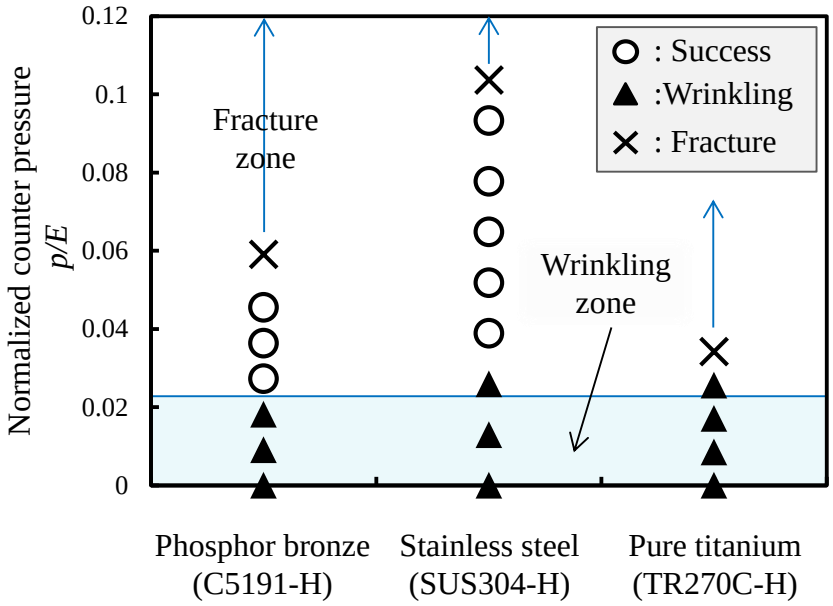

Fig. 3.24 Effect of counter pressure normalized by young modulus on occurrences of wrinkling and fracture in MHDD.

(2) Effect of fluid pressure on friction force in MHDD

Fig. 3.25(a) shows the effect of counter pressure on normalized punch force-stroke curves in stainless steel. The effective punch force is normalized to cup cross section at side wall $\pi \times (D_p + t)t$ and tensile strength σ_B. The maximum possible punch force is expressed by $(\pi \times (D_p + t)t)\sigma_B$. Thus, the normalized maximum effective punch force can be written for different blank materials by the above maximum possible punch force. The normalized effective punch force increases as the counter pressure increases. The difference in the effective punch force represents the difference in the friction force. Hence, it shows the increase of friction force. When the counter pressure excessively increases, the fracture occurs at punch shoulder. These behaviors are also observed in phosphor bronze and pure titanium.

Fig. 3.26 shows the effect of counter pressure on normalized maximum effective punch force and normalized counter pressure relations for various materials. In the experimental results, the maximum punch force of MDD decreases once when the counter pressure is applied. As the counter pressure is increased, the maximum punch force increases when counter pressure exceeds p_c/E =0.02. The change of normalized maximum effective punch force shows the change of friction force. This means that the friction force increases as the counter pressure increases in MHDD. As a result, the fracture occurs at the punch shoulder when the high counter pressure is applied, as shown in **Fig. 3.23**. This behavior is observed in all of the three materials.

The theoretical result shows the same tendency with the experimental result as shown in **Fig. 3.27**. This is because the application of counter pressure lubricates the blank and at the same time increases the contact pressure between the blank and blank holder as shown in Eq. (2.26). The counter pressure plays a role of blank holder pressure in the constant gap method. This means that the application of counter pressure almost linearly increases the friction force and the fracture occurs at punch shoulder due to the excessive punch force in MHDD using the constant gap method. It is why the fracture occurs before the applied fluid pressure reaches the ultra high pressure in MHDD.

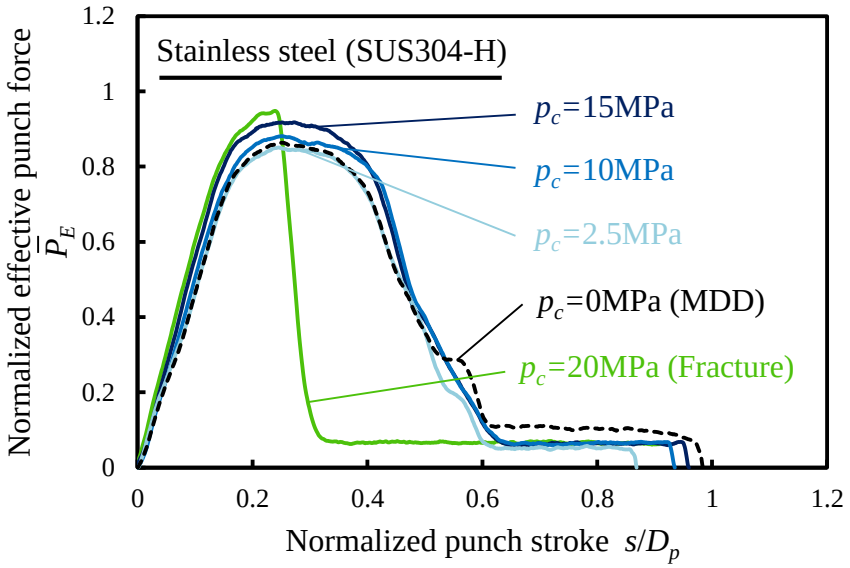

(a) Stainless steel (SUS304-H)

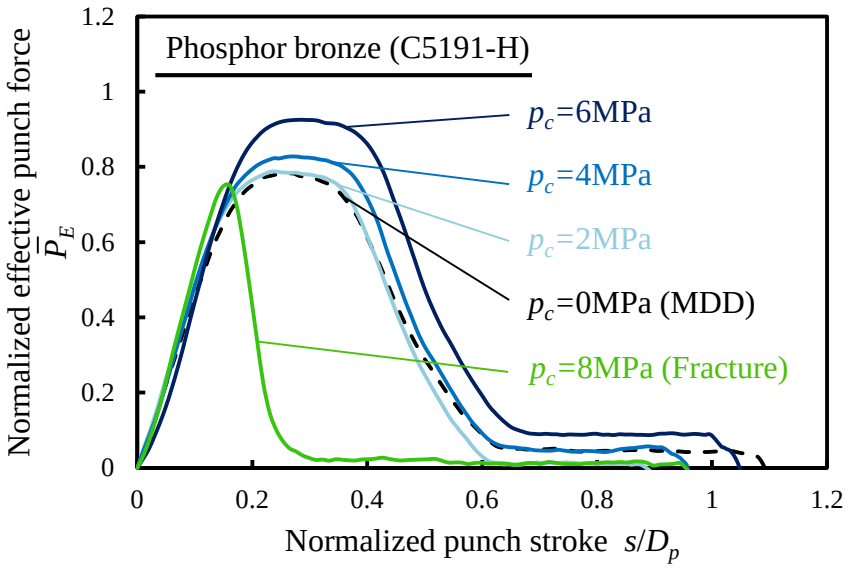

(b) Phosphor bronze (C5191-H)

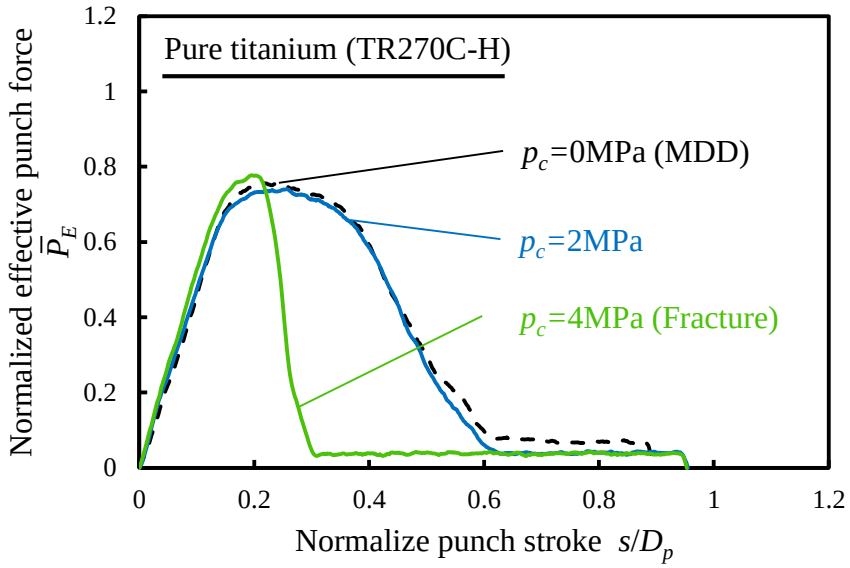

(c) Pure titanium (TR270C-H)

Fig. 3.25 Effect of counter pressure on normalized punch force-stroke curves.

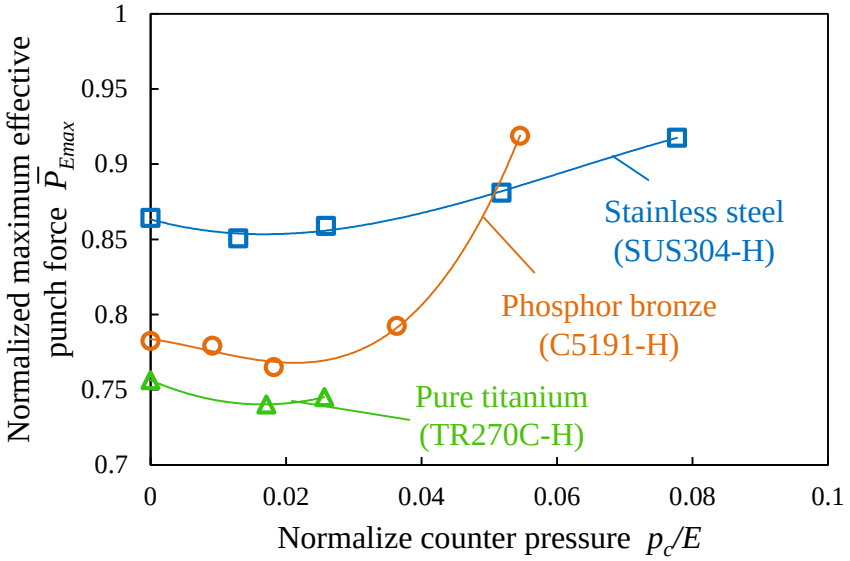

Fig. 3.26 Effect of counter pressure on normalized punch force-stroke curves.

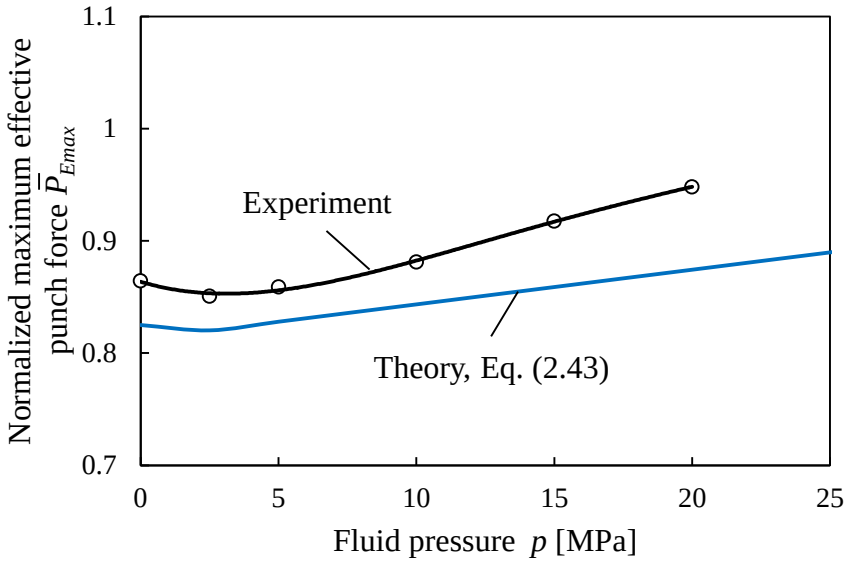

Fig. 3.27 Effect of fluid pressure on normalized maximum effective punch force in experiment and theory ($\mu_c = \mu_{dry} = 0.3$, $\bar{\alpha}_f = 0$ for MDD, $\mu_c = \mu_{dry} = 0.3$, $\mu_{fluid} = 0.25$, $\bar{\alpha}_f = 1/4$ for MHDD).

(3) Comparison of drawing characteristics and fluid behavior in HDD and MHDD

In conventional HDD, the fracture typically occurs at punch shoulder at high counter pressure as shown in **Fig. 3.28**. High fluid pressure induces the hydrodynamic lubrication which improves the tribological behavior and the friction holding effect, which can reduce the applied force to blank at the punch shoulder. Moreover, a friction holding effect which can reduce the applied force to blank at the punch shoulder. These mean that the fracture does not occur at the punch shoulder, but rather at the die shoulder when the blank is subjected to excessive reverse bulging deformation at the die shoulder [3-11]. It appears that the characteristics of fluid pressure are different in HDD and MHDD and these differences cause the difference in the type of fractures.

The differences in the tribological behavior and fracture types are resulted from the fluid behavior. In conventional HDD, the fluid pressure temporarily decreases at the early and middle stages which show the leakages between the blank-die and the blank-blank holder, respectively, as shown in **Fig. 3.29**. These leakages cause the hydrodynamic lubrication in the flange area and reduce the friction force but there is no decrease in fluid pressure in MHDD. This shows that there is no hydrodynamic lubrication in MHDD. This is the reason for the high friction force in MHDD.

According to Eq. (2.50), the required fluid pressure for hydrodynamic lubrication p_h can be obtained as shown in **Fig. 3.30**. The fluid pressure required for hydrodynamic lubrication increases with the decrease of D_p/t. In particular, the quite high fluid pressure is required to leak the fluid medium in micro scale in which D_p/t approximately ranges from 10 to 100. This is because the contact pressure at the die shoulder and the sealablity become high at the small D_p/t, in which the die shoulder radius is relatively small compared to the blank thickness. For this reason, the hydrodynamic lubrication cannot be obtained in MHDD even though the maximum pressure of pump p =20MPa is applied. These results indicate that the low lubrication in MHDD is caused by small D_p/t and low applied fluid pressure.

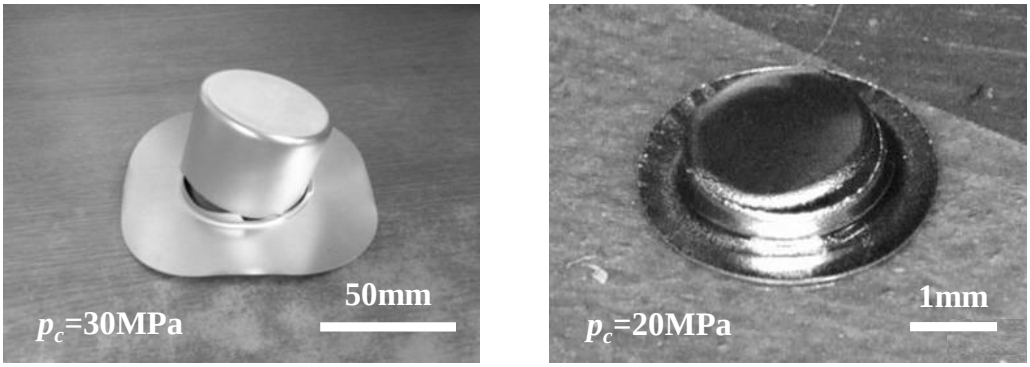

(a) Fracture at die shoulder in conventional HDD (b) Fracture at punch shoulder in MHDD

Fig. 3.28 Appearance of fractured cups in conventional HDD and MHDD.

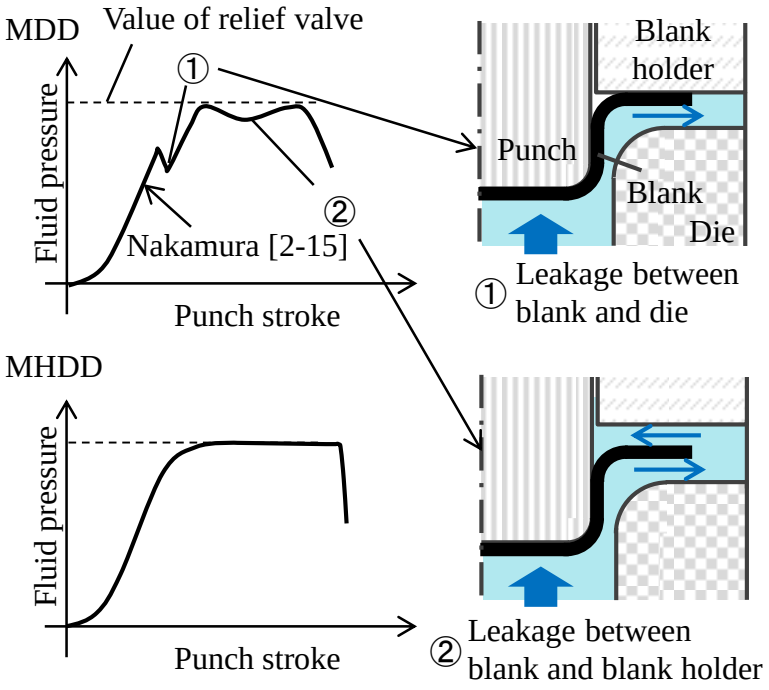

Fig. 3.29 Comparison of fluid behaviors between MDD and MHDD.

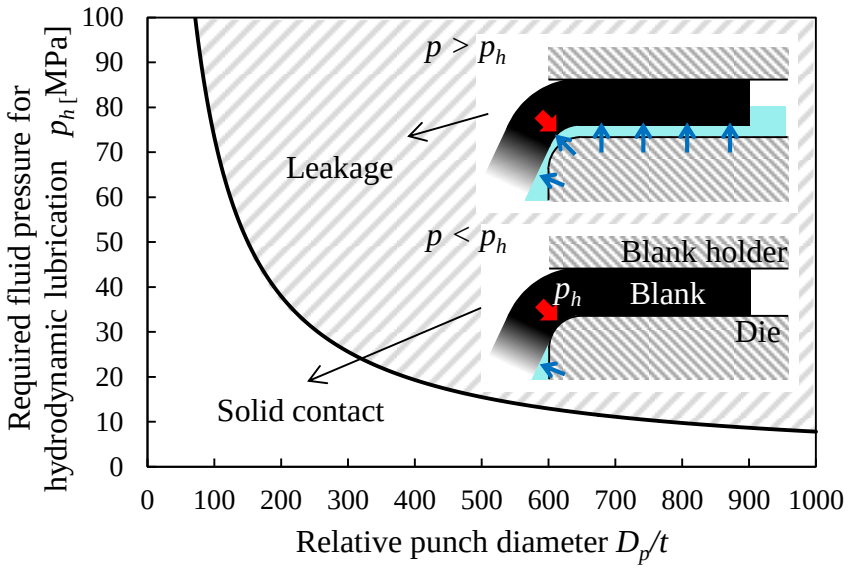

Fig. 3.30 Effect of D_p/t on required fluid pressure for hydrodynamic lubrication introduced in Eq. (2.50).

3.4.5. Effect of fluid pressure on shape accuracy

Fig. 3.31 shows the effect of counter pressure on the shape accuracy at the bottom of cups. In stainless steel, the bottom shape obtained by conventional MDD is convex with respect to the punch, whereas the bottom shape obtained by MHDD with the application of counter pressure is concave; thus, the bottom shape obtained by MDD is different from that obtained by MHDD. In addition, the concave deformation toward the punch increases with increasing counter pressure during MHDD. The same behavior was observed in phosphor bronze; nevertheless, the bottom shape is convex obtained even by applying counter pressure in pure titanium as shown in **Fig. 3.31(c)**. However, the convex shape at bottom of cup can be reduced by increasing counter pressure.

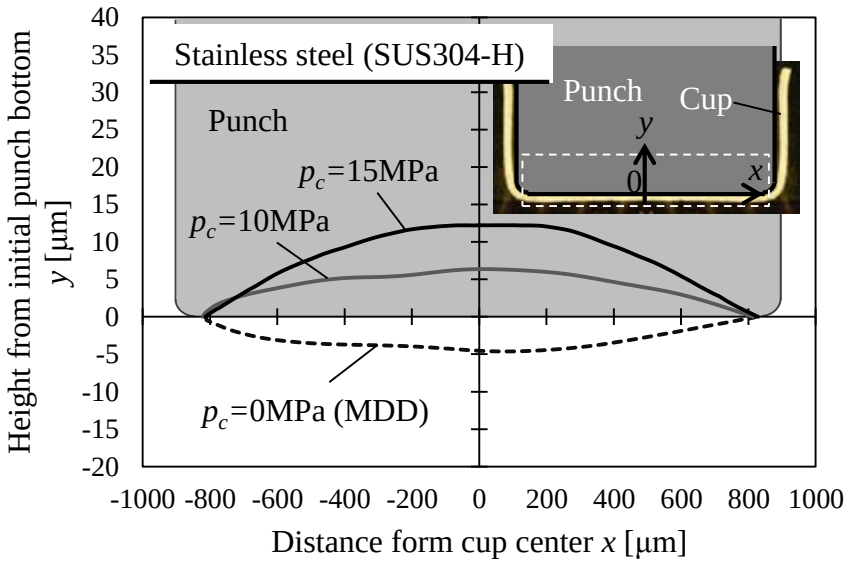

(a) Stainless steel

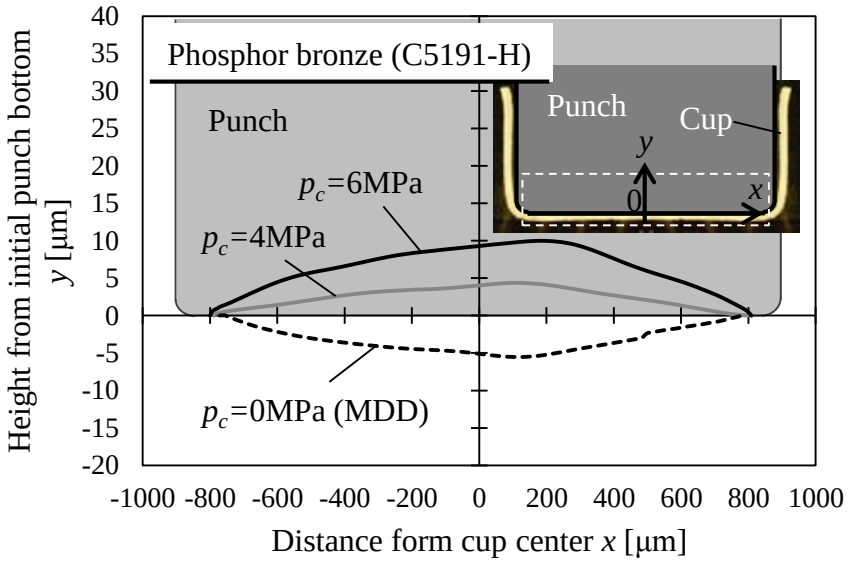

(b) Phosphor bronze

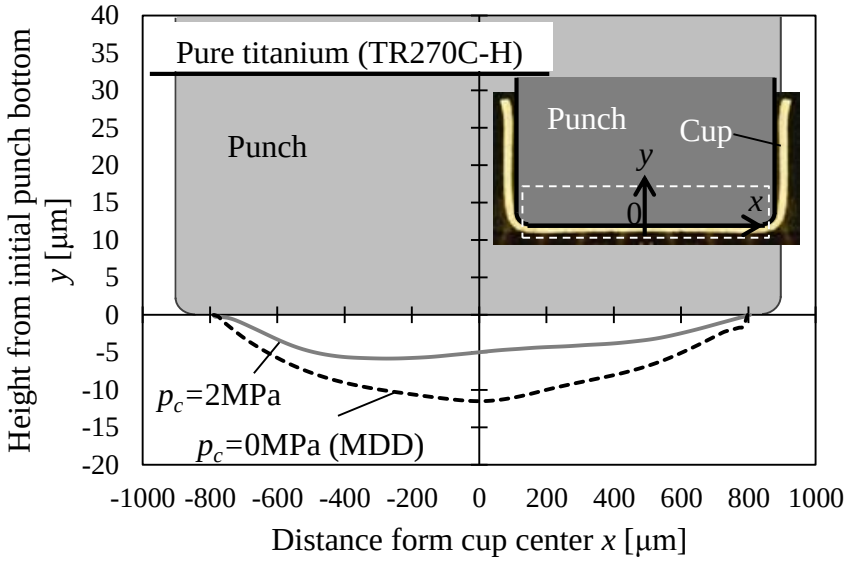

(c) Pure titanium

Fig. 3.31 Effect of counter pressure on drawn cup profiles at cup bottom.

Fig. 3.32 shows the blank statement during MDD and MHDD. In conventional MDD, the bottom of the cup is subjected to bulge deformation by the bending moment during deep drawing, resulting in a convex shape with respect to the punch. In contrast, when the fluid pressure that counters the bending moment is applied to the bottom during MHDD, the convex bulge deformation is suppressed and a flat cup bottom is formed. However, the fitness between the punch and the blank is increased by increasing the counter pressure and a negative pressure is generated during the knockout stage. The counter pressure is continuously applied until the end of the knockout stage, leading to a concave shape with respect to the punch. The negative pressure can be suppressed by making a hole at the center of the punch or a small groove on the side wall of the punch. The concave cup bottom obtained by MHDD can be made flat by controlling the tool and forming conditions. These results confirmed that the shape accuracy at cup bottom is improved by applying the counter pressure in MHDD.

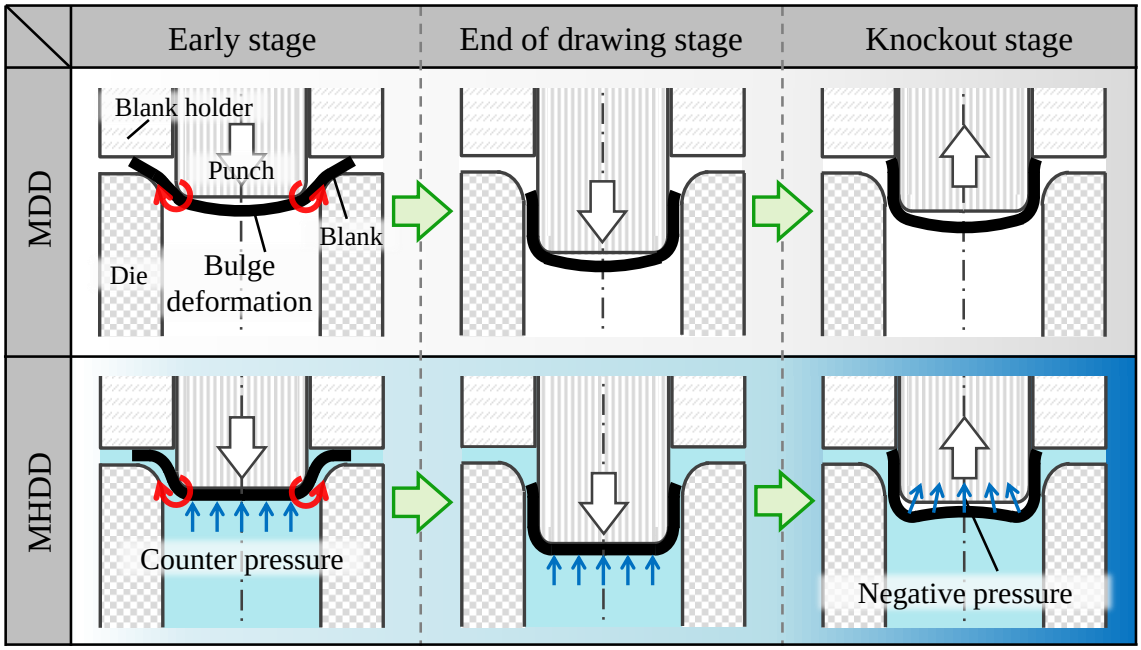

Fig. 3.32 Schematic illustration of blank states during forming process in MDD and MHDD.

Fig. 3.33 shows the effect of counter pressure on shape accuracy at side wall. The fitness at side wall is low in MDD; however, it can be improved by applying counter pressure p_c =20MPa in MHDD. It was revealed that the shape accuracy of micro cup can be improved by applying counter pressure in MHDD. However, the fitness near the punch shoulder is still low even though p_c =20MP is applied. It shows that the higher fluid pressure is required to obtain the good fitness at side wall; however, the fracture occurs at the punch shoulder before the applied fluid pressure is reached the ultra high fluid pressure as shown in **Fig. 3.24**. This result shows that the advantage of ultra high pressure cannot be obtained in MHDD due to the fracture.

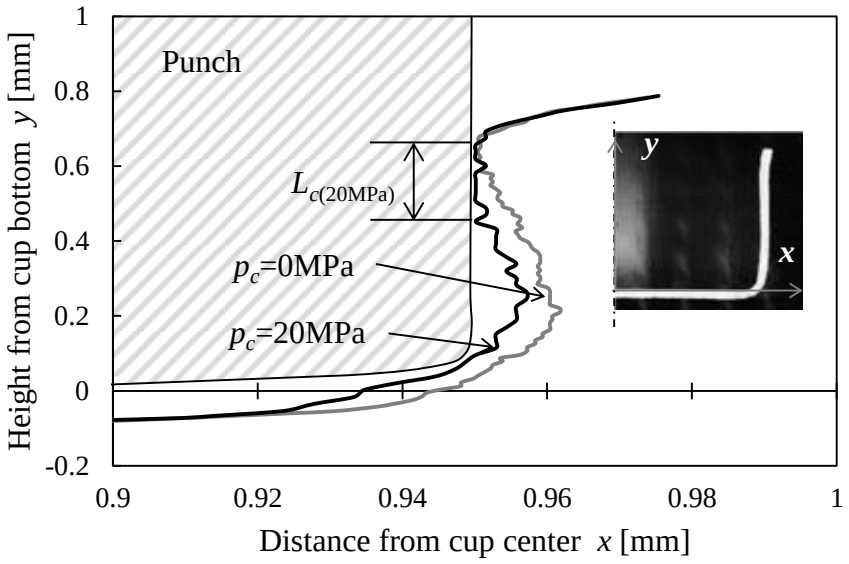

Fig. 3.33 Effect of counter pressure on drawn cup profile at side wall (Phosphor bronze).

Fig. 3.34 shows the effect of counter pressure on shape accuracy in tapered micro cups in MHDD. The shape accuracy at side wall is low in MDD. However, it can be significantly improved by applied p_c =16MPa in MHDD. It can be seen that the improvement of shape accuracy by applying the fluid pressure in the tapered punch is more significant than the flat punch. Furthermore, the cup height increases with increasing the counter pressure [3-12]. The aspect ratio of 0.7 can be obtained by applying p_c =16MPa in MHDD. However, the high aspect ratio cannot be achieved even though the tapered punch is used.

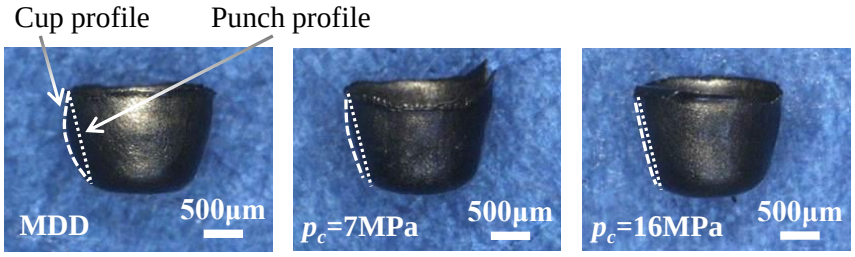

Fig. 3.34 Effect of counter pressure on shape accuracy in tapered micro cups (Pure titanium, TR270C-O).

Fig. 3.35 shows the effect of counter pressure on flatness at bottom of cup for each material. The flatness at bottom of cup is normalized to punch diameter to eliminate the difference of stiffness for each material and tooling dimension. The fitness at cup bottom increases with increasing the counter pressure. However, the fitness at bottom of cup decreases with increasing counter pressure in conventional macro HDD. The opposite behavior is observed for shape accuracy between the macro and micro HDD.

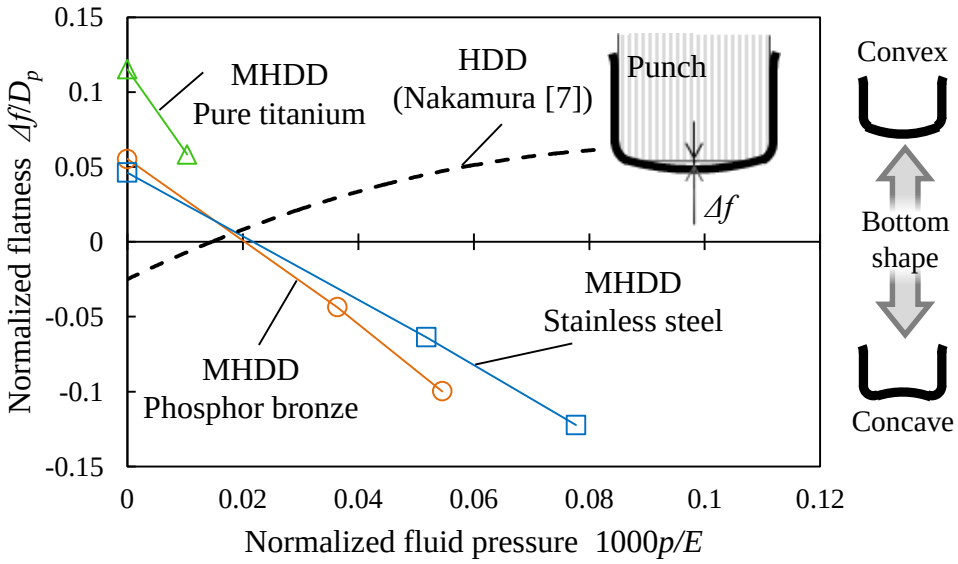

Fig. 3.35 Effect of normalized counter pressure on normalized flatness for each material.

3.5. Concluding Remarks

In this chapter, an MHDD apparatus with the simple forming processes and tooling structure, and the high shape accuracy of drawn components was developed. In addition, the effect of fluid pressure on basic drawing characteristics in MHDD was experimentally investigated. The following conclusions were obtained.

1) A servo-type MHDD apparatus with a simple structure and a small-clearance die structure was successfully developed, which can reproduce a multiaxial press by one-stroke forming and the constant-gap method.

2) It was confirmed that the developed MHDD apparatus can prevent the wrinkling with a constant gap of $h = 1.10t_o$ and generate the counter pressure with the clearance between tools of 1 μm that is sufficient to achieve a stable sealing. The micro cups with a diameter of 0.8 mm and a sharp cup with a diameter of 2.0 mm and a punch shoulder radius of 0.1 mm were successfully formed.

3) The application of appropriate counter pressure can successfully fabricate the micro cups without the wrinkling at the low counter pressure and the fracture at the excessive counter pressure. Furthermore, the shape accuracy at cup bottom and side wall can be improved by applying the counter pressure in MHDD. It was clarified that the counter pressure can improve the forming limit and shape accuracy in MHDD.

4) The fracture occurs at punch shoulder before the applied fluid pressure reaches the ultra high pressure. It means that the friction in flange area becomes significant due to the increase of contact pressure between the blank and blank holder before the friction reduction by hydrodynamic lubrication can be obtained with increasing the counter pressure.

5) The good fitness cannot be obtained near the punch shoulder even though the maximum applicable counter pressure is applied. It is because that the ultra high pressure is required to obtain the high fitness in MHDD due to the high stiffness in small D_p/t; however, the fracture occurs before the applied fluid pressure reaches the ultra high pressure. Furthermore, the high aspect ratio cannot be obtained even though the taper punch is used.

From the above, the effect of fluid pressure on basic forming characteristics in MHDD was

experimentally clarified. It was found that the fluid pressure is effective to improve the wrinkling limit and the shape accuracy in micro scale as with macro scale. However, the advantages of ultra high pressure cannot be obtained in MHDD due to the fracture. Therefore, the high shape accuracy, high friction reduction and significant improvement of forming limit cannot be achieved in MHDD. A new idea to realize the advantage of ultra high pressure without the fracture in micro scale is required.

References

[3-1] M. Koc, S. Mahabunphachai, Feasibility investigations on a novel micro-manufacturing process for fabrication of fuel cell bipolar plates: internal pressure-assisted embossing of micro-channels, with in-die mechanical bonding, Journal of Power Sources, 172, (2007), 725-733.

[3-2] Y. Kasuga, K. Kondo, Pressure lubricated deep drawing (3rd report, the pressure generated), Transactions of the Japan Society of Mechanical Engineers (in Japanese), 26-169, (1960), 1290-1297.

[3-3] S. Mahabunphachai, M. Koc, Fabrication of micro-channel arrays on thin metallic sheet using internal fluid pressure: Investigations on size effects and development of design guidelines, Journal of Power Sources, 175, (2008), 363-371.

[3-4] S. Mahabunphachai, M. Koc, Investigation of size effects on material behavior of thin sheet metals using hydraulic bulge testing at micro/meso-scales, International Journal of Machine Tools & Manufacture, 48, (2008), 1014-1029.

[3-5] H. Nishimura, Progress and future view of servo press, Press Working (in Japanese), 50-11, (2012), 18-21.

[3-6] http://www.hsk.co.jp/introduction/metal_forming_machines/feature.html

[3-7] T. Mori, Trend of multi-axis servo press, Press Working (in Japanese), 50-11, (2012), 51-55.

[3-8] K. Manabe, H. Hamano, Improvement of formability of sheet metals by effective application of blank holder, Journal of the Japan Society for Technology of Plasticity (in Japanese), 33-376, (1992), 480-487.

[3-9] S.H. Zhang, J. Danckert, Development of hydro-mechanical deep drawing, Journal of Materials Processing Technology, 83, (1998), 14-25.

[3-10] N. Kawai, Critical conditions of wrinkling in deep drawing of sheet metals (2nd report, analysis and considerations for conditions of blank-holding), Transactions of the Japan Society of Mechanical Engineers (in Japanese), 26-166, (1960), 857-863.

[3-11] K. Nakamura, T. Nakagawa, Radial pressure assisted hydraulic counter pressure deep drawing –studies on hydraulic counter pressure forming II-, Journal of the Japan Society for Technology of Plasticity (in Japanese), 26, (1985), 73-80.

[3-12] K. Manabe, D. Kondo, H. Sato, D.B. Wei, Z.Y. Jiang, Hydromechanical deep drawing of micro tapered cups, Proceedings of the 6th International Conference of Tube Hydroforming, (2013), 318-322.

Chapter 4

Process Design of MUDD Using Ultra High Pressure and Incremental Control

4.1. Introduction

As mentioned in Chapters 2, and 3, the fluid pressure has some advantages in micro sheet forming to improve the tribological behavior, shape accuracy, and drawability. In particular, the application of ultra high fluid pressure is required to realize the advantages of fluid pressure in MHDD. However, it seems that the simple scaling down of this technique cannot achieve the significant improvement of drawability in MHDD. It is because the fracture occurs before the applied fluid pressure reaches the ultra high pressure in MHDD. It shows that the advantages of ultra high pressure cannot be brought out in simple scale down of sheet hydroforming process. A new concept to realize the ultra high pressure in micro scale is required to realize the high forming limit and high shape accuracy.

From the above, an incremental forming technique is combined to the micro sheet hydroforming process to avoid the fracture and improve the forming limit significantly. A novel forming method, a micro incremental sheet hydroforming process is proposed. In particular, a deep drawing process in micro incremental sheet hydroforming, micro ultra deep drawing (MUDD), is focused on. In this chapter, MUDD process using the ultra high pressure and incremental control of tooling and pressure and its appropriate forming condition for high aspect ratio and high shape accuracy is designed by FEM simulation.

4.2. Design of MUDD Process

4.2.1. Difficulties in micro sheet hydroforming

The difficulties in MHDD process as mentioned in Chapters 2 and 3 are reviewed and summarized as follows:

(a) High relative bending stiffness

The relative bending stiffness increases with scaling down to micro scale due to the high relative punch diameter to minimum thickness D_p/t. It means that the friction holding effect, which can reduce the applied force at the punch shoulder, hardly occurs in micro sheet hydroforming. In addition, the shape accuracy cannot be improved under the fluid pressure of 100MPa. Therefore, the ultra high pressure is required to deform the blank and improve the shape accuracy in micro sheet hydroforming.

(b) High sealablity

The sealablity increases as the specimen size decreases due to the high relative die shoulder radius to minimum thickness r_d/t. It means that the hydrodynamic lubrication effect, which can reduce the friction force between the blank and tools, cannot be obtained at low fluid pressure. On the other hand, the lubrication in OLPs can improve the tribological behavior and its effect increases with scaling down to micro scale; however, the high fluid pressure is still required to obtain the sufficient improvement of tribological behavior in micro sheet hydroforming.

(c) Increase of friction force with increasing fluid pressure

With increasing the fluid pressure, the friction force between the blank and blank holder increases due to the increase of contact pressure between them. As a result, the excessive thinning and the fracture occur at punch shoulder before the friction holding and hydrodynamic lubrication effects are obtained. It means that the advantages of ultra high pressure cannot be obtained in MHDD due to the fracture.

Thus, the micro sheet hydroforming using ultra high fluid pressure can effectively improve the shape accuracy and tribological behavior; however, the simple application of ultra high pressure causes the large thinning at the punch shoulder. To develop the new MUDD process, these difficulties should be considered and overcome.

4.2.2. Concept of new MUDD process

As mentioned in Section 2, it was found that the ultra high pressure is useful to obtain the fracture restriction effects and improve the shape accuracy; however, it cannot be simply applied in MHDD process due to the fracture. A new technique to avoid the fracture and improve the forming limit is required. Generally, the thickness reduction is resulted because the blank is deformed by the traction force of punch and is subjected to the applied force at the punch shoulder in the conventional deep drawing. Furthermore, the deformation area is localized at the same place; punch shoulder. Therefore, the fracture is resulted at the punch shoulder.

To avoid the fracture and improve the forming limit, material flow control and control of deformation area is effective. These techniques are utilizing in the incremental forming [4-1] and the flange pressing [4-2], and the high improvement of forming limit was achieved. By controlling the material flow, the deformation state of blank during the forming process can be controlled. It is possible to reduce the tensile deformation at the punch shoulder and the fracture can be avoided. On the other hand, if the deformation area can be controlled, the deformed area is not localized at the same place, but can be moved to the desired area step by step as with the strain allocation [4-3]. As a result, the local thinning can be avoided and the fracture limit can be improved.

As mentioned above, the material flow control and the control of deformation effectively improve the forming limit. By combining the above incremental forming techniques in micro sheet hydroforming process, it is expected to obtain the advantages of ultra high pressure and significant improvement of forming limit in micro scale. Accordingly, a new forming process, micro ultra deep drawing (MUDD), is developed using the ultra high pressure and incremental control, such as the material flow control and control of deformation area. The concept of new MUDD process is shown in **Fig. 4.1**.

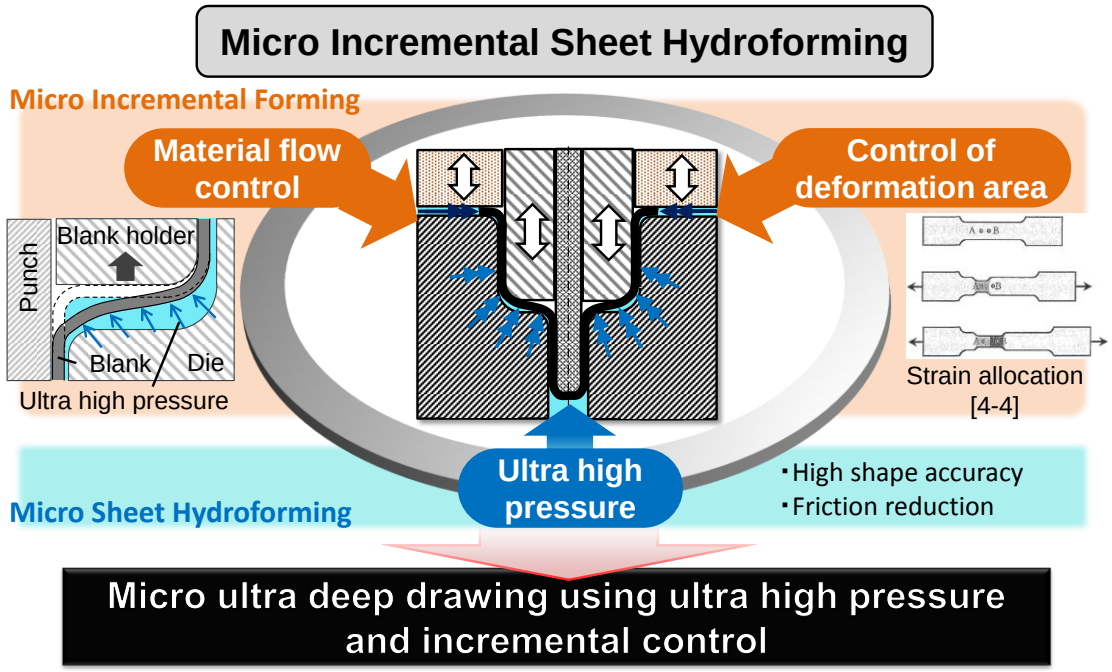

Fig. 4.1 Concept of new micro ultra deep drawing process.

4.2.3. Process sequence of MUDD

Fig. 4.2 shows the micro ultra deep drawing process. The newly proposed process is performed at the 2nd drawing stage. The 2nd punch is inside of the 1st punch to perform the 1st and 2nd drawings at the same axis.

1) The 1st drawing is performed to make cup shape. The 1st punch goes down until the blank contacts with the step part of die.
2) The 1st punch is lifted up and the space is made between the 1st punch and the blank. This 1st punch displacement is defined as Δs. At the same time, the stopper is made contact to the blank edge to restrict the upward movement of blank.
3) The ultra high pressure is applied so as to be disappeared the space between the 1st punch and the blank. The stopper is fixed when the ultra high pressure is applied. At this stage, the blank flows into the die cavity and contacts to the 1st and 2nd punches.
4) The 1st punch lifts down the total value of punch displacement Δs and the flange pressing amount Δt. The 2nd punch and stopper also lift down by keeping the contact with the cup bottom and the cup edge, respectively. The blank thickness at the flange area can be controlled by the flange pressing between the 1st punch and the step part of die in this stage.

These stages 2, 3 and 4 are regarded as 1 cycle. By continuing several cycles, the long micro cup can be drawn. Thus, the material flow can be controlled and the applied force at the punch shoulder may be reduced.

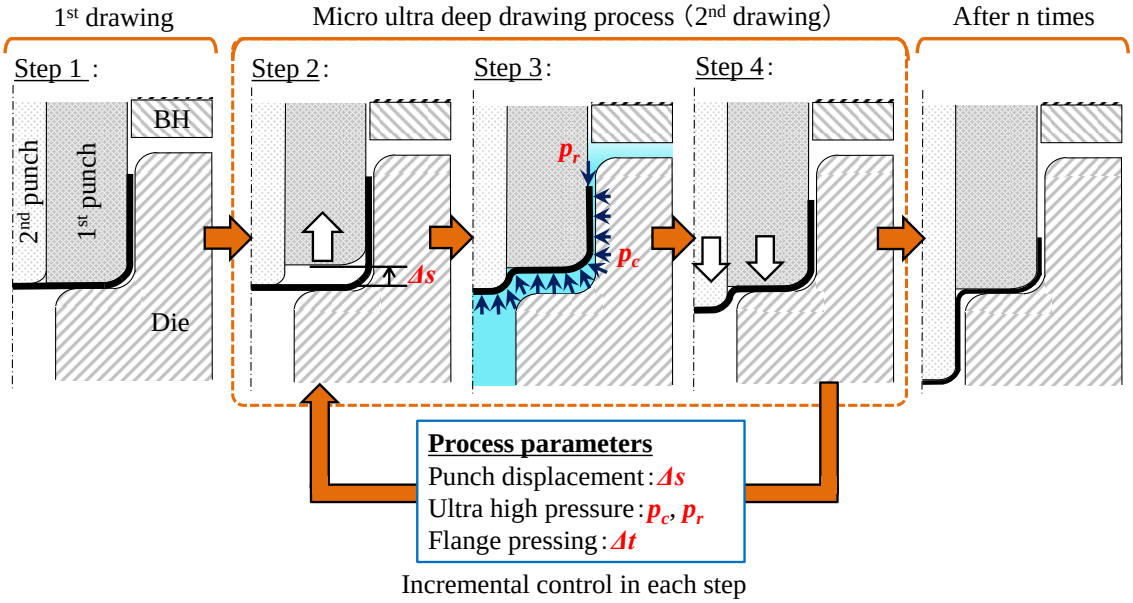

Fig. 4.2 Forming process of micro ultra deep drawing.

4.3. FEM modeling of MUDD

4.3.1. FEM model for MUDD

The numerical analysis was carried out with an explicit dynamic FE code, LS-DYNA ver.971. The blank was modeled as the solid of isotropic elastoplastic, and the tools were modeled as the shell of rigid body. The 8-node solid elements with isotropic elastic-plastic body model were used for the blank, and the tools were treated as the rigid bodies as shown in **Fig. 4.3**. Only one-quarter of the blank and the tools were simulated owing to symmetry. The blank has 5 elements in thickness direction, 100 elements in radial direction, and has the 10 integration points in thickness direction. The stainless steel foil (SUS304-H) of 50μm thickness was employed for FEM. The blank has 53613 solid elements and the tools totally have 13124 shell elements. To eliminate the vibration by upward and downward movement of 1st punch in MUDD process, the dumping coefficient was applied to the blank. The simulation time and the punch speed were 19s and 125mm/s. For the mechanical properties, Young's modulus $E = 197\text{GPa}$ and yield stress $\sigma_y = 589\text{MPa}$ were used. A real stress-strain curve obtained by tensile test shown in **Fig. 4.4** was input into FEM directly as the plastic stress-strain curve.

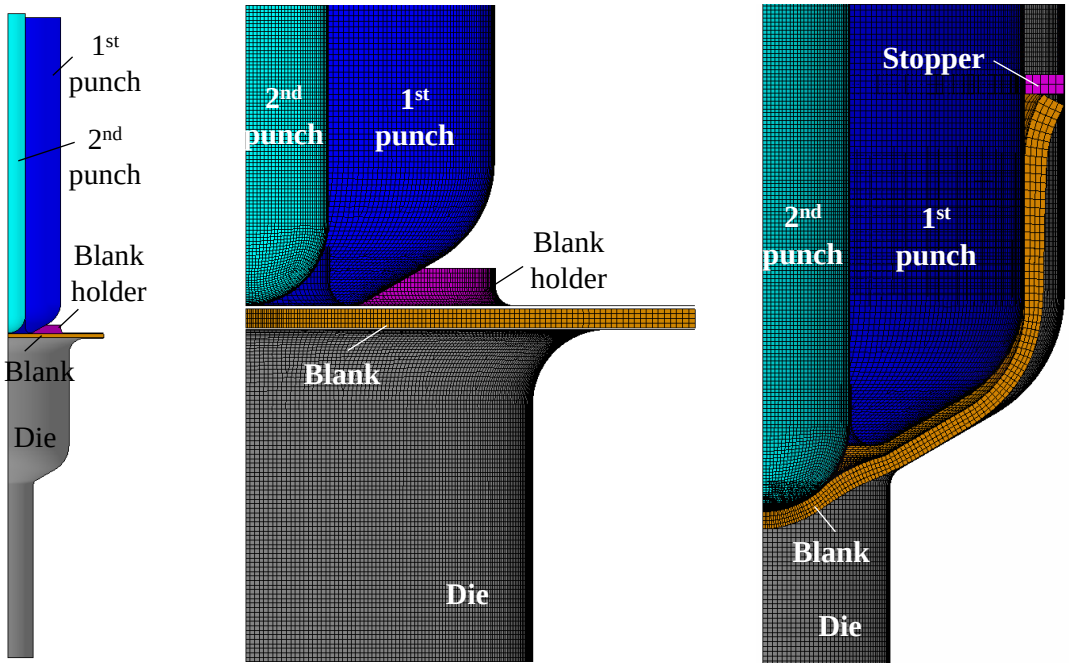

(a) Whole model (b) State in 1st drawing (c) State in 2nd drawing

Fig. 4.3 FEM model of MUDD.

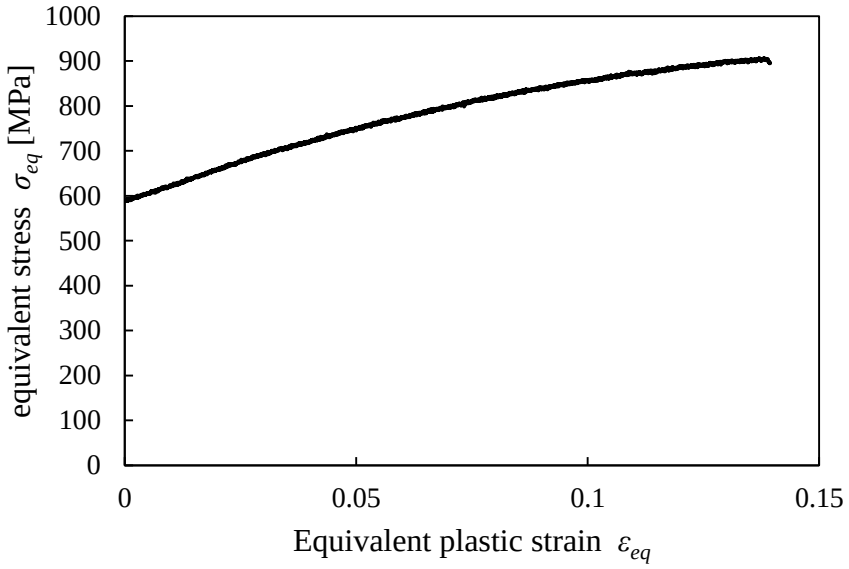

Fig. 4.4 Equivalent stress-strain curve used in FEM simulation.

4.3.2. Numerical conditions

The tooling dimensions used in MUDD are listed in **Table 4.1**. The geometrical parameter for tooling in MUDD is shown in **Fig. 4.5.** The tooling dimensions with the 1st, 2nd and total drawing ratios $DR = DR_1 \times DR_2$ =1.8×2.3=4.14 and DR_1 =1.8, DR_2 =3.0 and DR =5.4 was basically used to investigate the deformation behavior in MUDD. To investigate the drawability in MUDD, the tooling dimensions for $DR = DR_1 \times DR_2 = 2.0 \times 3.5 = 7.0$ and $DR = DR_1 \times DR_2$ =2.0×5.0=10.0 were also adopted. At the 1st drawing, the conventional MDD with constant gap method is adopted. The constant gap is h =0.055mm. The static and kinetic friction coefficients μ_s, μ_k are listed in **Table 4.2**. At the 2nd drawing, the process parameters used in MUDD, the punch displacement Δs, counter and radial pressures p_c, p_r, are listed in **Table 4.3**. The stopper was used to restrict the upward movement of cup edge. The counter and radial pressures were applied and varied in each cycle until the blank contacts with the bottom of 1st punch at flange area. The 2nd punch and stopper was fixed at the steps 2 and 3 and applied the force control to keep the contact with the cup bottom and cup edge at step 4, respectively. The loading paths for the application of counter and radial pressures, stopper, the 1st and 2nd punches are shown in **Fig. 4.6**. As the comparison, MDD and MHDD were also conducted in the 2nd drawing. The forming conditions for each forming method are listed in **Table 4.3**.

Table 4.1 Tooling dimension used in MUDD.

Total drawing ratio *DR*		3.8	5.4	7.0	10.0
1st and 2nd drawing ratios $DR_1 \times DR_2$		1.8×2.1	1.8×3.0	2.0×3.5	2.0×5.0
Initial blank diameter D_0 [mm]		1.700	2.400	3.100	4.440
Drawing punch	1st punch diameter D_{p1} [mm]	0.944	1.330	1.554	2.220
	2nd punch diameter D_{p2} [mm]	0.444	0.444	0.444	0.444
	1st punch shoulder radius r_{p1} [mm]	0.160	0.300	0.300	0.300
	1st punch inner shoulder radius r_{pi1} [mm]	0.060	0.060, 0.140	0.060	0.060
	2nd punch shoulder radius r_{p2} [mm]	0.222	0.222	0.222	0.222
	Taper angle ξ [°]	30	0, 30	30	30
Drawing die	1st die shoulder radius r_{d1} [mm]	0.200	0.200	0.200	0.200
	2nd die shoulder radius r_{d2} [mm]	0.050	0.050	0.050	0.050
Clearance between die and 1st punch c_1 [mm]		0.100	0.100	0.100	0.100
Clearance between die and 2nd punch c_2 [mm]		0.100	0.100	0.100	0.100

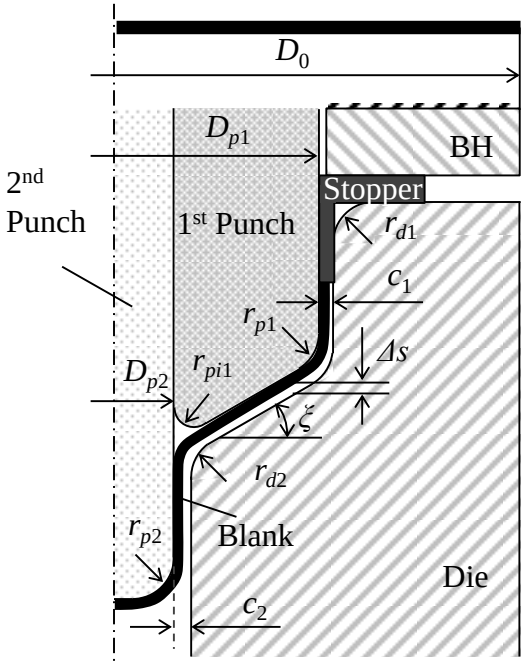

Fig. 4.5 Geometrical parameters for tooling in MUDD.

Table 4.2 Friction coefficient conditions for 1st and 2nd drawing.

Friction coefficient		Blank-1st punch	Blank-2nd punch	Blank-Die	Blank-Blank holder
1st drawing		μ_s=0.35, μ_k=0.30	μ_s=0.35, μ_k=0.30	μ_s=0.02, μ_k=0.01	μ_s=0.35, μ_k=0.30
2nd drawing	MDD	μ_s=0.35, μ_k=0.30	μ_s=0.35, μ_k=0.30	μ_s=0.02, μ_k=0.01	-
	MHDD	μ_s=0.35, μ_k=0.30	μ_s=0.35, μ_k=0.30	μ_s=0.02, μ_k=0.01	-
	MUDD	μ_s=0.02, μ_k=0.01, μ_s=0.35, μ_k=0.30	μ_s=0.02, μ_k=0.01, μ_s=0.35, μ_k=0.30	μ_s=0.02, μ_k=0.01,	-

Table 4.3 Process parameters for MDD, MHDD and MUDD in 2nd drawing.

	Constant gap h [mm]	1st punch displacement Δs [mm]	Counter and radial pressure p_c, p_r [MPa]
MDD	0.055	-	-
MHDD	0.055	-	p_c=p_r=100
MUDD	-	0.05, 0.10	p_c=p_r=100, 200~380, 400~560

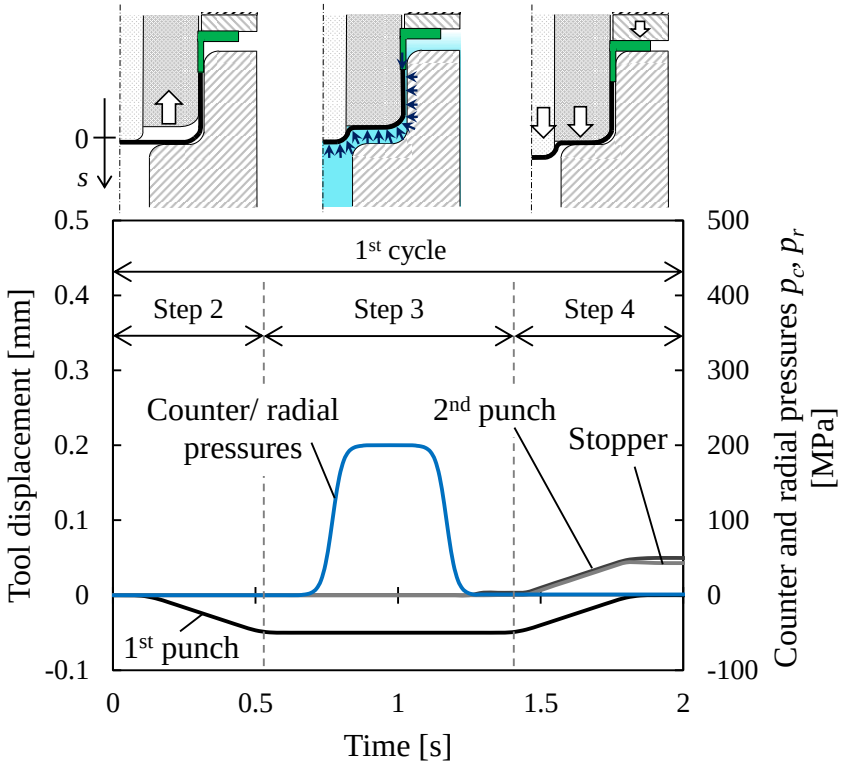

(a) Relationship between the application of ultra high pressures and tools displacements in 1st cycle

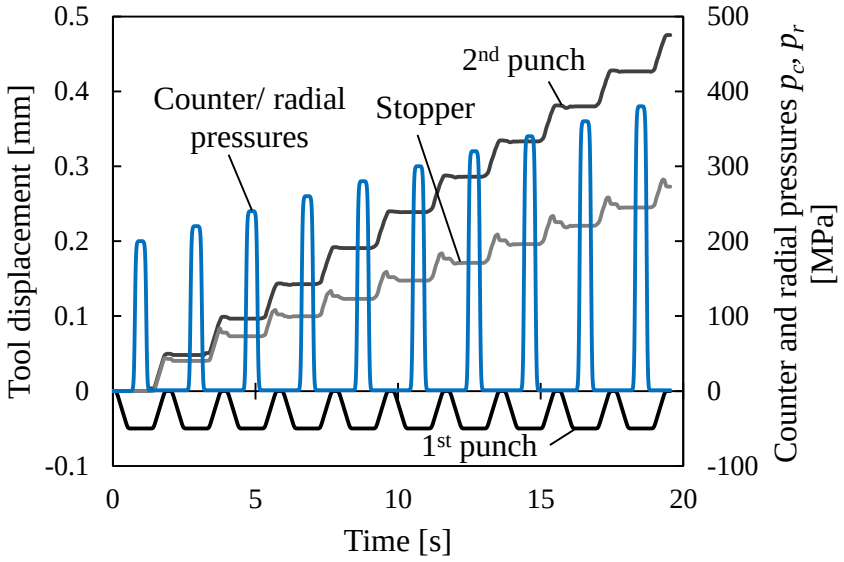

(b) Change of loading path from 1st cycle to 10th cycle

Fig. 4.6 Example of loading path used in MUDD.

4.4. Basic Deformation Characteristics in MUDD

4.4.1. Drawn micro cups

Fig. 4.7 shows the deformation process of blank during MUDD. Through the 1st and the 2nd drawings, the micro cup with total drawing ratio of 3.8 can successfully be fabricated by MUDD. **Fig. 4.8** shows the appearance of micro cups drawn by different forming methods. For the 2nd drawing of MDD and MHDD, the local thinning occurs at the 2nd punch shoulder and the micro cup cannot be drawn. On the other hand, the micro cup with aspect ratio of 2.0 can be successfully drawn in MUDD. It is because the thickness reduction at 2nd punch is prevented in MUDD although the thickness significantly decreases at the 2nd punch shoulder in conventional MDD and MHDD as shown in **Fig. 4.9**. It was found that MUDD can fabricate the micro cup with higher aspect ratio than that at the conventional micro redrawing [4-4].

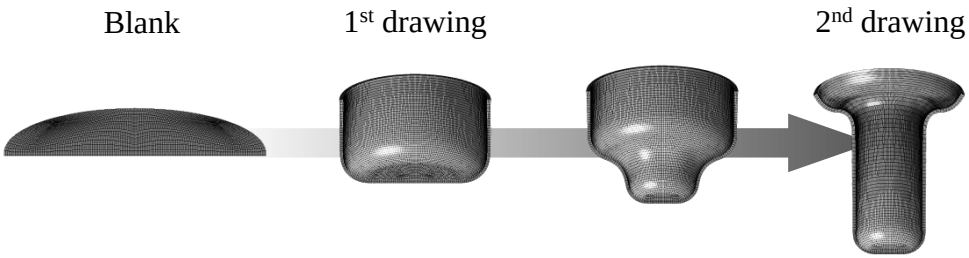

Fig. 4.7 Deformation process of blank during MUDD ($DR = 4.14$, $p_c = p_r = 100$MPa, $\Delta s = 0.03$mm, $\mu_s = 0.20$, $\mu_k = 0.15$).

Drawing stage	1st drawing	2nd drawing		
Forming method	MDD	MDD	MHDD	MUDD
Appearance of drawn micro cups	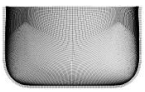 Aspect ratio *H/D*=0.6	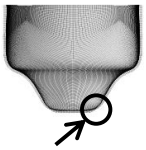 Fracture	 Fracture	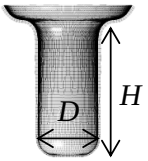 Aspect ratio *H/D*=2.0

Fig. 4.8 Appearance of micro cups drawn by different forming methods.

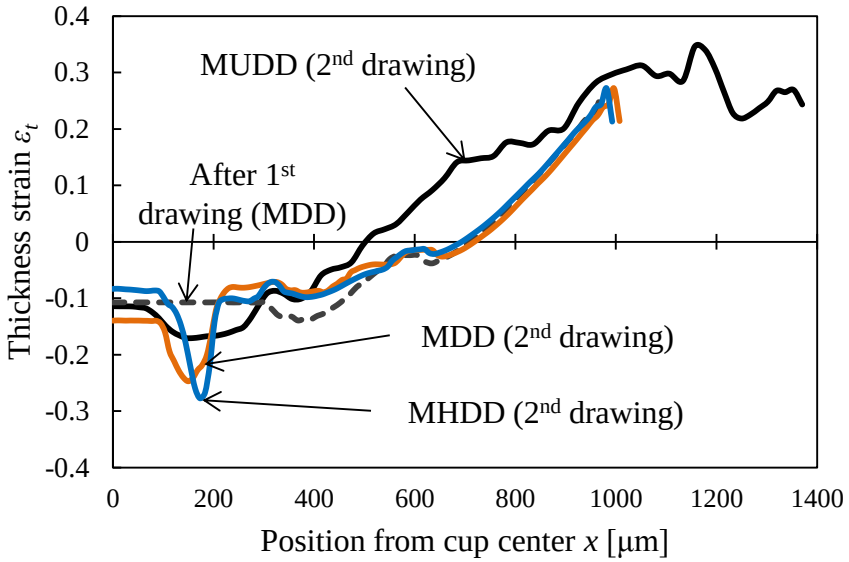

Fig. 4.9 Comparison of thickness strain distribution for each forming method.

4.4.2. Material flow in MUDD

Fig. 4.10 shows the material flow of blank at pressurization process in MUDD. By applying the ultra high pressure to the space between the blank and the 1st punch, the blank at the 2nd punch side wall and flange area flow into the inside. It shows that the application of ultra high pressure can enhance the material flow by counter pressure. In contrast, at the 1st punch side wall of, the blank goes up by counter pressure. It prevents the 1st punch material flow at the side wall unlike at the flange area.

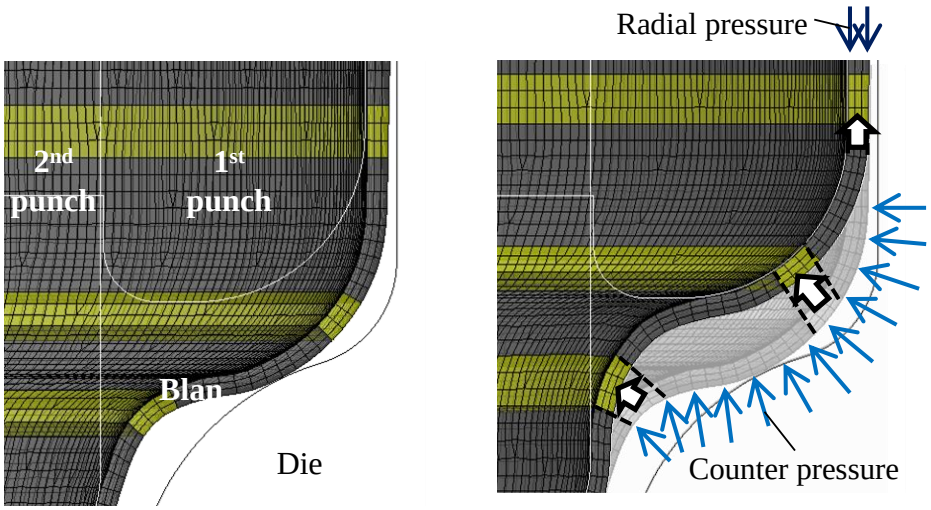

(a) Before applying ultra high pressure (b) After applying ultra high pressure

Fig. 4.10 Material flow of the blank at pressurization process.

4.4.3. Friction holding effect in MUDD

Fig. 4.11 shows the change of thickness distribution near the 2nd punch shoulder during micro ultra deep drawing process. The thickness decreases at the blank which does not contact with the 2nd punch. However, after the blank contacts with the 2nd punch, the thickness does not decrease due the friction holding effect. On the other hand, in MHDD, the thickness significantly decreases at the 2nd punch shoulder. It seems that the friction holding force at the 2nd punch shoulder is not enough to prevent the thickness reduction. In the 2nd drawing of MHDD, the friction holding force occurs not only at the 2nd punch shoulder but also the 1st punch shoulder. It increases the drawing resistance at the flange area. In addition, the blank is deformed by the traction force of punch in MHDD. The blank at the punch shoulder is subjected to the applied force during the forming process. Therefore, the applied force to blank becomes excessive and the fracture occurs. On the other hand, in MUDD, the blank is deformed by the ultra high pressure which enhances the material flow as shown in **Fig. 4.10**. Therefore, the applied force to blank can be reduced. It is because that the friction holding effect can be obtained in MUDD.

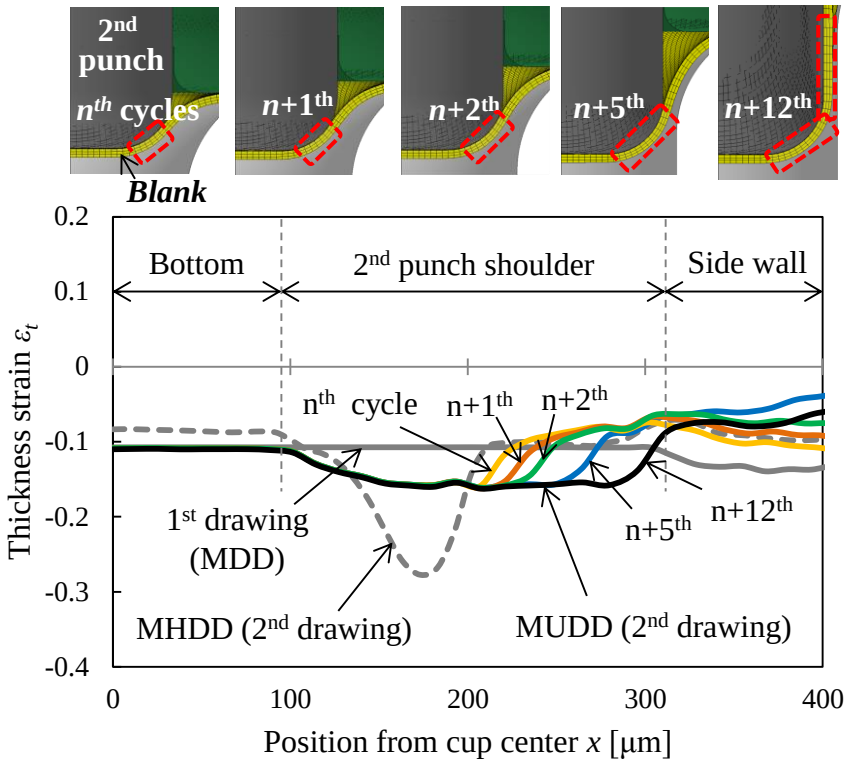

Fig. 4.11 Change of thickness strain distributions near the 2nd punch shoulder during MUDD.

4.5. FEM Based Design of MUDD Process

The basic deformation characteristics were clarified in Section 4. It can be seen that the material flow control by the ultra high pressure and punch displacement and the control of deformation area by constraint of blank deformation is important to achieve the high aspect ratio in MUDD process. They strongly depends on the tooling and process parameters. In MUDD, there are many parameters in MUDD and its relationship is not clarified. In this section, the effect of tooling and process parameters in MUDD are investigated and the forming condition is optimized.

4.5.1. Effect of friction coefficient on deformation behavior

Fig. 4.12 shows the effect of friction coefficient between the blank, the 1st and 2nd punches on change of strain distribution in thickness direction. For the low friction coefficient, the thickness reduces with repeating the cycles. In addition, the position of cup edge is almost the same during MUDD process. It is because the blank edge does not flow into the die cavity but moves upward at pressurization process as shown in **Fig. 4.10**. As a result, the excessive thinning occurs at punch shoulder due to no material flow and the concentration of deformation area at punch shoulder. On the other hand, for high friction coefficient, the thickness reduction occurs during at punch shoulder MUDD process, but is not significant. In addition, after the blank contacts with the 2nd punch, the thickness does not reduce as shown in **Figs. 4.12 (b)** and **4.13**. It is because the friction holding effect occurs and it restricts the thickness reduction at the contact area between the blank and the 2nd punch. Thus, the high friction coefficients between the blank, the 1st and 2nd punches are important to restrict the thickness reduction at punch shoulder by the friction holding effect.

However, because MUDD uses the fluid medium to apply ultra high pressure, there is some possibility of inserting the fluid medium into the gap between the blank and punches. It is difficult to keep the dry friction between the blank and punches. Furthermore, the tensile stress in meridional direction occurs at the punch shoulder at pressurization stage as shown in **Fig. 4.14**. The tensile stress at punch shoulder can be reduced in the case of high friction coefficient; however, the tensile stress in meridional direction cannot be zero. It means that this process possibly has the risks of thickness reduction and fracture. It shows that the quite high forming limit cannot be achieved using high friction coefficient alone.

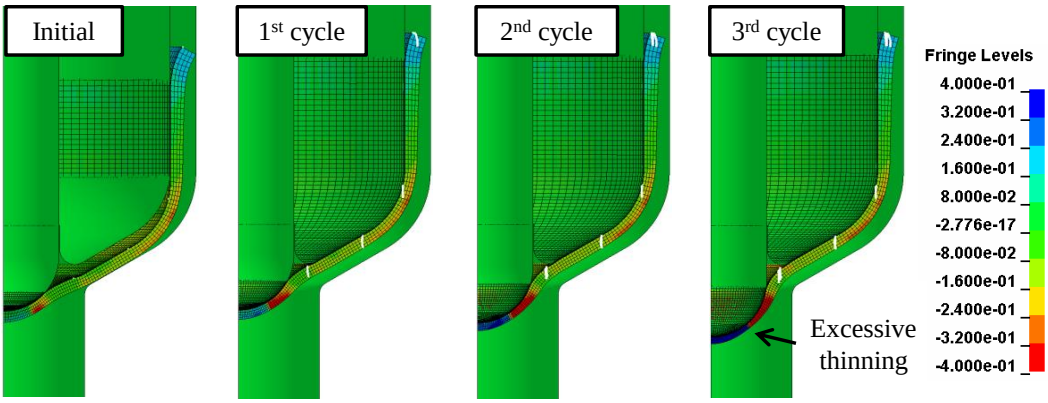

(a) Low friction coefficient between the blank, the 1st and 2nd punches (μ_s =0.02, μ_k =0.01)

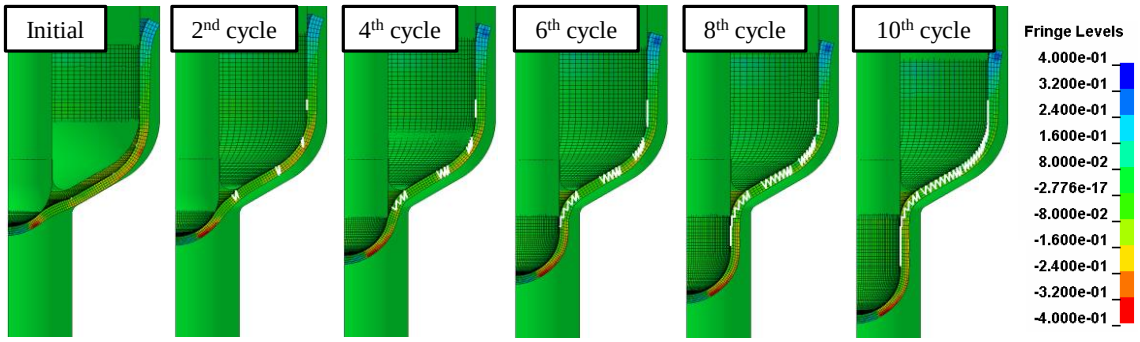

(b) High friction coefficient between the blank, the 1st and 2nd punches (μ_s =0.35, μ_k =0.30)

Fig. 4.12 Effect of friction coefficient between the blank, the 1st and 2nd punches on strain distribution in thickness direction at pressurization process in MUDD (DR =5.4, taper punch, r_{pi1} = 0.05mm, without stopper, Δs = 0.05mm, $p_c = p_r$ = 200~380MPa, t =50μm).

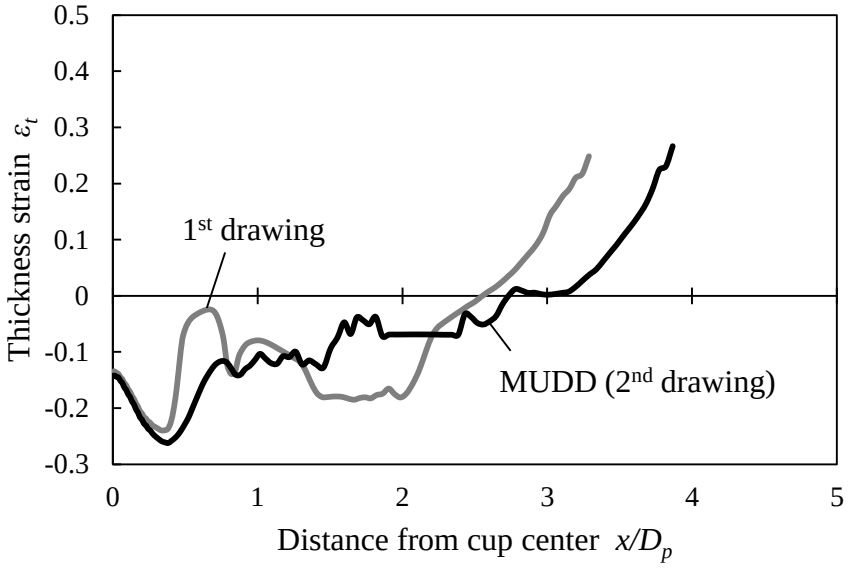

Fig. 4.13 Change of thickness strain distribution during MUDD process (DR =5.4, taper punch, r_{pi1} =0.05mm, without stopper, μ_s =0.35, μ_k =0.30 (Blank-1st and 2nd punches), Δs =0.05mm, $p_c = p_r$ =200~380MPa, t =50μm).

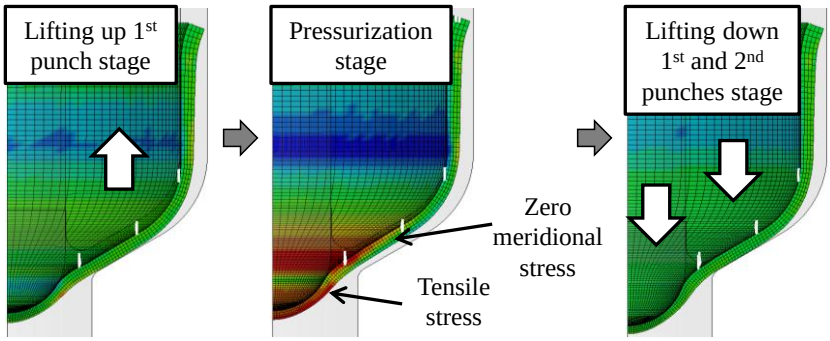

(a) Low friction coefficient between blank, 1st and 2nd punches (μ_s =0.05, μ_k =0.03)

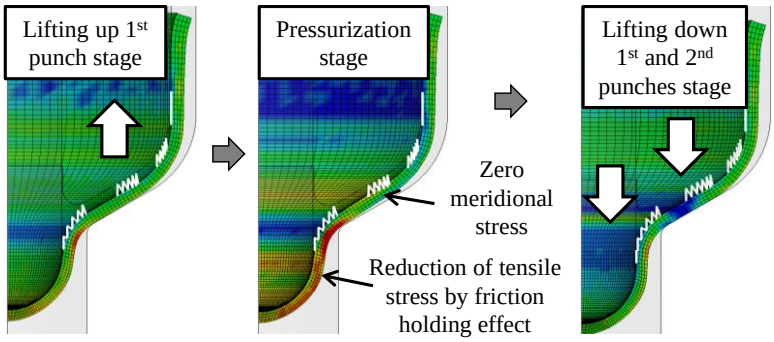

(b) High friction coefficient between blank, 1st and 2nd punches (μ_s =0.35, μ_k =0.30)

Fig. 4.14 Effect of friction coefficient between blank, 1st and 2nd punches on meridional stress distribution during MUDD (DR =5.4, taper punch, r_{pi1} =0.05mm, without stopper, Δs =0.05mm, $p_c = p_r$ =200~380MPa, t =50μm).

4.5.2. Effect of tooling conditions on deformation behavior

Fig. 4.15 shows the effects of existence of stopper and punch shape on change of strain distribution in thickness direction. In flat punch without stopper, the excessive thinning occurs at punch shoulder due to the low friction holding effect at low friction coefficient between the blank, the 1st and 2nd punches as shown in **Fig. 4.15.(a)**. By adding the stopper, the thickness reduction does not occur during MUDD process and the excessive thinning can be avoided even though the friction coefficients between the blank, 1st and 2nd punches are low as shown in **Fig. 4.15.(b)**. However, the thickness is still reduced at 2nd punch shoulder and the excessive thickening occurs at 1st punch shoulder as shown in **Fig. 4.16 (a)**. In the case of taper punch, the excessive thinning can also be avoided using the stopper, although it occurs without the stopper as shown in **Figs. 4.15(c) and (d)**. Moreover, the thinning does not occur at the 2nd punch shoulder and the excessive thickening can be restricted as shown in **Fig. 4.16(b)**.

By using the stopper in MUDD process, the blank is subjected to the compression stress in meridional direction unlike no stopper as shown in **Figs. 4.14(a)** and **4.17**. It is because the deformation and movement of blank at the 1st punch side wall is constrained by the stopper. Hence, the deformation area of blank is localized at the flange area and the material flows into the die cavity. Therefore, not the tensile stress, but the compression stress occurs in flange area by using the stopper in MUDD. It is why the excessive thinning can be avoided in flat and taper punch with stopper.

However, because the compression stress occurs in pressurization stage by using the stopper, the buckling in meridional direction occurs at flange area. Particularly, the buckling is large in the case of flat punch and the insufficient material flow is resulted in area A as shown in **Fig. 4.15(b)**. This insufficient material flow in area A causes the lack of material flow in area B and thinning at the 2nd punch shoulder is resulted. At the same time, the excessive thickening occurs because the material dose not flow from area A to the die cavity but the material flows from the 1st punch side wall to area A. As explained above, the nonuiform material flow in areas A and B causes the thinning behavior at the 2nd punch shoulder and the excessive thickening behavior at the 1st punch shoulder in the flat punch with stopper.

On the other hand, in the case of taper punch, the buckling in the meridional direction can be significantly improved and the material flow becomes uniform as shown in **Fig. 4.15(d)**. Therefore, the thinning at the 2nd punch shoulder and the excessive thickening at the 1st punch shoulder can be avoided because the material flows into the die cavity properly. As mentioned above, the stopper and taper are effective to avoid the thinning and fracture.

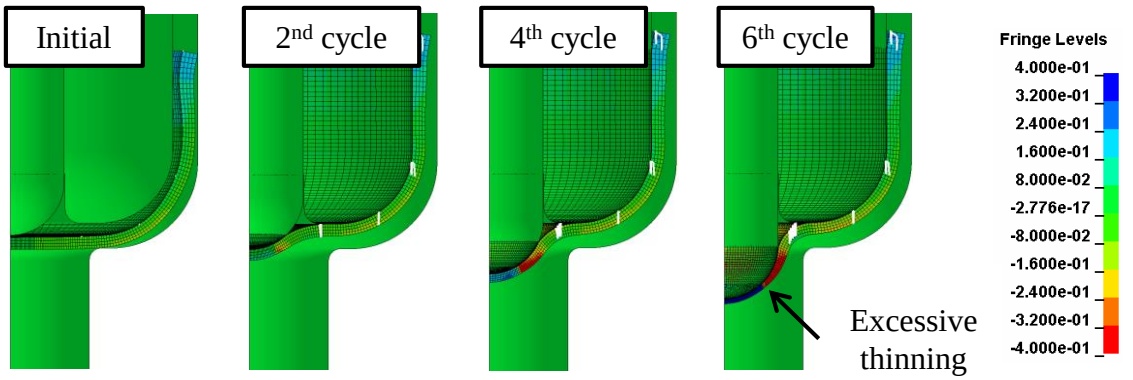

(a) Without stopper in flat punch

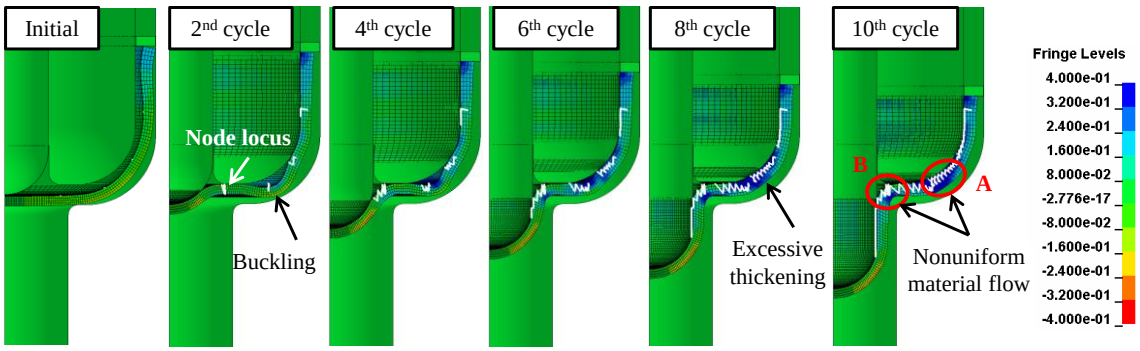

(b) With stopper in flat punch

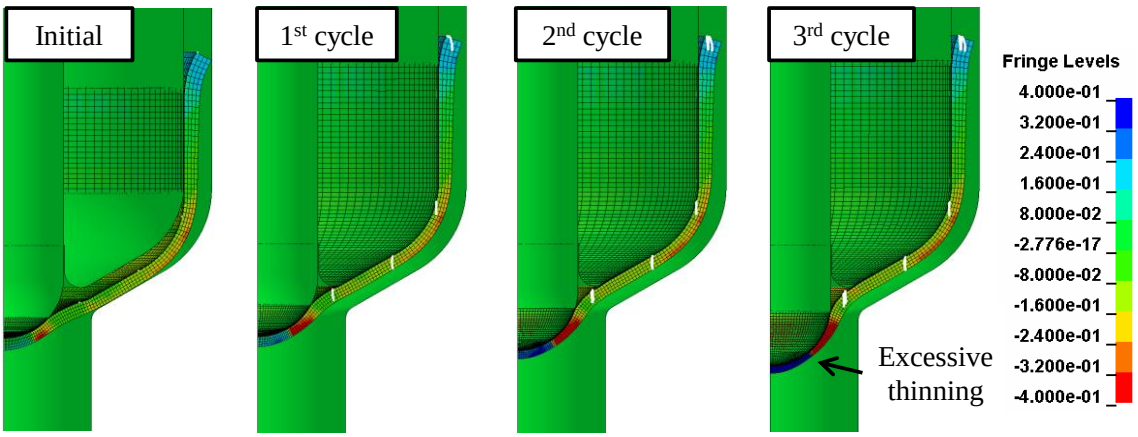

(c) Without stopper in taper punch

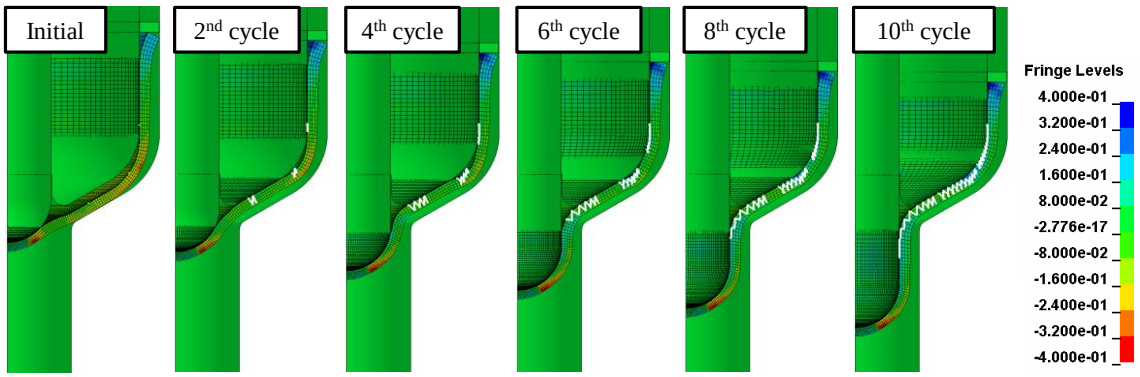

(d) With stopper in taper punch

Fig. 4.15 Effect of stopper and punch shape on strain distribution in thickness direction at pressurization process in MUDD (DR =5.4, r_{pi1} =0.05mm, μ_s =0.02, μ_k =0.01 (Blank-1st and 2nd punches), Δs =0.05mm, $p_c = p_r$ =200~380MPa, t =50μm).

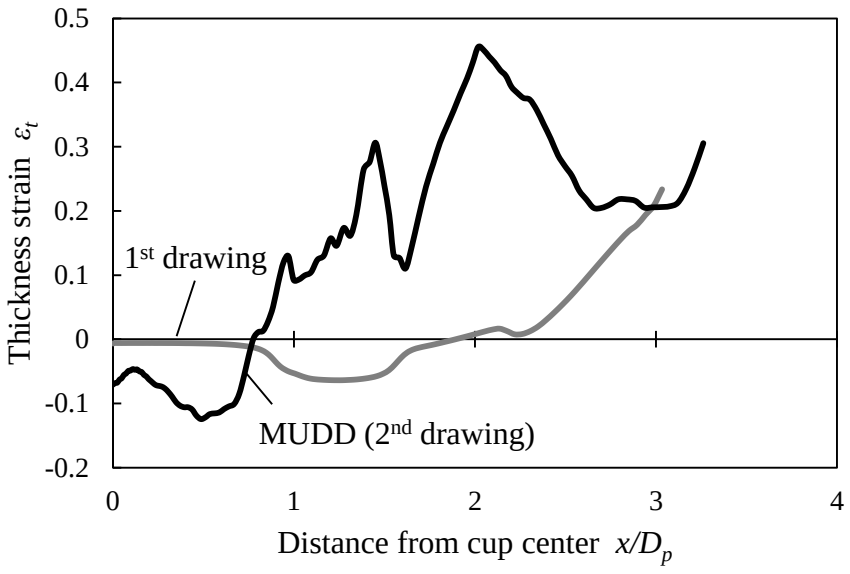

(a) In flat punch

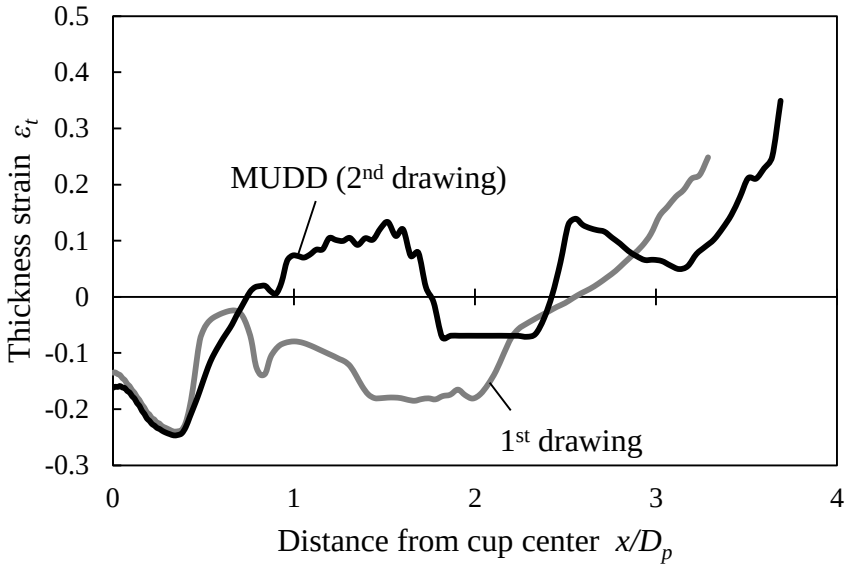

(b) In taper punch

Fig. 4.16 Change of thickness strain distribution during MUDD process (DR =5.4, r_{pi1} =0.05mm, without stopper, $\mu_s = 0.02$, $\mu_k = 0.01$ (Blank-1st and 2nd punches), $\Delta s = 0.05$mm, $p_c = p_r$ =200~380MPa).

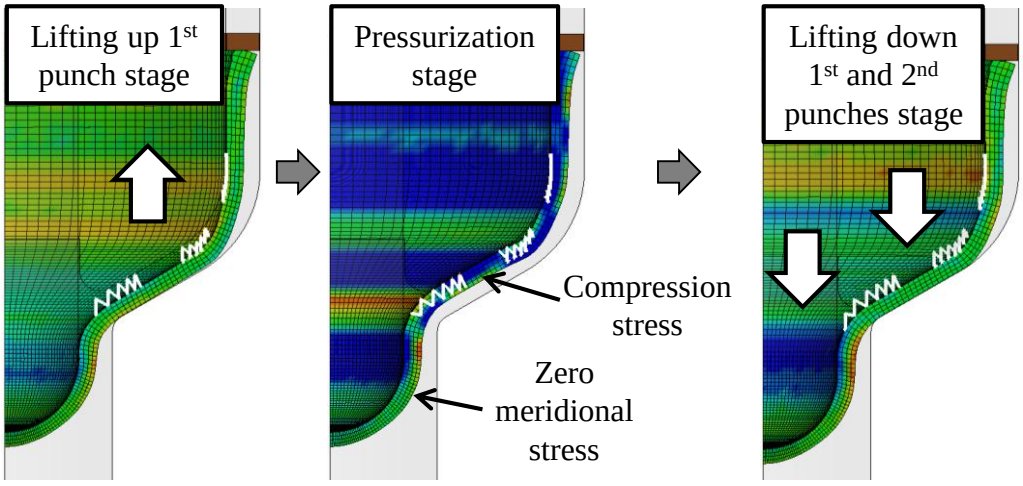

Fig. 4.17 Meridional stress distribution during MUDD with stopper (DR =5.4, taper punch, $\mu_s = 0.02$, $\mu_k = 0.01$ (Blank-1st and 2nd punches), $r_{pi1} = 0.05$mm, $\Delta s = 0.05$mm, $p_c = p_r$ =200~380MPa, t =50μm).

Fig. 4.18 shows the effect of the 1st punch inner shoulder radius on strain distribution in thickness direction. Using the large the 1st punch inner shoulder radius, the blank at the 1st punch inner shoulder is subjected the reverse bulge deformation. It causes that no material flow and no deformation at flange area by applying the ultra high pressure because the stiffness at the 1st punch inner shoulder area increases. Therefore, the micro cup cannot be fabricated in the large the 1st punch inner shoulder radius. Thus, the partial high stiffness interferes the material deformation at flange area. The nouniform material flow by partial high stiffness is also resulted in the small punch shoulder radius. The small punch inner shoulder radius and large punch shoulder radius are required to obtain the uniform material flow in MUDD.

Fig. 4.19 shows the effect of foil thickness on strain distribution in thickness direction. When the thickness of 20μm is used, not only the buckling in the meridional direction, but also the wrinkling in the circumferential direction occurs. The buckling can be eliminated by compressing it using the 1st punch and die because it occurs at flange area. On the other hand, the winkling occurs at die shoulder area. Accordingly, the wrinkles cannot be eliminated by compression using the 1st punch. By using the thickness of 50μm, the wrinkling can be prevented due to the high bending stiffness for the thick thickness. From these results, the foil thickness of 50μm is used in the MUDD.

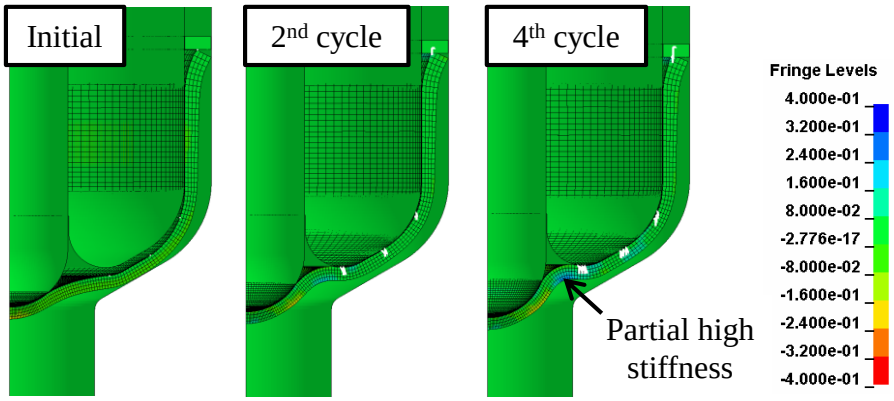

Fig. 4.18 Change of thickness distribution during MUDD with large 1st punch inner shoulder (DR =5.4, taper punch, r_{pi1} =0.10mm, with stopper, μ_s =0.02, μ_k =0.01 (Blank-1st and 2nd punches), Δs =0.05mm, $p_c = p_r$ =200~380MPa, t =50μm).

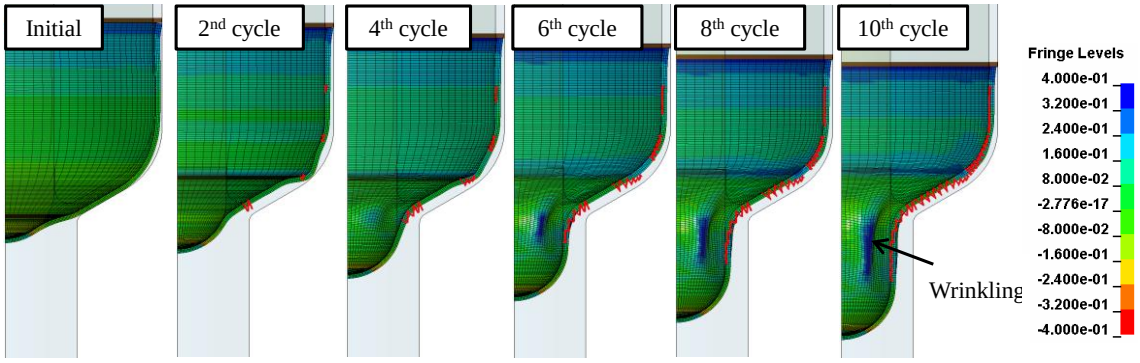

Fig. 4.19 Change of thickness distribution during MUDD for thickness t =20μm (DR =5.4, taper punch, r_{pi1} =0.10mm, with stopper, μ_s =0.02, μ_k =0.01 (Blank-1st and 2nd punches), Δs =0.05mm, $p_c = p_r$ =200~380MPa).

4.5.3. Effect of process parameters on deformation behavior

Fig. 4.20 shows the effect of punch displacement Δs and counter and radial pressure p_c, p_r on strain distribution in thickness direction. Δs in **Fig. 4.20(a)** is twice as large as that in **Fig. 4.14(d**). In this case, the deformation amount in a cycle is large and the thickness reduction at 2nd punch shoulder does not occur. In addition, the revers bulge deformation at the 2nd punch inner shoulder shown in **Fig. 4.18** can be avoided due to the improvement of material flow as shown in **Fig. 4.20(b)**. However, the large Δs causes the large buckling at 1st punch shoulder. It causes the insufficient material flow as with the flat punch shown in **Fig. 4.14(b)**. Furthermore, the shape accuracy of the blank surface decreases due to a nonuniform flange pressing between the 1st punch and die as shown in **Fig. 4.20(a)** and **4.21**.

On the other hand, the counter and radial pressures also affect the deformation behavior in MUDD. When the counter and radial pressures are too low, the blank cannot be deformed. The excessive counter and radial pressures, in contrast, results the reverse bulge deformation at the 2nd punch inner shoulder which causes no material flow due as shown in **Fig. 4.20(c)**. Therefore, the appropriate counter and radial pressures are required to deform the blank and enhance the material flow.

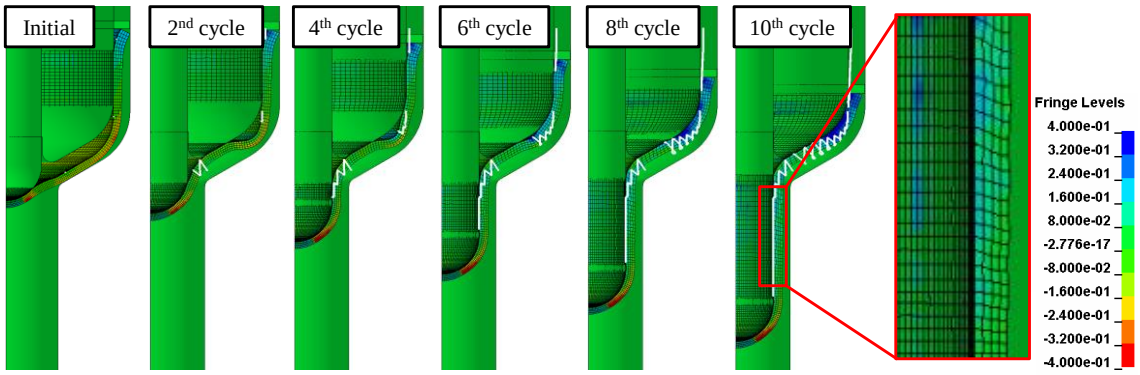

(a) Small punch inner shoulder (r_{pi1} =0.10mm, $p_c = p_r$ =200~380MPa)

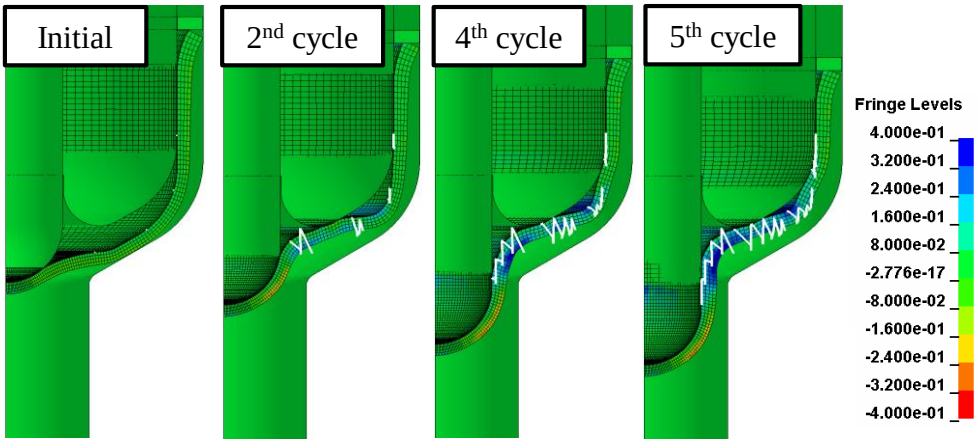

(b) Large punch inner shoulder (r_{pi1} =0.10mm, $p_c = p_r$ =200~380MPa)

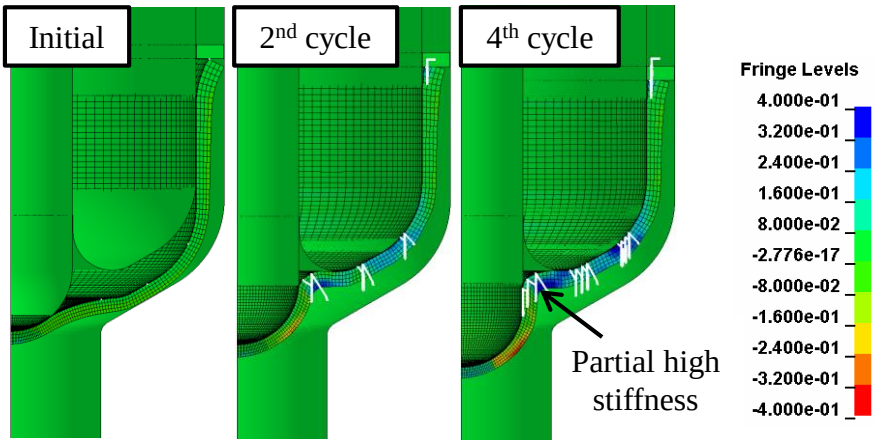

(c) Large punch inner shoulder with higher pressure (r_{pi1} =0.10mm, $p_c = p_r$ =400~560MPa)

Fig. 4.20 Effect of process parameters on change of thickness distribution during MUDD (DR =5.4, taper punch, with stopper, μ_s =0.02, μ_k =0.01 (Blank-1st and 2nd punches), Δs =0.10mm, t =50μm).

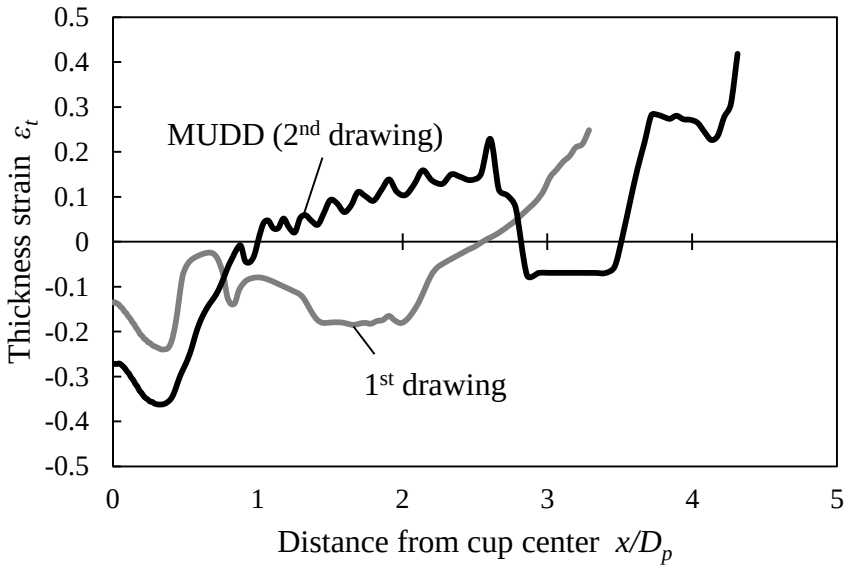

Fig. 4.21 Change of thickness strain distribution during MUDD process (DR =5.4, taper punch, r_{pi1} =0.05mm, without stopper, μ_s =0.02, μ_k =0.01 (Blank-1st and 2nd punches), Δs =0.10mm, $p_c = p_r$ =200~380MPa, t =50μm).

4.5.4. Design guideline for forming conditions in MUDD

Fig. 4.22 shows the effect of tooling and process parameters on failure types in MUDD. It was clarified that the excessive thinning and fracture at the 2nd punch shoulder is resulted by the low friction coefficient between the blank, the 1st and 2nd punches and no stopper to restrict the upward movement at blank edge. The large 1st punch inner shoulder radius and the excessive counter pressure cause no material flow and no material deformation at flange area. On the other hand, the flat punch and large punch displacement results the excessive thickening and low shape accuracy due to the nonuniform material flow. As a result, it was found that the appropriate forming condition to avoid the thickness reduction at the 2nd punch shoulder is the high friction coefficient, the use of stopper, the small 1st punch inner shoulder radius, the proper counter pressure, and the low punch displacement.

			Tooling condition					
			Flat punch		Taper punch			
			Without stopper	With stopper	Without stopper	Without stopper	With stopper	
			μ_s=0.02, μ_k=0.01 (between blank, 1st and 2nd punches)			μ_s=0.35, μ_k=0.30	μ_s=0.02, μ_k=0.01	
			r_{pi}=0.05mm					r_{pi}=0.10mm
Process parameters	Δs=0.05mm	$p_c=p_r$=200~380MPa	✕ Fracture	△ Thickening	✕ Fracture	○	○	✕ No material flow
	Δs=0.10mm	$p_c=p_r$=200~380MPa					△ Low accuracy	△ Low accuracy
	Δs=0.10mm	$p_c=p_r$=400~560MPa						✕ No material flow

Fig. 4.22 Effect of tooling and process parameters on failure modes in MUDD.

4.5.5. FEM based validation of proposed MUDD process for high aspect ratio cup

As mentioned in Section 4, the thickness reduction can be restricted and the uniform material flow and high shape accuracy can be obtained using the appropriate tooling and process parameters. Based on this appropriate forming condition, MUDD with high drawing ratios is conducted to fabricate the micro cup with the aspect ratio.

Fig. 4.23 shows the appearance of drawn micro cup for each drawing ratio. Using proper forming condition, the aspect ratio of 4.6 can be successfully fabricated in MUDD. The thickness at the 2nd punch shoulder does not significantly decreases in MUDD process even in DR =7.0. In addition, the uniform thickness distribution can be obtained at side wall in DR =5.4 and 7.0 due to the flange pressing as shown in **Fig. 4.24**, although it cannot be obtained at DR =3.8 because the flange are is not large enough to do the flange pressing. It shows that the desired thickness can be obtained by controlling the thickening and thinning behavior at the flange pressing stage in MUDD. From above results, it was revealed that MUDD can significantly improve the forming limit due to the deformation localization to restrict the thickness reduction and can improve the shape accuracy to control the thickening and thinning behavior.

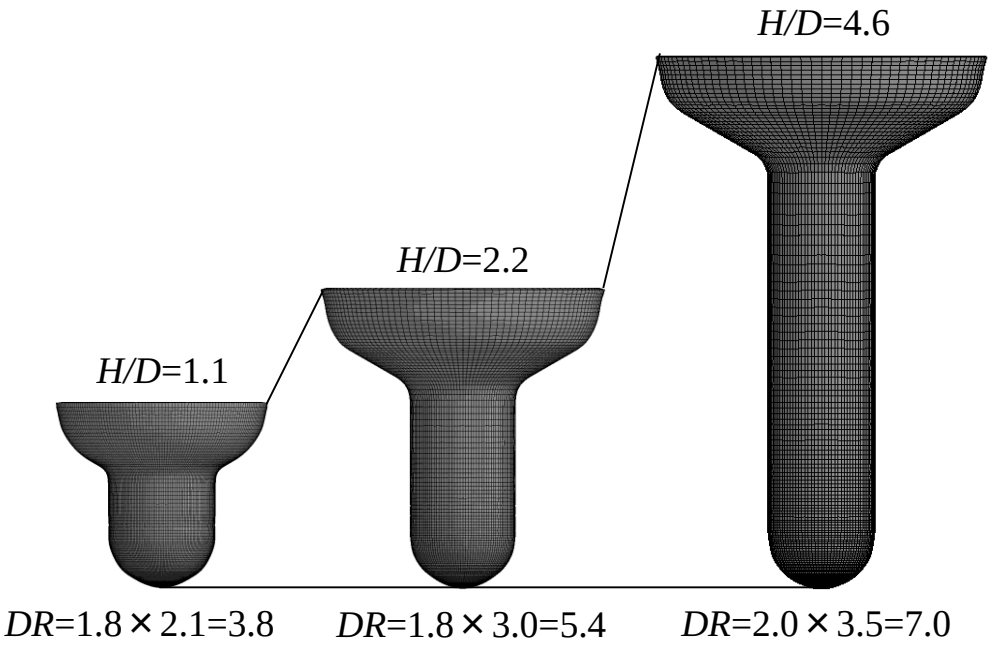

Fig. 4.23 Appearance of drawn micro cup with each drawing ratio.

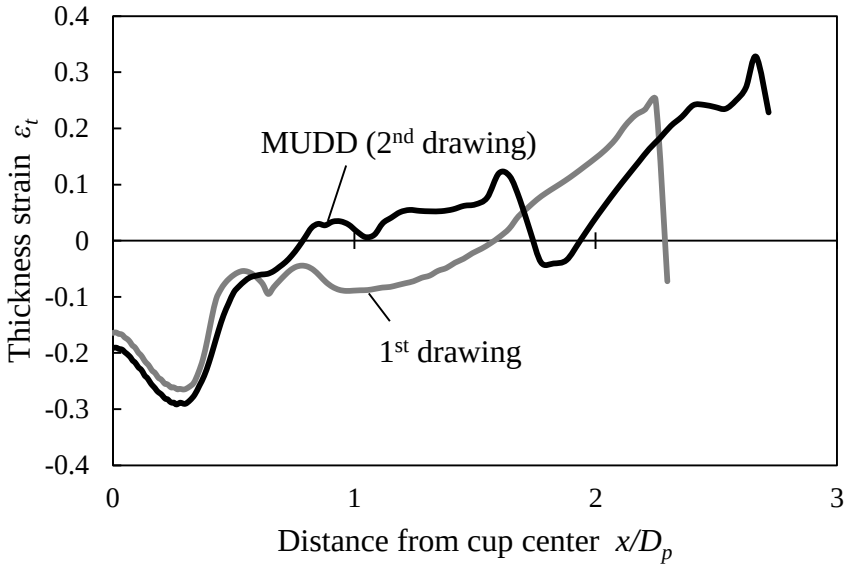

(a) DR =1.8×2.1=3.8

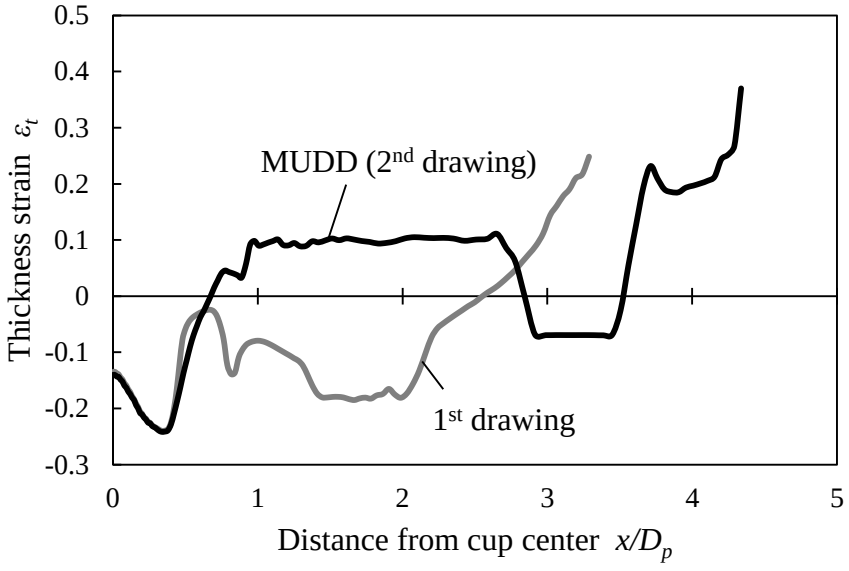

(b) DR =1.8×3.0=5.4

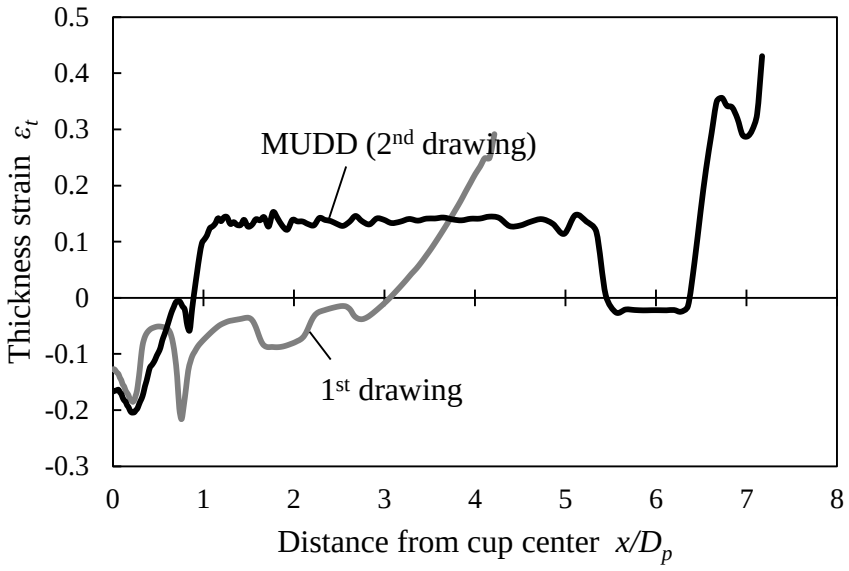

(c) DR =2.0×3.0=7.0

Fig. 4.24 Thickness strain distribution before and after MUDD.

4.4. Concluding Remarks

In this chapter, the newly micro ultra deep drawing (MUDD) process by combining the ultra high pressure and incremental control was developed. Furthermore, the appropriate forming condition to achieve the high aspect ratio and high shape accuracy in MUDD was designed by FEM simulation. The main conclusions are as follows;

(1) The MUDD process with 1st and 2nd punches in the same axis was developed, which can fabricate the long micro cup by repeating ① making the space between the 1st punch and blank by lifting up the 1st punch, ② applying the ultra high pressure so as to disappear this space, and ③ lifting down the 1st and 2nd punches at the same time.

(2) In MUDD process, the material flow can be induced by the ultra high pressure and incremental control of punch movement. The deformation area can be controlled by the material constraint at 2nd punch side wall by friction holding effect and at 1st punch side wall by the stopper. These effects can prevent the local thinning at 2nd punch shoulder and avoid the fracture. Due to these effects, the MUDD process can achieve larger drawing ratio than the conventional MDD and MHDD.

(3) The MUDD process and forming condition for the high forming limit and high shape accuracy was designed. It was found that the thickness reduction at 2nd punch shoulder can be avoided by the high friction coefficient, the use of stopper, the small 1st punch inner shoulder radius, the proper counter pressure, and the small punch displacement. Using the appropriate forming condition, the micro cup with aspect ratio of 4.6 and uniform thickness distribution can be obtained.

References

[4-1] J. Jeswiet, F. Micari, G. Hirt, A. Bramley, J. Duflou, J. Allwood, Asymmetric single point incremental forming of sheet metal, CIRP Annals – Manufacturing Technology, 54, (2005), 88-114.

[4-2] T. Iizuka, Fabrication of ultra long cup by the deep drawing of thin sheet using press compression, The Proceedings of the 3rd Integrated Advanced Conference in the Light Metal Educational Foundation, (2013), 47-53.

[4-3] K. Kitazawa, Incremental forming for new reuse technology, Journal of the Japan Society for Technology of Plasticity (in Japanese), 42-4889, (2001), 1001-1007.

[4-4] K. Manabe, T. Shimizu, H. Koyama, M. Yang, K. Ito, Validation of FE simulation based on surface roughness model in micro-deep drawing, Journal of Materials Processing Technology, 204, (2008), 89-93.

Chapter 5

Development of MUDD System and Its Experimental Verification

5.1. Introduction

In Chapter 4, micro ultra deep drawing (MUDD) process with ultra high pressure and incremental control was designed by FEM. The designed MUDD process can realize the material flow control and the control of deformation area. The material flow control is important to reduce the tensile stress during MUDD process to avoid the fracture. Furthermore, it is effective to obtain the uniform and desired thickness distribution. The material flow can be optimized by the ultra high pressure, taper punch, and small 1^{st} punch displacement. On the other hand, the control of deformation and undeformation areas is important to avoid the local thinning behavior. The deformation of blank at 2^{nd} punch shoulder and at the 1^{st} punch side wall should be constrained by the friction holding effect and stopper to avoid the local thinning behavior and fracture. The deformation area should be localized at the flange area. The designed MUDD process can realize the high aspect ratio and uniform thickness distribution. Thus, the possibility of MUDD process was numerically clarified.

To realize MUDD process, the blank holder, the 1^{st} and 2^{nd} punches should be incrementally and independently controlled. In addition, the application of ultra high pressure is required. However, the MUDD tool set will be complicated to realize the incremental and independent control of several tools in the limited space with high accuracy. Furthermore, the generation of ultra high pressure is normally not easy in macro scale due to its high energy and complex structure of hydraulic system. They should be realized in the limited space in the compact tool sets. In this section, a newly MUDD system with triple action servo press machine and ultra high hydraulic system is developed. Using the developed MUDD system, the possibility of MUDD process is experimentally discussed.

5.2. Development of MUDD System

The simple apparatus was developed by decreasing the number of control targets one stroke forming, constant gap method, small clearance between tools and multi axial tooling. However, to realize MUDD process, the blank holder force should be minutely controlled and multi axial should be realized to control several tools separately. Furthermore, the ultra high pressure can enhance the effect of fluid pressure and expand the scope of applicable target size and shape. For this reason, the MUDD system including high blank holder force control, multi axial press machine, and ultra high hydraulic system is developed.

5.2.1. Tooling structure

In MHDD tool, the one stroke forming [5-1] was adopted to conduct the blanking, the 1st drawing process coaxially. In MUDD process, not only the 1st drawing but also 2nd drawing should be conducted; however, they are normally conducted in different axials with transferring material. To conduct the 1st drawing, the 2nd drawing coaxially, the 2nd punch, which conducts the 2nd drawing, is placed at inside of 1st punch, which is for 1st drawing, as shown in **Fig. 5.1**. The MUDD tools consist of 4 parts. The bottom tools have almost same function with MHDD tool which can conduct the blanking and 1st drawing process. The 2nd drawing punch is assembled in the tool in the top to conduct the 2nd drawing. The blank holder is assembled in the second tool from the top to conduct blank holder control. Thus, this MUDD tool can conduct the blanking, blank holder control, the 1st and the 2nd drawings processes in the same axial. The tolerance of punches, die and blank holder is ±0.001 mm in flat area and ±0.010 mm in shoulder area. To measure the blank holder, the 1st and 2nd punches forces, the ultra compact load cell with high accuracy (KYOWA : LMB-A-200N) was assembled in the tool. Its maximum loading capacity is 200N. One load cell was used for the 2nd punch, and three load cells were used for the 1st punch and blank holder. The appearance of developed MUDD is shown in **Fig. 5.2**. The MUDD tool has approximately 100mm wide, 100mm long and 225mm tall. It is compact enough for triple axial tooling.

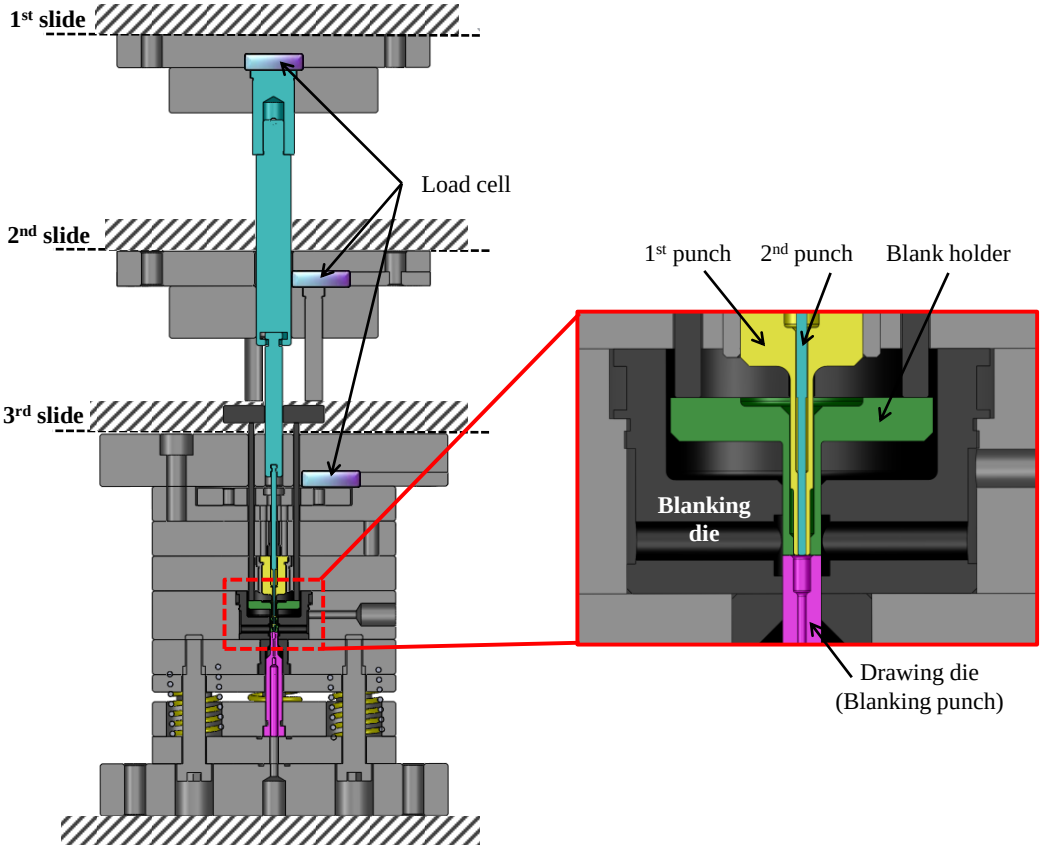

Fig. 5.1 Schematic of cross section of MUDD tool.

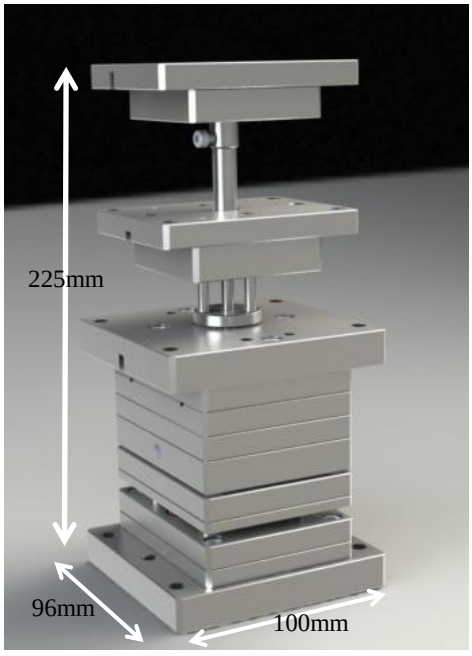

Fig. 5.2 Appearance of developed tool set.

5.2.2. Ultra high hydraulic system

In macro scale, to generate and control the ultra high pressure, the large, complex and expensive equipment is required because a quite high energy is needed to generate the ultra high pressure with large flow rate and it has a high risk. For this reason, it is limited to use the ultra high pressure in macro metal forming. On the other hand, in micro scale, the energy of generated ultra high pressure can be reduced significantly in micro scale because the required flow rate is small. It means that the ultra high pressure can be generated by simple equipment without the risk. Based on these advantages, the simple ultra high hydraulic system is developed.

(1) Ultra high pressure generator

Fig. 5.3 shows the schematic of ultra high hydraulic system. The fluid medium is filled in the cylinder and it is compressed by the piston connected to press machine. In this simple ultra high pressure generator, the generated pressure is determined by the cross section of piston and maximum capacity of press machine. The diameter of piston is 10mm and maximum capacity of press machine is 50kN. The design ultra high pressure is approximately 400MPa. **Fig. 5.4** shows the appearance of developed ultra high pressure system. As the hydraulic piping, the stainless steel small pipes and the ultra high pressure sensor with allowable pressure of 500MPa (WIKA Instrument: Type HP-2-S) was used.

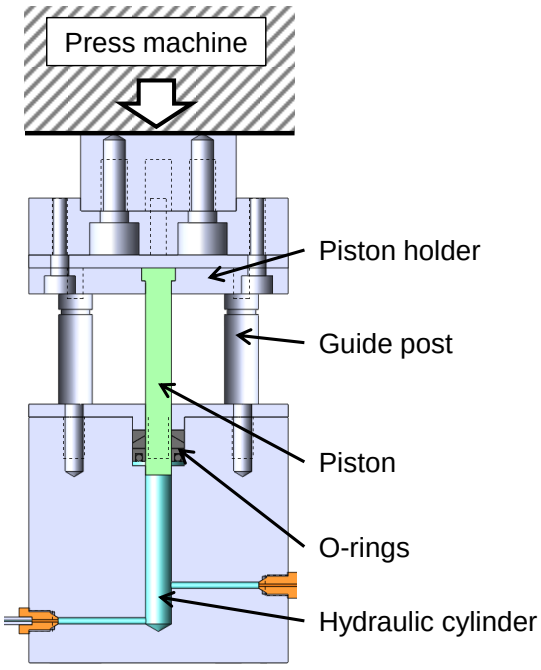

Fig. 5.3 Schematic of ultra high pressure generator.

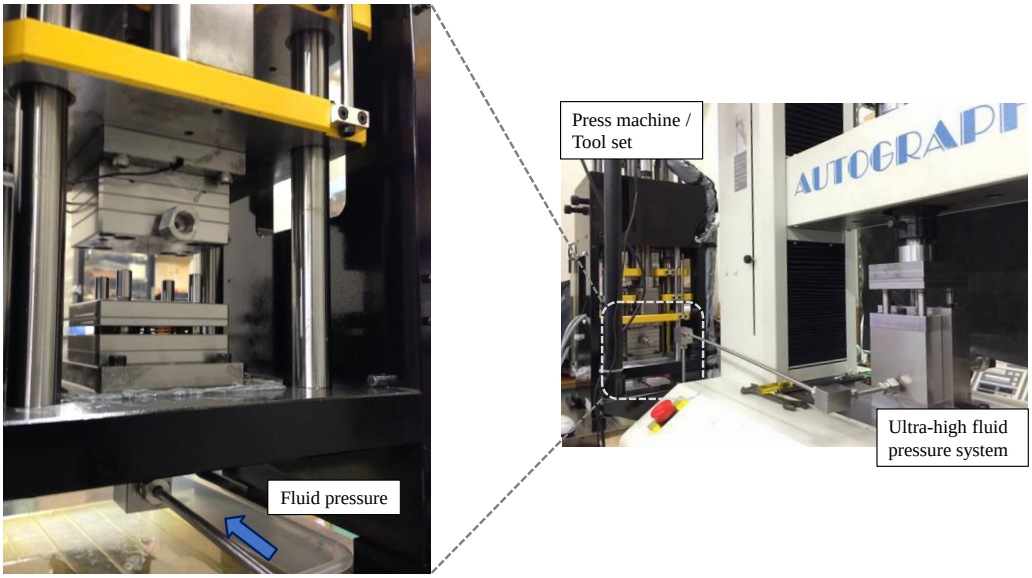

Fig. 5.4 Appearance of ultra high hydraulic system.

(2) Sealing and flow pass for counter and radial pressures

In MUDD system, not only counter pressure but also radial pressure can be applied. The counter pressure is applied from the bottom of MUDD tool as shown in **Fig. 5.5**. On the other hand, the radial pressure cannot be directly applied to blank edge due to the limitation of space and complex tool shape in the MUDD tool. Therefore, the fluid medium is applied from the side of MUDD tools and is enclosed 360 degree; then, the radial pressure is applied to blank edge from 4 holes in the blanking die bush as shown in **Fig. 5.5**. For the sealing, the O-rings and 1μm clearance between the tools mentioned at Section 3.2 were adopted as shown in **Fig. 5.6**.

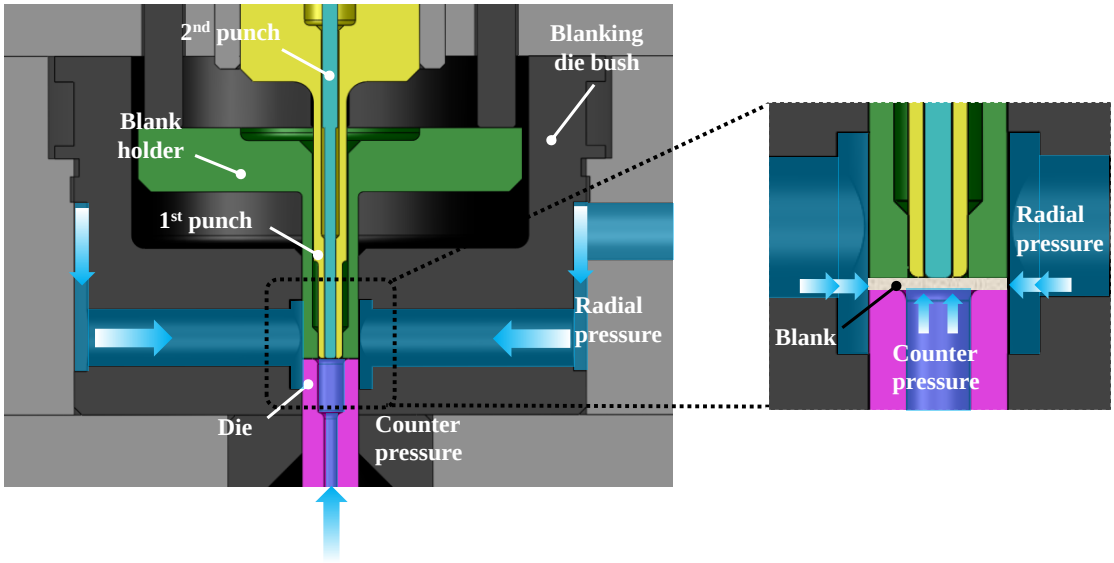

Fig. 5.5 Schematic illustration of fluid pressurized structure in developed apparatus.

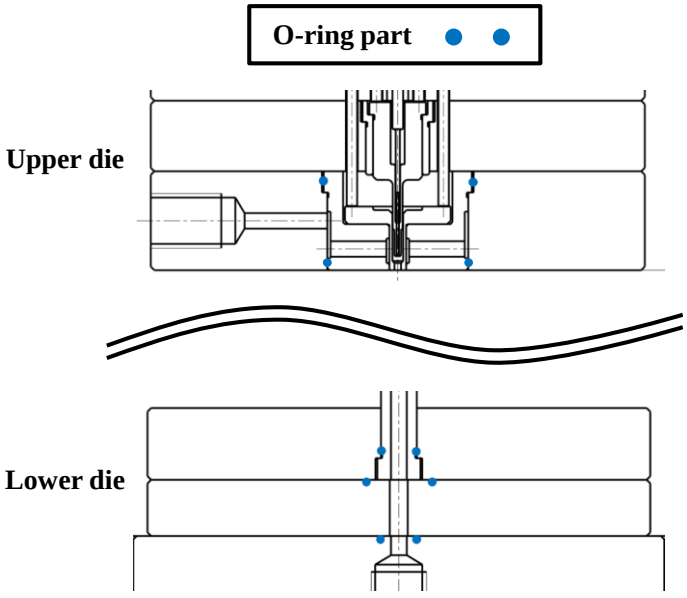

Fig. 5.6 Schematic illustration of sealing part by O-rings.

5.2.3. Triple action servo press machine

(1) Control of blank holder force

In MHDD, the constant gap method [5-2], in which the gap between the blank holder and die is fixed, is adopted to realize the stabilization of forming process in micro scale. However, the blank holder force and position cannot be controlled during the forming process. Accordingly, the multi slides set up in the press machine to control not only punches but also blank holder. Using the closed loop feedback control, the blank holder force and position were controlled continuously.

(2) Appearance of triple action servo press machine

Fig. 5.7 shows the appearance of developed MUDD system. The desktop type triple action servo press machine with high accuracy (LLC. MICRO FABRICATINO LABORATORY) was developed. This press machine can control the three slides separately. The 1^{st}, 2^{nd} and 3^{rd} slides control the 2^{nd} punch, blank holder and blanking die and 1^{st} punch, respectively. To realize slide position control with high accuracy, the servo mortar (MITSUBISHI ELECTRIC Co.: HG-MR23(B)) was adopted for control of the 2^{nd} slide and the stepping motors (ORIENTAL MOTOR Co., Ltd.: AR66SMK-N10-2) were adopted for control of the 1^{st} and 3^{rd} slides. Maximum working speed is 20mm/s and minimum operation amount of slide position by jog feeding is 0.001mm. Thus, the developed triple action servo press machine can control the slides separately and realize incremental control. The specification of developed triple action servo press machine is listed in **Table 5.1**.

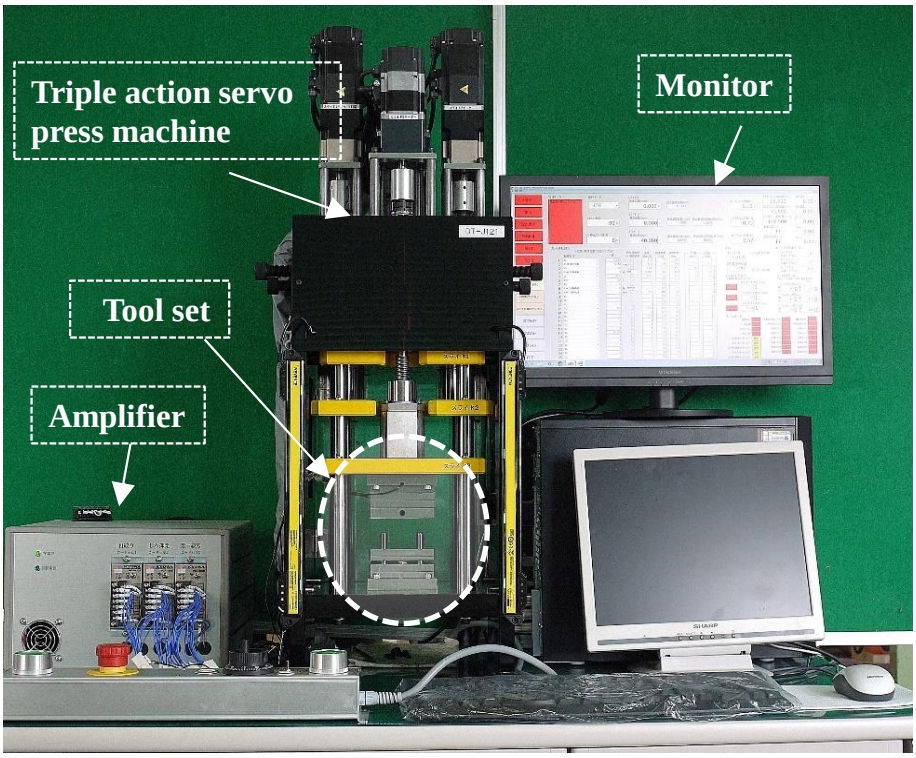

Fig. 5.7 Appearance of developed MUDD system.

Table 5.1 Specification of newly developed triple action servo press machine.

Triple action servo press machine	Press machine size [mm]		302W×330D×853H
	Maximum load capacity [kN]	1st slide	5
		2nd slide	10
		3rd slide	10
	Maximum stroke length [mm]	1st slide	80
		2nd slide	73
		3rd slide	44
	Maximum motion speed [mm/s]		20
	Load control resolution capability [g]		±10
	Hand motion JOG operation range [mm]		0.1 ~ 0.001
Tooling	Forming process	One-stroke forming	
	Blank holder	Blank holder force control method	
	Pressure generation	1μm clearance between tools	

(3) Operating system of triple action press machine

All of operation is performed using computer by inputting the data from motors, load cells and pressure sensors. Control program was made by Visual Basic. The operating modes for each slide are the position control (separately or simultaneously), force control (keep, above or below) and vibration (amplitude, time). The combination of these programs can realize several tooling motions. **Fig. 5.8** shows the monitor of operating system. The punch force-stroke and force, position-time curves for each punch and blank holder are displayed in this monitor.

Finally, the comparison of functions between MHDD and MUDD systems is listed in **Table 5.2**.

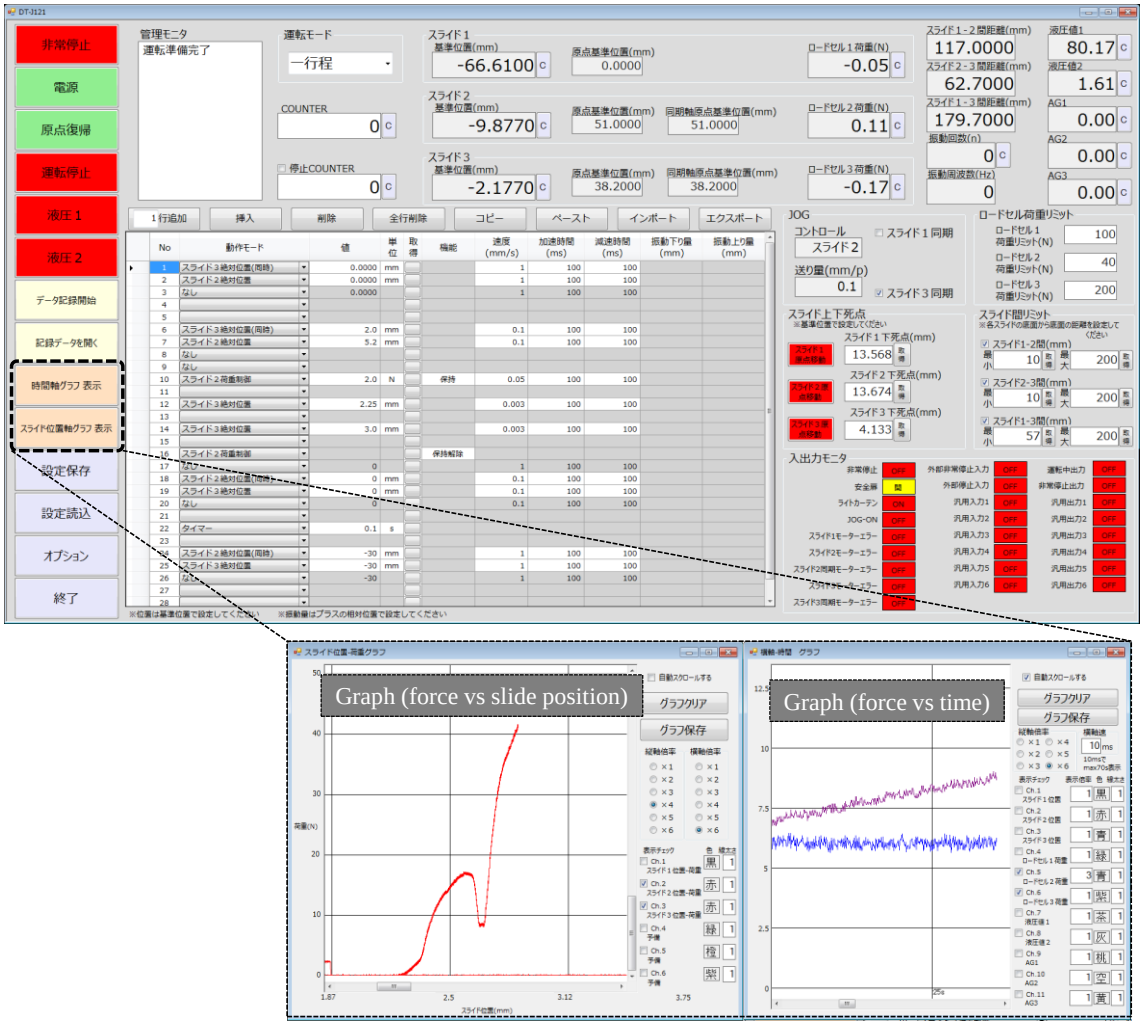

Fig. 5.8 Operating monitor for MUDD system.

Table 5.2 Comparison of functions between MHDD and MUDD systems

	MHDD apparatus	MUDD apparatus
Apparatus size [mm]	250W×265D×630H	302W×330D×853H
Press machine type	Single action servo press	Triple action servo press
Blank holder methods	Constant gap method	Constant gap, Blank holder and Displacement control methods
Maximum pressure [MPa]	20	400
Fluid pressure type	Counter pressure	Counter and radial pressures
Forming process	One stroke forming (Blanking and 1st drawing)	One stroke forming (Blanking, 1st and 2nd drawings)

5.3. Experiment of MUDD

5.3.1. Experimental procedure

(1) Material used

To fabricate the micro cup with high aspect ratio, the ultra-fine grained stainless steel foil (SUS304) of with thickness of 50μm were employed, which has the excellent material properties and can achieve the small dispersion. The average grain size is 2.29μm as shown in **Fig. 5.9**. The mechanical properties of the materials used are listed in **Table 5.3**.

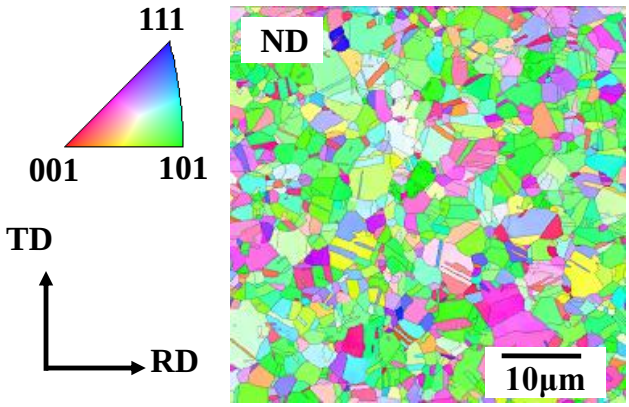

Fig. 5.9 EBSD image of micro structure for ultra-fine grained stainless steel foil.

Table 5.3 Material properties of ultra-fine grained stainless steel.

Yield stress σ_y [MPa]	Tensile strength σ_B [MPa]	Elongation δ [%]	Grain size d [μm]
522	875	46	2.3

(2) Experimental conditions

The tooling dimension used in experiment is listed in **Table 5.4**. The total drawing ratios for the MUDD tools are DR =3.8 and 7.0. The appearance of used tools is shown in **Fig. 5.10**. These tools are made of sintered WC-Co hard alloy (JIS: V20 tungsten carbide-cobalt alloy). The blank holder force used in the 1st drawing process, the punch displacement, the counter and radial pressure used in MUDD process are listed in **Table 5.5**. The counter and radial pressures were manually applied using the ultra high pressure generator shown in **Fig. 5.4**. They were kept several second at pressurization stage and increases with repeating the cycles. The loading path of MUDD used in experiment is shown in **Fig. 5.11**. To insert the stopper, the upper tool lifted up and the space was made between the upper and lower tools after the 1st drawing. When the stopper is inserted into die and contacts with the blank edge, the upper tool goes down and the 2nd drawing is conducted. The lubrication with high viscosity is applied to the material on the side of die. The drawing punch speed was 0.01mm/s.

Table 5.4 Tooling dimension used in experiment.

Total drawing ratio DR		3.8	7.0
1st and 2nd drawing ratios $DR_1 \times DR_2$		1.8×2.1	2.0×3.5
Initial blank diameter D_0 [mm]		1.700	3.100
Drawing punch	1st punch diameter D_{p1} [mm]	0.944	1.554
	2nd punch diameter D_{p2} [mm]	0.444	0.444
	1st punch shoulder radius r_{p1} [mm]	0.160	0.300
	1st punch inner shoulder radius r_{pi1} [mm]	0.060	0.060
	2nd punch shoulder radius r_{p2} [mm]	0.222	0.222
	Taper angle ξ [°]	30	30
Drawing die	1st die shoulder radius r_{d1} [mm]	0.200	0.200
	2nd die shoulder radius r_{d2} [mm]	0.050	0.050
Clearance between die and 1st punch c_1 [mm]		0.100	0.100
Clearance between die and 2nd punch c_2 [mm]		0.100	0.100

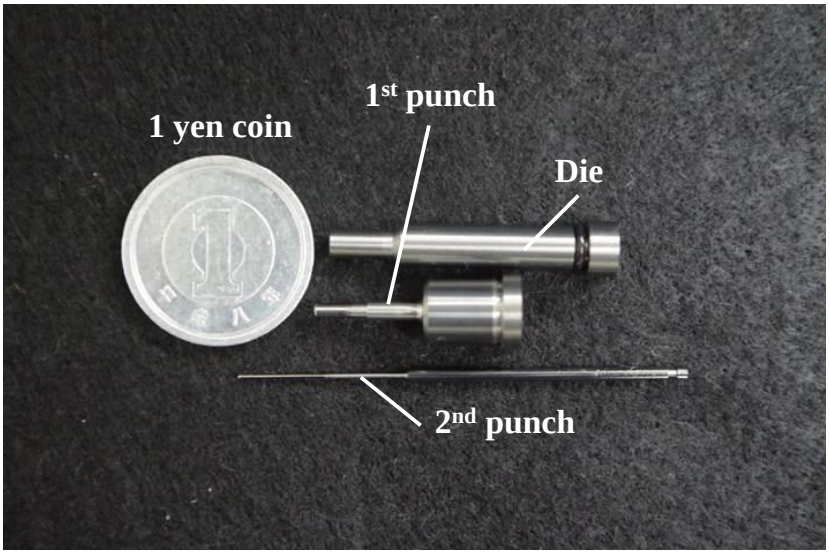

Fig. 5.10 Appearance of MUDD tools.

Table 5.5 Forming conditions used in experiment.

Tooling conditions	Blank holder force H [N]	1st punch displacement Δs [mm]	Counter and radial pressure p_c, p_r [MPa]
DR=1.8×2.1=3.8	4.0	0.03, 0.05, 0.10	100~150
DR=2.0×3.5=7.0	6.0	0.03, 0.05, 0.10	100~150

5.4.2. Experimental results

(1) Performance test for developed MUDD system

Fig. 5.11 shows the performance test results of tools displacement and generated counter pressure using the developed MUDD system. It can be seen that the ultra high pressure of 150MPa was successfully generated. The desired ultra high pressure can be applied and it can be maintained. Furthermore, the 1st punch, the 2nd punch and blank holder can be independently and incrementally controlled using triple action servo press machine. The developed MUDD system has enough performance and function to realize the MUDD process experimentally.

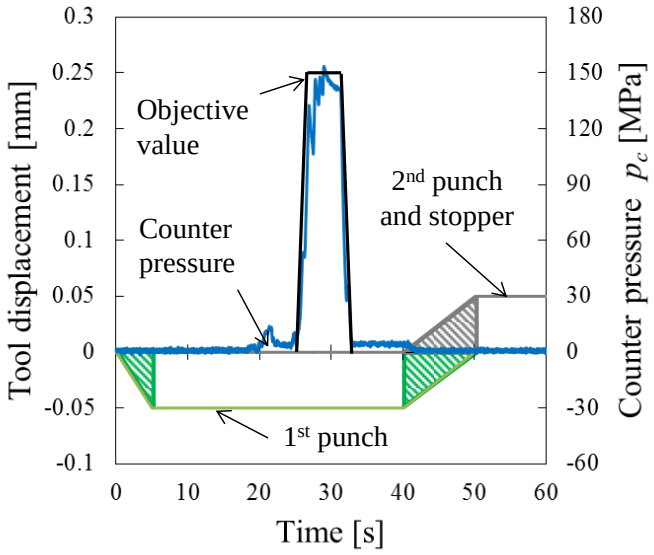

Fig. 5.11 Performance test results of tools displacements and generated counter pressure using developed MUDD system.

(2) Drawn micro cups

Fig. 5.12 shows the appearance of drawn cup at the 1st and 2nd drawings in FEM and experiment. In the 1st drawing, the micro cup can be fabricated in the experiment. The shape of drawn micro cup has a good agreement with the FEM result. **Fig. 5.13** shows the thickness strain distributions in the 1st drawing obtained in FEM simulation and experiment. The thickness strain distribution in experiment has a good agreement with that in FEM in the same manner as the cup shape shown in **Fig. 5.12**

For the 2nd drawing, the micro cup with aspect ratio of 0.92 was successfully fabricated without the fracture and wrinkling in the proposed forming conditions in Chapter 4. From these results, we can say that the MUDD process is realized in the experiment. To achieve the higher aspect ratio, the process parameters should be optimized in the experiment conditions.

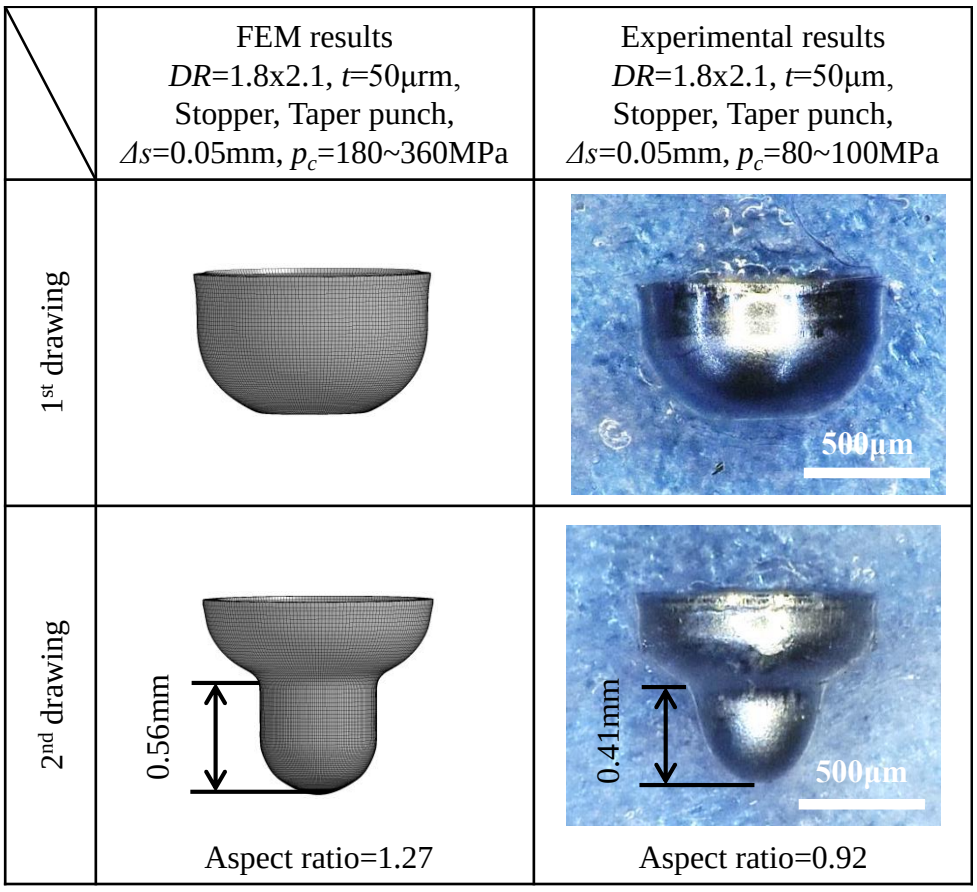

Fig. 5.12 Comparison of drawn micro cup between FEM and experiment.

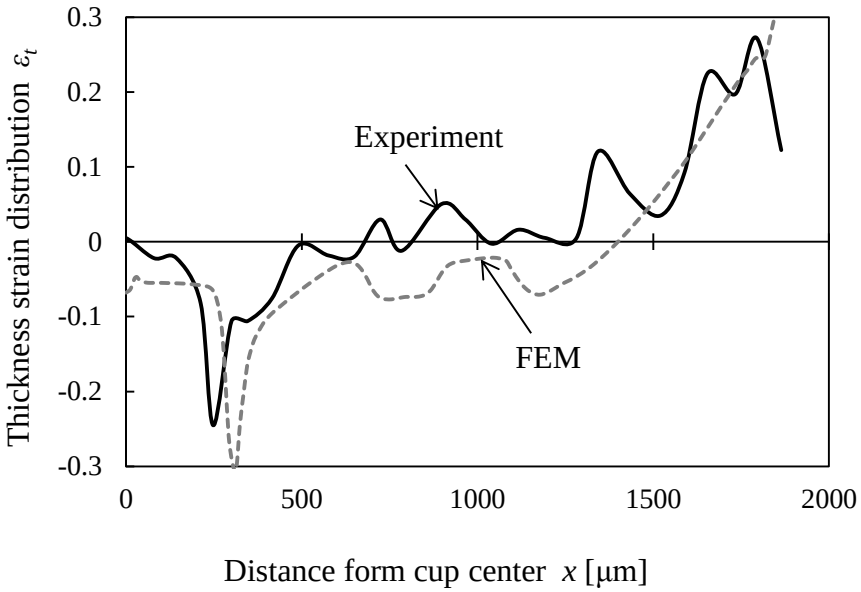

Fig. 5.12 Comparison of thickness strain distribution in the 1st drawing FEM and experiment.

5.5. Concluding Remarks

In this chapter, a newly MUDD system was developed on the basis of the design guideline in Chapter 4 and the experimental verification of the MUDD process was conducted. The main conclusions are as follows;

(1) A novel MUDD apparatus with triple action servo press and ultra high hydraulic system with designed maximum pressure of 400MPa was developed.

(2) The developed MUDD system can independently and incrementally control the displacements of the slides for blank holder, 1^{st} and 2^{nd} punches with the minimum control amount of 1 μm. The ultra high pressure of 150MPa can be generated and its level can be controlled and maintained using the developed ultra high hydraulic system.

(3) The micro cup with aspect ratio of 0.9 can be experimentally fabricated in MUDD. Using the developed MUDD system, the MUDD process combined the ultra high pressure and incremental control of tools and pressure was experimentally realized.

References

[5-1] H. Nishimura, Progress and future view of servo press, Press Working (in Japanese), 50-11, (2012), 18-21.

[5-2] K. Manabe, H. Hamano, Improvement of formability of sheet metals by effective application of blank holder, Journal of the Japan Society for Technology of Plasticity (in Japanese), 33-376, (1992), 480-487.

Chapter 6

Conclusions

6.1. Summary

The demand for micro components with an ultra fine, complicated shape, and high shape accuracy has been increasing in order to improve the performance of devices used in the fields of medicine, precision equipment, and communication, as well as develop multifunctional, compact, and highly integrated devices.

However, as the miniaturization advances, there are limitations in terms of shape and dimension in fabricating the components with a complicated three-dimensional shape due to the requirement of high accuracy for machine and tools. Another issue is the decrease in the lubrication effect and the deterioration in material properties as the specimen size decreases because of the tribological and grain size effects. In addition, due to a limitation of thinning of metal foil, the ratio of feature size to the minimum specimen size becomes small in micro scale and it has considerable influence on the deformation behavior. As a result, the forming limit decreases, the lifetime of dies shortens, and the surface property of the components deteriorates.

In macro sheet forming, several forming principles with special techniques such as multi steps, hydraulic pressure, flange pressing, local heating and cooling, and incremental forming are proposed. Especially, sheet hydroforming technique can achieve the high forming limit, high flexibility for complex shape and high accuracy. In addition, the incremental forming technique can significantly improve the forming limit and achieve the quite high aspect ratio in macro scale. If these technologies can be scaled down to micro scale, it is useful to fabricate micro parts with high aspect ratio, complex shape and high accuracy. However, it seems that the micro sheet hydroforming cannot achieve the high aspect ratio due to the decrease of formability by size effect. On the other hand, it is difficult to scale down the incremental control technique into the micro scale due to the problem of tooling and tribology.

With the above background, a new forming method, micro incremental sheet hydroforming was proposed in this study. In particular, this study aimed to develop a micro ultra deep drawing (MUDD) based on a micro hydromechanical deep drawing (MHDD) by combining the incremental control technique. However, the effect of hydraulic pressure on drawing characteristics in MHDD,

and its size effects have not been clarified in micro scale. Therefore, in the first stage, the MHDD process was designed on the basis of a new friction model considering open lubricant pockets and FEM model considering relative tooling feature size effect. Furthermore, the MHDD system was developed and its basic forming characteristics of fluid pressure were investigated. Based on these results of MHDD, in the second stage, a new forming process for MUDD with the ultra high fluid pressure and incremental control was designed and its forming principle was revealed by FE simulation. Finally, the MUDD system with ultra high hydraulic system and triple action servo press was developed and the MUDD process for micro cup with high aspect ratio was experimentally verified.

6.2. Outcomes

The main outcomes in this study can be divided into four parts. They can be drawn as follows,

1) Proposal of design guideline for micro hydromechanical deep drawing process based on tribological size effect and tooling feature size

The MHDD process was designed on the basis of the scale dependence of tribology and feature size effect. The new friction model considering OLPs and CLPs under fluid pressure was developed. In addition, the FEM simulation considering the relative tooling feature size was carried out, which is defined as the ratio of tooling dimension on minimum manufacturable thickness. Based on the mechanism in MHDD as described below, the design guideline in MHDD can be drawn as follows;

(a) The ultra high pressure which is more than 100MPa is required to induce friction holding and hydrodynamic lubrication effects in MHDD.

(b) The appropriate tooling conditions for fracture prevention effects and improvement of shape accuracy were clarified; hence, the punch shoulder radius should be small to obtain the high shape accuracy and friction holding effect. Meanwhile, the die shoulder radius should be small to induce the hydrodynamic lubrication.

(c) The application of radial pressure can improve the lubrication in OLPs in MHDD.

The increase of relative bending stiffness and the high contact pressure at die shoulder causes the feature size dependence of friction holding and hydrodynamic lubrication effects. Especially, when the ratio of punch diameter to thickness is less than 20, it is difficult to obtain the friction holding effect especially at small drawing ratio. On the other hand, it was clarified that the friction force

decreases with scaling down in MHDD, although it increases in conventional micro forming. The decrease of friction force is obvious when the blank diameter is approximately lower than 1~2mm. Thus, the design guideline of MHDD based on feature size effect and tribological size effect was clarified.

2) Development of simple and compact micro hydromechanical deep drawing system and confirmation of effects of fluid pressure on micro drawability

Based on the established design guideline, the MHDD systems were developed. The developed MHDD system has the following characteristics;

(a) The high precision and stable MHDD process was realized in simple and compact tooling by concept of one stroke forming (coaxial multiple processes).

(b) The sealing for hydraulic pressure of 20MPa can be realized in the compact tool sets by the 1μm clearance between the tools.

Using the developed system, the effect of fluid pressure on drawing characteristics in MHDD was confirmed. It can be summarized as follows;

- The micro drawability can be improved owing to the restriction of wrinkling and the reduction in friction force by applying the appropriate counter pressure.
- The shape accuracy at drawn cup bottom and side wall can be improved in micro scale by applying counter pressure.

However, the fracture occurs at punch shoulder before the applied fluid pressure reaches in the range of ultra high pressure. It is because the friction force between the blank and blank holder increases with increasing the fluid pressure and the load applied to the material at punch shoulder also increases. Therefore, the effect of ultra high pressure cannot be expected for further improvement in the shape accuracy and forming limit by applying only fluid pressure in MHDD.

3) Proposal of new micro ultra deep drawing process using the ultra high pressure and incremental control for high aspect ratio and high shape accuracy

The new MUDD process using the ultra high pressure and incremental controls of tools and pressure was proposed. In addition, the appropriate forming condition to achieve the high aspect ratio and high shape accuracy was designed using FEM simulation. The characteristics and design guideline of proposed MUDD are summarized as follows;

(a) The MUDD process consists of repeating three stages; ① making the space between the 1st punch and blank by lifting up the 1st punch, ② applying the ultra high pressure so as to disappear this space, and ③ lifting down the 1st and 2nd punches at the same time.

(b) The above process can be attained through the ultra high pressure and the alternative control of punch movement and pressure. The deformation area can be incrementally controlled and localized by friction holding effect and stopper in MUDD to prevent the thickness reduction and the fracture.

(c) The appropriate forming conditions to achieve the high aspect ratio and high shape accuracy are as follows; high friction coefficient between the 1st and 2nd punches and blank, the constraint of blank edge movement by stopper, the taper punch, the small 1st punch inner shoulder radius, and the small punch displacement.

(d) The micro cup with cup diameter of 0.5mm and aspect ratio of 4.6 can be successfully fabricated by the proposed MUDD process.

The appropriate forming condition in MUDD was design by FEM simulation. It can be concluded that the developed MUDD is an effective and innovative forming method to solve the problems in micro scale and realize the quite long micro cup with high accuracy.

4) Development of micro ultra deep drawing system with ultra high hydraulic system and multi axial press machine and experimental verification of micro ultra deep drawing process

To realize the designed MUDD process, the newly MUDD system was developed. Additionally, the experimental verification of MUDD process was conducted. The outcomes are summarized as

follows;

(a) The new MUDD system with the ultra high hydraulic system with designed maximum pressure of 400MPa and triple action servo press machine was developed.

(b) It was confirmed that the developed MUDD system can generate and keep the ultra high pressure and can incrementally and independently control the blank holder, 1^{st} and 2^{nd} punches with minimum control amounts of 1μm.

(c) The proposed MUDD process was experimentally verified using the develop MUDD system and micro cup with cup diameter of 0.5mm and aspect ratio of 0.9 was fabricated.

6.3. Contributions

The outcomes of present study are believed to contribute the academic value and industrial availability as follows.

6.3.1. Academic value

The present study clarified that the effects of fluid pressure on deformation behavior in MHDD and its size effect, which has never been reported in previous research in micro forming. The equations for friction holding effect, hydrodynamic lubrication effect and compression effect by radial pressure were derived and the influential parameters on these effects were theoretically revealed. The new friction model for MHDD was proposed and the tribological size effect under fluid pressure in MHDD was newly revealed, which can reduce the friction in micro scale. In addition, it was experimentally revealed that the application of fluid pressure can improve the wrinkling limit, the friction force and the shape accuracy in micro scale. The above findings can contribute to expand and incite the research of micro sheet hydroforming.

Furthermore, the new forming principle of material flow control and control of deformation area by combination of the ultra high fluid pressure and incremental control was realized in micro sheet forming. It can control the stress state and the thickness distribution of deformed blank by ultra high pressure, process parameters, the tool shape and size. This forming principle is a novel technique in micro forming and can contribute to potentially initiate a new academic research about ultra high pressure and incremental control.

6.3.2. Industrial availability

The industrial availability of present study can be described as follows:

The MHDD and MUDD systems with ultra high pressure and triple action serve press machine were developed. The one stroke forming was realized in the developed machines, which can conduct all of forming process in the same axis. It can significantly improve the handling and positioning with simple machine, tool set and process and also can realize the compact machine. In addition, the ultra high pressure can be generated and controlled in micro scale using the simple and compact ultra high hydraulic system. The application of ultra high pressure to micro forming can be easily realized due to the small required flow rate and the small energy for generated fluid pressure in micro scale, although the large and complex machine is required for the ultra high pressure generate in macro scale.

Secondly, the new findings about the lubricate OLPs and hydrodynamic lubrication in micro sheet hydroforming can effectively improve the tribological behavior and solve the previous tribological problem. Furthermore, the high fitness between the blank and punch can be obtained by applying the fluid pressure without the tiny die which is difficult to fabricate. It was shown that the dieless forming with high shape accuracy can be realized in micro sheet hydroforming. It also shows the applicability of micro sheet hydroforming to the tiny and complex shape components.

Additionally, the newly developed forming principle of MUDD can control the material flow and deformation area. It can realize the significant improvement of forming limit to achieve the quite high aspect ratio and can improve the shape accuracy and thickness uniformity. This innovative technique can solve the fundamental issue of low formability in micro forming and can be an universality and high flexible micro forming method.

6.4. Future Works

1) In-depth understanding of tribological characteristics under fluid pressure

The new friction model in micro sheet hydroforming was proposed in this study; however, its tribological behavior during the forming process has not been clearly clarified. In addition, its study is limited in the theoretical approach. This effect should be experimentally clarified in micro sheet hydroforming process.

Furthermore, the lubricant state in open and close lubricant pockets under lubricant or fluid pressure should be evaluated to relate it with the scale dependence of friction force. However, the contact state is drastically changed during the forming process and it is not stable in micro sheet hydroforming due to the change of fluid pressure during the process. Also, the high fluid pressure is required to induce this behavior. Therefore, the simple evaluation test to clarify this phenomenon and it practical application for micro forming process is necessary as the future works.

2) Modification of MUDD system and process to achieve the high aspect ratio

The developed MUDD system can realize the MUDD process and fabricate the micro cup with aspect ratio of 0.9. However, the micro cup with aspect ratio of 4.6 and drawing ratio of 7.0 cannot be fabricated in experiment. It seems that the developed MUDD system cannot realize the same condition with FEM. The main problem should be as follows;

○Insufficient sealablity in MUDD tool sets:

The ultra high fluid pressure cannot be stably generated because there are many small clearances in MUDD tool sets, the leakage of fluid medium is large.

○Micro elastic deformation of MUDD tool sets:

The elastic deformation of tool by applying ultra high fluid pressure is one to several tens μm. The stopper cannot constraint the blank edge and the designed and actual gap between the blank and die Δs may be different.

○Fluid pressure distribution in MUDD:

The fluid pressure has the distribution during MUDD process. It may cause the less material flow at 1^{st} punch shoulder.

These problems for MUDD system need to be modified to realize the same forming condition with FEM and achieve the high aspect ratio. Furthermore, the stopper was used to prevent the upward

movement of cup edge in 2nd drawing stage. However, to insert the stopper in the die after the 1st drawing, the upper tool should be lifted up once. The MUDD process using the stopper is coaxial multiple processes, but not purely the one stroke forming. The other method to restrict the upward movement of cup edge without the stopper or new principle for material flow control are required. The friction holding effect between the blank and 1st punch and the application of radial pressure can restrict the movement of cup edge. The new application method of fluid pressure, such as drastic or pulse pressurization, may be effective to enhance the material flow without stopper. From this, more simple, effective and productive forming process should be proposed in the future.

3) Expand of scope of application in micro incremental sheet hydroforming

The proposed MUDD process uses the thickness of 50μm because the wrinkling occurs when the thickness decreases. It means that the applicable thickness in MUDD is limited. A new concept to prevent and eliminate the wrinkling is required.

Additionally, the developed MUDD process uses the tiny punch to fabricate the micro cup. Even though the applied punch force is much smaller than conventional micro sheet forming process, there is the limitation of miniaturization of target size since the tiny punch is used. In addition, the target shape in this study is limit to the cylindrical cup. When the MUDD process is applied to the complex shape component, the deformation behavior, especially material flow control technique, will change.

If the punchless forming can be realized in micro scale, the components size can be further miniaturized. In addition, by controlling the material flow properly, the desired shape and dimension can be obtained. In macro scale, the deep drawing using rubber [6-1] and flange pressing [6-2] were developed to realize the punchless deep drawing. These forming methods induce the material flow by compression using tools to deform the blank; hence, the punch is not needed in the process. The developed MUDD process also can fabricate the cup by material flow. Therefore, this process is possibly applied to the further tiny and complex shape components by optimizing the material flow control and deformation area control. Through this, it is important to realize the further miniaturization and fabrication of complex shape component as the future works.

The achievement of aspect ratio by MUDD in this study and the feature target is shown in **Fig. 6.1**.

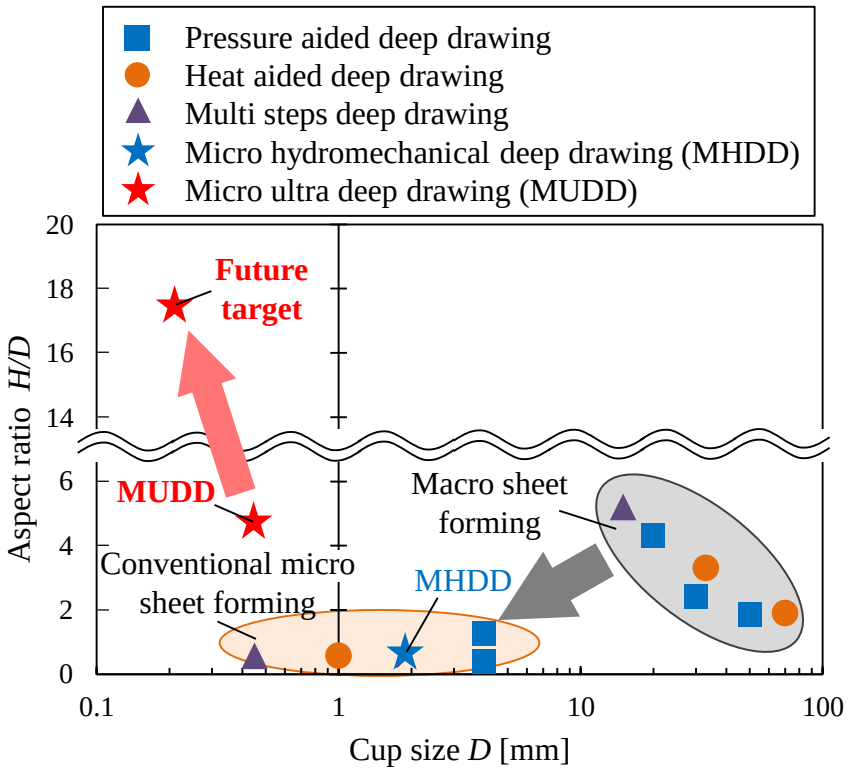

Fig. 6.1 Achievement of aspect ratio in this study and feature target.

Reference

[6-1] M.A. Hassan, N. Takakura, K. Yamaguchi, Friction aided deep drawing of sheet metals using polyurethane ring and auxiliary metal punch. part 1: experimental observations on the deep drawing of aluminium thin sheets and foils, International Journal of Machine Tools & Manufacture, 42, (202), 625-631.

[6-2] T. Iizuka, Fabrication of ultra long cup by the deep drawing of thin sheet using press compression, The Proceedings of the 3rd Integrated Advanced Conference in the Light Metal Educational Foundation, (2013), 47-53.